Integrated Advanced Oxidation and Membrane Reactor Technology for the Treatment of Industrial Wastewater

Hussien, Mukheled

Award date:
2019

Awarding institution:
University of Bath

Integrated Advanced Oxidation and Membrane Reactor Technology for the Treatment of Industrial Wastewater

Mukheled Amer Hussien Al-Sameraiy

A thesis submitted for the degree of Doctor of Philosophy

University of Bath

Department of Chemical Engineering

January 2019

Declaration of authorship

This is all my own work except where I have indicated via references or other forms of acknowledgement.

Signature:…….

Date:

Dedicated to the memory of

Dr. Darrell Alec Patterson

I worked with *Dr. Darrell Patterson* as a lead supervisor of my PhD study for two years. He was a wonderful man, very helpful, enthusiastic and an expert in my field of study.

I am grateful for the many meetings, discussions, constructive guidance, support, enthusiastic encouragement, useful critiques and words of motivation throughout that duration of time. These valuable matters have positively affected me and developed my academic skills in particular with working independently, thinking logically and writing academically.

Physically, he has gone but the life and memories with him can never be forgotten. Since his death until now, I have felt that he is still alive and very close to me in this hard track of my study.

I am forever indebted to him. I am sure that he will be happy when I finish my study.

I would like to say to him '*Thank You Very Much*'.

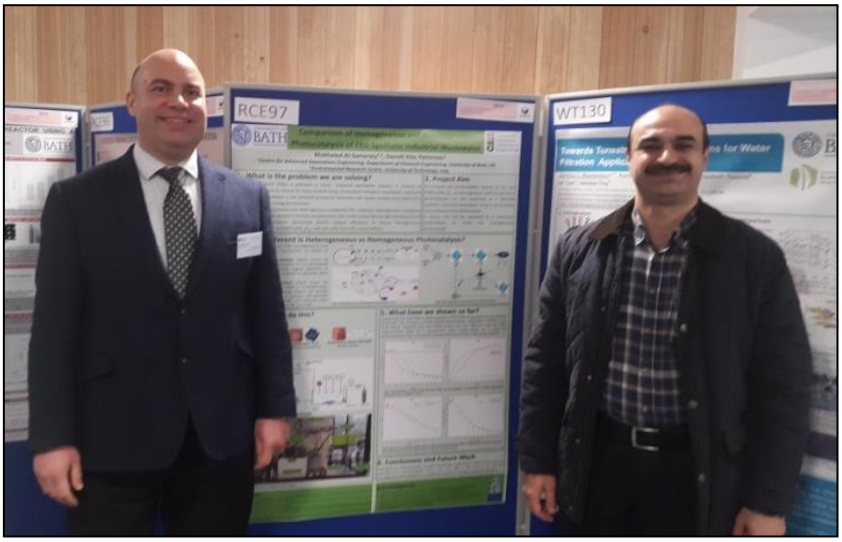

Acknowledgments

‘*In the Name of Allah, Most Gracious and Most Merciful*’

First of all, I would like to express my sincere gratitude to my previous supervisor Dr. Darrell Patterson for encouragement and support during the first two years period of my study.

I am thankful to my current supervisor Dr. Emma Emanuelsson Patterson for her work in supervising, guiding and assisting me during the last two years of my study.

Many thanks to the all technical staff in chemical engineering department, especially Fernando Acosta and Dr. Alexander Ciupa for their support in HPLC work. I want to thank Alan Carver who helped me in POM measurements. I owe much gratitude to Dr. Shaun Reeksting for his valuable help in POM and PEG identification. I also thank Dr. Antonio Exposito who helped in the design of experiments.

I would like to thank the members of ‘Patterson Research Group’ in UK, PhD students (Chris Davey, Kemi Lawal, Lili Xu, Abouther Al-Shimmery, Parimala Shivaprasad and Salida Mansor) and Post docs (Dr. Nicholas Low and Dr. Salman Shahid).

It is a pleasure to thank my colleagues (Dr. Arsalan Ashraf and Dr. Adrien Dartiguelongue) who shared the time of lab work with me. I express my gratitude to my dear friends within ‘Iraqi Student Union’ at bath for helps and sharing fun times together.

Most importantly, I would like to express my deepest gratitude to my beloved family (parents, brothers and sisters) for their continuous prayers and encouragements. I especially must restate my sincere appreciation to my dear wife for her continuous support, sacrifices, courage and help over the years of this study. My unlimited thanks and appreciation to my lovely children (Ahmed and Khaled) for their patience when I have stayed for a long time at the university and could not see them from day to day. Also, special thanks to her family (parents, brothers and sisters) for invaluable support to my family in Iraq.

Last but not least, I want to specially acknowledge the ‘*Environmental Research Center, University of Technology, Ministry of Higher Education and Scientific Research-IRAQ*’ for the scholarship awarded and financial support to pursue this study. Also, special thanks to the staff who work in the Iraqi Cultural Attach-London for their invaluable afford submitted during this long journey.

Abstract

Homogenous photocatalysis using polyoxometalates (POMs) is one of the effective and efficient advanced oxidation processes (AOPs) for the degradation of a wide range of refractory organic pollutants of industrial wastewater at comparable rates to TiO_2 heterogeneous photocatalysis. However, the main disadvantage of POM homogeneous photocatalysts is the separation and recycle of them due to their complete solubility in reactant solution (indeed the molecular size of the photocatalyst can be comparable to that of the pollutants). Such issue makes POM homogeneous photocatalysis unsuitable for any kind of environmental applications, thus limiting the real applications of POMs homogeneous photocatalysts in the field of industrial wastewater treatment.

The current project aims to address this issue as '*a big challenge in the literature*'. Therefore, a novel approach to separate and recycle homogeneous photocatalyst with reactant solution using a cross-flow photocatalytic membrane reactor (PMR) for the treatment of industrial wastewater was proposed. The performance of homogenous photocatalyst was compared with benchmark heterogeneous photocatalyst under batch and continuous modes of operation and assessed based on the evaluating parameters (percentage primary degradation (%PD), reaction kinetics (based on a pseudo-first order reaction constant-K_{app}) and mineralization (percentage total organic carbon (%TOC) removal). $H_3PW_{12}O_{40}$ (denoted as POM) was the homogeneous photocatalyst and TiO_2 was the benchmark heterogeneous photocatalyst. PEG1500 (denoted as PEG) was a selected polymer model of synthetic industrial wastewater. The experimental results of this work showed that:

Firstly, a dead-end membrane filtration process was used to examine the ability of membrane (NF270) to reject either POM or TiO_2 with PEG separately and together as feed (*no UV*). The used membrane could completely separate each of them from PEG reactant solution. These are very interesting results led to be used as a successful choice in the proposed cross-flow PMR approach.

Secondly, the effect of operating parameters including loading (mM), pH and conventional oxidant (mgO_2L^{-1}) on POM homogeneous photocatalysis (*no membrane*) for the treatment of PEG in a continuously recirculating annular photoreactor was examined using a central-composite experimental design (*CCED*) and neural network (*NN*) after several control experiments to confirm the suitable range for these investigated parameters. The optimal conditions were theoretically predicted, POM loading (0.35 mM), pH (3.3) and oxidant (14 mgO_2L^{-1}), using *CCED* and *NN* and then experimentally confirmed. *NN* as a model fitting allowed to determine the interaction effect of these parameters in terms of saliency analysis to be in the following order: pH > loading > oxidant. In general, pH and oxidant operating parameters showed a negative impact on the %PD of PEG. So, they were not controlled under the investigation of POM homogeneous PMR.

Thirdly, in terms of the concept *'membrane enhanced photocatalysis'* is feasible using batch PMR operation under each POM, TiO_2 and combined (POM-TiO_2) photocatalyst. The used membrane could successfully separate and recycle these photocatalysts with complete rejection. For POM and combined photocatalysts, this concept is feasible due to the ability of membrane to concentrate the concentrations of them in the retentate (and then to the photoreactor) to that of an optimal loading (*control photocatalysis-no membrane*), and then increasing the %PD of PEG and K_{app}. While for TiO_2, this concept is not feasible because the tendency of TiO_2 particles to be adsorbed onto the membrane surface increased with increasing the operating time, thus reducing the concentration in the photoreactor and then decreasing the overall %PD and K_{app}. For the membrane enhanced photocatalytic mineralization of PEG (%TOC removal) under the above investigated conditions, this concept is not feasible. This is due to the formation of a broad range of products including identified and unidentified intermediates, polymeric fractions and oxidized PEG oligomers. These products expressed by TOC concentration could not considerably pass through the membrane because of the effect of a *'secondary dynamic membrane'*, thus increasing the TOC concentration in the retentate. In addition, the identified intermediates (malonic, glycolic, formaldehyde, formic, acetic and propionic acids) are so resistant to total mineralization as reported in literature.

Fourthly, in terms of continuous PMR operation, it could successfully convert batch photocatalysis (*control process-no membrane*) to continuous photocatalysis under the optimal loading of POM (0.75 gL^{-1}), TiO_2 (0.25 gL^{-1}) and combined (POM-TiO_2) photocatalysts of Set 2 (POM-0.125 gL^{-1} and TiO_2-0.25 gL^{-1}) for the end course of operation, 9 h (POM or TiO_2) and 12 h (combined photocatalysts) with complete rejection, high photocatalytic efficiency in the degradation of PEG and continuous ability to promote good membrane flux. However, the membrane could not enhance photocatalytic mineralization of PEG as similar to batch PMR operation.

Overall, the proposed PMR approach under batch and continuous operations for the treatment of PEG confirms its ability for the complete separation and recycle of POM homogeneous photocatalyst under different investigated conditions. This successful achievement will make homogeneous photocatalysis using various types of POMs to be a suitable method for environmental applications and the starting point for the real applications of POMs in the industrial wastewater treatment field. Moreover, this approach has considerable advantages such as an environmentally friendly, economically feasible process that works under mild conditions (ambient temperature and pressure, and atmospheric oxygen is used as oxidant) and an effective process for the sustainable photocatalytic degradation of PEG that can be used as a pretreatment step before using conventional biological treatment systems. These results will be useful to facilitate easy benchmarking to real industrial wastewater process scale-up containing soluble polymers with similar properties.

Contents

List of figures

Chapter 3

Chapter 4

Chapter 6

Appendix A

Appendix B

Appendix C

Appendix D

List of tables

List of abbreviations

AAS	Atomic absorption spectrometer.
AOPs	Advanced oxidation processes.
AOTs	Advanced oxidation technologies.
ACN	Methylene cyanide.
BSR	Batch stirred reservoir.
BPMR	Batch cross-flow photocatalytic membrane reactor.
CPMR	Continuous cross-flow photocatalytic membrane reactor.
COD	Chemical oxygen demand.
CFV	Cross-flow velocity.
CCED	Central-Composite Experimental Design.
CPS	Counts per second (intensity unit used in HPLC-ESI-TOF analysis).
CO_2	Carbon dioxide.
DI	Deionized.
DAD	Diode array detector.
DO	Dissolved oxygen.
ELSD	Evaporative light scattering detector.
ESI-MicrOTO	Electrospray time-of-flight mass spectrometer.
FTIR	Fourier transform infrared spectroscopy.
HCl	Hydrochloric acid.
H_2O_2	Hydrogen peroxide.
H_2SO_4	Sulfuric acid.
HO	High molecular weight oligomer.
HPLC	High-performance liquid chromatography.
IC	Inorganic carbon.
K_{app}	Pseudo-first order reaction rate constant of simplified (L-H) kinetic model.
LC-MS	Liquid Chromatography–Mass Spectrometry.
L-H	Langmuir-Hinshelwood.
LO	Low molecular weight oligomer.
MO	Medium molecular weight oligomer.
MW	Molecular weight.
MWCO	Molecular weight cut-off.
MDL	Minimum detection limit of HPLC methodology for total PEG concentration.
MIDL	Minimum individual detection limit of HPLC methodology for oligomer concentration.

MALDI TOF	Matrix Assisted Laser Desorption/Ionization Time of Flight Mass Spectrometry.
NF	Nanofiltration.
NaOH	Sodium hydroxide.
NMR	Nuclear magnetic resonance.
NTU	Nephelometric turbidity unit.
NN	Neural network.
PEG	Polyethylene glycol using PEG1500.
PD	Primary degradation of PEG.
PMR	Photocatalytic membrane reactor.
POM	Polyoxometalate using phosphotungstic acid hydrate ($H_3PW_{12}O_{40}.xH_2O$).
PTFE	Polytetrafluoroethylene.
RID	Refractive index detector.
RO	Reverse osmosis.
SEM	Scanning electron microscopy.
TiO_2	Titanium (IV) oxide.
TMP	Transmembrane pressure.
TOC	Total organic carbon.
TC	Total carbon.
UV	Ultraviolet.
UF	Ultrafiltration.
UV-Vis	UV-Visible.
USA	United States of America.
UK	United Kingdom.
VFAs	Volatile fatty acids or short-chain acids.
W	Tungsten.
ZP	Zeta potential.

Chapter 1

Introduction

1.1 Background

There are many chemical organic pollutants such as polymers, dyes, surfactants, pharmaceuticals, petrochemicals and phenols in the wastewater effluents from industrial sources, which are highly refractory to be easily treated by conventional (physical, chemical and biological) wastewater treatment processes **[1-3]**. One example of these refractory pollutants is polyethylene glycol (PEG), which is a non-ionic synthetic water-soluble polymer. It is widely used in various industrial applications such as lubricants, antifreeze, food, cosmetic (in the form of surfactants and as dispersing agents) and pharmaceutical sector (emulsifiers, thickeners, skin conditioners, humectants, solvents, ointments, suppository bases and laxatives) **[4-6]**.

With these widespread applications, PEG is a common pollutant in conventional wastewater effluent streams. This pollutant is resistant to conventional biological oxidation, the most environmentally friendly and cheapest method of wastewater treatment, and thus can flow through these streams to be discharged into the environment. It might have a toxic effect on animals and soil microbial population, which in turn diminishes soil fertility **[2, 7, 8]**. As a consequence, environmental concerns regarding the fate of this pollutant have been risen **[6, 9-12]**.

In order to protect the environment from PEG pollution as well as other refractory pollutants, new wastewater treatment technologies and processes are required to treat it in industrial wastewater effluents to achieve the desired level of quality, to meet the discharge standards, and thus to protect the ground and surface waters in the environment.

1.2 Problem statement

In literature, it is agreed that advanced oxidation processes (AOPs) have become an attractive choice for degradation of refractory organic pollutants from industrial wastewater. In particular for PEG pollutant, these AOPs such as *wet air oxidation* **[6, 10, 13]**, *UV/H_2O_2* **[9, 14]**, *photo-Fenton* **[14]** and *UV/O_3* **[15]**, have proven to be of real interest as an efficient treatment for the oxidation of various types of PEGs in aqueous solutions (*except photocatalysis, it has not been used for the degradation of PEG yet*).

Photocatalysis, an AOP, is employing UV light in the presence of a photocatalyst to accelerate the photoreaction. *On one side,* heterogeneous photocatalysis generally uses powdered photocatalysts such as TiO_2, which is the most popular photocatalyst for photocatalytic performance, photostability, non-toxicity, low cost, highly abundant and safe to environment **[16, 17]**. It has shown to be effective process for the degradation of refractory organic pollutants **[18]**. An important drawback of this process is that a post treatment is required to separate and recover the TiO_2 photocatalyst (which is usually used as a particulate suspension). The use of a membrane separation process in combination with a photocatalysis process–producing a photocatalytic membrane reactor (PMR)–solves this issue. The membrane provides selectivity via a semi-permeable barrier for the reactor effluent, retention and recycle immediately the photocatalyst and other reactant species within the reactor via a facile separation of them. However, according to the literature, the major obstacle to the performance of PMRs is the fouling of the heterogeneous photocatalyst (e.g. from the suspension of TiO_2) on the surface of membrane. *To overcome these problems*, most research has moved to use immobilized systems, despite the overall lower reaction rates possible because of limitations in overall surface areas of photocatalyst used **[19, 20]**.

On the other side, homogeneous photocatalysis particularly uses homogeneous photocatalysts such as PolyOxoMetalates (POMs). The key advantages with POMs are high solubility in polar solvents (water, alcohols and acetonitrile), thermal stability, low toxicity, strong light absorption, high stability of their cluster shell structure during redox reactions in terms of acceptance and release a certain number of electrons reversely and re-oxidation of the reduced groups by using different oxidants such as O_2 or H_2O_2 **[21, 22]**. These characteristics enable POM homogeneous photocatalysis to photocatalytically degrade various refractory pollutants at comparable rates to TiO_2 heterogeneous photocatalysis such as *methylene orange* **[23]**, *azo dye naphthol blue black* **[24]**, *reactive brilliant red X3B as textile dye* **[25]**, *organchlorine pesticides and cholrophenols* **[26]**, *atrazine and fenitrothion* **[27]**, *methylene blue and congo red* **[28]** *and azo dye acid orange 7* **[29]**. However, a major disadvantage of POM photocatalysts is that they are difficult to separate molecular homogeneous photocatalysts from the reactant solution and recycle them due to their complete solubility in water (indeed their molecular size can be comparable to that of pollutants) as reported by several authors **[28, 30-34]**. Such issue makes POM homogeneous photocatalysis unsuitable for any kind of environmental applications, and thus limiting the real applications of POMs homogeneous photocatalysts in the field of industrial wastewater treatment. Therefore, *to overcome this issue*, research has moved to incorporating the homogenous POM photocatalysts with supporting materials such as TiO_2, ZrO_2, Ta_2O_5, carbon nanotube **[31]**, SiO_2 **[31, 35]**, carbonized resin **[36]**, Fe-POM fixed on a silica fabric structural matrix **[32]**, activated carbon **[37]**, yttrium-doped TiO_2 **[38]** and Ag-TiO_2

[39] to make them in a more recoverable form, despite the decrease of overall surface areas of used photocatalyst, and thus decreasing the overall photocatalytic degradation activity.

Up to now, there has been no research reported in the literature into the separation and recycling of POM homogeneous photocatalyst. *Janssen et al.*, **[40]** suggested that the use of cross-flow nanofiltration in the separation of POM is to be considered as having ***'Great Innovation Potential'*** but this has not yet been investigated. It is expected under this successful separation and recycling of POM that potentially POM as homogeneous photocatalyst will not foul the membrane to the same extent as compared with TiO_2 heterogeneous photocatalyst because the molecular size of POM is much smaller than that of TiO_2, and thus overcoming a reduction in membrane flux and flow throughput.

1.3 Project aim and scope

There is still a big challenge to separate and recycle POM homogeneous photocatalyst. Therefore, the overall aim of the current project is a major attempt to compare the use and recycle of homogeneous and heterogeneous photocatalysts with reactant in a photocatalytic membrane reactor (PMR) for the treatment of industrial wastewater. In this project, POM-$H_3PW_{12}O_{40}$ is the homogeneous photocatalyst and TiO_2 is the benchmark heterogeneous photocatalyst. PEG1500 is a selected model of synthetic industrial wastewater.

In order to achieve this aim, the main specific objectives of this project have been summarized as:

- Examining the ability of selected membrane for separation and recycling of POM and TiO_2 from PEG reactant solution using dead-end membrane filtration process. This membrane is to be used later in proposed cross-flow PMR.
- Producing a prototype PMR as an integrated technology based on combining advanced oxidation process (photocatalysis using conventional annular photoreactor) and membrane separation process (cross-flow nanofiltration cell).
- Developing a suitable and effective chromatographic method for the separation and quantification of PEG oligomers.
- Investigating the effect of operating parameters on POM homogeneous photocatalysis for the treatment of PEG (photocatalysis process-no membrane). These operating parameters are POM photocatalyst loading (mM), pH of the reactant solution and conventional oxidant (mgO_2L^{-1}). The optimal operating parameters will be used in POM homogeneous PMR later.

- Verifying the concept of *'membrane enhanced photocatalysis'* is to be feasible under POM homogeneous, TiO_2 heterogeneous and combined (POM-TiO_2) photocatalysts in a proposed cross-flow PMR under batch mode of operation.
- Verifying the ability of proposed cross-flow PMR under POM homogeneous, TiO_2 heterogeneous and combined (POM-TiO_2) photocatalysts to convert batch photocatalysis (control process-no membrane) to continuous process under the optimal loading of these photocatalysts.

In order to fulfil these objectives, a technical route has been formulated in Fig. 1.1.

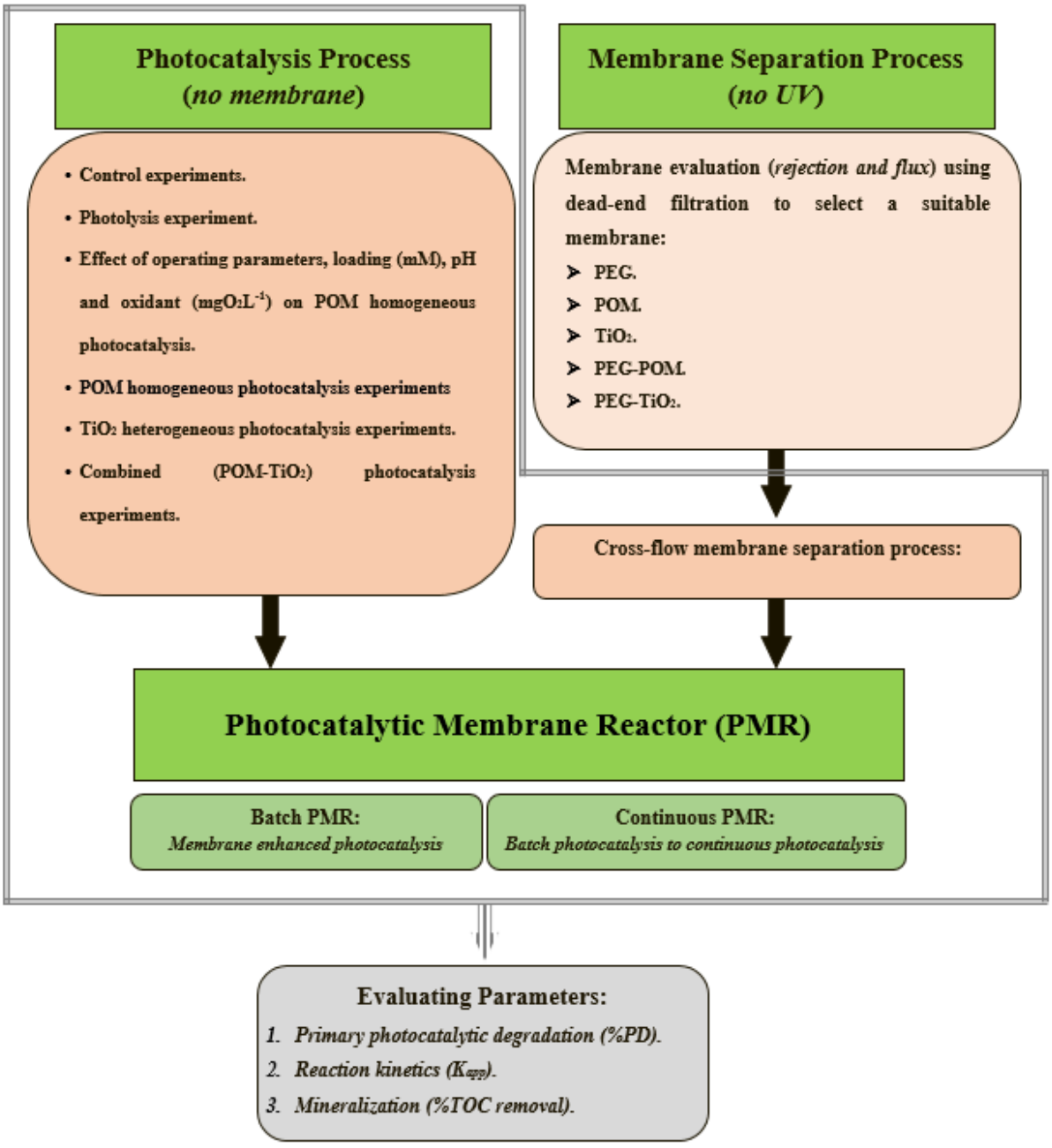

Fig. 1.1: Technical route for the fulfillment of specific objectives.

1.4 Thesis structure

This thesis has been divided into eight chapters and six appendices where four of which are the results and discussion of experimental work carried out to meet the overall aim and specific objectives set out in section (1.3). The results of each chapter contributes towards the general scope of this thesis. Brief descriptions of the scope of each chapter are given below:

- Chapter 1 focuses on the introduction and the motivations of the current project.
- Chapter 2 presents a systematic literature review in terms of advanced oxidation processes, membrane separation processes, photocatalytic membrane reactor and finally implications of the literature. This allows the research to be contextualized.
- Chapter 3 describes the methods and materials involved in this thesis and also all analytical techniques used.
- Chapter 4 investigates the effect of operating parameters, including loading (mM), pH of the reactant solution and conventional oxidant (mgO_2L^{-1}) on POM homogeneous photocatalysis for the treatment of PEG in a continuously recirculating annular photoreactor (photocatalysis process-no membrane) using a central-composite experimental design (*CCED*) and neural network (*NN*).
- Chapter 5 investigates the possibility of using and recycling the POM homogeneous photocatalyst in a proposed cross-flow PMR for the treatment of PEG under batch and continuous PMR operation.
- Chapter 6 investigates the possibility of using and recycling the TiO_2 heterogeneous photocatalyst in a proposed cross-flow PMR for the treatment of PEG under batch and continuous PMR operation.
- Chapter 7 investigates the use and recycle of combined (POM-TiO_2) photocatalysts in a proposed cross-flow PMR for the treatment of PEG under batch and continuous PMR operation. This investigation is evaluated based on the synergetic effect of combined photocatalysts as compared with separate photocatalyst.
- Chapter 8 concludes the results presented in chapters four to seven. It also presents recommendations for future work in this area.

Chapter 2

Literature Review

2.1 Oxidation processes

Oxidation processes used for wastewater treatment can be classified into two kinds, conventional and advanced **[41]**.

2.1.1 Conventional oxidation processes

Conventional oxidation processes, *which are not the subject of this PhD project*, refer to the chemical processes that utilized ordinary chemical oxidants such as hydrogen peroxide (H_2O_2), chlorine (Cl_2), peracetic acid (CH_3CO_3H), potassium permanganate ($KMnO_4$), ozone (O_3) and oxygen (O_2) to oxidize pollutants in wastewater **[42-44]**. The oxidizing potential of these oxidants is not high, thus incomplete oxidation of pollutants results and further treatment is required to meet discharge standards and to protect the environment **[43-45]**. The overall performance of these processes (e.g. in terms of the degradation rates) is slow compared with other advanced oxidation processes **[46]**. Consequently, they are not able to oxidize recalcitrant pollutants such as pesticides **[47]**, cyanides **[48]**, highly chlorinated aromatic compounds **[17]** and etc.,. Therefore, other *'advanced oxidation processes'* are needed for this.

2.1.2 Advanced oxidation processes

Advanced oxidation processes (AOPs) or advanced oxidation technologies (AOTs) can be described on the basis of forming the hydroxyl free radical ($HO^{\bullet}$) at appropriate levels to degrade a wide range of chemical organic pollutants in wastewater that are resistant to conventional chemical oxidants either partially to form intermediate compounds that are amenable to biological treatment or totally to mineralize them to CO_2, H_2O and inorganic ions as final compounds **[41, 42, 46, 49-51]**.

The efficiency and effectiveness of these processes to react with a wide spectrum of pollutants are due to the high oxidation potential or power (E_0) of $HO^{\bullet}$ (2.8 V) as shown in Table 2.1 with high reaction rates (with reaction rate constants of approximately between 10^6-10^9 M^{-1}. s^{-1} **[46, 52, 53]** when compared to conventional oxidants **[54]** where oxidation potential refers to the electromotive force measured in volt unit (V) of oxidation-reduction reaction and uses as an indicator for measuring the oxidant force **[55]**.

Table 2.1: Oxidation potential of various oxidants.

Oxidant	Oxidation potential (V)	References
Fluorine (F)	3.03	**[43, 56]**
Hydroxyl radical ($HO^{\cdot}$)	2.80	**[42, 43, 45, 56-58]**
Sulfate free radicals ($SO_4^{\cdot -}$)	2.60	**[59]**
Positive holes (h^+) on (TiO_2)	2.53	**[58, 60]**
Oxygen (atomic)	2.42	**[42, 56]**
Ozone (O_3)	2.07	**[43, 55]**
Persulfate anions ($S_2O_8^{-2}$)	2.01	**[58]**
Hydrogen peroxide (H_2O_2)	1.78	**[55, 56]**
Perhydroxyl radical ($HO_2^{\cdot}$)	1.70	**[56, 57]**
Magnesium permanganate ($Mg(MnO_4)_2$)	1.70	**[55]**
Permanganate ($MnO_4^{\cdot}$)	1.68	**[56]**
Potassium permanganate ($K(MnO_4)$)	1.67	**[43]**
Hypobromous acid (HBrO)	1.59	**[56, 61]**
Chlorine dioxide (ClO_2)	1.57	**[56]**
Hypochlorite or Hypochlorous acid (HClO)	1.49	**[56, 57]**
Hypoiodous acid (HIO)	1.45	**[56]**
Chlorine (Cl_2)	1.36	**[42, 45]**
Oxygen (molecular)	1.23	**[42, 45]**
Bromine (Br_2)	1.09	**[43, 57]**
Iodine (I_2)	0.54	**[56, 57]**

There are many different types of AOPs reported in open literature **[53]**. *For this PhD thesis, the three relevant processes among these processes are*:

2.1.2.1 Photolysis process

Photolysis process works from the ability of pollutants in water to absorb the ultraviolet (*UV*) irradiation from solar or artificial light, which has a wavelength lower than that of visible light and a sufficient energy to break down the covalent bonds of these pollutants in order to degrade them into fine fractions directly and indirectly (i.e. via the reaction of these degraded pollutants with another compounds) **[62-64]**. Direct photolysis has a limited effect on the degradation of most compounds in comparison with UV-based AOPs like photocatalysis **[65]**.

In the current PhD project, the photolysis process is to be used for examining whether PEG reactant pollutant can be effectively degraded under photolytic reaction conditions.

2.1.2.2 Photocatalysis process

This process can be categorized into the following classes depending basically on the type of photocatalyst phase used:

1) Heterogeneous photocatalysis process

i. Process description

This class of photocatalysis process uses a solid photocatalyst phase, which is different from the phase of pollutants in the solution to accelerate the chemical photoreactions **[17, 66-68]**.

Photocatalysis can be described as a combination process of applying an energetic light source (usually *UV*) and a photocatalyst. A photocatalyst is a solid phase semiconductor material and consists of atoms or molecules that are linked with each other in a certain arrangement and energy levels. These energy levels in terms of band gap theory lead to generate the valence band (VB)-the highest occupied molecular orbitals **(**HOMO) and the conduction band (CB)-the lowest unoccupied molecular orbitals **(**LUMO). They have a definite level of energy, a difference between these levels of energy is known as band gap energy (E_{BG}) **[16, 64, 69]**.

The principal advantages of using a heterogeneous photocatalysis process are **[18, 70, 71]**

- It operates at standard conditions of ambient temperature and pressure.
- It has a good ability to oxidize a broad range of refractory pollutants in wastewater either partially to generate reaction intermediates that are amenable to biological treatment or totally to final products (CO_2, water and inorganic ions).
- It uses generally not expensive photocatalysts with high stability.
- It is to be considered as an eco-friendly applicable method.

The principal disadvantage of using a heterogeneous photocatalysis process is their limitation in the industrial scale application **[69]**. In addition **[18, 72]**:

- Unless immobilized photocatalysts are used, an additional technology is needed to separate the photocatalyst particles.
- It is relatively less economic due to high levels of UV irradiation energy requirements. It can be more economic when using solar irradiation however.

There are several types of semiconductor photocatalysts used in heterogeneous photocatalysis as shown in Table 2.2. They are excited by visible light of a range of different wavelengths and used for degradation of many organic pollutants **[71, 73]**. Among these photocatalysts, TiO_2 is the most generally applied photocatalyst in the photocatalysis processes where it has several significant characteristics such as cheap cost, insoluble in water, nontoxic, high photostability, high UV

absorption and high catalytic performance (high adsorptive ability) because of the availability of effective sites at its surface **[45, 69, 74]**.

There are generally two different phases of TiO_2, including amorphous and crystalline polymorphous (anatase, rutile and brookite). Their photocatalytic performances are unequal where the photocatalytic activity of polymorphous is higher than amorphous **[75, 76]**. Anatase has higher photocatalytic activity and stability than rutile and brookite, so it is more applicable in real applications. However, a combination of anatase and rutile at a certain ratio has been found to be more active than anatase alone, which is a typical crystalline composition of titanium (IV) or titanic oxide (TiO_2, titania, Degussa P-25) **[18, 71, 73]**. TiO_2 (P-25), a standard photocatalyst, is the most extensively photocatalyst utilized in the research of water and wastewater treatment due to its greater photocatalytic activity in the degradation of most pollutant species. Consequently, it is used as a benchmark of performance of photocatalysis at various operating conditions **[70, 77, 78]**.

Table 2.2: Various types of photocatalysts as a function of band gap energy and activation wavelength **[79, 80]**.

Photocatalyst	Band gap energy (V)	Activation wavelength (nm)
$BaTiO_3$	3.3	375
CdO	2.1	590
CdS	2.5	497
CdSe	1.7	730
Fe_2O_3	2.2	565
GaAs	1.4	887
GaP	2.3	540
SnO_2	3.9	318
$SrTiO_3$	3.4	365
TiO_2 (Anatase)	3.2	388
TiO_2 (Rutile)	3.0	414
WO_3	2.8	443
ZnO	3.2	390
ZnS	3.7	336

ii. Heterogeneous photocatalytic reaction mechanism

The basic reaction mechanisms of photocatalysis process can be generally described by the following 9 steps, which incorporates the classic '7 steps of heterogeneous photocatalysis' with the required photoinitiation and photoreaction needed for photocatalysis to occur **[16, 18, 71, 80-83]**.

1. *First external mass transfer of reactants from bulk solution phase to the surface of photocatalyst.*
2. *(If the photocatalyst is porous): internal mass transfer of reactants' molecules through diffusion to the active surface sites of the photocatalyst particles.*
3. *Adsorption of the reactants onto the active sites of the photocatalyst.*

4. *Photoexcitation.*

The action of UV irradiation under a certain wavelength can strongly affect the activation of semiconducting photocatalyst via absorption of a sufficient quantity of photons at energy level (≥) the band gap energy of photocatalyst. As a result of this activation, accelerating the photoreactions and then photoexcitation phenomena occur accordingly in terms of transferring electrons from (VB) to (CB). The results of this transfer generate the electronic vacancies or positive holes (h^+_{VB}) and electrons (e^-_{CB}) in the (VB) and (CB) respectively as shown in Eq. 2.1. The photoabsorption and electron/hole pair formation occur simultaneously in the same process.

$$TiO_2 + h_v \xrightarrow{\geq E_{BG}} h^+_{VB} + e^-_{CB} \quad (2.1)$$

5. *Recombination of electron/hole pair.*

In the absence of electron scavenger, both h^+_{VB} and e^-_{CB} can transfer very fast (around less than 10 nanosecond) to pick up free sites on the surface of catalyst particles, thus the recombination of (h^+_{VB}/e^-_{CB}) occurs, which is one of main drawbacks of the application of heterogeneous photocatalysis process. This recombination in terms of exothermic reaction leads to generate thermodynamically a waste of heat energy and then reducing the overall photocatalytic activity. Therefore, this recombination as shown in Eq. 2.2. should be avoided as much as possible by adding conventional oxidant like hydrogen peroxide (H_2O_2) or molecular dissolved oxygen (O_2) in order to trapping the (e^-_{CB}).

$$h^+_{VB} + e^-_{CB} \rightarrow Heat \quad (2.2)$$

6. *Photocatalytic reactions.*

The holes (h^+_{VB}) act as conventional oxidant to oxidize pollutants directly (Eq. 2.3) and indirectly to form $HO^{\bullet}$ via the reaction with adsorbed water molecules on the outer surface of semiconductor (Eq. 2.4).

$$h^+_{VB} + \text{pollutants} \rightarrow \text{oxidized pollutants} \quad (2.3)$$

$$h^+_{VB} + H_2O \rightarrow HO^{\cdot} + H^+ \quad (2.4)$$

While, electrons (e^-_{CB}) can react with adsorbed oxygen molecules on the outer surface of semiconductor to generate the superoxide radical ions ($O^{\cdot -}_2$) as shown in Eq. 2.5.

$$e^-_{CB} + O_2 \rightarrow O^{\cdot -}_2 \quad (2.5)$$

After these main reactions shown in Eqs. (2.3-2.5), several chemical reactions can be occurred to generate perhydroxyl radicals ($HO_2^{\cdot}$), H_2O_2 and finally $HO^{\bullet}$. These chemical reactions are presented by the following equations:

$$O_2^{\cdot -} + H^+ \rightarrow HO_2^{\cdot} \quad (2.6)$$

$$e_{CB}^- + HO_2^{\cdot} \rightarrow HO_2^- \quad (2.7)$$

$$HO_2^- + H^+ \rightarrow H_2O_2 \quad (2.8)$$

$$H_2O_2 + h_v \rightarrow 2HO^{\cdot} \quad (2.9)$$

$$H_2O_2 + e_{CB}^- \rightarrow HO^{\cdot} + OH^- \quad (2.10)$$

$$H_2O_2 + HO^{\cdot} \rightarrow HO_2^{\cdot} + H_2O \quad (2.11)$$

7. *Desorption of produced compounds (intermediates) from the active sites of photocatalyst.*

8. *(If porous): internal mass transfer to the external surface of the photocatalyst.*

9. *Second external mass transfer of produced compounds from the external surface of the photocatalyst to the bulk solution.*

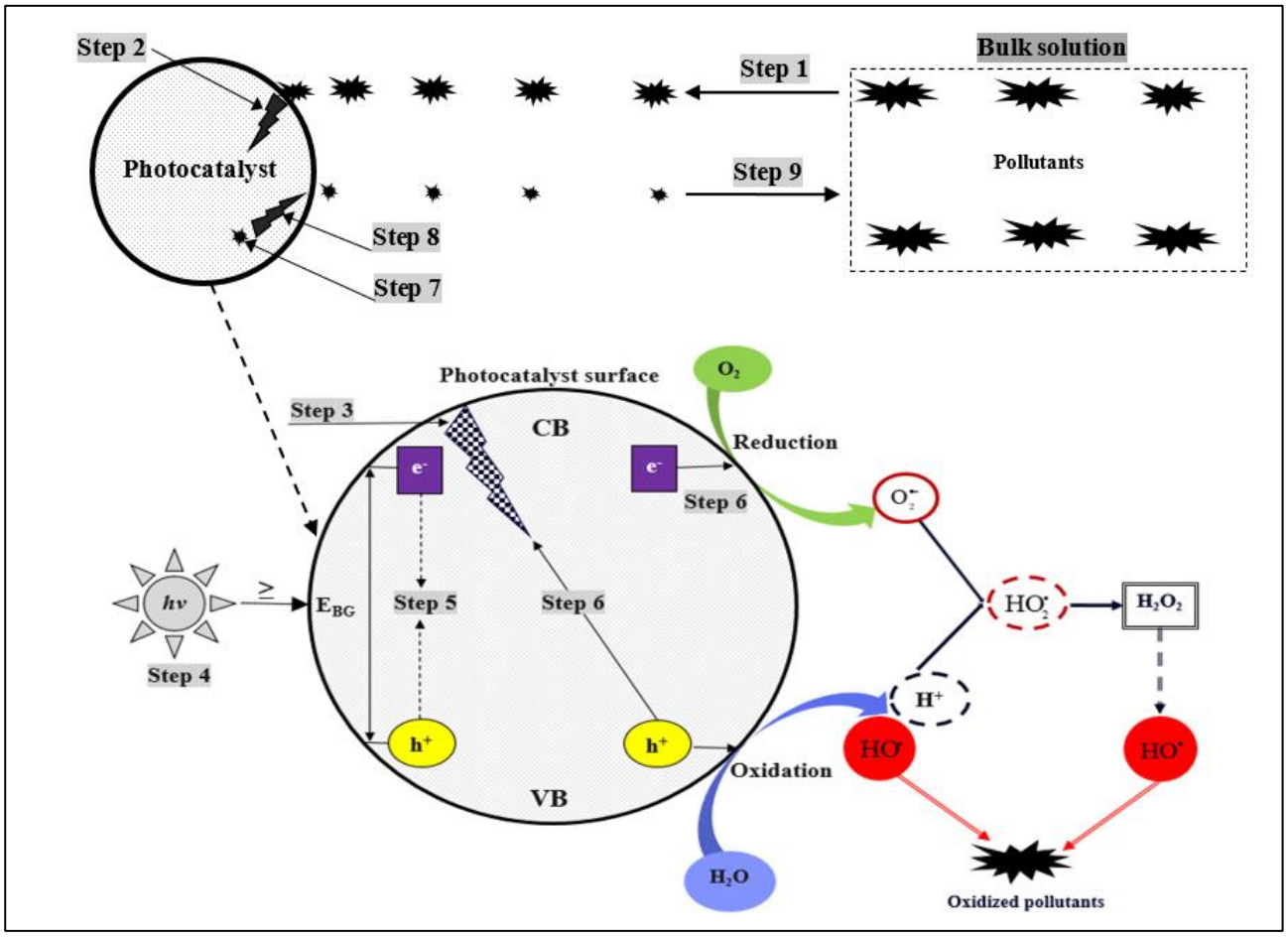

Fig. 2.1: Schematic representation of mechanism of photocatalysis process. VB: valence band; CB: conduction band; E_{BG}: band gap energy; h^+: positive holes; e^-: electrons; *hv*: ultraviolet (UV). Adapted from **[16, 18, 71, 80-83]**.

iii. Reaction kinetics

The reaction kinetics of heterogeneous photocatalysis process can be usually described well by the Langmuir-Hinshelwood (L-H) kinetic model. This model was basically built on the following assumptions **[17, 81, 84]**:

- At equilibrium adsorption conditions, the number of surface sites of the catalyst is constant.
- One reactant may occupy one surface site of catalyst only.
- The heat of adsorption is equal for all adsorption sites on the surface of catalyst.
- There is no contact between each adsorbed molecule.
- The rate of surface adsorption of reactant is higher than the rate of any chemical reaction.
- It is not necessary for reactants to occupy all active sites on the catalyst.

The (L-H) kinetic model can be expressed by Eq. 2.12 **[81, 82, 85]**.

$$r = -\frac{dc}{dt} = \frac{kKC}{1+KC} \tag{2.12}$$

Where *r* is the degradation rate of a pollutant ($mgL^{-1}min^{-1}$), *C* is the concentration of the pollutant in the solution (mgL^{-1}) at any time, *t* is the reaction time (min), *k* is a true rate constant ($mgL^{-1}min^{-1}$) and *K* is the Langmuir adsorption equilibrium constant (Lmg^{-1}). The equation above can be simplified according to two main cases:

(A) When the concentration of reactant solution is high (> 0.005 $molL^{-1}$), the Eq. 2.12 can be mathematically simplified into the form of zero-order reaction kinetic as follows:

$$r = -\frac{dc}{dt} = k_{app} \tag{2.13}$$

The above equation can be integrated and rearranged into the following equation:

$$C = -k_{app}t + C_0 \tag{2.14}$$

Where *k* is the zero order reaction constant ($mgL^{-1}min^{-1}$) that can be calculated from plotting *C* versus *t*.

(B) When the concentration of reactant solution is highly diluted (< 0.001 $molL^{-1}$), the Eq. 2.12 can be mathematically simplified into the form of first order reaction kinetic as follows:

$$r = -\frac{dc}{dt} = kKC = K_{app}C \tag{2.15}$$

The above equation can be integrated and rearranged into the following equation:

$$ln\frac{C}{C_0} = -k_{app}t \tag{2.16}$$

Where k_{app} is the pseudo-first order reaction constant (min^{-1}) that can be calculated from plotting (*ln C*) or (*ln C/C₀*) versus *t*.

Generally, literature **[65, 86, 87]** shows that most of heterogeneous photocatalytic degradations of organic pollutants follow kinetically the first order approximation of the Langmuir-Hinshelwood model (Eq. 2.15).

2) Homogeneous photocatalysis process

This class of photocatalysis process uses a photocatalyst in the same phase as that containing pollutants or a photocatalyst is dissolved in reactant solution **[17, 79]**.

For this PhD project, the homogenous photocatalyst is a powder that fully dissolves in PEG reactant solution, so finally both of them are liquid phase.

i. Homogeneous photocatalysts

The most commonly used homogeneous photocatalysts are "PolyOxoMetalates" (POMs). This term 'POMs' refers to huge group of anionic clusters based on high valent transition metals.

From a molecular chemical point of view, generally there are two categories of POMs, isopolyanions $[M_mO_y]^{n-}$ and heteropolyanions $[X_xM_mO_y]^{n-}$ where M is the main transition metal constituent of POMs such as Vanadium (*V*), Niobium (*Nb*), Tantalum (*Ta*), Molybdenum (*Mo*) and Tungsten (*W*), O is the oxygen atom, X (heteroatom) may be a wide range of different elements of the periodic table except the noble gases and n is the overall cluster charge **[21, 88, 89]**. The most common transition metal atoms present in the clusters are (*Mo*) and (*W*), whereas (*V*), (*Nb*) and (*Ta*) are less frequent **[22, 34]**.

From a structural point of view, they have a wide range of molecular structural diversity, resulting in various dimensions, shapes, sizes, charge density, surface reactivity and high redox reactions. There are various structural types of them such as *Lindqvist* $[M_6O_{19}]^{n-}$, *Anderson* $[XM_6O_{24}]^{n-}$, *Keggin* $[XM_{12}O_{40}]^{n-}$ and *Wells-Dawson* $[X_2M_{18}O_{62}]^{n-}$ cluster anions as shown in Fig. 2.2 **[34, 90]**.

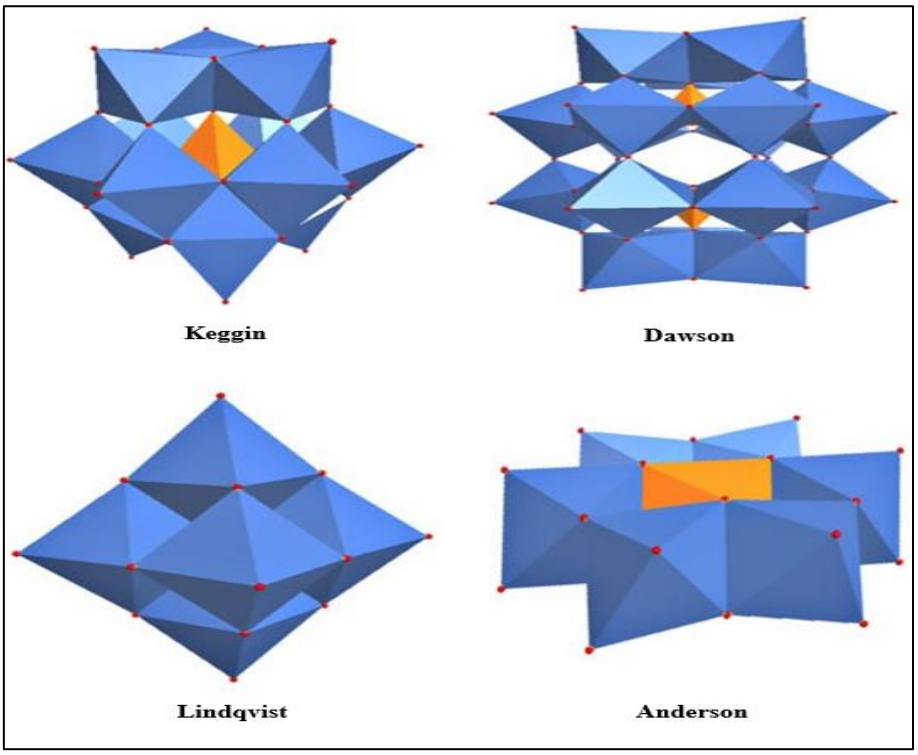

Fig. 2.2: Different structural types of POMs where blue polyhedra, orange polyhedra and red balls refer to M, X and O respectively. Taken from **[88]**.

POMs have several characteristics such as being soluble in polar solvents like (water, alcohols and acetonitrile), thermal stability, low toxicity, strong light absorption, high stability of their cluster shell structure during redox reactions in terms of acceptance and release a certain number of electrons reversely and re-oxidation of the reduced groups by using different oxidants such as O_2 or H_2O_2 **[21, 22, 91]**. In addition, these photocatalysts are acidic and negatively charged in aqueous or reactant solutions **[38, 92-94]**.

The most common structural types of POMs used is the Keggin cluster due to its easy synthesis, commercial availability and excellent chemical characteristics. Phosphotungstic acid (PTA) or tungstophosphoric acid (TPA) with molecular chemical formula ($H_3PW_{12}O_{40}$) is one typical example of a Keggin cluster **[92, 93]**. These characteristics enable POMs homogeneous photocatalysis to be used in the photocatalytic degradation of various refractory pollutants at comparable rates to TiO_2 heterogeneous photocatalysis as explained in the next section. In addition, they have a wide range of applications such as in medicine, photography as recording materials, dyes or pigments, fire resistance coating, electrochemistry, magnetism and catalysis **[1, 34, 92]**.

In terms of POMs chemical stability, it is generally accepted that POMs under aqueous solutions are chemically stable at pH 1, when varying pH, they decomposed partially into several lacunary species **[95]**. These lacunary species are oxidative agents **[92, 96]**. More detailed information about the chemical stability of POMs is shown in chapter 4.

ii. Application of POMs homogeneous photocatalysis in the treatment of wastewater

The application of POMs as homogeneous photocatalysts shows an appropriate photocatalytic activity to oxidize an extensive range of organic pollutants. Some examples of this application of POMs in terms of a powder (acidic salt) that fully dissolves in reactant solution are methylene orange **[23]**, methylene blue and congo red **[28]**, azo dye naphthol blue black **[24]**, azo dye acid orange 7 **[29]**, reactive brilliant red X3B as textile dye **[25]**, atrazine **[97]**, fenitrothion **[98]**, atrazine and fenitrothion **[27]**, chloroaromatic 1,2-dichlorobenzene **[99]**, 3,4,5-trichlorophenol, 3,4-dichlorophenol and 3-chlorophenol **[100]**, 2,4,6-trichlorophenol **[101]**, 2,4-dichlorophenol and organchlorine pesticides with two types: lindane and hexachlorobenzene **[26]**.

However, in the practical application of POMs-based homogeneous catalysis, there is a principal problem by which they are so difficult to separate POMs from their reactant solution for recycling them. From this point of view, several techniques have been developed to immobilize POMs on different supports such as TiO_2, ZrO_2, Ta_2O_5, carbon nanotube **[31]**, SiO_2 **[31, 35]**, carbonized resin **[36]**, Fe-POM fixed on a silica fabric structural matrix **[32]**, activated carbon **[37]**, yttrium-doped TiO_2 **[38]** and Ag-TiO_2 **[39]** to make them in a more easily recoverable form, despite the decrease of overall surface areas of used photocatalyst, and thus decreasing the overall photocatalytic degradation activity.

Up to date, the separation and recycling of POMs homogeneous photocatalysts are still a big challenge in the literature. This gives the principal motivations for the current PhD project to have a great opportunity of novel investigation.

iii. Homogeneous photocatalytic reaction mechanism

Two mechanisms have been generally accepted in the literature–one has the photocatalysis reaction mechanism using POM as similar to the TiO_2 as heterogeneous photocatalyst mechanism in which both of them generate ($HO^{\bullet}$) **[27]**. The other is quite different and is as follows **[26, 97-104]**.

1) Photoexcitation step

POMs have an excellent ability to absorb high quantities of UV light below 400 nm at energy level ≥ band gap energy (E_{BG}) of photocatalyst (for example, E_{BG} of POM-$H_3PW_{12}O_{40}$ is 2.8 V), resulting in the excitation of POM via transferring electron from highest occupied molecular orbital (HOMO) to the lowest unoccupied molecular orbital (LUMO) to form an excited state of POM cluster as (POM^*).

$$\mathrm{POM} + h\nu \rightarrow \mathrm{POM}^* \qquad (2.17)$$

2) Reactions step

POM^* as a powerful oxidizing reagent can react directly with organic pollutants to oxidize them and generate reduced POM cluster (POM^-) as shown Eq. 2.18 and indirectly with water molecules to form POM^-, $HO^{\bullet}$ and positive hydrogen ion (H^+) as shown in Eq. 2.19:

$$POM^* + \text{polltants} \rightarrow POM^- + \text{oxidized products} \quad (2.18)$$

$$POM^* + H_2O \rightarrow POM^- + HO^{\cdot} + H^+ \quad (2.19)$$

After that, $HO^{\bullet}$ as a strong oxidant can react with organic pollutants to mineralize them either partially into oxidized products and short chain acids or totally into final products (CO_2, H_2O and inorganic ions).

3) Re-oxidation step

Molecular dissolved oxygen (O_2) can regenerate (reoxidize) POM^- to form POM cluster and superoxide radical ions ($O_2^{\cdot -}$), which are able to further participate in oxidization of the organic pollutants as shown Eq. 2.20:

$$POM^- + O_2 \rightarrow POM + O_2^{\cdot -} \quad (2.20)$$

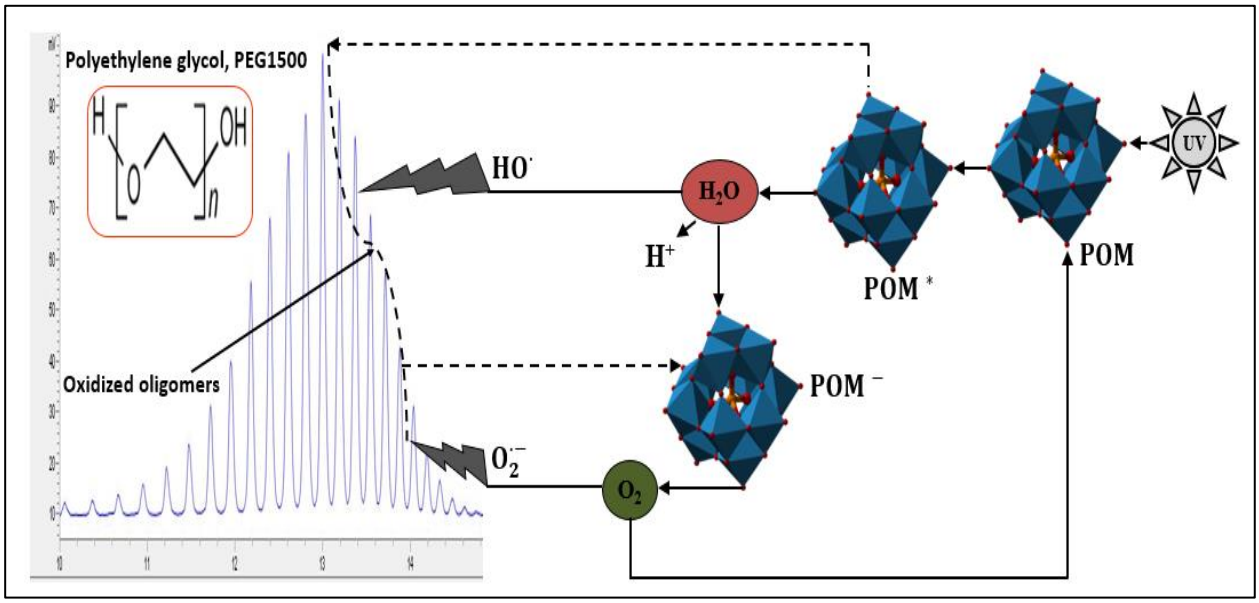

Fig. 2.3: Schematic representation of the mechanism of POM homogeneous photocatalysis process of PEG. Adapted from **[26, 97-104]**.

iv. Homogeneous reaction kinetics

There are very limited numbers of studies done to investigate the kinetics of POM as a homogeneous photocatalyst, especially when comparing with TiO_2 as heterogeneous photocatalyst. Some researchers reported **[38, 39, 105-107]** that the Langmuir-Hinshelwood kinetic model (pseudo-first order reaction model) can be applied to describe the POM homogeneous kinetics.

2.2 Membranes

2.2.1 Membrane filtration processes

2.2.1.1 Basic description

Filtration is a traditional separation process to remove particulate matters (suspended and colloidal solids) in water and wastewater as a liquid phase using conventional filter media **[42, 108]**. Membrane filtration processes as a mechanism for separation is defined by permeation of liquids or gases through semipermeable or selective barrier membrane under a specific driving force *i.e.* pressure, concentration and electrical potential gradients. An applied driving force to the initial feed solution (feed stream) flowing into the membrane separates it into two streams: the first stream (permeate or permeating or product or filtrate) refers to the liquid that passes through the membrane where this permeate flow through the total surface area of membrane expressed by the flux as a rate. While the second stream (concentrate or retentate or retained phase or reject or waste) refers to the liquid that does not pass through the membrane. **[109-111]**.

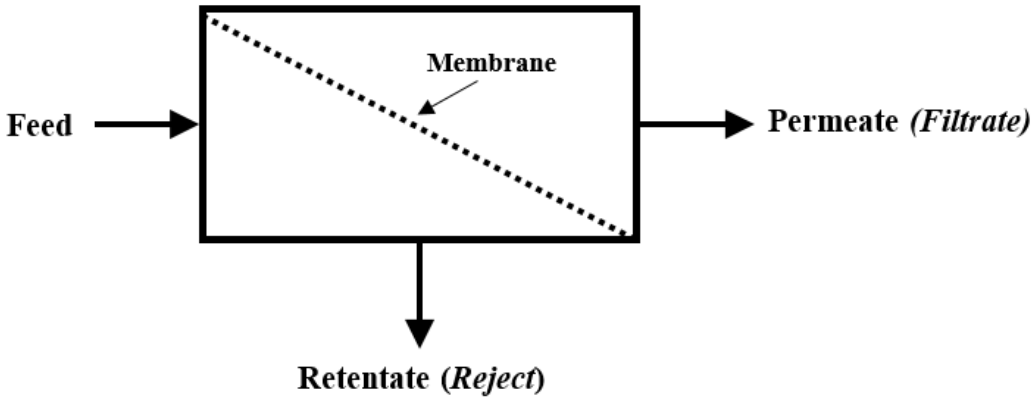

Fig. 2.4: Schematic membrane process.

2.2.1.2 Criteria of membranes

There are several parameters that play an important role as criteria to evaluate the membranes, involving **[112]**:

- Diameter pore size of membrane.
- Manufacturing material of membrane.
- General shape of membrane as geometry.
- Type of solid material to be treated.
- Type of water to be treated.

2.2.1.3 Characteristics of membranes

There are several important characteristics that enable the membranes to be suitable for commercial applications such as **[111, 113]**:

- A high flux (permeance).
- Highly selectivity to the species to be separated.
- Robust-including good mechanical strength.
- Fouling resistance.
- High resistance to temperature change.
- Low aging–i.e. they last long in a process.

2.2.2 Membrane separation classification

Membrane separation processes can be generally categorized on the basis of driving forces into pressure, concentration and electrical potential gradients. *The current PhD project focuses on pressure-driven membrane processes*. So, this literature review focuses on these processes.

Pressure-driven membrane separation processes are principally classified depending on their pore size or molecular weight cut off (MWCO) into four different processes: microfiltration (MF), ultrafiltration (UF), nanofiltration (NF) and reverse osmosis (RO). The pore sizes of these membranes are differentiated as macropores (> 50 nm), mesopores (2-50 nm) and micropores (< 2 nm). MF membranes are usually specified by pore size (in particular with macropores), whereas the others are generally described by MWCO, which describes the retention performance of a membrane where 90% of a solute molecular weight (MW) is rejected by the membrane **[42, 109-111, 114]**.

2.2.2.1 Microfiltration process

Microfiltration (MF) process uses a membrane with a pore size in the range of 0.1-10 μm where above 10 μm, the separation is considered as a conventional filtration using filters. MF membranes are used to retain various types of solids as shown in Table 2.3. It can be used as pre-filtration step before UF process. The rejection of these membranes are described by size exclusion (pore flow model) **[42, 108, 110, 111, 115]**. Generally, this process has several features as shown in Table 2.3:

Table 2.3: Features of MF process, adapted from **[42, 108, 110, 111, 115]**.

Features	Description
Operating mode	cross flow and dead-end.
Operating pressure	(0.1-3) bar.
Molecular separation size	solids > 0.1 μm (100 nm).
Material retained	suspended solids, small particles, large colloids, microbial cells, bacteria and yeast.
Material passed	water and dissolved solutes.
Membrane type	symmetric polymer or ceramic.
Module type	tubular, hollow fibre, spiral-wound, and plate and frame.

2.2.2.2 Ultrafiltration process

Ultrafiltration (UF) process uses a membrane with a pore size in the range of 0.005-0.1 μm. UF membranes are suitable for the removal of different solids as shown in Table 2.4. The rejection of these membranes is described by size exclusion (pore flow model) **[108, 110, 111, 114, 115]**. Table 2.4 shows the important features of UF process.

Table 2.4: Features of UF process, adapted from **[108, 110, 111, 114, 115]**.

Features	Description
Operating mode	cross flow and dead-end.
Transmembrane pressure	(0.5-10) bar.
Molecular separation size	solids > 0.005 μm (5 nm) and colloidal solids (MW > 20,000 $gmol^{-1}$).
Material retained	macromolecules, colloids, proteins, emulsions, cells, starch and enzymes.
Material passed	water and dissolved salts.
Membrane type	asymmetric polymer composite or ceramic.
Module type	tubular, hollow fibre, spiral-wound, and plate and frame.

2.2.2.3 Nanofiltration process

Nanofiltration (NF) process uses a membrane with a pore size around 1 nm. It is basically characterised as having characteristics between ultrafiltration and reverse osmosis. The separation of NF membranes is described by a combination of the pore flow and solution-diffusion models **[42, 110, 115]**. General features of NF processes are presented in Table 2.5.

Table 2.5: Features of NF process, adapted from **[42, 110, 115]**.

Features	Description
Operating mode	cross flow and dead-end.
Transmembrane pressure	(2-40) bar.
Molecular separation size	solids > 0.001 μm (1 nm) and dissolved solids (MW > 200 $gmol^{-1}$).
Material retained	dissolved multivalent salts and low molar mass organics.
Material passed	water.
Membrane type	asymmetric polymer or composite.
Module type	tubular and spiral-wound.

In the field of industrial wastewater treatment, NF is extensively used to **[110, 111, 115]**:

- Pretreat wastewater before being applied (RO) process.
- Remove colour in wastewater from textile, and pulp and paper industries.
- Demineralize wastewater including surfactants.
- Retain multivalent ions such as cadmium and chrome.
- Separate low organic MWs from water/solvent.

In literature, *the membrane (NF270)*, has been successfully used for the treatment of different types of synthetic and real industrial wastewater such as pharmaceutical (ciprofloxacin, CIPRO **[116]** and sulphamethoxazole **[117]**), veterinary pharmaceutical (sulfamethoxazole-SMETOX, trimethoprim-TMP, ciprofloxacin-CIPRO, dexamethasone-DEXA and febantel-FEBA) **[118]**, meat processing **[119]**, paper industry **[120]**, dairy industry (real wastewater and model from commercial skim milk) **[121]**, gold mining and ore processing **[122]**, abandoned mine drainage **[123]**, olive mill effluent **[124]**, printing wastewater containing heavy metals and dyes **[125]**, Argo-industrial effluent (dairy, tomato, artichoke and olive oil) **[126]**, palm oil mill effluent **[127]** and synthetic dyes (methylene red-MR, crystal violet-CV, reactive orange 16-RO16 and methylene blue-MB) and synthetic polymers (polyethylene glycols-PEGs (PEG200, PEG400, PEG600 and PEG1000)) **[128]**.

This membrane has shown a higher rejection of the above pollutants with a higher rate of flux until the end of operation time under the examined conditions of dead-end and cross-flow membrane filtration processes. *These viable advantages make this membrane to be potentially the best candidate for selection in the current PhD study.*

2.2.2.4 Reverse osmosis process

Reverse osmosis (RO) process as a hyperfiltration uses a dense membrane with pore diameter < 1 nm. RO process has higher efficiency than NF process in separation of solids. It is widely applied in desalination of seawater and brackish water. The rejection of RO membranes is described by the solution-diffusion model **[111, 115, 129, 130]**. General features of RO process are presented in Table 2.6.

Table 2.6: Features of RO process, adapted from **[111, 115].**

Features	Description
Operating mode	cross flow.
Transmembrane pressure	(5-70) bar.
Molecular separation size	solids < 0.001 μm (1 nm) and dissolved solids (MW < 200 $gmol^{-1}$).
Material retained	dissolved salts and organics.
Material passed	Water and solvent.
Membrane type	asymmetric polymer or composite.
Module type	tubular, spiral-wound, and plate and frame.

2.2.3 Membrane material

Membranes are broadly categorized into three types: organic, inorganic and hybrid. Organic membranes can be made from a variety of polymers such as polyamide (PA), polysulfone (PS), polyethersulfone (PES), polyvinylidene fluoride (PVDF), polypropylene (PP), polyaniline and cellulose acetate (CA). Inorganic membranes can be made of different materials such as ceramics, glasses and metals like alumina (Al_2O_3), titania (TiO_2), silica (SiO_2) and zirconia (ZrO_2). While, a combination of organic and inorganic membranes (incorporating an inorganic dispersed phase within a polymer matrix) produces hybrid membranes (MMMs) such as mixed matrix membranes **[110, 131, 132]**. Generally, polymeric membranes have several characteristics such as low cost, ease of production in different shapes like flat sheets, tubular, capillaries and hollow fibers compared with inorganic membranes **[133]**.

In the current PhD project, commercially synthetic organic membrane (polyamide, NF270) is used for dead-end and cross-low NF processes.

2.2.4 Membrane characterization

There are a wide range of techniques used for the characterization of membranes. The used techniques depend on the information which is required. *The specifications of the commercial membrane (NF270) used, in the current PhD project, are available from the supplier and open literature.* So, specific information relating to membrane characterization in terms of membrane fouling and cleaning is not necessary, which is beyond the scope of this project. This project focuses mainly on the performance of membrane based on rejection and flux. However, this section is just to give some information about the commonly used methods for membrane characterization in terms of the surface conditions.

1) Membrane hydrophobicity

The hydrophobicity or wettability of a membrane can be determined by measuring the contact angle that forms between the solid surface (membrane) and a liquid (drop of water). This contact angle can identify the nature of membrane where if it is less or greater than 90^0, the membrane is hydrophilic and hydrophobic respectively **[134, 135]**. The wettability can affect the separation through the interactions between the feed and the membrane **[136]**. Generally, hydrophilic membranes exhibit less tendency of pollutant for adsorption than hydrophobic membranes, leading to make them more resistant to fouling and thus increasing the flux **[120, 137]**.

In the current PhD project, commercially synthetic organic membrane (polyamide, NF270) is hydrophilic as reported in the literature **[117, 120]**.

2) Membrane surface charge

The charge on the surface of membrane during a filtration process can affect the adsorption of species on the membrane surface (fouling tendencies). The surface charge on a membrane is related to the zeta potential (ZP), which arises from the dissociation of certain species on the surface, leaving behand a charged functional group. ZP is useful to identify any particle-particle and surface-particle interactions and then these interactions play a significant role in membrane fouling **[138, 139]**.

Among factors affecting ZP, pH is the most important factor that affects the ZP of the membrane. It is accepted generally that most membrane surfaces have a negative charge at neutral pH conditions **[139, 140]**. This negative charge on the surface of membrane based on the ZP will be significantly affected under acidic and basic conditions of the reactant solution, thus the interaction between membrane and either solute or suspended particles in the solution results in adsorption. This adsorption and then fouling can be minimized when the surface of membrane and particles (solute or suspended) having the same charge due to higher electrostatic repulsion between them **[139, 141]**.

In the current PhD project, the surface of used membrane (NF270) is negatively charged at natural pH as reported in the literature **[120, 142]**.

3) Scanning electron microscopy (SEM)

SEM is a common technique used to image the surface or cross-section of a membrane. Images allow the membrane surface to be analyzed and give a clear indication of fouling and cleaning when comparing with a virgin membrane.

In the current PhD project, the SEM images of the top surface of used membranes (NF270) only are taken under different investigated conditions in order to give an indication about the deposited material (rejected) on the surface of membrane. The cross-section of used membranes will not considered in the current work since it relates to the mechanistic study of fouling and cleaning, which is beyond the scope of the current study.

2.2.5 Filtration modes

There are two principal operating modes of membrane filtration processes, namely dead-end (or direct feed or static) filtration and cross-flow (or dynamic) filtration.

In the mode of dead-end filtration (Fig. 2.5-a), the feed is perpendicularly pumped to the surface of membrane leading to a pressure gradient across the membrane. This pressure gradient is because of the accumulation of rejected components on the membrane surface in the form of a cake layer. The build-up of a cake layer over time leads to a reduction in the flux. This flux reduction increases significantly with increasing the rejected components in the feed. To enhance the dead-end

performance, a rapid stirring of the feed side is used to reduce the effect of build-up of a cake layer at the surface of membrane and provides a pseudo-cross-flow filtration environment. However, due to intensive fouling formation, this fouling is limited their industrial applications. Generally, this mode is applied to MF and UF processes that are required to remove complete species in the feed or for laboratory applications **[111, 115, 143]**.

In the mode of cross-flow filtration (Fig. 2.5-b), the feed is pumped parallel and tangential to the surface of membrane. In this case, some feed passes through the membrane and then is collected as a permeate. While, the others pass over the membrane as cross-flow retentate flowrate and next reuse again to control fouling. The shear forces by the action of continuous flow of retentate stream lead significantly to reduce the accumulated layer of solid components as fouling on the surface of membrane and then achieving a continuous operation **[111, 115, 134, 137, 143]**.

The advantages of cross-flow filtration, it can be generally applied for the commercial large scale of membrane processes such as MF, UF, NF and RO. It is widely applied to NF and RO in various industrial applications due to its ability to control fouling by which the rate of fouling is decreased by increasing the cross-flow velocity of feed **[115, 143, 144]**.

The disadvantage of cross-flow filtration when compared with the traditional and simplest operational mode (dead-end filtration) is the high energy required in order to maintain a continuous volumetric flowrate of feed. Therefore, another type of operating mode of membrane filtration processes named "semi-cross-flow" or "semi-dead-end" mode was modified by a combination of two modes of cross-flow and dead-flow principles so as to decrease the energy requirements by using discontinuous intervals of backwashing **[115]**.

In the current PhD project, the dead-end filtration will be initially used to examine the ability of used membrane (NF270) to reject the POM homogeneous and TiO_2 heterogeneous photocatalysts from the PEG reactant solution. The same membrane will be used later in the proposed cross-flow filtration process in conjunction with the photocatalysis process to produce the photocatalytic membrane reactor (PMR).

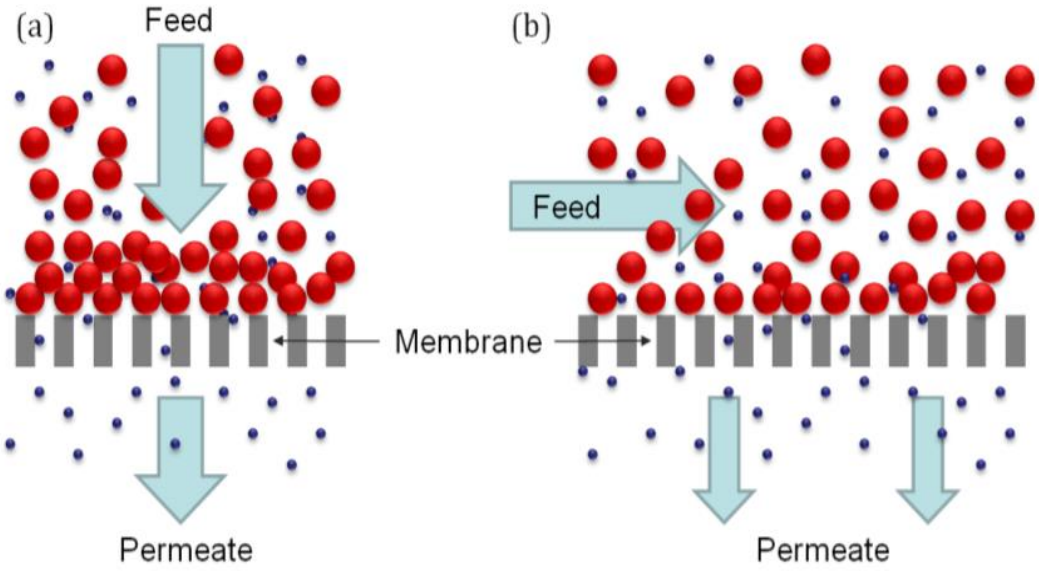

Fig. 2.5: Membrane operating modes: (a) dead-end mode and (b) cross-flow mode.

2.2.6 Membrane configurations

The active surface area of a membrane is important to be able to have the largest membrane surface area in the smallest possible volume. So, a number of membrane modules have been designed to achieve this. The term 'module' refers to the total unit, which is fully supported with suitable equipment. The design of the membrane module should be considered the throughput, flow dynamics, fouling and total cost of the membrane process. In terms of the industrial membrane filed scale operation, currently there are four common kinds of these membrane modules, which are used in cross-flow mode of operation where each has its own advantages and disadvantages **[42, 143]**:

1) Tubular modules

In this configuration, the membrane is fixed within a porous support tube, which is usually made of a stainless steel pipe or other proper materials. The feed is entered into the tubes and then permeate flow is to be perpendicular on the fiber walls. This flow is collected outside of tubes as shown in Fig. 2.6 **[42, 143, 145]**. The advantages of this unit:

- It is normally applied to high suspended solids loading.
- It can work at a turbulent flowrate (Re > 10,000).
- It is easy to clean by using a circulating chemical solutions.

The disadvantages of this unit are:

- It uses to small flowrate.
- Low membrane's surface area compared with total dimensions.
- Low permeate rate compared with total volumetric flowrate of feed.
- The cost of membranes is relatively high.
- The cost of operation is high.

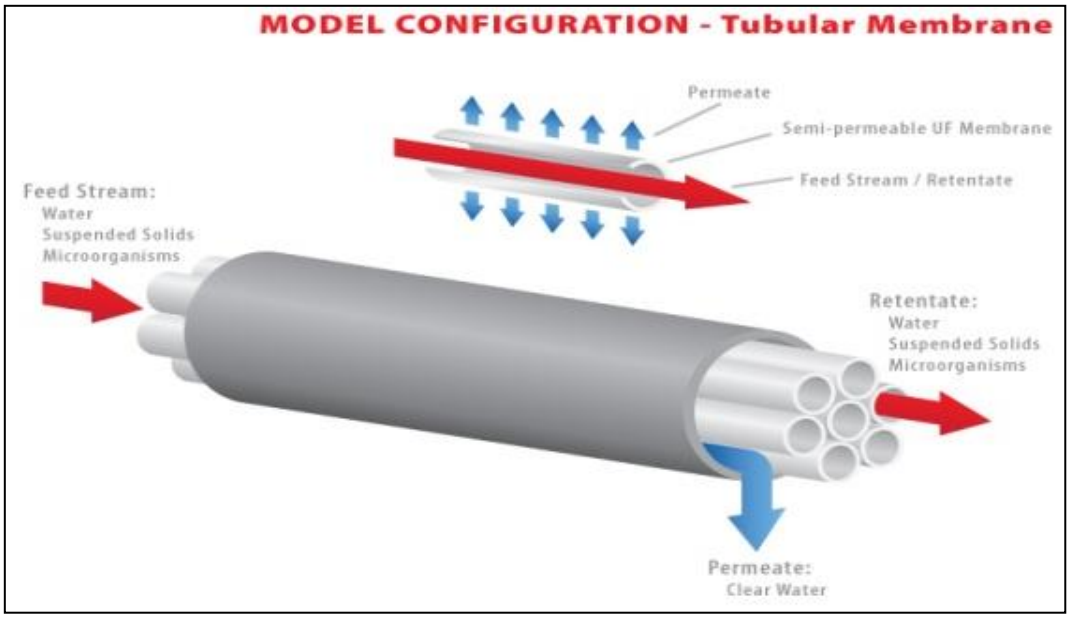

Fig. 2.6: Tubular module.

2) Hollow-fiber modules

In this configuration, the module includes a package of hollow or capillary fibers at diameter of (0.1-2 mm), which are arranged inside a tube **[134, 145]**. The action of this module as shown in Fig. 2.7 is similar to that of tubular model. The advantages of this unit are:

- It is normally applied to low suspended solids loading.
- It can be used at high flowrate.
- It is designed to easy clean generally.
- High level rates of mass transfer.
- Low energy cost.

The disadvantage of this unit is its propensity for clogging due to high suspended solids loading, and thus the membranes are difficult to clean. Therefore, a pretreatment process is normally used before treating the feed with a hollow-fiber module.

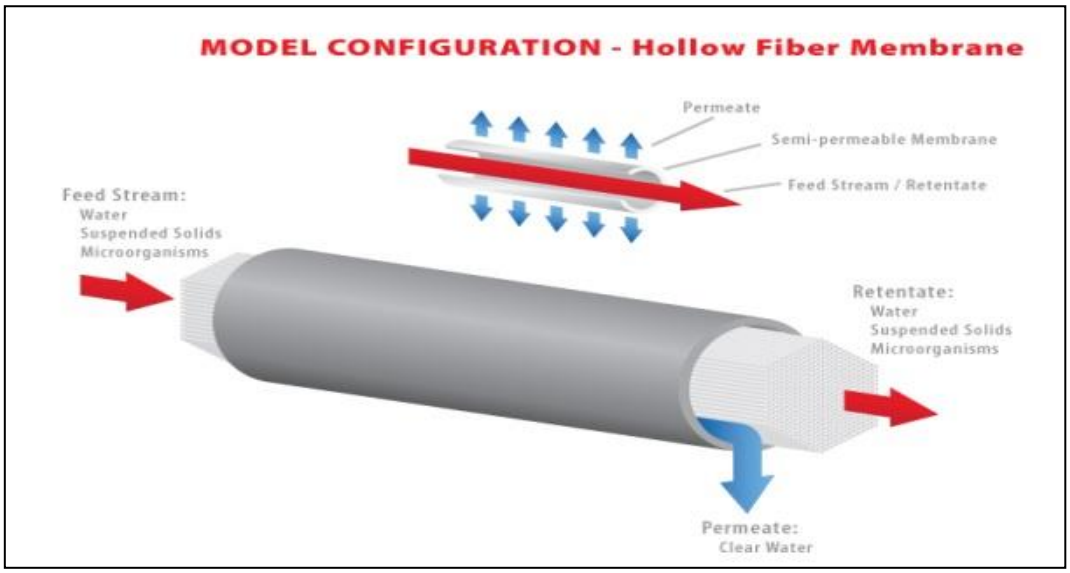

Fig. 2.7: Hollow-fiber module.

3) Spiral-wound modules

In this configuration, the module comprises of various flat sheet membranes, which are set in the form of spiral **[137, 143, 145]** and separated by mesh (Fig. 2.8). The advantages of this unit are:

- It is relatively inexpensive.
- Its performance generally is better than tubular and flat-sheet modules.
- Low energy cost.
- High level rates of mass transfer.
- High throughput can be processed.

The main disadvantage of this unit is the propensity for fouling and consequently, it is not easy to clean and thus limiting its use at high levels of suspended solids.

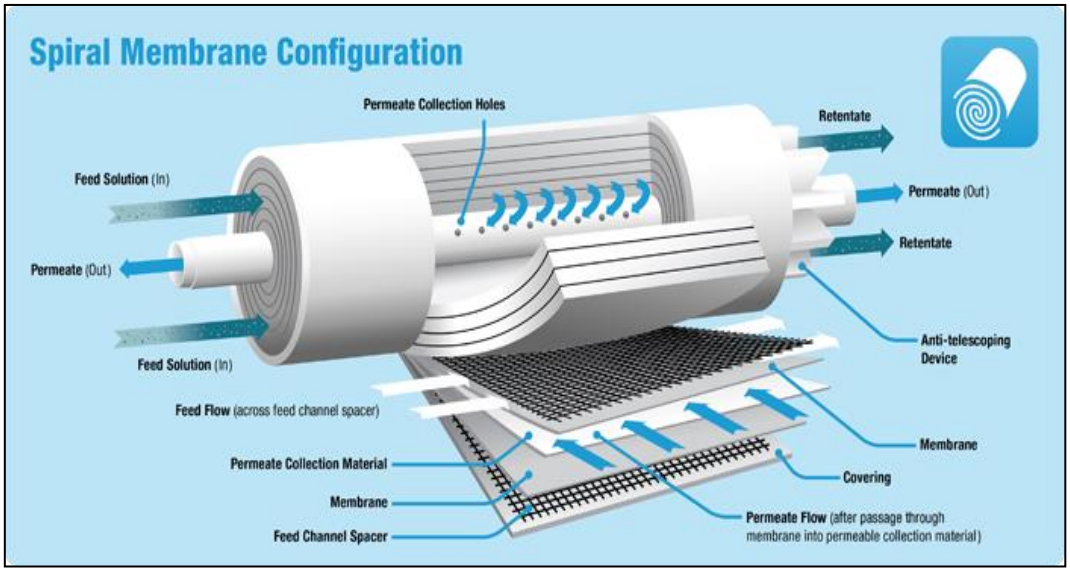

Fig. 2.8: Spiral-wound module.

4) Plate and frame modules

In this configuration, the module is the simplest form of membrane module and generally consists of several flat sheet membranes in a sandwich arrangement, which is separated by spacer to allow permeate to flow out (Fig. 2.9) **[143-145]**. It is similar approximetly to traditional filter presses. The advantages of this unit are:

- It can work at a laminar flowrate (Re < 2,100).
- The membranes can be easily replaced.

The disadvantages of this unit are high capital cost and fouling. This fouling is not easy to clean, thus limiting its use at high levels of suspended solids.

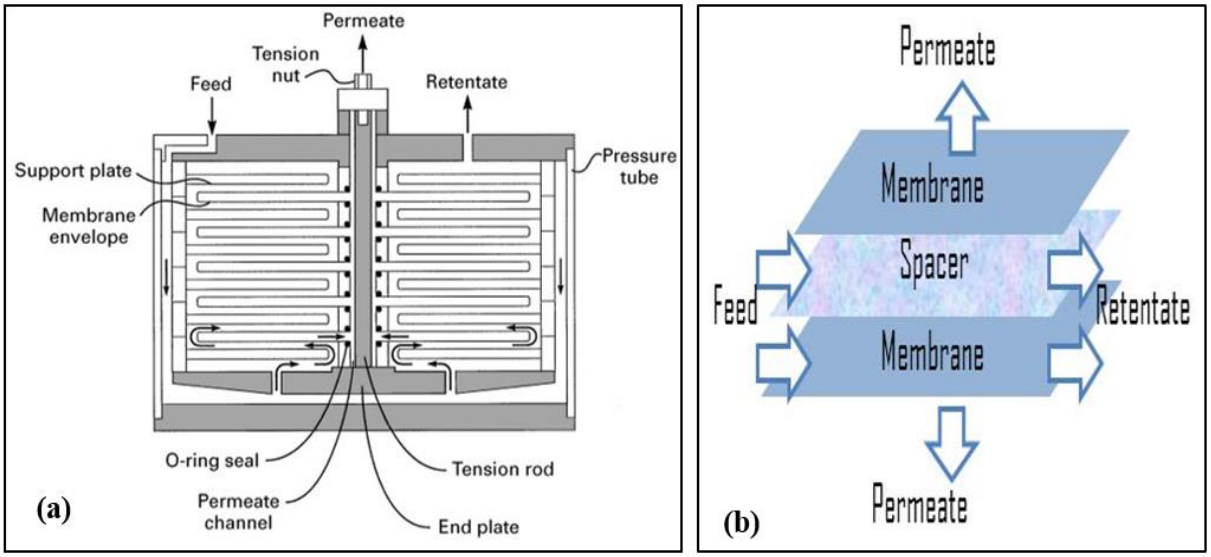

Fig. 2.9: (a) General schematic of a plate and frame module and (b) cross-sectional view of flat sheet membrane.

The work presented in the current PhD project deals solely with flat-sheet membranes, which have been applied in laboratory scale plate and frame type modules in terms of dead-end and cross-flow modes of operation with low laboratory scale surface areas (14.6 cm^2). More detail information about these modules is shown in chapter 3.

2.2.7 Mechanism of membrane separation

There are three principal mechanisms of mass transport in the permeation processes, which are applied depending on the type of membrane and feed molecules: the pore-flow model, solution-diffusion model and Donnan exclusion model.

1. The pore-flow model

This model assumes that the material of membrane has defined pores and does not change in their sites or size with time due to the movement of permeating species. Permeants (solutes and solvent) are transported through the pores of the membrane by the pressure driven convective flow. A separation process in this model takes place by solutes being excluded from pores of the membrane, which other permeants can move through it, i.e. size exclusion. Darcy's law is used to describe this model as follows **[108, 146, 147]**:

$$J_i = -kc_i \frac{dp}{dx} \tag{2.21}$$

Where J_i is the flux of species i, c_i is the concentration of species i in the medium, and (dp/dx) is the pressure gradient existing in the porous medium and k is the coefficient reflecting the nature of medium.

This model is used to describe the separation of macromolecular or colloidal solids using MF or UF membranes **[111, 146, 147]**. On the other hand, the pore concept in NF is considered to be only hypothetical due to a change in pore size and/or free volume and/or other properties that produce exclusion during the filtration. A molecular sieving (known as surface diffusion of adsorbed species on the surface of pores to diffuse through the membrane) model has been proposed to describe the separation process in NF membranes **[108, 111]**.

2. The solution-diffusion model

This model assumes that the material of membrane is a dense polymer layer and does not include any defined pores. It has very tiny free volume elements, which is the space between the polymers chains of membrane material. The permeating species can dissolve in the material of membrane. After that, they diffuse in these free volume elements. A separation process in this condition occurs on the basis of difference in the concentrations between the solubility of permeating species in the membrane and the rate of diffused permeating species through the membrane. This model can be mathematically described (in the most basic sense) by Fick's first law as follows **[111, 146]**:

$$J_i = -D_i \frac{dc_i}{dx} \tag{2.22}$$

Where J_i is the flux of species *i*, D_i is the diffusion coefficient and (dc_i/dx) is the concentration gradient of species *i* across the membrane.

This model is used to describe the separation of permeating species at molecular weights (< 200 $gmol^{-1}$) via using the membranes of NF and RO **[111, 146, 148]**.

3. Donnan exclusion model

This model is used to describe the ability of charged or conductive ions of electrolytes to pass through the membrane thermodynamically. In membrane equilibrium, the charged membrane has an ability to select counter ions and then exclude certain characterized charged ions, which is called 'co-ions'. It can be successfully used to describe NF process **[111, 149, 150]**.

All the above models can play a major role in the NF mechanism via the transport properties of solutes through the membrane. In the current PhD project, the flux and rejection of PEG based on individual oligomers and total organic carbon (TOC) as well as two photocatalysts (POM and TiO_2) will be used to characterize the transport through the used membrane.

2.2.8 Membrane performance characteristics

2.2.8.1 Flux

Flux refers to the rate of permeate flow through the membrane. It can be presented by volume per unit time per unit area of the membrane at a given operating pressure. Also, it is expressed as a velocity of permeate. Generally, flux is used as the basis for calculating the membrane performance and allows a quantitative comparison with various membrane configurations. It can be mathematically presented by using a modified form of Darcy's law as follows **[42, 112, 151]**:

$$J = \frac{Q}{A} = \frac{1}{A}\frac{dV}{dt} = \frac{\Delta p}{\mu R_m} \quad (2.23)$$

Where J is the volumetric water flux of permeate stream through membrane ($Lm^{-2}h^{-1}$) or (LMH), Q is the volumetric flowrate of permeate stream, (Lh^{-1}), A is the membrane surface area (m^2), dv/dt is the change of volume per time (Lh^{-1}), ΔP is the transmembrane pressure (kPa), μ is the dynamic viscosity of feed solution (Pa.s) and R_m is the membrane resistance coefficient, (m^2L^{-1}).

This flux remains constant when using a pure water through the membrane and is used as an indication of membrane resistance and benchmark for all other filtrations with that membrane. While, this flux changes when using a real solution (not pure water) significantly over the filtration time (more detailed information about this change in flux is shown below).

2.2.8.2 Membrane rejection

The general model used to describe a membrane performance is rejection or retention factor (*R*), which gives a good indication for membrane selectivity and permeate quality of membrane process. This model can be defined by efficiency equation as follows **[111, 151]**:

$$R_i = \left(\frac{C_{i,f} - C_{i,p}}{C_{i,f}}\right) * 100\% \quad (2.24)$$

Where (R_i) is the membrane rejection or retention factor of any solute component *i*, ($C_{i,p}$) is the concentration of any solute component *i* in the permeate and ($C_{i,f}$) is the concentration of any solute component *i* in the feed.

The concentration can be measured in mgL^{-1} or other appropriate unit. While (R_i) is dimensionless group. The general limits of membrane rejection (R_i) in Eq. 2.24 can be found in the range between 0 and 100% as follows:

⇨ At $C_{i,p} = 0$, R = 100%. This means that all the solute components in the feed are totally removed.
⇨ At $C_{i,p} = C_{i,f}$, R = 0%. This means that there is no separation process.

2.2.8.3 Fouling

During separation process (Fig. 2.10), the solute or suspended solid components in the feed stream are transported towards the membrane surface due to the convective (drag) force. After that, the concentration of these components increases with increasing the permeation through the membrane. Thus, forming a concentration gradient in the feed side. This concentration gradient leads to diffuse the concentrated components close to the surface of membrane back into the feed stream or retentate due to diffusive force based on Fick's first law. Under the competitive conditions between the convective transport towards the membrane and diffusive transport away from the membrane, a final steady state concentration distribution near the membrane surface occurs. Under these conditions, the surface of membrane is to be polarized via the accumulation of these rejected solid components in the boundary layer adjust to the surface of membrane where this phenomenon is referred to as 'concentration polarization'. Due to this concentration polarization, a rapid solid components build-up near the membrane surface, thus an initial flux declines. This developed concentration polarization layer over the membrane surface plays a significant and dominant role in controlling the permeate flux mechanism **[137, 152-154]**.

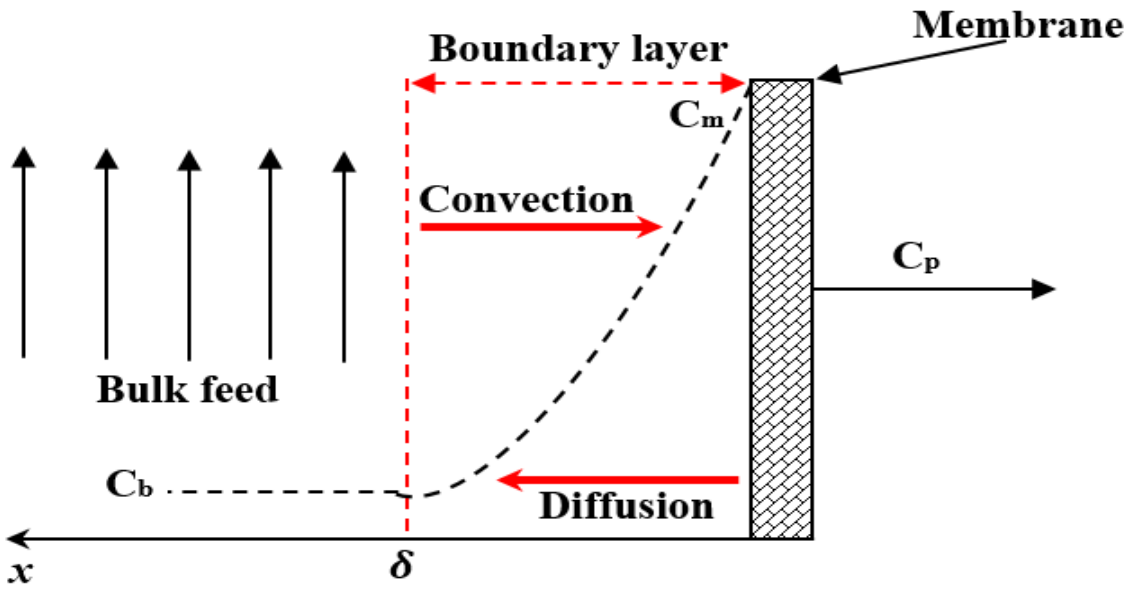

Fig. 2.10: Representation of concentration polarization, showing the convective and diffusive solute mass transfer over the concentration polarization boundary layer thickness (δ). *X* is the distance from the surface of membrane, C_b is the bulk concentration, C_m is the concentration at the membrane surface and C_p is the concentration of solute in the permeate. Adapted from **[137]**.

In general, the consequences of this concentration polarization is to initiate a membrane fouling. The term 'fouling' refers to the accumulated layer of various types of solid components in the feed stream on the surface of membrane. Also, it refers to the gradual reduction in permeate flux through the membrane at constant pressure or it refers to an increase in transmembrane pressure to remain a flux to be constant **[42, 112]**.

Membrane fouling plays a restricted factor to apply the membrane processes in some applications. It leads to decrease the rate of permeate stream flow and reduce the active pores' diameter of membrane. It depends strongly on the characteristics of the feed applied and the type of membrane utilized. The appropriate selection of membrane process based on the type of solids in the feed play a vital role to extent the membrane fouling. Under some conditions, it is more applicable for the feed to be pretreated before being applied to RO membrane process. Membrane fouling is a significant parameter to be considered when designing and operating membrane systems in terms of cleaning needs, cost, maintenance and efficiency **[143]**.

Generally, membrane fouling is a complex process and has not been precisely defined. However, in terms of membrane fouling mechanism, a number of different forms of membrane fouling are shown below:

i. Complete pore blocking

Complete pore blocking occurs when a particle, present in the original feed having a pore size greater than that of the membrane as shown in Fig. 2. 11-a, blocks a pore of the membrane and thus

prevents anything passing through it. So, the active area of membrane based on pores are completely blocked **[155-157]**.

ii. Standard (internal) pore blocking

Standard (internal) pore blocking occurs when a particle, which has a pore size less than that of the membrane as shown in Fig. 2.11-b, is deposited onto the internal pore of membrane walls, leading to reduce the pore size of membrane. So, the active area of membrane based on pores are partially blocked **[155-158]**.

iii. Intermediate pore blocking

Intermediate pore blocking occurs when a particle is deposited on an existing particle at the surface of membrane or block completely some membrane pores as shown in Fig. 2.11-c **[156, 157, 159]**.

iv. Cake formation

Cake formation occurs when particles deposit onto the existing particles (Fig. 2.11-d), which are already present over the surface of membrane, leading to build a cake layer that grows in thickness gradually with the progress of filtration time **[158, 159]**.

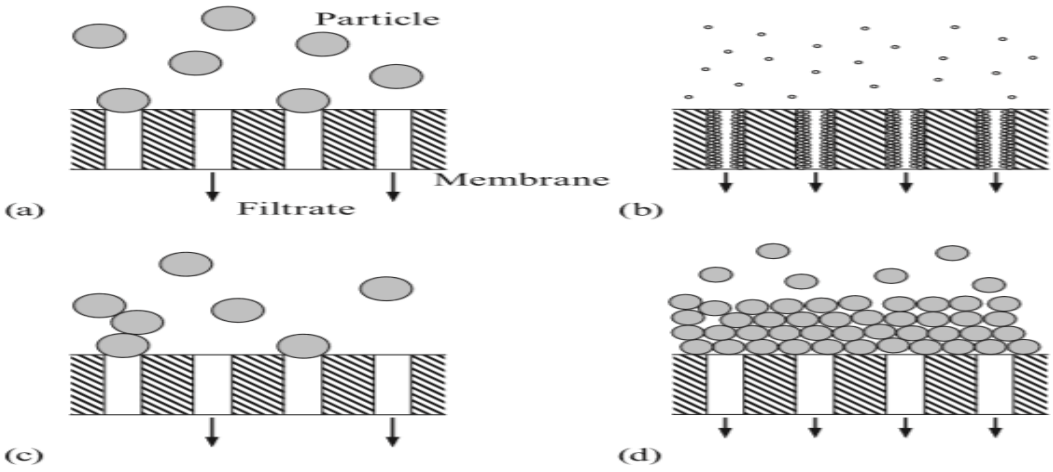

Fig. 2.11: Fouling mechanism of pores membranes, (a) complete pore blocking, (b) standard pore blocking, (c) intermediate pore blocking and (d) cake formation. Taken from **[158]**.

The concentration polarization in terms of membrane fouling is inevitable phenomenon and a major problem in the design of membrane separation processes. *However, in the current PhD project, photocatalytic membrane reactor (PMR) is potentially an answer to this problem* since this fouling in terms of organic solutes can be continuously controlled under the photocatalytic degradation reactions to be minimized as reported in literature **[160, 161]**.

2.2.9 Factors affecting membrane performance

There are many factors affecting the performance of membrane and only those relevant to the current PhD project are described herein:

2.2.9.1 Transmembrane pressure

An increase in pressure applied across the membrane, i.e. transmembrane pressure TMP (if a pressure driven filtration is being used) with a given feed under a certain set of hydrodynamic conditions is directly proportional to the flux of permeate until to reach a level that there is no effect of increased pressure on the rate of permeate where in this case, the flux is referred as a limiting flux **[151]**.

For the cross-flow filtration, the TMP can be described as the difference of pressures between the average pressure driving force and permeate pressure for mass transfer in the feed stream over the membrane and represented by the following equations **[42, 111, 151]**:

$$P_m = P_a - P_p \tag{2.25}$$

$$P_a = \frac{P_f + P_r}{2} \tag{2.26}$$

Where P_m is the transmembrane pressure gradient, P_a is the average pressure driving force, P_f is the feed pressure stream, P_r is the retentate pressure stream, P_p is the permeate pressure stream. These pressures are measured with relevant pressure units.

The overall pressure drop (P) over the membrane module for this mode of operation can be calculated as follows **[42]**:

$$P = P_f - P_p \tag{2.27}$$

While, for the dead-end filtration, the TMP can be described as the difference of pressures between two streams of the feed and permeate, and can be expressed by Eq. 2.28 **[42, 115]**:

$$P_m = P_f - P_p \tag{2.28}$$

2.2.9.2 Cross-flow velocity

In cross-flow filtration mode, the cross-flow velocity (CFV) can be changed with the type of flowrate conditions in terms of laminar or turbulent. Industrially, turbulent flowrate conditions are commonly used. Under these conditions, the CFV increases the shear rate at the surface of membrane, and thus reducing the fouling in terms of the concentration polarization layer thickness through increasing swapping away the rejected solid components on the membrane surface. This leads to increase significantly the permeate flux through the membrane. Increasing the CFV based on

increased flowrate increases the required consumption of energy, so this point should be considered when investigating the process efficiency **[144, 151, 162]**.

2.3 Reactors

2.3.1 Conventional reactors

Generally conventional chemical reactors-in chemical engineering-can be basically a piece of equipment that are well designed in terms of economy, efficacy and construction to deal with chemical feed to obtain the desired yield product without adding any photocatalyst materials. These conventional reactors can be classified in terms of the content flow into: batch reactors and continuous flow reactors such as continuous stirred tank reactors (CSTR), plug flow reactors (PFR), fluidized bed reactors (FBR) and packed bed reactors (PBR) **[163, 164]**.

2.3.2 Photocatalytic reactors

Photocatalytic reactors are designed to carry out the photocatalysis advanced oxidation process via utilizing photocatalysts in combination with solar or artificial light. There are many photocatalytic reactors in the literature, including: stirred tank reactors (STR), fluidized bed reactors (FBR), packed bed reactors (PBR), spinning disc reactors (SDR) and plug flow reactors (PFR).

This PhD study focuses on a plug flow reactor using an annular photoreactor, which is the simplest form of continuous flow reactor. It consists of two concentric tubes and the reactant solution flows between them. The UV light source is placed inside the inner tube as shown in Fig. 2.12. It has several advantages when comparing with other photoreactors **[164, 165]**:

- High throughput.
- It is easy to scale up by connecting several reactors to get either a better conversion in series or a higher volume conversion in parallel.
- It is simple in design with no moving mechanical parts.
- It can be constructed with various photocatalytic configurations such as slurry, coated walls and coated mesh.
- The reactant molecules can absorb all emitted photons due to the well-designed configuration in terms of uniform radiation.
- Limited back mixing.

The disadvantages of this type are:

- Relatively expensive.

- Controlling the temperature inside it, especially as the type of reaction is exothermic.
- High operating cost such as maintenance and cleaning.

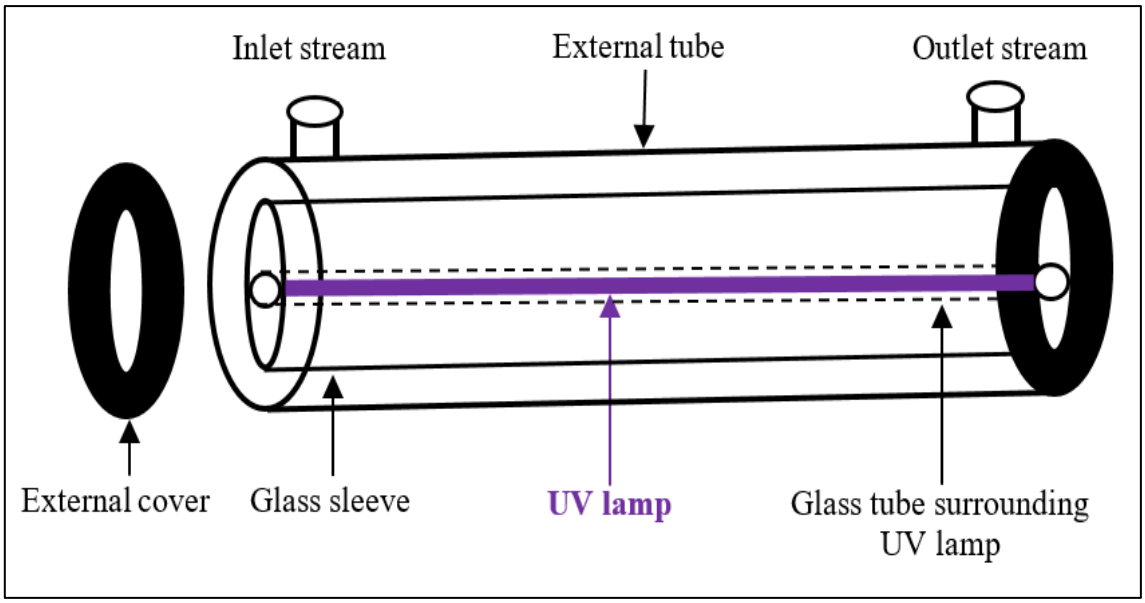

Fig. 2.12: Schematic of annular photoreactor. Adapted from **[165]**.

2.3.2.1 Photocatalytic reactor configurations

There are two main types of heterogeneous photocatalytic reactor configurations depending exactly on the state of photocatalyst used such as slurry (suspended) or immobilised (attached-supported) **[166]**.

(i) Slurry photocatalytic reactors

In this reactor, the photocatalyst is used in the form of powder like TiO_2, mixed with the feed stream and then fed together into the reactor. The principal advantage of this type of reactor is highly photocatalytic performance when compared with immobilised reactor due to provide a large surface area of photocatalyst particles per unit volume, which in turn plays a significant role in photocatalysis process. On the other hand, the main disadvantage of this reactor is the separation of photocatalyst used. Numerous post treatment methods are available to separate the photocatalyst particles from the treated water such as using sedimentation or filtration systems. As a result, the total cost of photocatalysis process is to be relatively high **[67]**.

In the current PhD project, this type of configuration will be used and evaluated with the TiO_2 heterogeneous photocatalyst. It is important to mention that POM homogeneous photocatalysts are generally used in this configuration as like in the current project, however since the POM photocatalyst fully dissolves in the liquid feed, it is not a 'slurry' reactor, but rather an 'in-flow' photocatalytic reactor.

(ii) Immobilised photocatalytic reactors

In this reactor, the photocatalyst is set in various coating configurations to support the reactor, such as transparent wall coating **[165]**, coated plate **[167]**, coated beads **[168]** and coated meshes **[169]**. The advantage of this type of configuration is that photocatalyst separation is not required. Normally the performance of immobilised photocatalytic reactor is lower than that of slurry photocatalytic reactor due to a reduction of the available photocatalytically active surface area that can be loaded **[170]**. For example, *Galvez and Rodriguez* **[171]** showed that the efficiency of the immobilised photocatalytic reactor using TiO_2 in aqueous solution is less by 60-70% when comparing with the slurry photocatalytic reactor.

2.3.2.2 Factors affecting the photocatalytic reactors

There are several operational parameters that influence the performance of photocatalytic reactors. Some of the main parameters relevant to the current PhD work are summarized below:

1) Type of photocatalyst

As previously discussed, the type of photocatalyst significantly affects the reaction and operation of the reactor–especially when considering heterogeneous vs homogeneous photocatalysts.

For heterogeneous photocatalysts, different types of these photocatalysts have been studied and compared, which have various structure characteristics in terms of surface morphology (such as the size of photocatalyst particle) and the number of sites onto the surface of photocatalyst particles in addition to the band gap energy. For example, titanium oxide (TiO_2) is the most extensively heterogeneous photocatalyst used in the literature where there are different forms of TiO_2 such as UV100, PC500, TTP and P25. Several studies **[64, 67]** stated that the performances of these photocatalysts are not equal in which P25, a standard photocatalyst, exhibits more active than others.

Similarly for homogeneous photocatalysts, there are different types of POMs photocatalysts based on molecular structural diversity, which their photocatalytic activates are not equal **[34, 90]**. The most common structural type of POMs used in the literature is the Keggin cluster. One typical example of a Keggin cluster is $H_3PW_{12}O_{40}$, which is widely investigated in the photocatalytic degradation of various refractory pollutants **[92, 93]**.

In the current PhD study, the typical POM ($H_3PW_{12}O_{40}$) and TiO_2 (P25) as homogeneous and heterogeneous photocatalysts respectively will be used for the treatment of PEG.

2) Photocatalyst loading

One of the most important parameter affecting the photocatalysis performance is the loading of photocatalyst. The overall performance of photocatalysis increases proportionally with the increase in the loading of photocatalyst and then starts decreasing at the optimal photocatalyst loading due to the effect of light scattering and then photons capture. This phenomenon occurs for both TiO_2-heterogeneous **[64-66]** and POM-homogeneous **[24-26]** photocatalysts. It is important to consider this optimal photocatalyst loading when designing the photocatalytic reactors to get a maximum photocatalytic performance **[64, 166]**. In addition, it plays a significant role in the calculation of photocatalytic reactor dimensions in process scaling up **[67, 79, 170]**.

It is generally agreed in the literature that identifying an optimal loading of heterogeneous and homogenous photocatalysts in the field of wastewater treatment is a problem that should be solved experimentally. So, a range of various photocatalyst loadings is selected to identify this optimal loading depending on the proposed evaluating parameters like TOC removal, %PD and K_{app}. This optimal loading is significantly dependent on the experimental conditions in terms of the type and concentration of pollutant, pH of the reactant solution, UV exposure time, light intensity and light wavelength **[25, 27, 86, 172]**.

As reported earlier, there is no literature available into the application of POM ($H_3PW_{12}O_{40}$) and TiO_2 (P25) for the treatment of PEG, so in the current PhD study, the optimal loadings of these photocatyst will be experimentally investigated under different examined conditions shown in chapters (4-7).

3) pH of the solution

pH is a significant operating factor in the heterogeneous photocatalysis since it has a strong influence on the adsorption rate of pollutants onto the surface of photocatalyst particles, aggregation (particle attraction) and band energy. Thus, affecting the photocatalytic activity **[64, 67, 166]**. This influence can be described qualitatively based on the photocatalyst surface charge in terms of the point of zero charge (pzc). The pzc refers to the pH value at which the total net of electrical charge conditions on the photocatalyst surface is neutral (zero charge). For example, the pHpzc of TiO_2 particles is in the range 5.6-6.9 depending on the type of TiO_2 used **[18, 71, 173]**. At pH < pHzpc, the surface of photocatalyst is positively charged and then can attract the negatively charged (anionic) compounds, and vice versa as shown in Fig. 2.13 **[64, 82]**.

Also, pH has the same effect on the immobilized photocatalysis systems where some pollutants may favour a positively or negatively charged surface with thin film applications **[174]**.

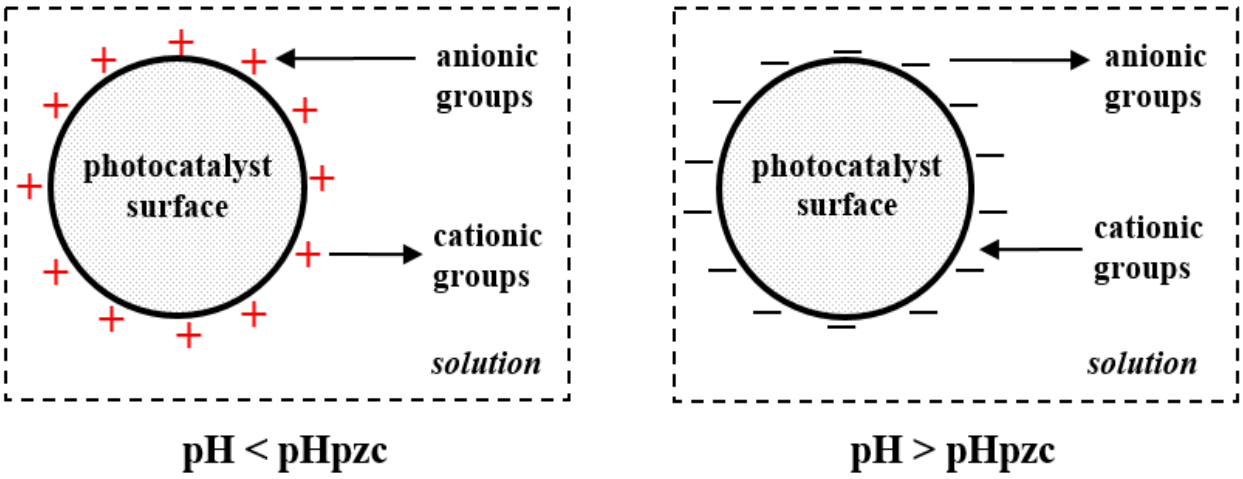

Fig. 2.13: Effect of pH solution on the pzc of TiO_2 particles. Adapted from **[64]**.

It is important to mention that the effect of acidic pH conditions plays a significant role in enhancing the heterogeneous photocatalytic reactions where for example under HCl conditions, the oxidation of chloride ions (Cl^-) in the solution through the reaction with either free hydroxyl radicals ($HO^{\cdot}$), Eq. 2.29-2.30 or positive holes (h^+_{VB}), Eq. 2.31 generates chlorine radical ($Cl^{\cdot}$) that in turn reacts with (Cl^-), Eq. 2.32 to form dichloride radical anions ($Cl^{\cdot}_2{}^-$) as reactive species. As a result, these reactive species can further oxidize the organic pollutants **[67, 175, 176]**.

$$HO^{\cdot} + Cl^- \rightarrow HOCl^{\cdot -} \quad (2.29)$$

$$HOCl^{\cdot -} + H^+ \rightarrow Cl^{\cdot} + H_2O \quad (2.30)$$

$$h^+_{VB} + Cl^- \rightarrow Cl^{\cdot} \quad (2.31)$$

$$Cl^{\cdot} + Cl^- \rightarrow Cl^{\cdot}_2{}^- \quad (2.32)$$

In general, the redox reactions of heterogeneous photocatalysis are sensitive to pH of the solution and the conditions of surface photocatalyst (i.e. pHpzc) where during these reactions, the generation of intermediate reaction compounds can directly result in changing the pH value of solution and then in turn influence the rate of oxidation **[64, 173]**.

While for POMs homogeneous photocatalysis, pH has significant influences on POMs homogeneous reactions and POMs chemical stability during these reactions **[95, 177]**. The nature of POMs in aqueous and real solutions is acidic (pH < 7) depending on their applied loadings **[38, 93]**. In literature, it is generally agreed that POMs under aqueous solutions are chemically stable at pH 1. When varying pH, they decomposed partially into several lacunary species **[95]**.

In the current PhD study, the pH parameter is to be considered for POM homogeneous and TiO_2 heterogeneous photocatalysis of PEG.

4) Conventional oxidant

In the conventional reaction mechanism of both heterogeneous and homogeneous photocatalysis as shown in section 2.1.2.2, the presence of molecular dissolved oxygen (DO) as a conventional oxidant plays a pivotal role in these reactions. For TiO_2 heterogeneous reactions, DO traps the excited e^-_{CB} and prevents it from recombining with h^+_{VB} **[16, 18]**. While for POM homogeneous reactions, DO regenerate (reoxidize) POM^- to form POM cluster. The final products of trapping (Eq. 2.5) and regenerating (Eq. 2.20) steps are the formation of superoxide radical ions ($O_2^{\cdot -}$), which are able to further participate in oxidization of the organic pollutants.

Another role of DO in a slurry photocatalytic reactor is to support sufficient forces to suspend the particles of photocatalyst in the solution **[178]**. Operating an open photocatalytic reactor with pure oxygen seems to be not economic in commercial scale since there is no significant difference between pure oxygen and air in terms of mass transfer of oxygen in the process **[178]**. Accordingly, it is sensible to operate the photocatalytic reactor under ambient conditions (using air as a free sustainable source) **[166]**.

Also, hydrogen peroxide (H_2O_2) uses as a conventional oxidant in photocatalysis processes, increasing the generation of $HO^{\bullet}$ and then the oxidation rate **[179, 180]**. It can be used in the case of nonexistence of oxygen to replacing its action **[64]**. Generally, it uses for enhancing the total photocatalytic mineralization of pollutants.

In the current PhD study, the DO as suppling bubbles based on lab scale is to be used as conventional oxidant only for POM homogeneous and TiO_2 heterogeneous photocatalysis of PEG.

5) Temperature

Generally, temperature is an important operating variable for chemical reactions **[163]**. In terms of the photoreactions, the activation energy of these photoreactions is approximately constant. In other words, it does not change significantly with changing the temperature. It can be considered as a variable that has an insignificant effect on photoreactions **[64]**. However, *Gaya and Abdullah* **[181]** showed that an increase in temperature more than 80 ^oC leads to the recombination of charge carriers of e^-_{CB} and h^+_{VB} in the photocatalysis process and effects on the rate of adsorption. As a result, desorption processes are to be the rate limiting step at this temperature. Another study was carried out by *Palmer et al.,* **[182]** showed that the impact of temperature between 10-68 ^oC on the photocatalysis process was not precisely clear. They stated that above 68 ^oC, there is a direct effect of temperature on the solubility of dissolved oxygen in the solution phase and hence increasing the recombination of these charge carriers. For this reason, decreasing the photocatalytic activity. The best temperature reported for photocatalysis process is in the range of 20-80 ^oC **[67, 183]**.

For practical applications, during the photocatalysis process in the photocatalytic reactor, the temperature raises due to the generation of heat by UV-lamp. So, it is important to consider keeping a constant reaction temperature during the reaction time.

In the current PhD study, the temperature of photocatalytic reaction under POM homogeneous and TiO_2 heterogeneous photocatalysis is to be constant at room temperature and monitored during these processes.

6) Light wavelength and intensity

Photocatalysis needs ultra violet (UV)-irradiation source with sufficient quantity of photons and energy level (≥ the band gap energy of the photocatalyst) to start the photoreactions **[102]**. This UV-irradiation source may be either naturally like sunlight or artificially like low and medium pressure mercury lamps, black and white light lamps, fluorescent lamps and light-emitting diodes (LEDs) lamps **[184]**. This UV-irradiation source varies significantly the wavelength and intensity.

i. light wavelength

The spectrum of UV irradiation can be classified into three types: near ultraviolet (UVA with wavelength 315-400 nm and photon energy 3.10-3.94 V), far ultraviolet (UVB with wavelength 280 to 315 nm and photon energy 3.94-4.43 V) and extreme ultraviolet (UVC with wavelength 100-280 nm and photon energy 4.43-12.4 V) **[185, 186]**. Generally, the lower the wavelength of the light source, the more energy is available per photon and thus a higher effectiveness **[80]**. Based on this, sunlight with wavelength > 300 nm has a lower energy around 4-5% of the sunlight, thus limiting the application of solar light in photocatalysis processes although it is cheap, available and more economic. However, a lot of improvements and modifications on photocatalysts are required in order for them to work effectively with solar irradiation **[67, 187]**. On the other hand, artificial light with UVA, UVB and UVC is extensively utilized for the oxidation of organic contaminants **[45]**. Many studies used a UV wavelength of 254 nm generated by a low pressure mercury lamp for TiO_2 photocatalysis where at this wavelength, 85-90% of the UV light can be used when comping with other wavelengths such as 350 nm **[188]** and 365 nm **[189]**. Similarly for POM homogeneous photocatalysis, this wavelength has been used by several authors for photocatalytic degradation such as formic acid as a model compound **[106]**, 1,2-dichlorobenzene **[99, 190]** and methylene orange **[23]**.

ii. Light intensity

The impact of UV light intensity on photocatalytic degradation kinetics in terms of reaction rate can be described by two cases **[166]**. The first case is that the reaction rate is dependent on UV light

intensity where this dependency may be either linear relationship (first order form) at low light intensity (< 20 $mWcm^{-2}$) because the formation of charge carriers of e^{-}_{CB} and h^{+}_{VB} is dominant when compared with the recombination of them or nonlinear relationship (square root-half order form) at intermediate light intensity (20-25 $mWcm^{-2}$) because the formation of these charge carriers is not dominant when compared with recombination of them **[191, 192]**. While the second case is that the reaction rate is independent on UV light intensity because of the recombination of these charge carriers, and thus decreasing the overall performance of photocatalytic process **[84]**.

In the current PhD study, the wavelength of UV light and light intensity to be used in the photoreactor are 254 nm and 20 W respectively.

2.4 Photocatalytic membrane reactors

2.4.1 Basic description

'Photocatalytic membrane reactors' (PMRs) or 'membrane photoreactors' can be defined as a hybrid reactor in which the photocatalysis process is in conjunction with a membrane process. The membrane plays a significant role as a simple barrier in retaining the photocatalyst and recycles it in a continuous process, and as selective barrier for the molecules of various stages of degradation; controls the residence time of reactant molecules inside the reactor and also improves a quality of effluent **[81, 193, 194]**.

PMRs have a synergistic effect when comparing with conventional photocatalytic reactors and membrane separation process (one-step separation) **[194, 195]**. In addition, they offer several advantages such as less energy consumption, reducing the size of installation, and separating the used photocatalyst and recycling it in the photoreactor for further runs. Consequently, these PMRs are a promising approach in terms of green and sustainable chemistry **[81, 196, 197]**. However, PMRs are not widely applied due to the use of the suspended heterogeneous photocatalytic reactors that lead to membrane fouling and reduced photoreactor throughput as a result **[81, 198]**. This can be overcome by using immobilized photocatalysts instead of suspended. However, this then decreases the reaction rate and reactor productivity, since immobilized photocatalysts have a lower surface area and photocatalyst loading possible for the same reactor volume **[195, 198, 199]**.

Homogeneous photocatalysts using POMs are potentially an answer to both these problems. However, up to date, this has not yet investigated.

2.4.2 PMR design

In practical applications, there are various configurations of PMR designs that depend on the used characteristics of photocatalysis process and membrane separation process. For photocatalysis process, these characteristics are the state of photocatalyst (suspended or immobilized), type of reactor and type of light source. While for membrane separation process, these characteristics are the process mode (dead-end or cross-flow), flow type (batch or continuous), membrane process (MF, UF and NF) and membrane module (flat-sheet, hollow-fiber, spiral-wound and tubular) **[40, 200]**.

Generally, the most common popular configurations of PMR design are **[81, 201]**:

(i) Reactors with photocatalyst suspended in the feed that are separated by the membrane. UV light can be placed in different positions including: irradiation of the feed tank (Fig. 2.17-A), irradiation of the membrane module (Fig. 2.17-B) and irradiation of the reservoir tank (Fig. 2.17-C).

(ii) Reactors with photocatalyst supported in or on the membrane (i.e. photocatalytically active membrane). UV light is placed above the membrane (Fig. 2.17-D).

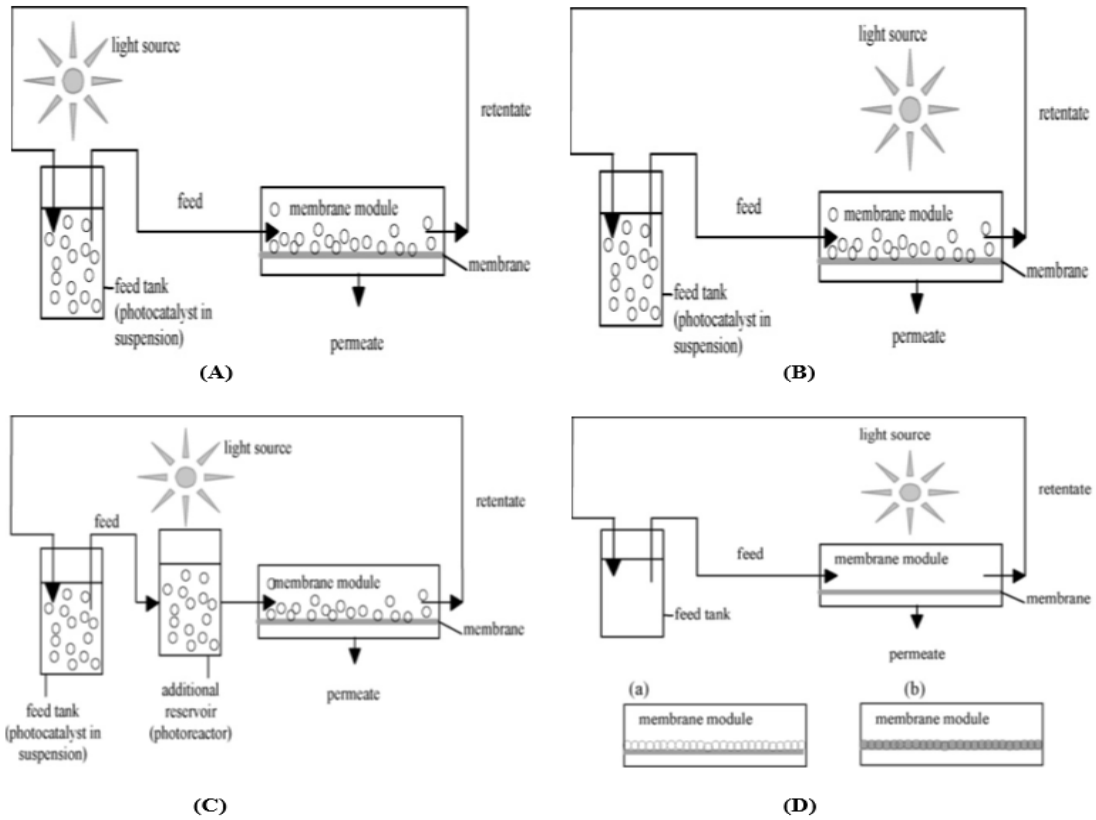

Fig. 2.14: PMR configurations: (A) suspended photocatalyst-irradiation of the feed tank, (B) suspended photocatalyst-irradiation of the membrane model, (C) suspended photocatalyst-irradiation of the reservoir tank and (D) immobilized photocatalyst: (a) on a membrane and (b) within a membrane structure. Taken from **[81]**.

2.4.3 Selection of PMR in the current study

In literature, the earliest example of separating and recycling the TiO_2 heterogeneous photocatalyst from wastewater, reported in a patent by *Cooper and Ratcliff* **[202]** who invented a novel PMR approach in terms of combining photocatalysis with cross-flow MF process. From that time, many configurations of PMRs have been modified. For example, *Sopajaree et al.*, **[203, 204]** modified the earlier PMR configuration by *Cooper and Ratcliff*. This modified PMR is shown in Fig. 2.15 where it consists of three parts. The first one represents photocatalysis process (annular photoreactor) connected with the second part (batch reservoir tank). The second part connected with the third part, which represents a membrane separation process (cross-flow UF unit using hollow-fiber membrane). This PMR used for the treatment of methylene blue using TiO_2 photocatalyst (P25) on the basis of recirculating batch mode of operation.

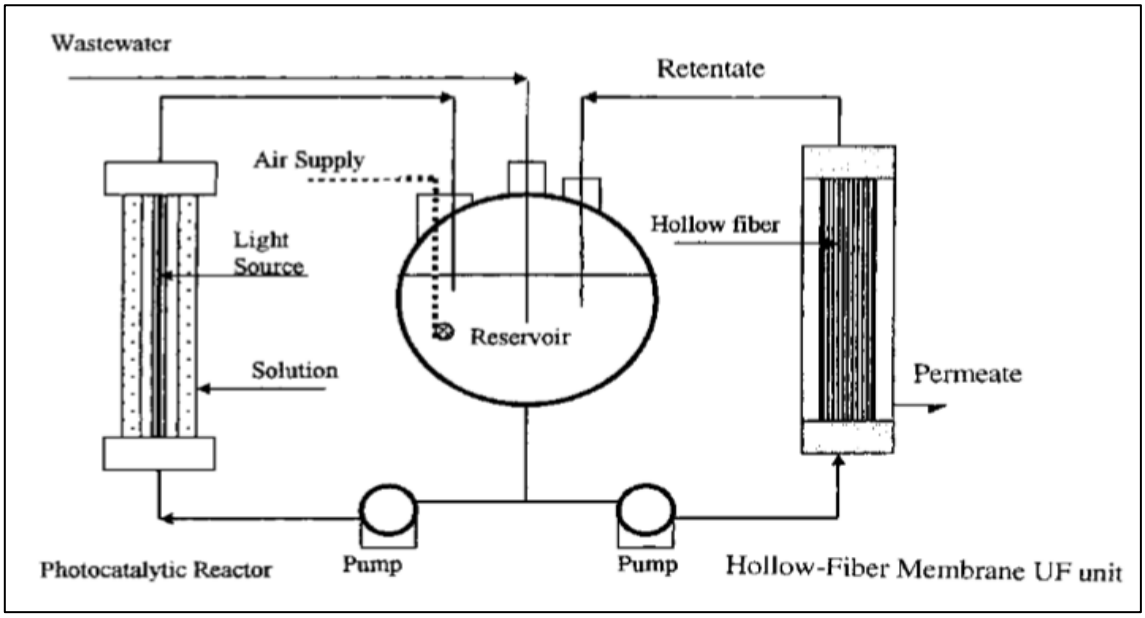

Fig. 2.15: Schematic diagram of PMR. Taken from **[203, 204]**.

In the current PhD study, the PMR approach by *Sopajaree et al.*, **[203, 204]** is selected to investigate the possibility of separation and recycling POM homogenous and TiO_2 heterogeneous photocatalysts with PEG reactant solution. Based on our experience in this field, this approach has several advantages such as:

- It is easy to setup.
- It can be used for controlling the photocatalysis and membrane separation processes either separated or combined.
- There is no direct effect of UV light on the material of used membrane as similar to conventional configurations **[205]** shown in Fig. 2.14 (B, D).

- It can be operated based on recirculating batch mode of operation.
- There is a possibility to convert a batch PMR mode of operation (i.e. batch photocatalysis) to continuous PMR mode of operation (i.e. continuous photocatalysis) since *this continuous mode of operation has not been explored yet* **[160]**.

Our proposed PMR approach consists of advanced oxidation process (homogeneous or heterogeneous photocatalysis process) using annular photoreactor in combination with a membrane separation process (cross-flow NF unit). This approach will be operated under batch PMR mode of operation (batch photocatalysis). In addition, this approach will be modified to work under continuous PMR mode of operation (continuous photocatalysis). More details about this proposed approach is shown in chapter 3.

The successful results of the current proposed PMR approach in terms of the separation and recycle of POM homogeneous photocatalyst from PEG reactant solution under batch and continuous modes of operation will enable this proposed approach to be the first valuable attempt in this field, and thus it should be considered as 'A Novel Homogenous PMR Approach' in the literature.

2.4.4 The concept '*membrane enhanced photocatalysis*'

The combination of membrane separation process with heterogeneous photocatalysis produces a PMR that is a perfect example of a process intensification technology **[111]**. This intensification technology has a synergistic effect when comparing with conventional photocatalytic reactors and membrane separation process (one-step separation) **[194]**.

In literature, the concept of PMR in terms of enhancing the photocatalytic degradation of used pollutant based on this synergistic effect have been discussed by several authors. They either claimed it **[206]** or supposed it **[111, 194]**. Generally, the proof of this concept is still unclear since their reported results do not support it effectively based on the comparable investigating conditions despite their success in separating the heterogeneous photocatalyst from reactant solution and recycling it through the photoreactor.

The main reasons behand this can be related to using different comparable conditions between photocatalysis process and photocatalysis with membrane (PMR) such as the operating time used with membrane is longer than that of oxidation time, changing the operating parameters such as CFV and TMP with PMR only (without considering these parameters with photocatalysis) and adding continuously fresh water to maintain a constant working volume in the reactant feeding tank (this leads to dilute the original concentration of reactant solution when compared with photocatalysis).

Therefore, their final results did not show the difference in terms of primary degradation (%) or reaction rate or reaction rate constant between photocatalysis as control process and PMR.

In the current PhD study, the proof of concept 'membrane enhanced photocatalysis' is to be built on the proposed protocol based on the same comparable conditions between control photocatalysis (no membrane) and photocatalysis with membrane-PMR-to identity exactly the performance of each of them separately. This performance is assessed with proposed evaluating parameters (primary degradation, reaction kinetics-based on reaction rate constant and mineralization-based on %TOC removal). The photocatalysis process is investigated under either POM homogenous photocatalyst or TiO_2 heterogeneous photocatalyst or combined photocatalysts.

2.4.5 Continuous PMR mode of operation

The majority of works in literature have focussed on the batch PMR mode over a short time of operation **[201]**. However, the practical applications of a continuous PMR mode over a long time of operation in industrial wastewater treatment are still limited with laboratory and bench-scale investigations **[193, 205, 206]**. These limited applications can be attributed to the membrane fouling over this long time due to using a suspended TiO_2 heterogeneous photocatalyst, which in turn deposits on the surface of membrane, and thus decreasing significantly the permeate flux through the membrane **[81, 207]** and also the overall photocatalytic degradation activity.

In the current PhD project, potentially the applying POM homogeneous photocatalyst will not foul the membrane based on PMR to the same extent as a suspended TiO_2 heterogeneous photocatalyst overcoming this problem and then speeding up the real applications of POM homogenous PMR in the field of industrial wastewater treatment.

2.5 Model compound

Polyethylene glycol (PEG) with a molecular formula [HO-$(CH_2CH_2O)_n$-H] is a non-ionic synthetic polymer composed of repeating units of ethylene oxide (CH_2CH_2O) that terminated with hydroxyl groups of water to from ethylene glycol ($C_2H_6O_2$) monomer. This monomer is chemically reacted with repeating units in terms of polymerization to produce PEG. Each unit represents an oligomer. PEG is synthesized in a wide range of molecular weights where the numerical value of PEG (*n*) refers to the average molecular weight (e.g., PEG1500). When a unique type of PEG consists of well-defined chain length and molecular weight is referred as 'monodispersed', while a mixture of chain length and molecular weight based on a Gaussian distribution is referred as 'polydispersed' **[4, 5, 208-211]**.

PEG has several characteristics such as hydrophilic, soluble in water with colourless and other solvents like benzene, methanol and dichloromethane; thermally stable; non-volatile; low toxic and inexpensive. It is widely used in various industrial applications such as lubricants, antifreeze, food, cosmetic (in the form of surfactants and as dispersing agents) and pharmaceutical sector (emulsifiers, thickeners, skin conditioners, humectants, solvents, ointments, suppository bases and laxatives) **[4-6]**.

With these widespread applications, PEG is a common pollutant in conventional wastewater effluent streams. This pollutant is resistant to conventional biological oxidation, the most environmentally friendly and cheapest method of wastewater treatment, and thus can flow through these streams to be discharged into the environment. It might have a toxic effect on animals and soil microbial population, which in turn diminishes soil fertility **[2, 7, 8, 212]**. As a consequence, environmental concerns regarding the fate of this pollutant has been risen **[6, 9-12]**. In order to protect the environment from PEG pollution, new wastewater treatment technologies and processes are required to treat it in industrial wastewater effluents to achieve the desired level of quality, to meet the discharge standards, and thus to protect the ground and surface waters in the environment.

In literature, it is generally accepted that advanced oxidation processes (AOPs) have become an attractive choice for degradation of refractory organic pollutants from industrial wastewater. In particular for PEG pollutant, among these AOPs such as *wet air oxidation* **[6, 10, 13]**, *UV/H_2O_2* **[9, 14]**, *photo-Fenton* **[14, 212]** and *UV/O_3* **[15]**, have proven to be of real interest as an efficient treatment for the oxidation of various types of PEGs in aqueous solutions. The oxidation of PEG under these processes produces two types of reaction intermediate groups. The first group is polymeric fractions, which are formed by fragmentation of the original PEG into ethylene glycol and oligomers with different MWs. While the second group is non-polymeric fractions (short chain or violate fatty acids) **[6, 9, 13]**, which are amenable to biological treatment **[50, 51, 53, 213]**.

PEG is an ideal molecule to assess a PMR, since the products are smaller than the reactants, allowing the effect of reactant retention to be rigorously assessed as well as photocatalyst retention. It is the established reference polymer for the treatment of industrial wastewater containing soluble polymers with similar properties. In terms of identification and quantification, PEG oligomers can be identified and then quantified using high performance liquid chromatography (HPLC) **[214-216]**.

To the best of our knowledge, there is no literature available pertaining to the oxidation of PEG by using either POM homogenous photocatalysis or TiO_2 heterogeneous photocatalysis. Therefore, in the current PhD project, the PEG 1500 is selected as a synthetic industrial wastewater to be treated under POM homogeneous and TiO_2 heterogeneous PMR.

2.6 Implications of the literature review

The preceding literature review illustrates the wide scope and significant amount of research that has been carried out into the application of POM homogenous photocatalysis as one of the effective and efficient AOPs for the degradation of a wide range of refractory organic pollutants in industrial wastewater field at comparable rates to TiO_2 heterogeneous photocatalysis. However, the main disadvantage of POM homogeneous photocatalysts is the separation and recycle of them due to their complete solubility in reactant solution. Such issue makes a POM homogeneous photocatalysis unsuitable for the environmental applications, thus limiting the real applications of POMs homogeneous photocatalysts in the field of industrial wastewater treatment. In literature, this issue has been overcome by using immobilized system (incorporating the POM homogeneous photocatalysts with supporting materials). However, POM as an immobilized photocatalyst has an active surface area lower than that of suspended (dissolved) photocatalyst, thus significantly decreasing the overall photocatalytic degradation activity.

The current project addresses this issue as '*a big challenge in the literature*'. Therefore, this project attempts to fill the gap by developing a novel cross-flow PMR approach to separate and recycle homogeneous photocatalyst with reactant solution. This PMR consists mainly of annular photoreactor in conjunction with cross-flow nanofiltration unit.

The literature highlights that there has been no research on the oxidation of PEG by homogenous or heterogeneous photocatalysis. Therefore, the performance of this PMR approach will be evaluated under POM-$H_3PW_{12}O_{40}$ homogeneous photocatalyst with PEG as a synthetic polymer model of industrial wastewater and then compared with TiO_2 benchmark heterogeneous photocatalyst under batch and continuous PMR modes of operation. Under these conditions, it is expected that the use of POM homogeneous photocatalyst in this proposed PMR approach will not foul the membrane to the same extent as compared with TiO_2 heterogeneous photocatalyst, and thus overcoming a reduction in membrane flux and flow throughput as usual in TiO_2 heterogeneous PMR.

The significant motivations and contributions of this PhD project to fill several literature gaps can be listed below:

1) This work is the first through investigation of the effect of operating parameters (POM photocatalyst loading (mM), pH of the reactant solution and conventional oxidant (mgO_2L^{-1})) on POM-$H_3PW_{12}O_{40}$ homogeneous photocatalysis for the treatment of PEG in a continuously recirculating annular photoreactor. The treatment of PEG as a selected polymer model of synthetic industrial wastewater will facilitate easy benchmarking for a real industrial wastewater containing soluble polymers with similar properties.

2) This work in terms of separation and recycle of POM homogenous photocatalyst will be one of the first in depth investigation in this area. So, this successful work will contribute to make homogenous photocatalysis under various types of POMs for the treatment of real industrial wastewater to be a suitable method for environmental applications with regard to batch PMR mode of operation and continuous PMR mode of operation (continuous photocatalysis).

3) This work is the first investigation of TiO_2 heterogeneous photocatalysis for the treatment of PEG using batch and continuous PMR modes of operation.

4) New protocol in terms of validating the concept *'membrane enhanced photocatalysis'* based on batch PMR mode of operation with POM homogenous or TiO_2 heterogeneous photocatalyst will be proposed and tested with proposed evaluating parameters.

5) A comprehensive assessment of PEG oligomers degradation conditions based on the comparison between individual concentrations of these oligomers with different MWs and total concentration of PEG will be investigated. This assessment is the first to establish an insight with particular emphases into understanding and monitoring the photocatalytic degradation characteristics of polymers based on the same function since PEG is as an adequate model for this.

6) This work is to be one of first attempt to investigate the formation of reaction intermediates and then to open up an opportunity towards their photocatalytic degradation pathway under POM homogeneous and TiO_2 heterogeneous photocatalysis.

The above significant motivations and contributions give the current PhD study further novelty and originality.

Chapter 3

Materials and Methods

3.1 Materials

3.1.1 Photocatalysis process

3.1.1.1 Model compound

Polyethylene glycol, PEG1500, form: powder, colour: white to off-white, pH-value (100 gL^{-1}) 5-7 at 20 ^{o}C, solubility in water 500 gL^{-1}, Alfa-Alsafer, A Johnson Matthey Company, Inc., UK. Note that, in the current project, *PEG1500 is referred to as PEG*.

3.1.1.2 Photocatalyst

- Phosphotungstic acid hydrate ($H_3PW_{12}O_{40}.xH_2O$), reagent grade, MW: 2880.05 $gmol^{-1}$, Sigma-Aldrich Company Ltd., UK. Note that, in the current project, *$H_3PW_{12}O_{40}.xH_2O$ is referred to as POM*.
- Titanium (IV) oxide, TiO_2, Degussa P25, nanopowder, 21 nm particle size (TEM), MW: 79.87 $gmol^{-1}$, density: 4.26 gmL^{-1} at 25 ^{o}C, Aldrich Company Ltd., UK.

3.1.1.3 Chemicals and compounds

- Several types of short chain acids-volatile fatty acids (VFAs) including malonic (MW: 104.06 $gmol^{-1}$), glycolic (MW: 76.05 $gmol^{-1}$), formaldehyde (MW: 30.03 $gmol^{-1}$), formic (MW: 46.02 $gmol^{-1}$), acetic (MW: 60.05 $gmol^{-1}$) and propionic (MW: 74.07 $gmol^{-1}$) were obtained from Sigma-Aldrich and used to prepare external standard solutions for the investigation of reaction intermediates.
- The pH of the reactant solution was adjusted with HCl and NaOH (Sigma-Aldrich).
- Oxygen gas from (BOC with 99.5% purity, UK) was supplied continuously as a conventional oxidant for oxygenation of PEG reactant solution.
- Nitrogen gas from (BOC with 99.998% purity, UK) was used for membrane evaluation under dead-end membrane filtration process.
- Analytical grade acetonitrile, methyl cyanide ACN, colourless, MW: 41.05 $gmol^{-1}$, Sigma-Aldrich Company Ltd., UK.

- Deionized (DI) water was obtained from a purifying machine (Milli-Q, Millipore S.A.S. 67120, Laboratory ultra-pure water unit, France).

3.1.2 Membrane separation process

The membranes used in all experiments of dead-end filtration process and cross-flow photocatalytic membrane reactor (batch and continuous modes of operation) were purchased from Sterlitch (USA), DOW FILMTEC flat-sheet membrane, NF270, Polyamide, Size (305 x 305 mm), MWCO (200-400 Da), pH range (2-11).

3.2 Analytical techniques

3.2.1 Chromatographic method development for PEG oligomers separation and quantification

A reverse phase high performance liquid chromatography (RP-HPLC) coupled with an evaporative light scattering detector (ELSD) showed to be a powerful chromatographic technique for the separation of PEG oligomers **[217, 218]**. However, various chromatographic methods that uses this technique suffer from either a non-linear baseline or a weak peak resolution, or both **[214, 219]**. Therefore, in the current project RP-HPLC/ELSD method was developed based on past methods **[214, 216]**. This developed method achieved a high chromatographic resolution of individual PEG oligomers and, stable and straight baseline enabling to obtain an accurate peak area quantification.

An Agilent Technologies (1260 Infinity) HPLC system consisting of a quaternary pump (G1311B), autosampler (G1329B), column oven (G1316A) and ELSD (GB1530001) equipped with Zorbax extend-C18 (4.6 x 150 mm, 3.5 µm) column was used. The analytical column was connected with an Agilent guard column (4.6 x 12.5 mm, 5 µm). The ELSD detector was set to a nebulizer temperature of 25 ^{o}C, a nitrogen gas pressure of 1.5 bar and an evaporator temperature of 25 ^{o}C. The chromatographic conditions utilized an injection volume of 50 µL, a flow rate of 1 mLmin^{-1}, a column temperature of 50 ^{o}C and a gradient elution of water and acetonitrile outlined in Table A1 (*Appendix A*).

3.2.2 Identification of individual PEG oligomers

The initial PEG reactant solution was run using the developed method, yielding that a well resolved normal (Gaussian) distribution chromatogram of PEG oligomers-a series of several unidentified peaks (Fig. 3.1). As shown in Fig. 3.1, this developed method could separate the individual peaks efficiently with a precise and stable baseline. It was found that 23 peaks were identified with the major peak, which locates at the center corresponding to average molecular weight (Mn). Each peak corresponding to an oligomer with different molecular weight (MW).

The MW of each PEG oligomer was identified analytically using Matrix Assisted Laser Desorption/Ionization Time of Flight Mass Spectrometry, MALDI TOF (Model: Autoflex speed MALDI TOF/TOF, Bruker Daltonik GmbH, 2014, DHB 10 mg mL^{-1} as matrix), which is the most analytical tool for the determination of MW of synthetic polymers such as PEG **[220, 221]**. The MALDI TOF mass spectrum (Fig. 3.2) shows a well resolved MW distribution of PEG into individual peaks. Each individual peak representing an oligomer with a certain MW. Thus, the Mn of the major peak is 1537.9 $gmol^{-1}$ by matching Fig. 3.1 and Fig. 3.2. In general, as shown in these Figs., RP-HPLC/ELSD and MALDI TOF provided similar quantitative profiles of the PEG oligomers. This result further supports that the developed RP-HPLC/ELSD method was efficient in the separation of PEG oligomers. This is the main aim of using the MALDI TOF in the current project.

This project does not address the fate of MW of each PEG oligomer during photocatalytic reactions since this is beyond the scope of the work. This will be part of future work.

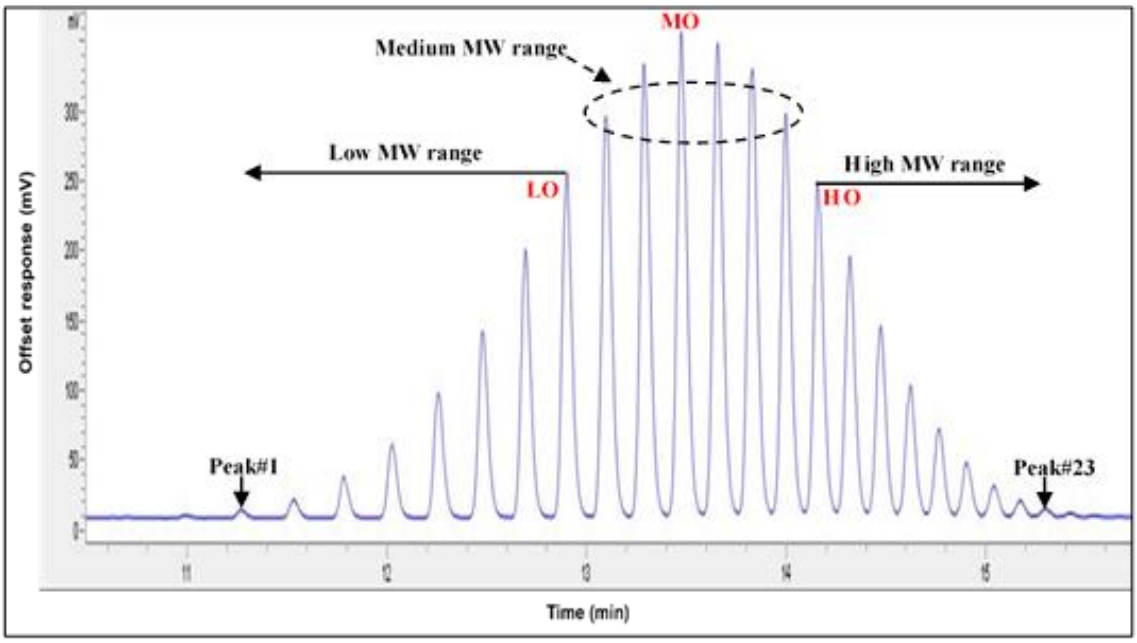

Fig. 3.1: RP-HPLC/ELSD chromatogram of PEG1500.

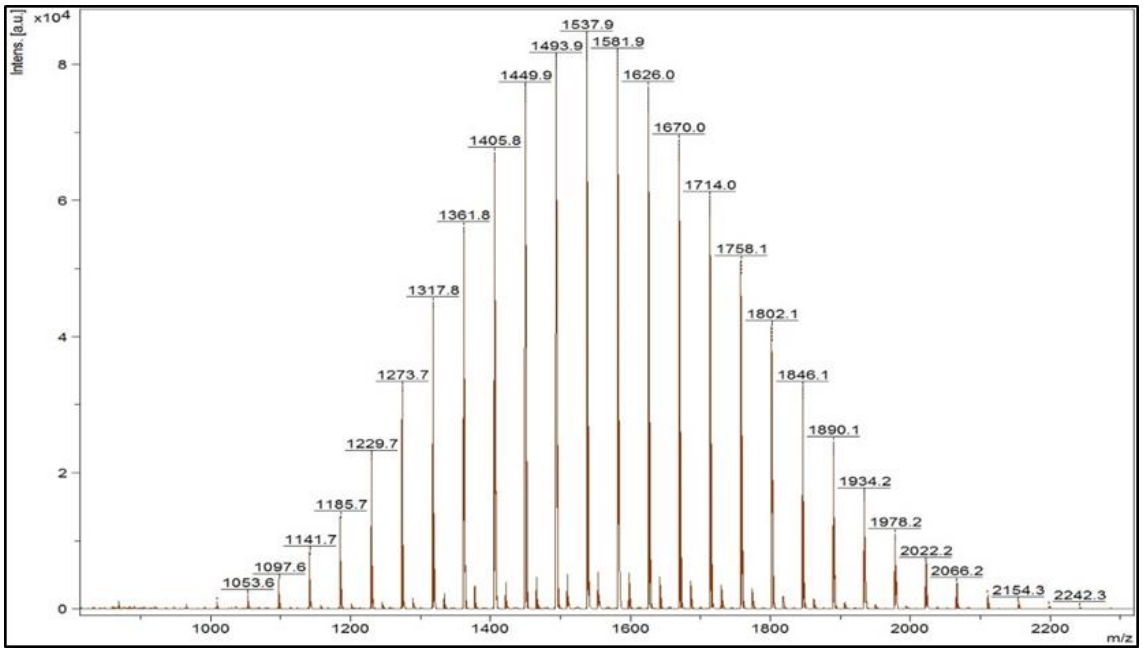

Fig. 3.2: MALDI-TOF mass spectrum of PEG1500.

In order to establish a fundamental understanding of the PEG reaction conditions as a function of the 23 individual oligomers identified, the oligomeric profile (Fig. 3.1) was divided into three ranges of different MWs: the low MW range, medium MW range and high MW range. To simplify the reaction conditions in each range separately, one oligomer was selected and designated as low MW oligomer-LO (1361.8 $gmol^{-1}$), medium MW oligomer-MO (1537.9 $gmol^{-1}$) and high MW oligomer- HO (1714 $gmol^{-1}$). These three selected oligomers would give a comprehensive coverage of the characteristic reaction conditions of PEG.

3.2.3 Determination of PEG oligomer concentration

The stock solution of PEG was diluted from 1000 to 100 mgL^{-1}, considering the sensitivity of the ELSD detector used. At the total concentration of PEG solution (100 mgL^{-1}), the concentration of each oligomer could be identified obviously and referred as the minimum individual detection limit (MIDL) of HPLC methodology. While, below 100 mgL^{-1}, the detector baseline appeared to drift and showed an excessive noise and referred as the minimum detection limit (MDL) of HPLC methodology. These diluted concentrations were run using the developed method to establish the calibration curves in terms of individual oligomer concentration versus individual peak area for every oligomeric peak in PEG. The individual concentration of each PEG oligomer was calculated using Eq. (3.1) **[214, 216]**:

$$C_i = \left(\frac{A_i}{\sum_i^n A_i}\right) * C_t \tag{3.1}$$

Where C_i and A_i is the concentration and area of each individual oligomer corresponding to peak i respectively, C_t is the total concentration of PEG and n is the total number of oligomer peaks in RP-HPLC/ELSD chromatogram.

The resulting calibration equations exhibited a non-linear relationship (power model) (see Fig. A1 and Table A2 in *Appendix A*). This is expected since the characteristics of this type of detector in most applications showed a nonlinear response **[217]**. This result is in agreement with that reported by *Davey et al.*, **[215]** and *Barman et al.*, **[222]** who found the same model for various types of PEG (200-8000). These equations were used to calculate the concentrations of the 23 individual oligomers under different reaction conditions. In terms of total concentration of PEG, it was calculated by the sum of 23 individual oligomeric concentration and *referred to as (total PEG) in the text and (PEG) in the figures.*

The percentage primary degradation, %PD was calculated according to the Eq. (3.2).

$$\%PD = \left(\frac{C_{oi} - C_i}{C_{oi}}\right) * 100\% \tag{3.2}$$

Where C_{oi} is the concentration of selected oligomer or total PEG after the adsorption period in (mgL^{-1}) and C_i is the concentration of selected oligomer or total PEG in (mgL^{-1}) during reaction time.

3.2.4 Identification of reaction intermediates

Information regarding the formation of reaction intermediates under homogeneous and heterogeneous photocatalysis of PEG is not available in the literature. However, the detailed information on the oxidation of PEG using AOPs are available **[6, 9, 10, 14, 223]**. It has been reported that these AOPs could generate short chain organic acids or volatile fatty acids (VFAs) reaction intermediates. The major VFAs are malonic, glycolic, formaldehyde, formic, acetic and propionic acids. Therefore, in this project, these VFAs formed during different examined conditions were identified and quantified with external standards using HPLC with the same specifications as shown in section 3.2.1 equipped with a refractive index detector (RID) and separated on an Agilent Hi-Plex H (300 x 7.7 mm) column. The analytical column was connected with an Agilent PL Hi-Plex H (50 x 7.7 mm) guard column. The conditions used an injection volume of 100 µL, a flow rate of 0.6 $mLmin^{-1}$, a column temperature of 60 ^{o}C and sulphuric acid of 0.005 M as mobile phase. The chromatographic analysis and calibration curves of these acids are shown in Fig. A2 and Fig. A3 respectively (*Appendix A*).

3.2.5 Identification of POM and its lacunary species

Experimental techniques are still facing a big challenge to analyze polyoxometalate compounds in aqueous solution and (synthetic and real) reactant solutions due to their complexity **[177]**. POM is very sensitive to decompose partially into various lacunary species in these solutions, so in the PhD current project several analytical techniques including Nuclear Magnetic Resonance Spectroscopy (NMR), Liquid Chromatography–Mass Spectrometry (LC-MS), HPLC couples with DAD, Fourier Transform Infrared Spectroscopy (FTIR) and Ultraviolet-Visible Spectroscopy (UV.vis) were used to identify POM and its lacunary species in PEG reactant solution. Unfortunately, some of these techniques (NMR, HPLC-DAD and LC-MS) could not identify it because its concentration in PEG reactant solution used was $\leq 1\ gL^{-1}$, making a detection of it is less than that of a minimum detectable limit of these techniques. While the other techniques were not accurate in their identifications.

The POM and its lacunary species in aqueous solution and PEG reactant solution under various investigating conditions were identified using HPLC-ESI-TOF analysis. This analysis was conducted using an electrospray time-of-flight mass spectrometer ESI-MicrOTOF (Bruker Daltonik GmbH, Bremen, Germany), which was coupled with an Agilent HPLC stack (Agilent, Santa Clara, CA, United States) consisting of Agilent G1312A binary pump with G1329A autosampler and G1316A column oven. Analyses were performed in ESI negative mode. The capillary voltage was set to 4500 V, nebulizing gas at 2.2 bar, drying gas at 10.2 $Lmin^{-1}$ at 220 °C in each case. The TOF scan range was from 50-1500 mass-to-charge ratio (m/z) where this ratio (m/z) was used as an indicator to

identify some types of lacunary species of POM based on the accurate mass and isotope calculator. In each case 10 µL injections were made. The TOF was calibrated with a 10 µL sodium formate calibrant solution injection prior to the chromatographic/flow injection run. The calibrant solution consisted of 3 parts of 1 M NaOH to 97 parts of 50:50 water: isopropanol with 2% formic acid. Automated data processing was performed using the Compass Data Analysis software scripts (Bruker Daltonik GmbH, Bremen, Germany).

Note that, this analysis was applied for identifying the original POM ($H_3PW_{12}O_{40}$) in the form $[PW_{12}O_{40}]^{3-}$ and formed lacunary species only. It could not be used to quantifying them.

3.2.6 Determination of concentration of POM

Due to the limitation of suggested analytical techniques shown above to identify POM and then quantify it. Therefore, the concentration of POM-$H_3PW_{12}O_{40}$ in the form $[PW_{12}O_{40}]^{3-}$ and its lacunary species with external standards and PEG reactant solutions under different investigating conditions was determined on a basis of the total elemental concentration of tungsten (*W*) in the solution. This total concentration of POM based on the *W* was used to evaluate the performance of dead-end membrane separation process (*no UV*) in terms of the rejection as well as batch and continuous PMR modes of operation in terms of the rejection and retentate concentration in the BSR.

This total concentration of *W* was analyzed using an Atomic Absorption Spectrometer-*AAS* (Perkin-Elmer, AAnalyst 100) equipped with a nitrous oxide burner head. A hollow-cathode tungsten lamp (Perkin-Elmer, Lumina^{TM}, wavelength 400.9 nm, Singapore) was the radiation source. Air-acetylene gas, a carrier, was supported by nitrous oxide. All samples prepared were analyzed under the optimum flame conditions. The prepared calibration curve is shown in Fig. A4 (*Appendix A*). *Note that, a minimum detection limit of an AAS device was 3 mg W L^{-1}.*

3.2.7 Total organic carbon-TOC

TOC content was measured with a Shimadzu TOC-L CPH analyzer equipped with an auto sampler, Shimadzu ASI-L. It works based on the combustion/non-dispersive infrared (NDIR) gas analysis. Total carbon (TC) was first measured and then inorganic carbon (IC). The TOC was determined by subtracting IC from TC.

3.2.8 pH and dissolved oxygen monitoring

The pH and dissolved oxygen (DO) of PEG reactant solution were continuously monitored using multiparameter device (Thermo Scientific™ Orion™ Versa Star, Advanced Electrochemistry Meter, Sn V 05133, Indonesia).

3.2.9 Turbid meter

The concentration of TiO_2 in the PEG reactant solution was measured using a turbid meter (EUTECH TN-100IR, Thermo Scientific, Singapore) and expressed in (mgL^{-1}) based on the prepared calibration curve of various TiO_2 loadings in PEG reactant solution as shown in Fig. A5 (*Appendix A*). The turbidity range of this device is 0-2000 NTU. The dilution factor was considered for some cases (out of the measurement range of this device).

3.2.10 Scanning electron microscopy (SEM)

The SEM images of the top surface of used membranes were taken using an instrument (JEOL JSM6480LV, Sweden) after sputter-coating with gold 4 minutes using an Edwards S150B sputter coater.

3.3 Experimental set-up

3.3.1 Dead-end membrane filtration process

Dead-end membrane filtration experiments were performed in a Sterlitech HP4750 stirred cell made of stainless steel with an active membrane area of 14.6 cm^2. A magnetic stirrer was placed above the membrane surface and used for mixing the feed at a constant stirring speed (300 rpm) to minimize the fouling. The dead-end cell was placed in a water bath on a heater-stirrer and operated at room temperature. Pressure was applied using compressed nitrogen from nitrogen cylinder and measured with a pressure gauge. Weight of permeate was recorded using a Sartorius LC3201D-00MS balance with data logging program developed in Labview. Flat-sheet membrane discs of 47 mm, NF270 were cut out from larger flat-sheet with a scalpel. A schematic of dead-end filtration and photograph of its components is shown in Fig. 3.3. Detailed information about the cell components and operating parameters is given in Fig. A6 and Table A3 respectively (*Appendix A*).

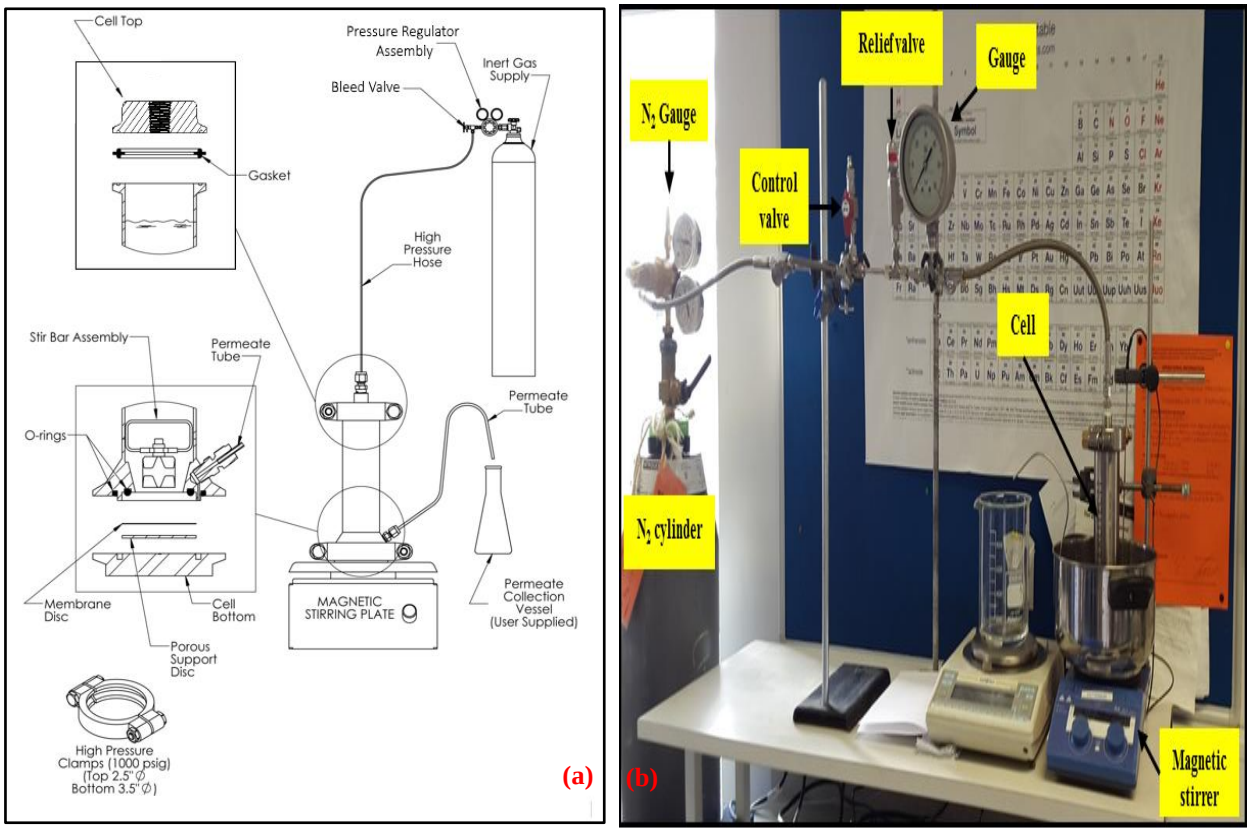

Fig. 3.3: Sterlitech HP4750 dead-end cell used for filtration: (a) schematic diagram, (b) overall experimental assembly photograph.

3.3.2 Cross-flow photocatalytic membrane reactor

A schematic diagram of experimental setup of a cross-flow photocatalytic membrane reactor (PMR) is shown in Fig. 3.4. The PMR is comprised of three parts. The first part (Fig. 3.4-a) is an advanced oxidation (photocatalysis process). This part was adopted on the basis of a continuously recirculating batch mode of operation to combine the following components: a pump 1 (peristaltic type, Millipore Corporation, model 01N 038, USA), a flowmeter-F_1 (model: KDG1100, England), annular photoreactor (Davey Steriflo Domestic and Commercial UV system, model SF300, light intensity 20 W, light wavelength 254 nm with an outer radius of 44 mm, an inner radius of 25 mm and a length of 410 mm supplied standard with a low pressure mercury UV lamp from New Zealand, more information about this photoreactor reactor is given in Fig. A7, *Appendix A*) and a cooling tank containing a metal cooling coil using tap water via control valve 1. Polytetrafluoroethylene (PTFE) tubing was used to connect these components of this part due to its high chemical residence and low potential adsorption for PEG solution.

The second part (Fig. 3.4-b) is a batch-stirred reservoir (BSR) with a total volume of 2.5 L as a feeding reactant tank (PYREX, QUICKFIT, UK), which was placed above a heater-stirrer (IKA, CE, model: RCT BS002, laboratory equipment, Germany) and covered with aluminum tin foil to prevent any degradation effects via ambient light in the lab. It contained a magmatic stirrer, a pH

probe, a DO probe, a thermocouple and a gas bubbling stone connected with oxygen cylinder via control valve 2.

The third part (Fig. 3.4-c) is a cross-flow membrane separation process that consisted of a control valve 3 (Swagelok, SS-4558, USA), a pump 2 (plunger type, Grosvenor, model: 5583, max pressure 45 bar, England), a pulsation damper (FLOWGURD, SA 351, CF8M, England), a safety valve (Swagelok, AFTA, USA), a metal cross-flow cell (METXF-2.5-040-02, stainless steel, Membrane Extraction Technology, UK) with effective membrane area of 14.6 cm^2, PI_1 and PI_2 gauges (WIKI, 316SS, USA), pressure regulator (TESCOM, ELK RIVER, MN, 44-2369-24-55, USA), control valve 4 (Swagelok, W, CF8M, USA) and permeate tank (beaker, squat form with graduations and spout borosilicate glass 1 L, Fisher brand, Fisher Scientific, UK). This tank was placed above a balance (Sartorius LC3201D-00MS) with data logging program developed in Labview. Stainless steel tubing was used to connect the components of part three. The BSR connected the photocatalysis process and cross-flow membrane separation process together to procedure a batch cross-flow PMR mode of operation as shown in Fig. 3.4 (a-c).

A PEG continuously feeding tank with the same specifications of BSR and a peristaltic pump (Watson-Marlow, model 101U, England), Fig. 3.4-d, connected with the BSR (Fig. 3.4-b) to produce a continuous cross-flow PMR mode of operation (Fig. 3.4).

The samples under batch and continuous PMR experiments were taken from the points of S1 and S2 for experimental analysis as shown in Fig. 3.4.

The overall assembly photograph of cross-flow PMR with batch and continuous modes of operation is shown in Fig. 3.5.

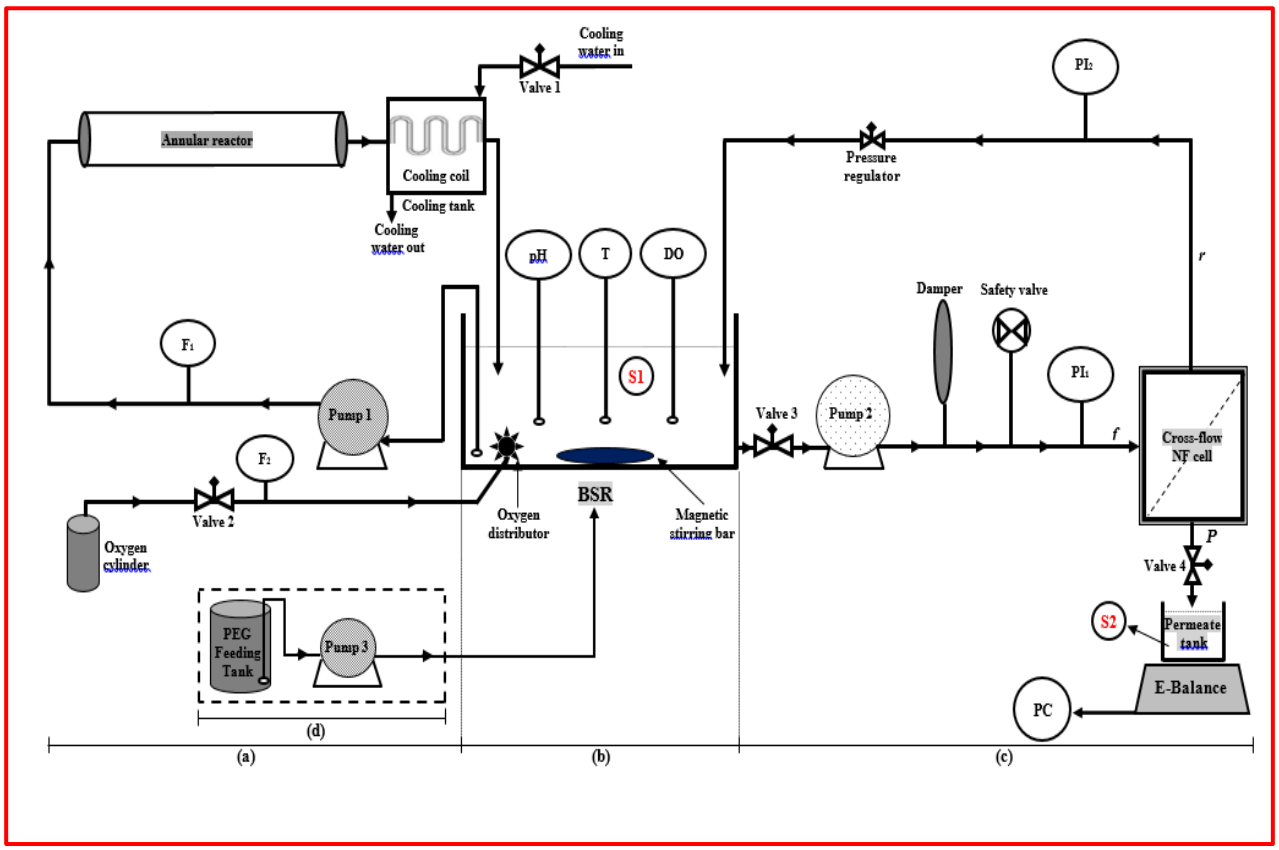

Fig. 3.4: Schematic diagram, (a) photocatalysis process, (b) batch-stirred reservoir (BSR), (c) cross-flow membrane separation process**,** (a-b-c) batch cross-flow PMR operation and (a-b-c-d) continuous cross-flow PMR operation.

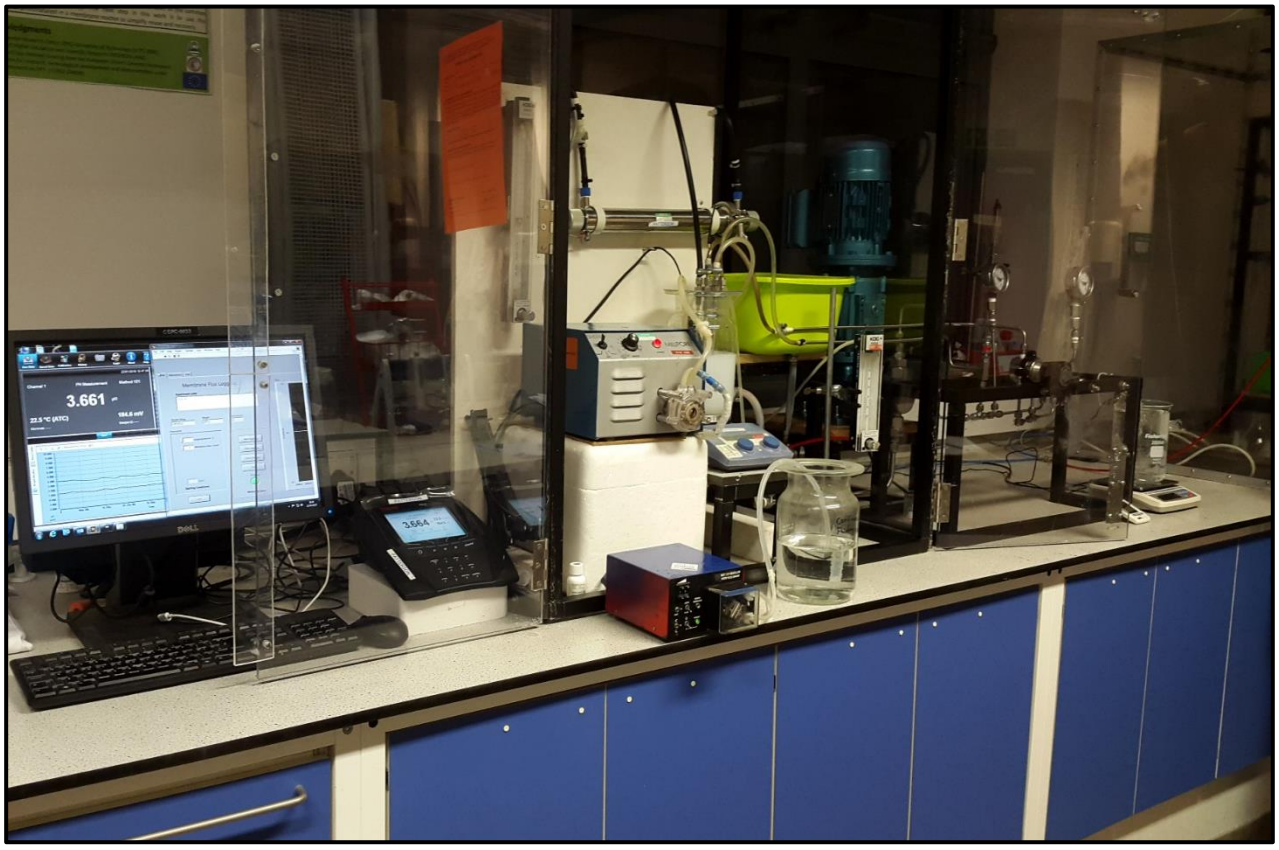

Fig. 3.5: Overall PMR assembly photograph.

3.4 Experimental procedure

3.4.1 Dead-end membrane filtration process

Dead end membrane filtration procedure was performed according to standard methodology reported by several studies **[214, 224]**. All membranes were initially pre-conditioned with 300 mL of DI water under a driving force of 15 bar of compressed N_2 for a constant stirring speed (300 rpm) and temperature (25 ^oC) until a steady state flux was obtained. If the membrane did not achieve a stable flux after this run, the same procedure was repeated again with a new fresh DI water until achieving a stable flux. After that, the remaining water was emptied from the filtration cell and the desired solution of 50 mL under various investigating cases including PEG, POM, TiO_2, PEG with POM, PEG with TiO_2 and combined (POM-TiO_2) with PEG at a specified condition for each of these cases shown later was loaded under the same driving force of N_2 until 25 mL of the permeate was collected in a measuring cylinder. This permeate collection was used to determine the flux of membrane via recording the permeate volume versus filtration time. The SEM was used to image the surface of used membrane in these experiments.

Rejection of PEG was calculated using Eq. (3.3):

$$R\ (\%) = \left(1 - \frac{C_p}{C_f}\right) * 100\% \tag{3.3}$$

Where R is the rejection of membrane, C_p refers to the concentration in the permeate in (mgL^{-1}) for either total PEG or each PEG individual oligomer or TOC or POM or TiO_2 and C_f refers to the concentration in the feed in (mgL^{-1}) for either total PEG or each PEG individual oligomer or TOC or POM or TiO_2.

Mass balances were calculated using Eq. (3.4):

$$\text{Recovery}\ (\%) = \left(\frac{V_p C_p + V_r C_r}{V_f C_f}\right) * 100\% \tag{3.4}$$

Where *Vp, Vr and Vf* refer to the volume of the permeate, retentate and feed respectively and C_p, C_r and C_f refer to the concentration (mgL^{-1}) in the permeate, retentate and feed respectively for either total PEG or each PEG individual oligomer or TOC.

3.4.2 Effect of POM loading, pH and oxidant on photocatalysis of PEG

This section describes the experimental design and work in ***chapter 4***. This work was carried out by two steps:

3.4.2.1 Experimental design

A Central-Composite Experimental Design (*CCED*) was applied to investigate the effects of three operating parameters including POM loading, pH and oxidant concentration on the selected response functions (%PD and K_{app}) of POM photocatalysis of PEG.

The design process consisted of three series of experiments (Table 4.2): *Set 1*: a factorial design of 2^k trials with all possible combinations of codified values +1 and -1, where k=3 variables, resulting in 8 experiments (1-8). *Set 2*: selection of the axial distance of the star point (codified values $\alpha=2^{k/4}=\pm1.6817$) consisting of $2k$=6 experiments (9-14). *Set 3*: replicates of the central point, 4 experiments (15-18). A neural network (*NN*) was used to fit the obtained experimental results with two neurons using a simple exponential activation function and a solution strategy based on a back-propagation algorithm **[225-230]**. Parameters were fitted using the solver tool in a custom spreadsheet in Microsoft Excel using a nonlinear fitting method. A measure of the saliency of the input variables was used to analyze the relevance of each variable with respect to others (expressed as percentages) based on the connection weights of the neural network. The general factors (N_1 and N_2) are first and second neurons respectively. While W_{11}-W_{13} and W_{21}-W_{23} are the contribution parameters relating to first and second neurons respectively, and representing the influence of each of these operating parameters used.

3.4.2.2 Experimental work

It was carried out using two parts of PMR system only, which are a photocatalysis process in conjunction with BSR only (Fig. 3.4 (a-b)) without using a membrane separation process. The operating parameters, POM loading and oxidant concentration, were selected in the range (0.35-1.05 mM) and (14-58.65 mgO_2/L) respectively based on the relevant literature **[25-27, 98, 102, 231-233]**. While for pH operating parameter, detailed information in terms of selecting the suitable range of pH is shown in chapter 4, section 4.2.3. The pH was adjusted by using HCl and NaOH. Note that POM-$H_3PW_{12}O_{40}$ is acidic in aqueous solution depending on its applied loading **[38, 93]** where the relationship between the pH of PEG reactant solution and applied POM loading is shown in Fig. A8 (*Appendix A*).

In terms of preparation of PEG initial reactant solution, a weighted mass of PEG (2 g) was added to 2 L of DI water in the BSR and then mixed under constant magnetic stirring of 350 rpm for

15 min to prepare the initial reactant solution (1 gL^{-1}) with pH~3.1 and TOC (560±10 mgL^{-1}) according to standard methods. This initial reactant solution was treated with different experimental conditions as explained by the following consecutive steps:

- ***Step 1-Adsorption and photolysis control experiments (PEG only with circulation, without and with UV):***

The initial reactant solution in the BSR was circulated in the dark (*no UV light*) for 180 min to allow for the adsorption of PEG oligomers to reach equilibrium. Quantifiable adsorption occurred only in the first 30 min and after that the concentration of these oligomers remained nearly constant. Thus, 30 min was chosen as the dark equilibrium time prior to starting the photolytic reaction. Any subsequent change in the concentration of these oligomers during this reaction is due to photolytic degradation only.

- ***Step 2-Non-photocatalytic reaction experiments without adsorption (PEG-POM, no circulation and no UV)*:**

Various POM loadings (mM) based on a *CCED* conditions as is explained in chapter 4, section 4.3 were mixed with initial reactant solution inside the BSR at a constant stirring speed of 500 rpm to ensure perfect mixing for 180 min without circulating the prepared (PEG-POM) solution through the system to avoid the effect of adsorption. Any subsequent change in the concentration of PEG and POM is thus due a non-photocatalytic reaction of POM with PEG only. Oxygen was supplied continuously from an oxygen cylinder using a gas bubbling stone as an oxygen diffuser into the BSR at various flowrates based on a *CCED* conditions to maintain a fixed concentration (mgO_2L^{-1}) inside the BSR during this period. The lower level of oxidant concentration (14 mgO_2L^{-1}) was achieved by circulated the PEG reactant solution through the system (oxygenation of the solution through mass transfer from ambient air only). pH was adjusted using either HCl or NaOH based on a *CCED* conditions. The pH and oxidant concentration were continuously monitored using multiparameter device. More details about a non-photocatalytic reaction of POM with PEG are shown in chapter 4, section 4.2.2. A non-photocatalytic reaction time of 30 min was selected to ensure that there is no significant change in concentration of PEG and POM prior to carrying out the step 3.

- ***Step 3-Adsorption and photocatalytic reaction experiments (PEG-POM with circulation, without and with UV)*:**

The reactant (PEG-POM) solution from step 2 was circulated through the system for 30 min in the dark (*no UV light*) to allow the PEG reactant solution to reach adsorption equilibrium. Thereafter, the lamp was switched on for 180 min and the photocatalytic reaction started.

It is important to mention that as the photocatalytic reaction proceeded, under the lower level of oxidant concentration (14 mgO_2L^{-1}), the concentration of oxygen would reduce slightly, so very limited quantities of oxygen bubbles was supplied into the reactant solution to sustain this concentration.

All samples were withdrawn from the BSR before, during and after a non-photocatalytic reaction, adsorption and then periodically every 15 min photocatalytic time.

3.4.3 Batch cross-flow PMR operation

*This section describes the experimental work in **chapter 5, 6 and 7**.*

3.4.3.1 POM homogeneous photocatalytic membrane reactor

*This section describes the experimental work in **chapter 5**.*

3.4.3.1.1 POM homogeneous photocatalysis (*no membrane*)

After identifying the optimum conditions of operating parameters from the above section 3.4.2 where POM photocatalyst loading was found to be 1 gL^{-1} under controlling pH and oxidant concentration. In this section, POM loadings were varied from 1 to 0.25 gL^{-1} to investigate the effect of POM homogeneous photocatalysis on PEG as a control process (*no membrane*) under monitoring the pH and DO during photocatalytic reaction (since these two parameters showed a negative impact on photocatalytic degradation of PEG when controlling them, detailed information about them is shown in chapter 5, section 5.3).

In order to establish a comparable performance between the POM homogeneous photocatalysis of PEG as a control process (*no membrane*) and the proposed PMR later, *to achieve this*, it was decided to use the whole components of PMR system in which the permeate valve was totally closed to prevent any permeation through the permeate stream. The reacting solution of PEG was initially prepared inside the BSR and then various POM loadings for each experiment was separately added to the PEG reactant solution and mixed for 30 min of a non-photocatalytic reaction time prior to starting the adsorption period. Any subsequent change in the concentration of PEG and POM together is due to the effect of adsorption. At this stage, the reacting solution was being continuously fed and circulated from the BSR to the photocatalysis process (Fig. 3.4 (a-b)) using a pump 1 at 0.5 $Lmin^{-1}$ and to membrane separation process (Fig. 3.4 (b-c)) using a pump 2 at a transmembrane pressure of (TMP) of 15 bar with cross-flow velocity (CFV) of 1.3 cms^{-1}. This circulation through the system was continued for 30 min in the dark (*no UV light*) to obtain adsorption equilibrium. Thereafter, the lamp of photoreactor was switched on for 180 min and the photocatalytic reaction started.

3.4.3.1.2 Cross-flow homogeneous PMR

In terms of membrane pre-conditioning, a new membrane was initially put inside a metal cross-flow cell. DI water (2 L) was put inside the BSR that was being continuously circulated from the BSR to membrane separation process using a pump 2 under a constant pressure filtration mode, TMP of 15 bar and CFV of 1.3 cms^{-1}. This pressure was obtained by adjusting a pressure regulator. The flux through the membrane was monitored at 1 min intervals and measured using a balance that recorded the water permeate through the membrane via data acquisition software connected with a personal computer. Due to the action of pump 2, the temperature of DI water inside the BSR increased gradually, so to keep this temperature at room condition, a pump 1 was operated to circulate DI water from the BSR to a cooling coil (using a tap water) and then this circulating water was cooled to room temperature. The membrane pre-conditioning was being continued until achieving a stable flux. After that both pumps were tuned off and the remaining DI water in the system was emptied.

After membrane pre-conditioning, the PEG reactant solution was initially prepared inside the BSR and then a certain POM loading was added to the solution and mixed for 30 min of a non-photocatalytic reaction time prior to starting the adsorption period. Pump 1 at 0.5 $Lmin^{-1}$ and pump 2 (15 bar and 1.3 cms^{-1}) were being continuously operated together to circulate the (PEG-POM) solution from the BSR towards both sides of photocatalysis process and membrane separation process with two separate closed loop for 30 min in the dark (*no UV light*) to obtain adsorption equilibrium. Afterward, the lamp in the photoreactor was switched on to start the photocatalytic reaction for180 min as well as the permeate valve was opened entirely to collect the permeation through the membrane in the permeate tank.

Note that, in terms of the investigation of influence hydrodynamic conditions on homogeneous PMR, the same experimental procedure shown above was done under TMP (25 bar) with CFV (1.3 cms^{-1}) and TMP (15 bar) with CFV (0.65 cms^{-1}).

3.4.3.2 TiO_2 heterogeneous photocatalytic membrane reactor

This section describes the experimental work in ***chapter 6****.*

3.4.3.2.1 TiO_2 heterogeneous photocatalysis (*no membrane*)

To identify the best conditions to be applied in TiO_2 heterogeneous photocatalysis without membrane, several preliminary experiments were carried out in three steps. After that the TiO_2 photocatalytic reaction of PEG under identified conditions above was achieved in two sets of experiments. Note that, PEG initial reactant solution used in this section was prepared inside the BSR according to the method shown in section 3.4.2.2. A TiO_2 loading was added to the prepared solution. The prepared (PEG-TiO_2) solution was circulated from the BSR to the whole components of PMR

system using pump 1 and pump 2 together under the volumetric flowrate (0.5 $Lmin^{-1}$) and hydrodynamic (TMP-15 bar and CFV-1.3 cms^{-1}) conditions respectively.

A. Preliminary experiments:

- ***Step 1-Non-photocataytic reaction of TiO_2 with PEG experiments (PEG-TiO_2 with no circulation and no UV):***

Various TiO_2 loadings were mixed with PEG initial solution inside the BSR at a constant stirring speed of 500 rpm for 180 min without circulating the prepared (PEG-TiO_2) solution through the system to avoid the adsorption of PEG oligomers and TiO_2 onto the components of PMR system. More details about the identification of a non-photocatalytic reaction of TiO_2 with PEG are shown in chapter 6, section 6.3.1.3. The non-photocatalytic reaction time (30 min) was selected prior to carrying the adsorption period (step 3).

- ***Step 2-Effect of pH on the adsorption of PEG oligomers onto TiO_2 particles experiments (PEG-TiO_2 with no circulation and no UV):***

To investigate the effect of pH under acidic (pH 3) using HCl and basic (pH 11) using NaOH on the adsorption of PEG oligomers onto the active sites of TiO_2 particles, different TiO_2 loadings were mixed with PEG initial solution inside the BSR at 500 rpm stirring speed for 180 min without circulating the prepared (PEG-TiO_2) solution through the system to avoid the effect of adsorption of these oligomers and TiO_2 on the components of PMR system. Detailed information about the effect of pH on the adsorption of these oligomers is shown in chapter 6, section 6.3.1.2. Based on the obtained results from this investigation, the pH was not controlled in all coming experiments.

- ***Step 3-Effect of adsorption on TiO_2 concentration experiments (PEG-TiO_2 with circulation, no UV):***

To identify the required dark equilibrium time for the adsorption of TiO_2 in the PMR system (Fig. 3.4, a-b-c) under the conditions with no membrane (the permeate valve was totally closed to prevent any permeation through the permeate stream), various TiO_2 loadings were added to the PEG initial solution and mixed for 30 min of a non-photocatalytic reaction period. The prepared (PEG-TiO_2) solution was circulated in the dark for 210 min. An adsorption equilibrium time of 60 min was identified depending on the minimum effect of adsorption to take place and used prior to carrying out any photocatalytic reactions later.

B. Photocatalytic reaction of TiO_2 with PEG

- ***Set 1-Adsorption and photocatalytic reaction experiments (PEG-TiO_2 with circulation, without and with UV)-<u>Effect of oxidant concentration</u>:***

Three experiments were carried out at a TiO_2 loading of 0.25 gL^{-1} to investigate the effect of oxidant concentration (DO) on the TiO_2 photocatalytic reaction of PEG under monitoring the DO (experiment 1) and controlling it at the concentrations of 20 mgO_2L^{-1} (experiment 2) and 75 mgO_2L^{-1} (experiment 3). Powdered TiO_2 was mixed with PEG initial reactant solution inside the BSR at a constant stirring speed of 500 rpm for 30 min of a non-photocatalytic reaction of TiO_2 with PEG. After that the prepared (PEG-TiO_2) solution was circulated through the PMR system for 60 min to allow the solution to reach adsorption equilibrium and then the lamp was switched on for 180 min and the photocatalytic reaction started. The best conditions were found under the experiment 2, so the oxidant concentration in the range 20-25 mgO_2L^{-1} was chosen prior to carrying out the set 2.

- ***Set 2-Adsorption and photocatalytic reaction experiments (PEG-TiO_2 with circulation, without and with UV)-<u>Effect of TiO_2</u> <u>loading:</u>***

The aim of this section is to investigate the TiO_2 heterogeneous photocatalysis of PEG as control process (*no membrane*) under different loadings. Numerous TiO_2 loadings in the range of 0.125 to 0.50 gL^{-1} were mixed with PEG initial solution inside the BSR at 500 rpm for 30 min of a non-photocatalytic reaction period. Then, the prepared (PEG-TiO_2) solution was circulated through the system for 60 min adsorption period. During this adsorption period, the oxidant concentration (20-25 mgO_2L^{-1}) was continuously supplied into the BSR. Finally, the UV lamp was switched on for 180 min and the photocatalytic reaction started.

3.4.3.2.2 Cross-flow heterogeneous PMR

After membrane pre-conditioning as explained in section 3.4.3.1.2 earlier, the PEG reactant solution was initially prepared inside the BSR and then two TiO_2 loadings of 0.25 and 0.5 gL^{-1} were separately added to PEG prepared solution and mixed for 30 min of non-photocatalytic reaction period prior to starting the adsorption period. Pump 1 and pump 2 were being continuously operated together to circulate the (PEG-TiO_2) solution from the BSR through the PMR system for 60 min in the dark (*no UV light*) as well as the oxidant concentration (20-25 mgO_2L^{-1}) was continuously supplied into the BSR. Afterward, the lamp of photoreactor was switched on to start the photocatalytic reaction for 180 min as well as the permeate valve was entirely opened to collect the permeation through the membrane in the permeate tank.

3.4.3.3 Combined (POM-TiO_2) photocatalytic membrane reactor

*This section describes the experimental work in **chapter 7**.*

3.4.3.3.1 Combined (POM-TiO_2) photocatalysis (*no membrane*)

The concept of synergistic combination of POM and TiO_2 was adopted based on two proposed scenarios. Several preliminary experiments to identify which scenario would be better to be applied in investigating the optimal loadings of combined (POM-TiO_2) photocatalysts later. These experiments were done in two steps. Note that, PEG initial solution used in this section was prepared inside the BSR according to the method shown in section 3.4.2.2. The final prepared PEG solution with the addition of POM and TiO_2 under different examined conditions was circulated from the BSR to the whole components of PMR system using pump 1 and pump 2 together under the volumetric flow rate (0.5 $Lmin^{-1}$) and hydrodynamic (TMP-15 bar and CFV-1.3 cms^{-1}) conditions respectively.

A. Preliminary experiments:

- ***Step 1-First scenario***

The first scenario assumed that POM is a primary photocatalyst and TiO_2 is a secondary photocatalyst. Firstly, POM was added to the PEG initial solution inside the BSR and mixed for 30 min of non-photocatalytic reaction period. Secondly, TiO_2 was added after that time and mixed for 30 min of non-photocatalytic reaction period. The prepared (PEG-POM-TiO_2) solution was circulated through the PMR system for 60 min adsorption period to allow the PEG oligomer, POM and TiO_2 to reach adsorption equilibrium under the conditions with no membrane (the permeate valve was totally closed to prevent any permeation through the permeate stream) and then the lamp was switched on for 180 min and the photocatalytic reaction started.

- ***Step 2-Second scenario***

The second scenario assumed that TiO_2 is a primary photocatalyst and POM is a secondary photocatalyst. Firstly, TiO_2 was added to the PEG initial solution inside the BSR and mixed for 30 min of non-photocatalytic reaction period. Secondly, POM was added after that time and mixed for 30 min of non-photocatalytic reaction period. The prepared (PEG-TiO_2-POM) solution was dealt with the same experimental procedure shown in step 1 (first scenario).

More details about the results of these scenarios are shown in chapter 7, section 7.2.1 where the first scenario showed a better %PD of PEG, and thus it was selected to carry out the experiments in the following section (B).

B. Exploration of the optimal synergistic effect loadings:

The aim of this section is to explore the optimal synergistic effect loadings of combined (POM-TiO_2) photocatalysts under the conditions of first scenario. The experimental results of this section will be used as a basis of combined (POM-TiO_2) photocatalysis (no membrane). *To achieve this*, experiments started with optimal loading of individual POM (0.75 gL^{-1}) and TiO_2 (0.25 gL^{-1}), which were investigated before in chapters (5-6) and the further investigation was done under two sets of experiments referred to as Set 1, Set 2 and Set 3. Full details are shown in chapter 7, section 7.2.2. These experiments were followed the experimental procedure of first scenario shown above.

3.4.3.3.2 Cross-flow combined (POM-TiO_2) PMR

After membrane pre-conditioning as explained in section 3.4.3.1.2 earlier, the PEG reactant solution was initially prepared inside the BSR and then POM and TiO_2 were used based on their optimal conditions of Set 1, Set 2 and Set 3. These photocatalysts were added to PEG prepared solution according to the experimental procedure of first scenario shown above until the adsorption period. After this adsorption period, the lamp of photoreactor was switched on to start the photocatalytic reaction for 180 min as well as the permeate valve was entirely opened to collect the permeation through the membrane in the permeate tank.

3.4.4 Continuous cross-flow PMR operation (*Continuous photocatalysis)*

The main aim of this work is to convert batch cross-flow photocatalysis (control process-no membrane) to a continuous photocatalysis mode of operation by using PMR. *To achieve this*, the same experimental procedure shown in terms of batch cross-flow PMR operation, sections 3.4.3.1, 3.4.3.2 and 3.4.3.3, was followed until the end of stage of adsorption equilibrium. After this stage, the lamp of photoreactor was switched on to start the photocatalytic reaction for 9 h with POM continuous photocatalysis or TiO_2 continuous photocatalysis and 12 h for combined (POM-TiO_2) continuous photocatalysis, the permeate valve was entirely opened to collect the permeation through the membrane in the permeate tank and pump 3 (Fig. 3.4-d) was switched on to pumping a constant mass rate ($gmin^{-1}$) of fresh PEG feed (1 gL^{-1}) from its feeding tank to the original PEG reactant solution inside the BSR.

This added mass rate of fresh PEG feed was approximately calculated from the result of permeate flux of batch PMR operation for each case of POM, TiO_2 and combined (POM-TiO_2) photocatalysts. Since this mass rate of fresh PEG feed was added constantly to the original PEG reactant solution, it is expected that there is a significant difference between the rate of addition and the rate of filtration due to membrane fouling during the operating time, causing a considerable effect on the concentration of these photocatalysts and thus affecting the %PD of PEG and also formed

VFAs and then the monitoring the pH. This difference between the two rates of addition and filtration was described in terms of permeate flux under batch PMR mode of operation (*referred to as BPMR*) and continuous PMR mode of operation (*referred to as CPMR*). More information is discussed for each case later.

Under BPMR and CPMR modes of operation for POM, TiO_2 and combined (POM-TiO_2) photocatalysts:

- The pH, DO and flux were being monitored during the course of reaction.
- In terms of sampling, all samples were withdrawn from the BSR before, during and after a non-photocatalytic reaction, adsorption and then periodically every 15 min photocatalytic time as well as the permeate from the permeate tank at the end of experiment. These samples were analyzed with suitable analytical techniques.
- The SEM images of the top surface of used membranes in these experiments were taken.

Note that, most of experiments in the current research were repeated in duplicate in order to confirm the reproducibility of the results and these results are presented as the average ± one standard deviation.

The total concentration of PEG was selected as a basis of calculating the primary degradation and reaction kinetics unless otherwise stated.

Chapter 4

Effect of POM Loading, pH and Oxidant on Photocatalysis of PEG

4.1 Introduction

As shown in chapter 2, there has been no research reported in the literature into the application of POM homogeneous photocatalysis on PEG. Therefore, in order to extend the knowledge and real application of POMs in the field of industrial wastewater treatment, the current chapter is the first through investigation of the effect of operating parameters on POM homogeneous photocatalysis for the treatment of PEG in a continuously recirculating annular photoreactor. These operating parameters are POM photocatalyst loading (mM), pH of the reactant solution and conventional oxidant (mgO_2L^{-1}). Essentially, understanding the impacts of these parameters on the performance of photocatalysis process is of importance from the design and the operational points of view when selecting a sustainable and efficient process for the treatment of industrial wastewater.

To achieve this aim, a central-composite experimental design (*CCED*) and neural network (*NN*) fitting as a mathematical tool was used to design and assess the significant effect of these parameters on photocatalytic degradation conditions (primary degradation and degradation kinetics) and mineralization. A comprehensive assessment of these degradation conditions based on the comparison between individual concentrations of three selected oligomers with different MWs and total concentration of PEG was investigated. This assessment is the first to establish an insight with particular emphases into understanding and monitoring the photocatalytic degradation characteristics of polymers based on the same function since PEG as an adequate model for this.

This chapter is divided into two main sections where the experimental procedures of these sections were performed in chapter 3, section 3.4.2. The first section (4.2) investigates several control experiments in terms of photolysis, non-photocatalytic reaction of POM with PEG and the effect of pH on the stability of this non-photocatalytic reaction, to be used for identifying the best conditions of the photocatalytic reaction of POM with PEG in the second section.

The second section (4.3) investigates the combined effect of operating parameters (POM loading, pH and oxidant concentration) on the primary degradation of PEG and reaction kinetics based on a *CCED* to identify the optimal conditions of these operating parameters to be used later in the next chapter 5 (POM homogeneous PMR). The degradation pathway, formation of reaction intermediates and mineralization of PEG are considered.

4.2 Control experiments

4.2.1 Photolysis

The photolysis process (*no photocatalyst, UV only*) was examined to ascertain whether PEG can be effectively degraded under 180 min of photolytic time (Fig. 4.1). It can be seen that the selected oligomers LO, MO and HO were partially degraded by 5, 11 and 13% respectively. While for total PEG, it was 11%. This result confirms that UV alone has a limited effect on the degradation of PEG.

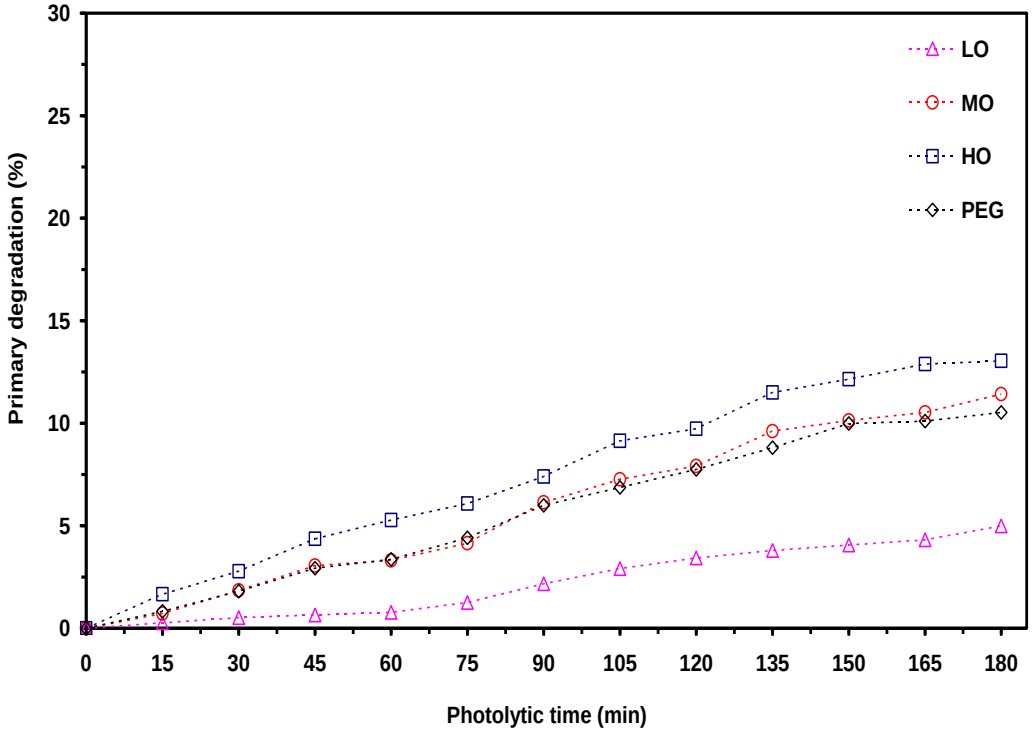

Fig. 4.1: Percentage primary degradation of PEG under photolysis process.

4.2.2 Non-photocatalytic reaction of POM with PEG

In literature, many POMs can react with some pollutants under dark condition (*no UV*) due to the mechanism of homogeneous-phase outer-sphere electron-transfer reactions between POM anions and organic or inorganic electron donors or acceptors **[94]**. So, several preliminary control experiments (without pH control) were carried out to examine the ability of POM to react with PEG under this condition. These experiments showed that POM-$H_3PW_{12}O_{40}$ has undergone a non-photocatalytic reaction with PEG. It was found that the concentration of PEG as well as POM decreased significantly within the first five minutes and then remained nearly constant for 180 min depending on the POM loading applied. One example of POM loading (0.35 mM) is shown in Fig. 4.2.

On one side of PEG, the selected oligomers LO, MO and HO were degraded by 9, 19 and 25% respectively when compared with total PEG (19%). *On the other side of POM*, it was decreased by 13%. The percentage consumption of POM increased with increasing its applied loading (Fig. 4.3) and followed a non-linear relationship (power model), for further data (see Fig. B1 in *Appendix B*). The reason for this is that POM loadings are proportional to the charge densities in the form $[PW_{12}O_{40}]^{3-}$ anions in which a higher POM loading has a greater charge density in comparison with a lower one and consequently increasing its consumption **[94]**.

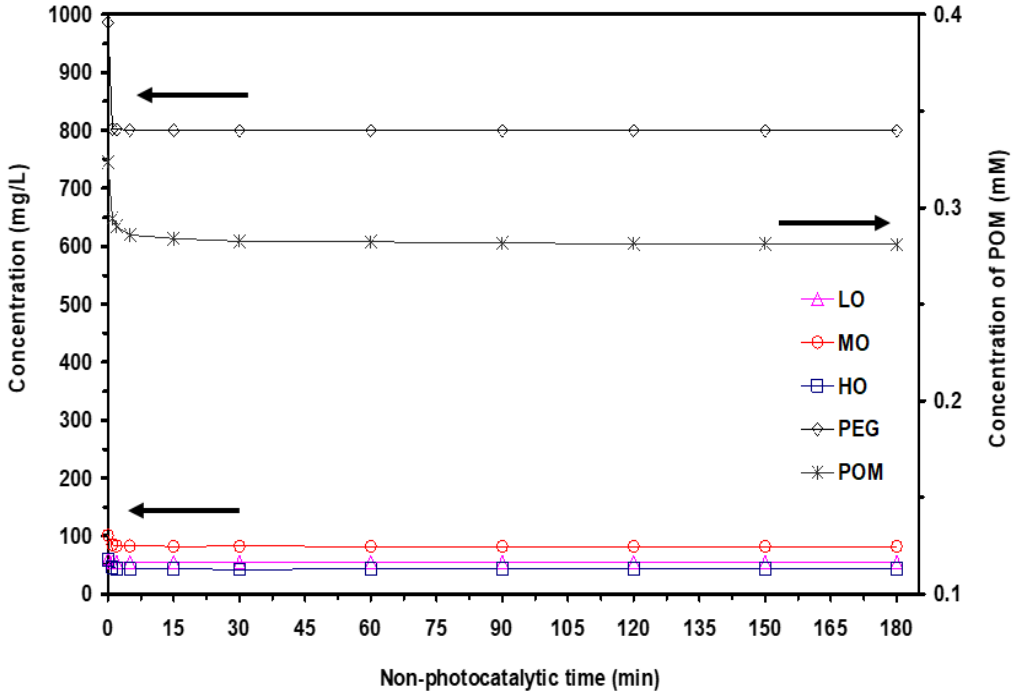

Fig. 4.2: The change in concentration of PEG and POM during a non-photocatalytic reaction at POM loading (0.35mM).

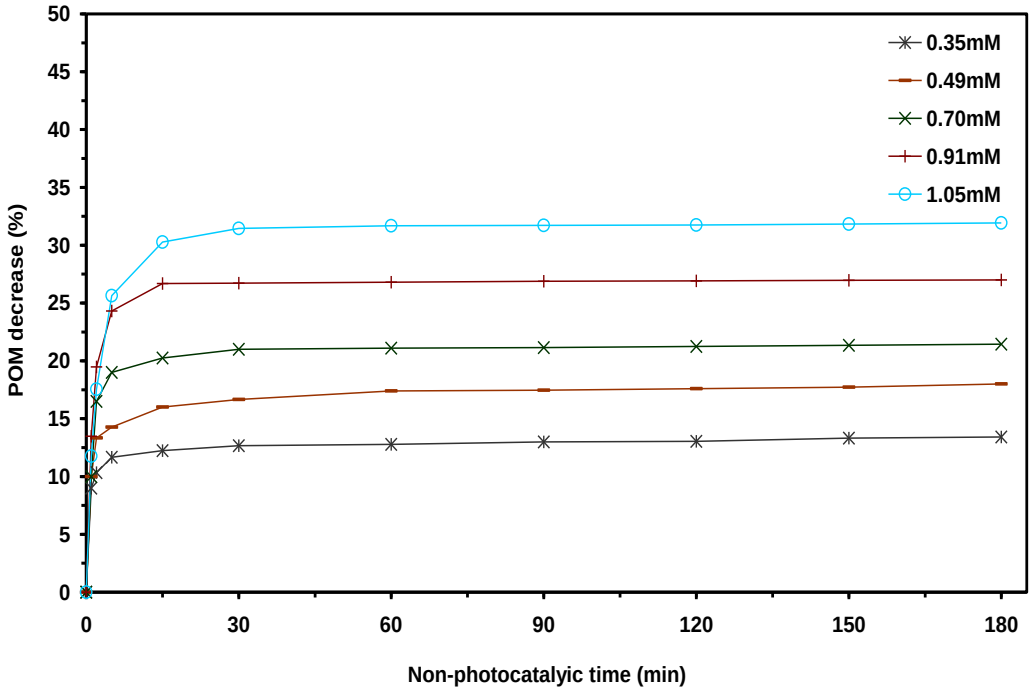

Fig. 4.3: Effect of a non-photocatalytic reaction of POM with PEG on the POM consumption (%) under various loadings.

4.2.3 Effect of pH on the non-photocatalytic reaction of POM with PEG and POM chemical stability

Homogeneous photocatalytic reactions are significantly pH-dependent **[173]**. Similarly, pH can affect non-photocatalytic reactions. As shown earlier, POM has undergone a non-photocatalytic reaction with PEG, so several experiments were performed to examine the effect of pH on this reaction stability.

In literature, POM homogeneous photocatalyst is stable in aqueous solution at pH 1 only **[95, 177]**. Above this value, POM can convert rapidly and reversibly to the lacunary species of tungsten element (*W*). Examination of a non-photocatalytic reaction of POM with PEG, pH 1, was carried out at a lower extreme level of POM loading (0.35 mM) where the actual pH of the prepared (PEG-POM) solution at this condition was ~3.1 (Fig. A8, *Appendix A*) and denoted as (PEG-POM) control in Fig. 4.4 (*no pH adjustment*) and then it was adjusted to be 1 using HCl.

In Fig. 4.4, at pH 1, the concentration of each oligomer MW ranging from 1097.6 to 1714 $gmol^{-1}$ decreased significantly to be below the MIDL of HPLC methodology (based on the sensitivity of the ELSD used) at MW ≥ 1758.1 $gmol^{-1}$. Under this condition, the LO, MO and HO were degraded by 53, 69 and 85% respectively in comparison with PEG-POM control. While for total PEG, it was degraded by 69%. These results confirm that the non-photocatalytic reaction between POM and PEG is greatly accelerated at pH 1. Also, it was observed that a white, thick and very sticky material was formed and it precipitated inside the BSR, which caused a significant reduction in POM concentration (see Fig. B2 in *Appendix B*). This can be potentially explained by the presence of chloride ions (Cl^-), which could further increase the charge densities of POM in the form $[PW_{12}O_{40}]^{3-}$ anions, and thus accelerating the non-photocatalytic reaction of POM with PEG oligomers via electron transfer mechanism **[94]**. This explanation is confirmed by another experiment (the addition of HCl to PEG reactant solution, pH 1, without using POM). It was found that there was no effect in terms of the reduction of PEG oligomers concentration under this condition. Confirming that chloride ions alone cannot react with the PEG oligomers via electron transfer mechanism as like POM, and thus strengthening the explanation mentioned above.

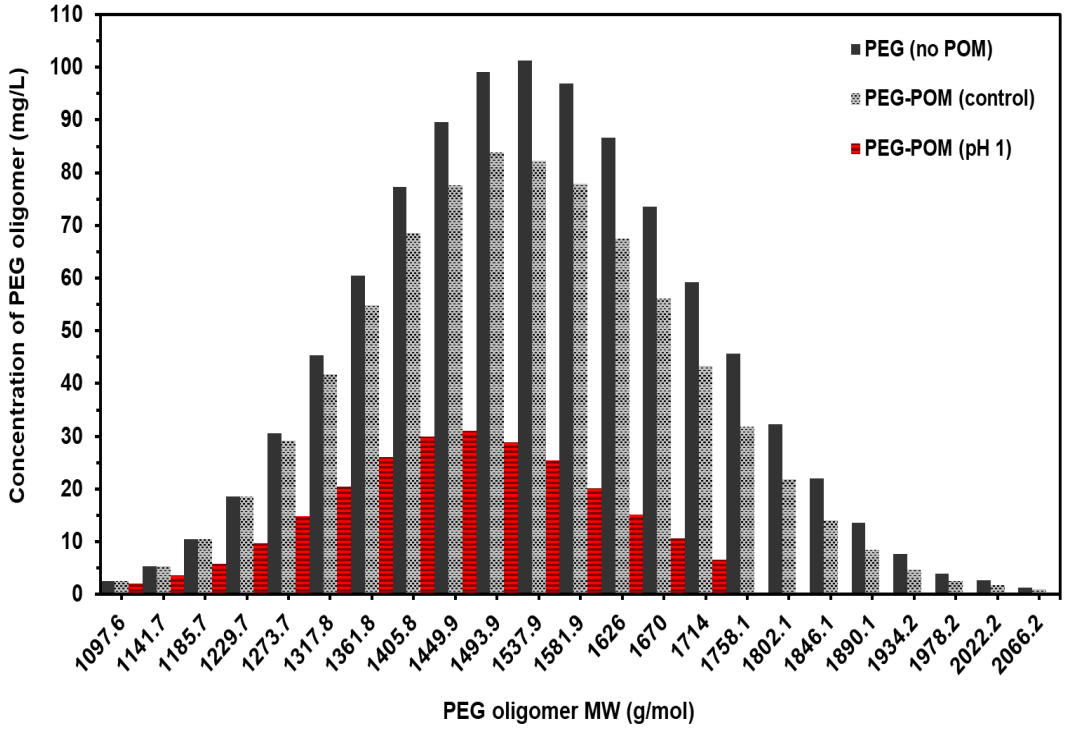

Fig. 4.4: Effect of pH condition on POM non-photocatalytic reaction with PEG, loading (0.35 mM) and oxidant concentration (42 mgO_2L^{-1}) for 30 min.

In terms of the chemical stability of POM under the examined condition (pH 1), it was found that the original POM-$H_3PW_{12}O_{40}$ in the form $[PW_{12}O_{40}]^{3-}$ decomposed partially into several lacunary species by HPLC-ESI-TOF analysis (results shown later). Surprisingly, this finding is totally different from the literature where POM should be chemically stable at pH 1. This decomposition of POM into several lacunary species may be related to the non-photocatalytic reaction of POM with PEG, affecting the chemical structure of POM by the electron-transfer mechanism. However, *this is just a prior claim*, and further investigation is required before any conclusive reason can be given.

To achieve this, an extensive investigation was achieved to examine the chemical stability of POM under different conditions including POM in aqueous solution without control pH (*case* 1), POM in aqueous solution at pH 1 (*case* 2), POM in PEG reactant solution without control pH (*case* 3) and POM in PEG reactant solution at pH 1 (*case* 4). These cases were experimentally carried out at PEG (1 gL^{-1}) and POM (0.35 mM-1 gL^{-1}).

The experimental results of these investigated cases in terms of HPLC-ESI-TOF chromatograms are shown in Fig. 4.5. It is clear to see from Fig. 4.5 that POM-$H_3PW_{12}O_{40}$ in the form $[PW_{12}O_{40}]^{3-}$ decomposed into several lacunary species in all investigated cases. *These are very strange results and totally different from reported literature in this regard*.

Now, these obtained results in Fig. 4.5 are still a subject of debate when comparing with the published literature. In order to give consecutive reasons behand these results, first of all, we will

start discussing the chemical stability of POM, in aqueous solution and in reactant solution, with specific literature in this respect as follows.

1) In terms of POM in aqueous solution

In literature, *Zhu et al.,* **[95]** investigated the decomposition of POM ($H_3PW_{12}O_{40}$) in aqueous solution under a wide range of pH (1-12). The prepared solution at pH 1 was obtained by adding a certain weight of POM (288 g) in 1 L water. Under this condition, the final concentration of solution was 0.1 M. After this stage, the pH was adjusted with 0.2 N NaOH. They found that POM is stable at pH 1 (*no decomposition of POM*). When pH increased from 1.1 to 12, POM decomposed gradually into various lacunary species as shown in Table 4.1. This finding in terms of a full stability of POM at pH 1 is similar to that reported by a well-known reference in literature, *Pope* **[177]**.

One possible explanation for this stability of POM at pH 1 is related to a higher concentration of used POM when compared with our prepared concentration (0.35 mM-1 gL^{-1}) at *case* 1. This implies that POM is stable under a restricted condition only, *in particular*, when using a massive concentration of POM to get a pH 1 without using any chemical adjustments.

Experimental results of HPLC-ESI-TOF chromatograms in Fig. 4.5 show that POM is not stable in aqueous solution under *case* 1 (no pH control) and *case* 2 (pH 1). Concluding that a fair comparison based on pH 1 between the obtained results from *case* 2 with that of *Zhu et al.,* is not valid. In practical point of view, it is impossible to use this higher concentration to get a stable POM at pH 1, in particular with photocatalysis due to the significant effect of light scattering.

In conclusion, the work was achieved by Zhu et al., and Pope is solely an investigation of POM chemical stability in aqueous solution. Therefore, this study cannot be dependent in terms of POM in reactant solution based on photocatalysis process as is explained below.

Table 4.1: Effect of pH on the decomposition of POM-$H_3PW_{12}O_{40}$ **[95]**.

pH	Principal components
1.0	$[PW_{12}O_{40}]^{3-}$
2.2	$[PW_{12}O_{40}]^{3-}$, $[P_2W_{21}O_{71}]^{6-}$, $[PW_{11}O_{39}]^{7-}$
3.5	$[PW_{12}O_{40}]^{3-}$, $[P_2W_{21}O_{71}]^{6-}$, $[PW_{11}O_{39}]^{7-}$, $[P_2W_{18}O_{62}]^{6-}$, $[P_2W_{19}O_{67}]^{10-}$
5.4	$[P_2W_{21}O_{71}]^{6-}$, $[PW_{11}O_{39}]^{7-}$, $[P_2W_{18}O_{62}]^{6-}$
7.3	$[PW_9O_{34}]^{9-}$
8.3	PO_4^{3-}, WO_4^{2-}

2) In terms of POM in reactant solution

In literature, several authors who controlled pH at 1 in order to get a full chemical stability of POM ($H_3PW_{12}O_{40}$) in reactant solution under POM homogeneous photocatalysis process such as *Jun Bo* **[107]** used perchloric acid ($HClO_4$) to adjust 10 mgL^{-1} of prepared solution of methylene orange (MO) with POM loadings (0.1-1 gL^{-1}). *Hu and Xu* **[25]** used $HClO_4$ to adjust 0.06 mM of textile dye (X3B) solution with POM loadings (0.1-0.6 gL^{-1}). *Antonaraki et al.,* **[100]** used 0.1 M $HClO_4$ to adjust various types of chlorophenols (CPs) at 0.4 mM with POM loading (2 gL^{-1}). *Troupis et al.,* **[24]** used $HClO_4$ to adjust naphthol blue black (NB) solution at 0.05 mM with POM loading (0.7 gL^{-1}). *Kormali et al.,* **[27]** used 0.1 M $HClO_4$ to adjust various reactant solutions of atrazine (0.07 mM), fenitrothion (0.05 mM), 4-chlorophenol (0.1 mM) and 2,4-dichlorophenoxyacetic acid (0.07 mM) with POM loading (2 gL^{-1}).

These authors claimed that POM is chemically stable, *at pH 1 using either HCl or $HClO_4$,* depending on published literature like *Zhu et al.,* **[95]** and *Pope* **[177]**, and other researchers who used a secondary referencing relating to *Zhu et al., and Pope.* They did not try to confirm experimentally the chemical stability of POM in their reactant solutions under the examined conditions. ***Therefore, their claims in terms of POM is chemically stable at pH 1 without proper experimental evidences are dubious.*** This might be a misconception in terms of comparing their studies (**POM in reactant solution**) with that of *Zhu et al.,* and *Pope* (**POM in aqueous solution**) and/or lack in particular with experimental techniques to testify the chemical stability of POM.

When comparing their results with that of *Zhu et al.,* it can be seen that they used a limited range of POM loadings from 0.1 to 2 gL^{-1} compared with that used by *Zhu et al.,* (288 gL^{-1}). Under this range, they adjusted the pH of reactant solution to be 1 using either HCl or $HClO_4$, and thus their studies are absolutely different from *Zhu et al*. Accordingly, this is most likely an unfair comparison. It can be recommended that a restricted stability of POM in aqueous solution at pH 1 only obtained by *Zhu et al*., and *Pope* should not be generalized to be a well-known principle in literature for POM homogeneous photocatalysis.

Experimental results of HPLC-ESI-TOF chromatograms in Fig. 4.5 show that POM is not stable in PEG reactant solution under *case* 3 (no pH control) and its decomposition increased significantly under pH 1 (*case* 4). This finding is expected since POM in aqueous solution under *case* 1 (no pH control) and *case* 2 (pH 1) was not stable.

In terms of the HPLC-ESI-TOF intensity (counts per second, cps), Fig. 4.5, it should be noted that POM in the form $[PW_{12}O_{40}]^{3-}$ was significantly affected under pH 1 of *case* 2 and *case* 4 when compared with that of *case* 1 and *case* 3 respectively. This means that the stability of POM in the form $[PW_{12}O_{40}]^{3-}$ at pH 1 is so weak and it decomposed greatly into many lacunary species. As shown

in literature **[91]**, POM ($H_3PW_{12}O_{40}$) can be prepared by the reaction of sodium tungstate ($Na_2WO_4.{}_2H_2O$) with phosphoric acid (H_3PO_4) acidified with HCl. It seems that the presence of HCl played a negative role in its chemical structure and stability.

In the current research, in order to avoid any influence of HCl on the POM non-photocatalytic reaction with PEG and the chemical stability of POM, it was decided to select a new pH range. As shown earlier, the actual pH of prepared (PEG-POM) solution at a POM loading (0.35 mM) was~3.1. So, the pH was selected to be higher than this value between 3.3 to 8 using NaOH.

The effect of pH 3.3 and pH 8 on the POM non-photocatalytic reaction with PEG was studied. It was found that there is no significant difference in the concentration of the 23 identified PEG oligomers. Similarly, the concentration of POM under these conditions did not change.

In terms of chemical stability of POM in PEG reactant solution under these pH conditions, it was investigated at pH 3.3 (*case* 5), pH 5 (*case* 6) and pH 8 (*case* 7) as shown in HPLC-ESI-TOF chromatograms (Fig. 4.6). Investigation on the stability of POM in the form $[PW_{12}O_{40}]^{3-}$ in Fig. 4.6 shows that its intensity (cps) decreased significantly with increasing the pH from 5 to 8, indicating that the decomposition of POM into several lacunary species increased accordingly. From the obtained results in terms of POM non-photocatalytic reaction with PEG and POM chemical stability at NaOH conditions, ***the range of pH was selected from 3.3 to 5 in the coming section (photocatalytic reaction of POM with PEG)***.

Overall, in the current investigation, POM ($H_3PW_{12}O_{40}$) in the form $[PW_{12}O_{40}]^{3-}$ is not stable in aqueous solution and PEG reactant solution, it can convert partially into various lacunary species. The identification of names of these lacunary species is so complex and difficult that are required specific analytical techniques as reported in literature **[177]**. However, some lacunary species like $[PW_{11}O_{39}]^{7-}$ and $[P_2W_{21}O_{71}]^{6-}$ were identified by the methodology shown in chapter 3, section 3.2.5. These identified lacunary species and other unidentified lacunary species of *W* have a high oxidizing ability **[33, 34, 155]**. It is important to mention that POM in the form $[PW_{12}O_{40}]^{3-}$ is still dominant in the selected range of pH so far and will be expected to play a significant role with other lacunary species of *W* under UV reaction in the section below.

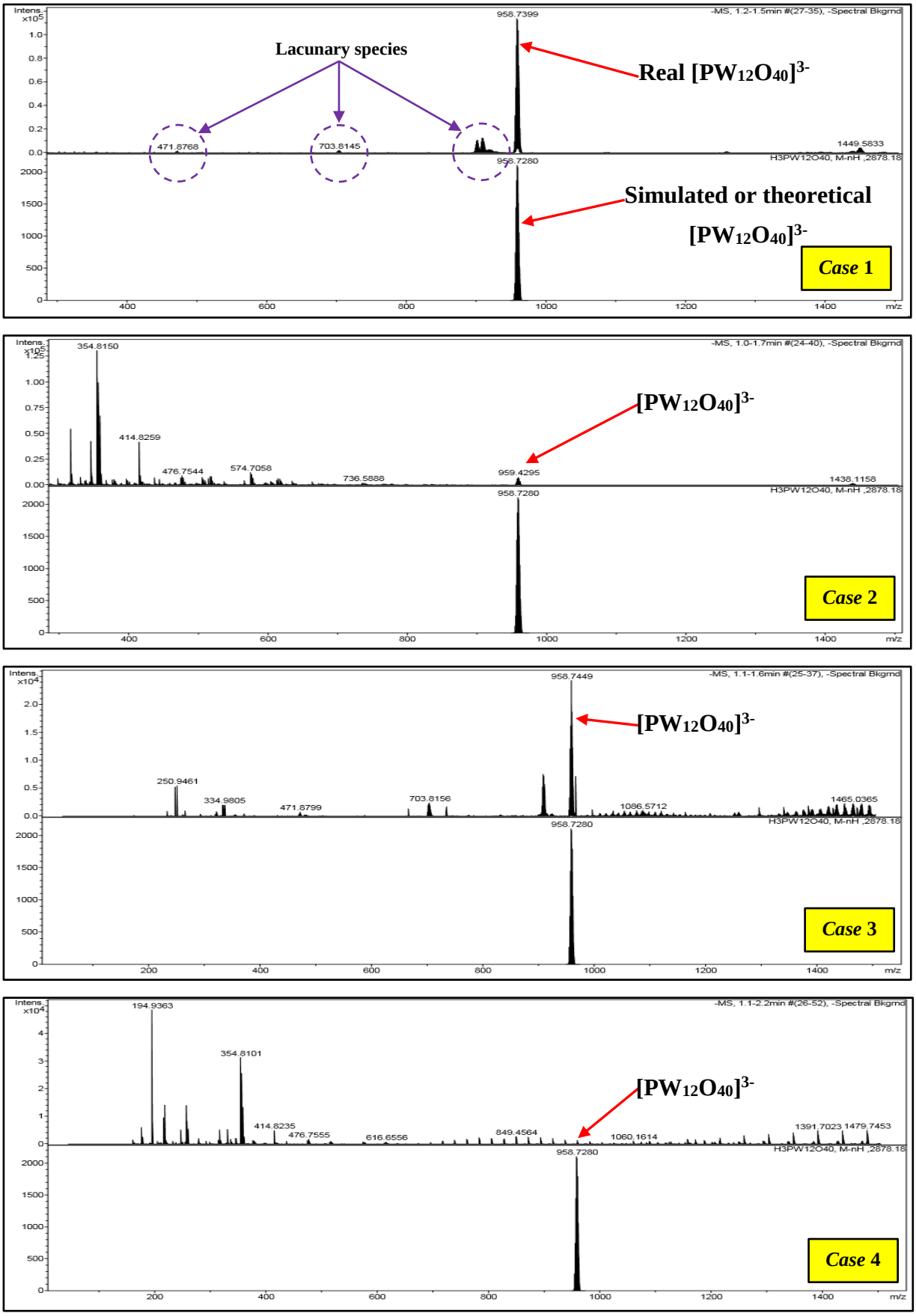

Fig. 4.5: HPLC-ESI-TOF chromatograms for the investigation of chemical stability of POM under case 1: POM in aqueous solution, case 2: POM in aqueous solution at pH 1, case 3: POM in PEG reactant solution and case 4: POM in PEG reactant solution at pH 1.

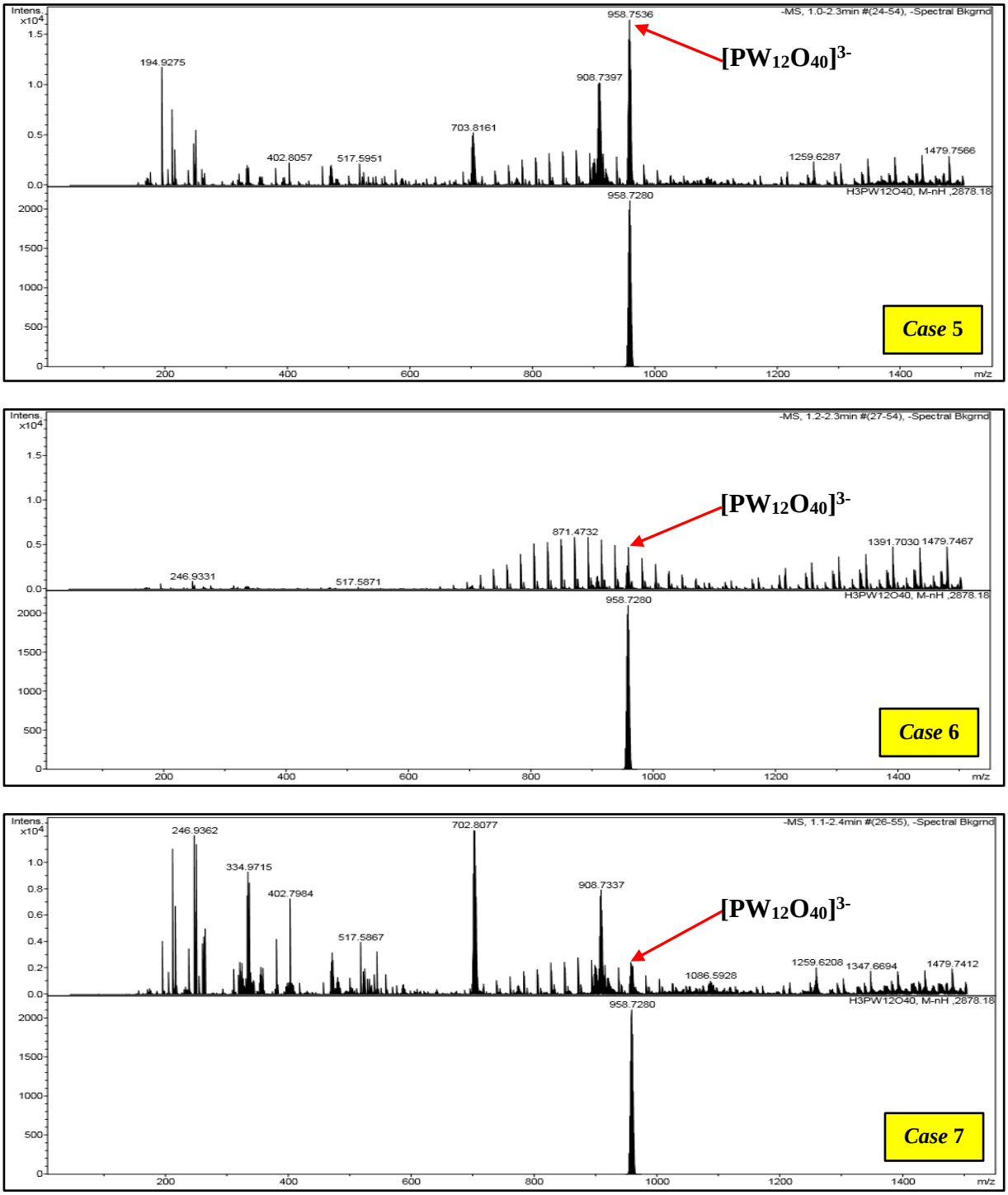

Fig. 4.6: HPLC-ESI-TOF chromatograms for the investigation of chemical stability of POM in PEG reactant solution under pH 3.3 (*case* 5), pH 5 (*case* 6) and pH 8 (*case* 7).

4.3 Photocatalytic reaction of POM with PEG

The effect of operating parameters including POM loading (0.35-1.05mM), pH (3.3-5) and oxidant concentration (14-58.65 mgO_2L^{-1}) on the selected response functions (%PD and K_{app}) of POM photocatalysis of PEG was investigated by a *CCED*. A complete *CCED* with the obtained experimental results and the additional experiments performed to obtain the optimal conditions are shown in Table 4.2. These experimental results were fitted with a *NN* to simulate the effect of these parameters on response functions as shown in Fig. B3 (*Appendix B*) after the end of photocatalytic treatment time (180 min). The equations and fitting parameters are shown in Table B1 (*Appendix B*).

Table 4.2: Three factors of *CCED* matrix for POM homogeneous photocatalysis of PEG.

Factorial design				***Response function***									
Exp.	**POM (mM)**	**pH**	**Oxidant (mgO_2L^{-1})**	**Primary degradation (%)**				**K_{app} (min^{-1})**				**TOC removal (%)**	**VFA (mgL^{-1})**
				LO	***MO***	***HO***	***Total PEG***	***LO***	***MO***	***HO***	***Total PEG***		
1	0.91	4.66	58.65	17.40	33.20	52.30	32.11	0.0010	0.0023	0.0042	0.0020	5.88	30.85
2	0.49	4.66	58.65	20.86	42.10	65.10	41.24	0.0013	0.0028	0.0054	0.0027	4.96	20.23
3	0.91	3.65	58.65	26.88	54.00	74.70	51.87	0.0019	0.0048	0.0081	0.0043	3.39	35.87
4	0.49	3.65	58.65	35.24	61.60	79.62	57.99	0.0025	0.0055	0.0100	0.0056	2.38	31.28
5	0.91	4.66	25.35	20.51	36.70	55.23	35.81	0.0012	0.0027	0.0045	0.0025	5.66	26.83
6	0.49	4.66	25.35	23.66	44.98	68.56	43.98	0.0015	0.0030	0.0057	0.0031	3.67	24.25
7	0.91	3.65	25.35	40.65	64.53	80.99	57.40	0.0029	0.0056	0.0086	0.0050	4.58	35.87
8	0.49	3.65	25.35	46.95	69.99	84.56	68.98	0.0033	0.0065	0.0110	0.0063	4.19	26.11
9	1.05	4.15	42.00	21.18	43.65	63.26	42.38	0.0015	0.0033	0.0059	0.0032	3.88	29.99
10	0.35	4.15	42.00	43.19	63.00	82.49	62.05	0.0031	0.0060	0.0095	0.0060	3.09	22.81
11	0.70	5.00	42.00	17.04	33.17	49.01	31.93	0.0010	0.0021	0.0037	0.0020	2.44	24.96
12	0.70	3.30	42.00	40.01	60.96	79.98	60.05	0.0029	0.0057	0.0089	0.0059	2.97	36.44
13	0.70	4.15	70.00	20.90	33.50	50.10	31.99	0.0012	0.0026	0.0042	0.0025	4.62	24.82
14	0.70	4.15	14.00	23.50	36.55	56.51	38.56	0.0015	0.0030	0.0047	0.0029	4.98	25.68
15	0.70	4.15	42.00	22.00	34.89	53.99	33.53	0.0014	0.0028	0.0044	0.0028	3.77	27.00
16	0.70	4.15	42.00	21.46	33.77	54.00	34.11	0.0013	0.0027	0.0043	0.0027	3.77	26.50
17	0.70	4.15	42.00	22.50	34.19	55.32	35.06	0.0014	0.0028	0.0044	0.0028	3.77	26.95
18	0.70	4.15	42.00	21.33	33.65	53.00	33.09	0.0013	0.0027	0.0043	0.0027	3.77	26.33
Additional experiments for determination of optimum conditions													
19	0.35	3.30	14.00	49.18	80.98	93.22	72.78	0.0035	0.0076	0.0119	0.0068	3.65	39.02
20	0.49	3.30	14.00	46.83	75.11	88.31	70.91	0.0033	0.0069	0.0100	0.0058	3.43	36.73
21	0.70	3.30	14.00	40.12	68.20	80.30	68.31	0.0031	0.0057	0.0088	0.0050	3.15	35.58
22	0.91	3.30	14.00	36.33	60.81	70.11	63.05	0.0027	0.0048	0.0079	0.0042	2.99	33.30
23	1.05	3.30	14.00	33.82	54.50	65.20	53.41	0.0022	0.0042	0.0073	0.0036	2.74	37.30
24	0.17	3.30	14.00	41.60	71.60	86.80	68.08	0.0032	0.0068	0.0090	0.0065	3.26	35.87

Coded levels				***Levels***
(+α)	1.05	5.00	70.00	Superior extreme
(+1)	0.91	4.66	58.65	Superior level
(0)	0.70	4.15	42.00	Central point
(-1)	0.49	3.65	25.35	Lower level
(-α)	0.35	3.30	14.00	Lower extreme

4.3.1 Primary degradation

1) Effect of POM loading and pH

An example of the effect of POM photocatalysis on the degradation of total PEG and selected oligomers is shown in Fig. 4.7. It can be seen that the %PD of HO is higher than MO and LO. The behavior of primary degradation for all investigated conditions (Table 4.2) was found in the following order: HO > MO > LO.

In terms of polymers' degradation, this behavior is generally expected where *Guo et al.,* **[7]** and *Santos et al.,* **[9]** showed that higher MW oligomers of PEG3550 degraded rapidly into lower MW oligomers under UV/H_2O_2 process due to increasing the number of polymer chain scissions by UV irradiation, and thus lowering the average molar masses of the polymer. Also, this behavior could be explained by the separation mechanism of RI-HPLC/ELSD method based on the competition between the solubility of MW of each PEG oligomer in the mobile phase and the selective adsorption on the C18 column. The higher the MW of PEG oligomer, the longer the non-polar chain and the more non-polar the PEG oligomer becomes, and thus prolonging the retention time **[214, 234]**. Higher MW oligomers tended to be initially degraded by a considerable reduction in height of their peaks with longer retention times, and thus reducing the calculated area and then the final concentration of each oligomer accordingly, (see the resulting HPLC chromatograms in Fig. B4, *Appendix B*).

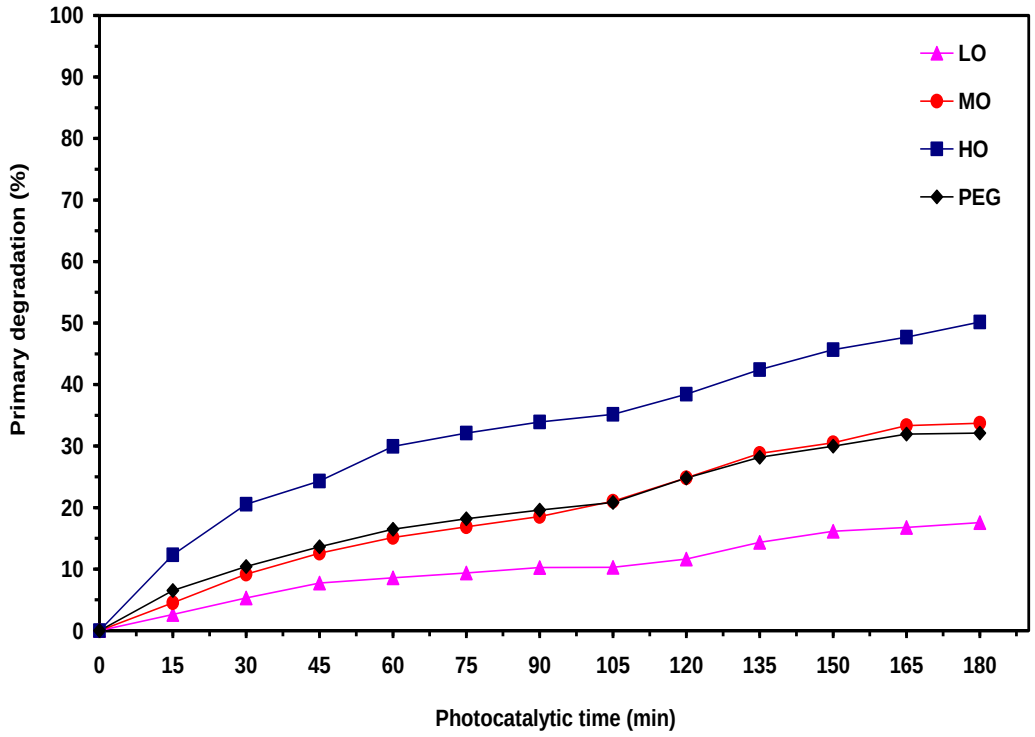

Fig. 4.7: Percentage primary degradation of PEG under POM homogeneous photocatalysis: loading (0.91mM), pH (4.66) and oxidant concentration (58.65 mgO_2L^{-1}).

A simulation influence of POM loading and pH on the %PD of PEG, based on the obtained results in Table 4.2, is shown in Fig. 4.8. It can be observed from Fig. 4.8 (a-c) that the %PD of the LO, MO and HO decreased with increasing POM loading and pH. A similar trend was observed for the total PEG (Fig. 4.8-d). There are two possible explanations for this:

Firstly, in terms of POM homogeneous photocatalysis, POM photocatalytic activity decreased gradually with the increase of loading, meaning that POM reached a critical level of photon capture and consequently its photocatalytic activity decreased as well **[24, 25, 38]**. In this regard, a lower extreme level of POM loading (0.35mM) as highlighted in red in Fig. 4.8 (a-d) showed the maximum %PD corresponding to the pH of 3.3. This indicates that further investigation is required below this loading to identify exactly the optimum loading, this is shown in section 4.3.3 later.

Secondly, since homogeneous photocatalytic reactions are affected by pH **[173]**, the potential oxidation of $HO^{\bullet}$ formed during these reactions decreases significantly with increasing pH. Generally, the oxidation of PEG decreased under alkaline (NaOH) conditions because of the deprotonation of $HO^{\bullet}$ under these conditions **[235]**.

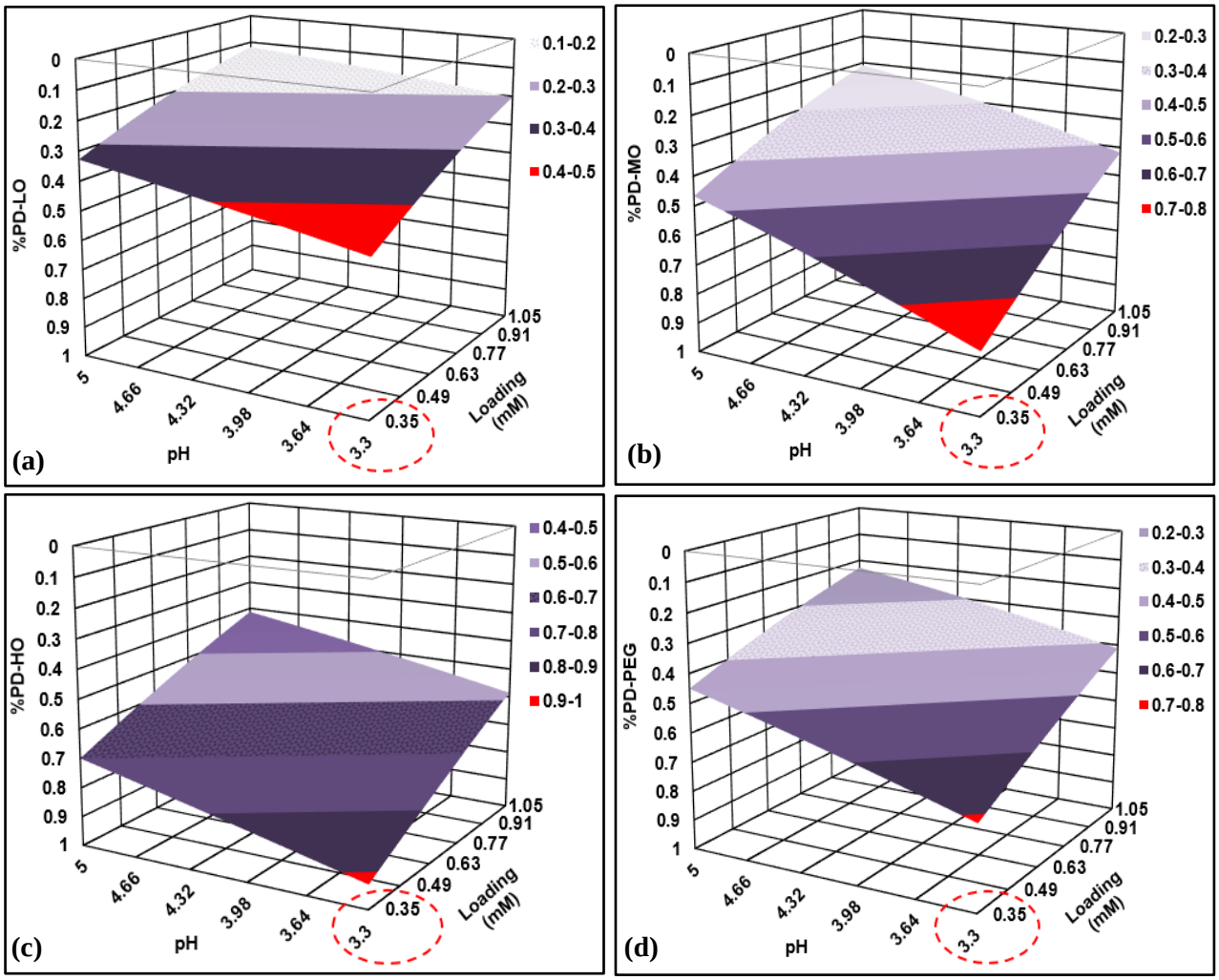

Fig. 4.8: NN simulation of percentage primary degradation under two operating conditions, POM loading (mM) and pH: (a) LO, (b) MO, (c) HO and (d) total PEG.

2) Effect of POM loading and oxidant concentration

The interaction effect of POM loading and oxidant concentration on the %PD of PEG is shown in Fig. 4.9. It shows that increasing the oxidant concentration (>14 mgO_2L^{-1}) led to a decrease in the %PD of LO, MO, HO and total PEG. This could be explained by the fact that dissolved molecular oxygen (DO) could hinder the photodegradation by acting as '*inner filter*'. DO could absorb UV in the range 185-254 nm, reducing considerably the UV light intensity in the photoreactor and then the photocatalytic degradation **[170, 236]**. On the other hand, the oxidant concentration of 14 mgO_2L^{-1} corresponding to the POM loading of 0.35 mM as shown with dashed red circle in Fig. 4.9 (a-d) has a positive effect on the %PD of PEG where the maximum %PD is achieved at this level.

Apart from the inner filter effect, DO plays a significant role in POM homogeneous photocatalysis where as shown in chapter 2, the reduced POM cluster POM^- can react with DO to form superoxide radical ions ($O_2^{\cdot -}$), which are able to further react with organic pollutants, thus increasing the overall primary degradation **[21, 89, 102, 235]**. It is important to mention that as shown in chapter 3, section 3.4.2.2, a lower extreme level of oxidant concentration (14 mgO_2L^{-1}) was achieved by the oxygenation of the PEG reactant solution through mass transfer from ambient air without supplying a continuous oxygen feed. The obtained results at 14 mgO_2L^{-1} confirmed that the DO at this concentration is so enough to sustain the POM photocatalytic reactions of PEG for 180 min.

It becomes evident that these results would support the selection of optimal conditions and suggest that the oxidant concentration of 14 mgO_2L^{-1} should be considered to avoid the effect of inner filter.

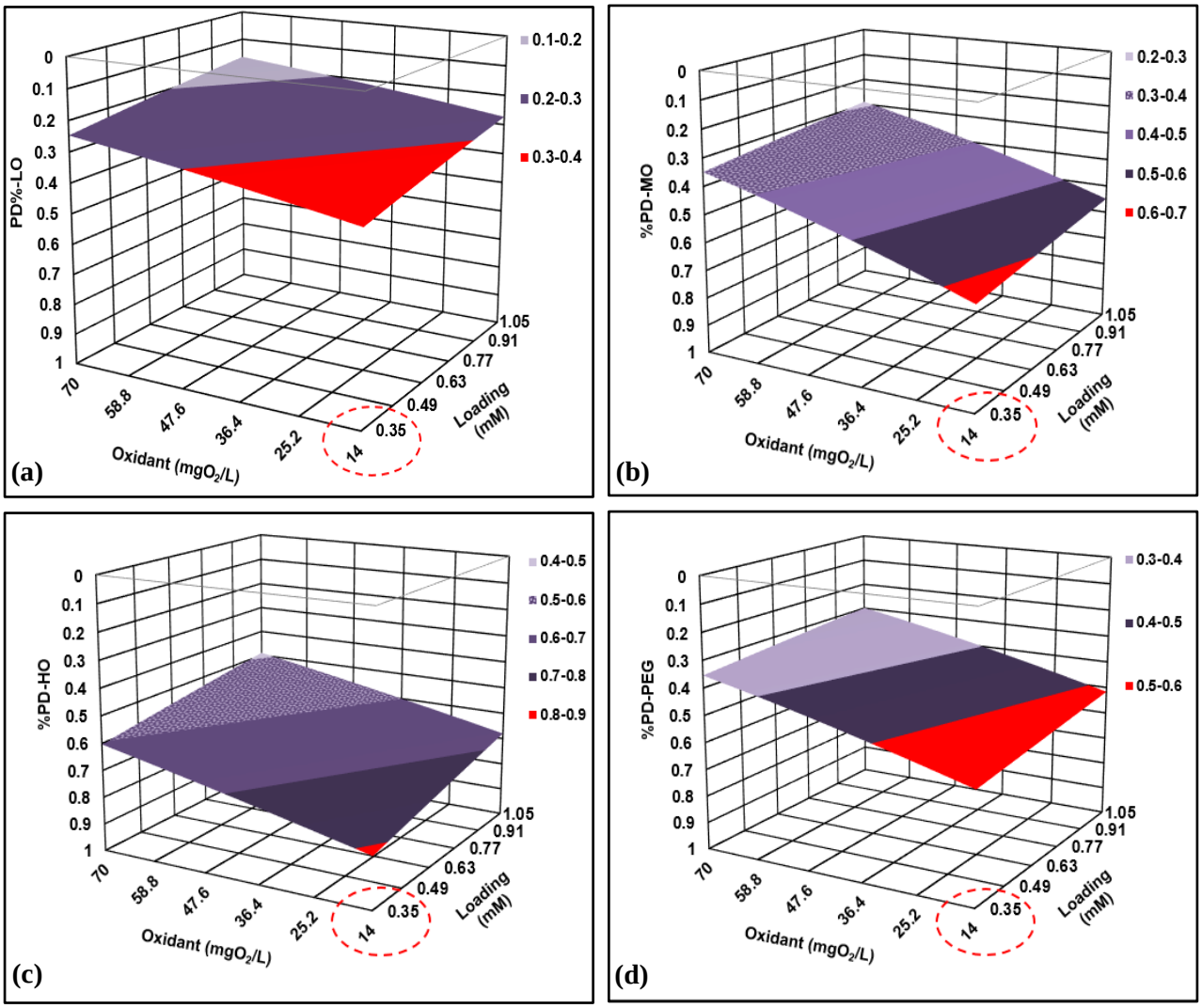

Fig. 4.9: NN simulation of percentage PEG degradation under two operating conditions, POM loading (mM) and oxidant concentration (mgO_2L^{-1}): (a) LO, (b) MO, (c) HO and (d) total PEG.

The influence of saliency analysis as percentage on operating parameters as input variables for three selected oligomers and total PEG using a *NN* to deduce the effect of each investigated parameter on primary degradation as a response function is shown in Table 4.3. This analysis confirms that the primary degradation of these oligomers and total PEG was mainly influenced by the pH and then POM loading, while the oxidant was a less significance.

Table 4.3: Saliency analysis of %PD of PEG under POM homogeneous photocatalysis.

Oligomer	*Influence*		
	pH	**POM (mM)**	**Oxidant (mgO_2L^{-1})**
LO	52.9	26.3	20.8
MO	48.4	40.6	11.0
HO	49.3	31.2	19.5
Total PEG	47.7	40.5	11.8

Further investigation using the combined effect of pH and oxidant concentration (*without POM loading*) on %PD of total PEG (Fig. 4.10) shows that decreasing the pH and oxidant concentration causes an increase in the %PD. A similar trend was also observed for the three selected oligomers (see Fig. B5 in *Appendix B*). These results confirmed the earlier findings in terms of pH (3.3) and oxidant concentration (14 mgO_2L^{-1}) that would be supportive in prediction of the optimal conditions.

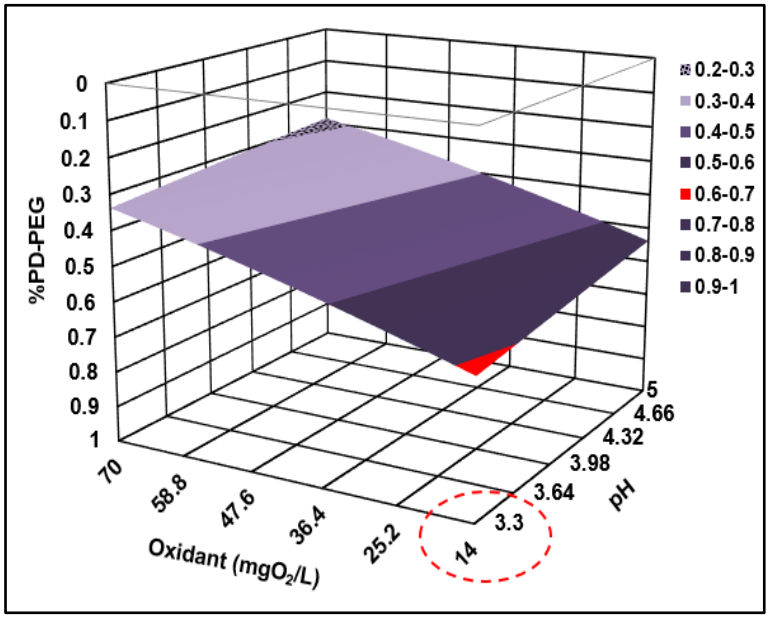

Fig. 4.10: *NN* simulation of %PD on the total PEG under pH and oxidant concentration (mgO_2L^{-1}).

4.3.2 Reaction kinetics

A kinetic reaction analysis of POM photocatalytic degradation on three selected PEG oligomers and total PEG was examined based on a simplified Langmuir-Hinshelwood (L-H) kinetic model Eq. (4.1), which is commonly used in photocatalysis process under low dilute reactant concentration **[65]**. A linear relationship was observed for all investigated photocatalytic data of first order logarithmic kinetic plots, an example data fit is shown in Fig. B6 (*Appendix B*), indicating that the photodegradation of PEG oligomers as well as total PEG followed the pseudo-first order reaction kinetic model. This model is more mechanistically applicable fit for POM photocatalysed reactions **[23, 39, 100]**. The validity of this model was tested with the experimental data (Fig. 4.11) and it gave a good fit with a percent deviation (≤ 1%) for all investigated cases.

Note that the annular photoreactor in the current project showed an induction period at the start (0-15 min), which is common in radical reactions **[237]**. As the induction period does not represent the true degradation kinetics, the first data point was excluded from fitting. The values of K_{app} for three selected oligomers and total PEG as a function of operating parameters investigated are tabulated in Table 4.2.

$$\ln C_i = -K_{app}t + \ln C_{oi} \quad (4.1)$$

Where C_i is the concentration of selected PEG oligomer in (mgL^{-1}) at any time of reaction, C_{oi} is the concentration of selected PEG oligomer after adsorption period in (mgL^{-1}) and k_{app} is a pseudo-first order reaction constant (min^{-1}). Also, the same Eq. (4.1) was used for the total PEG.

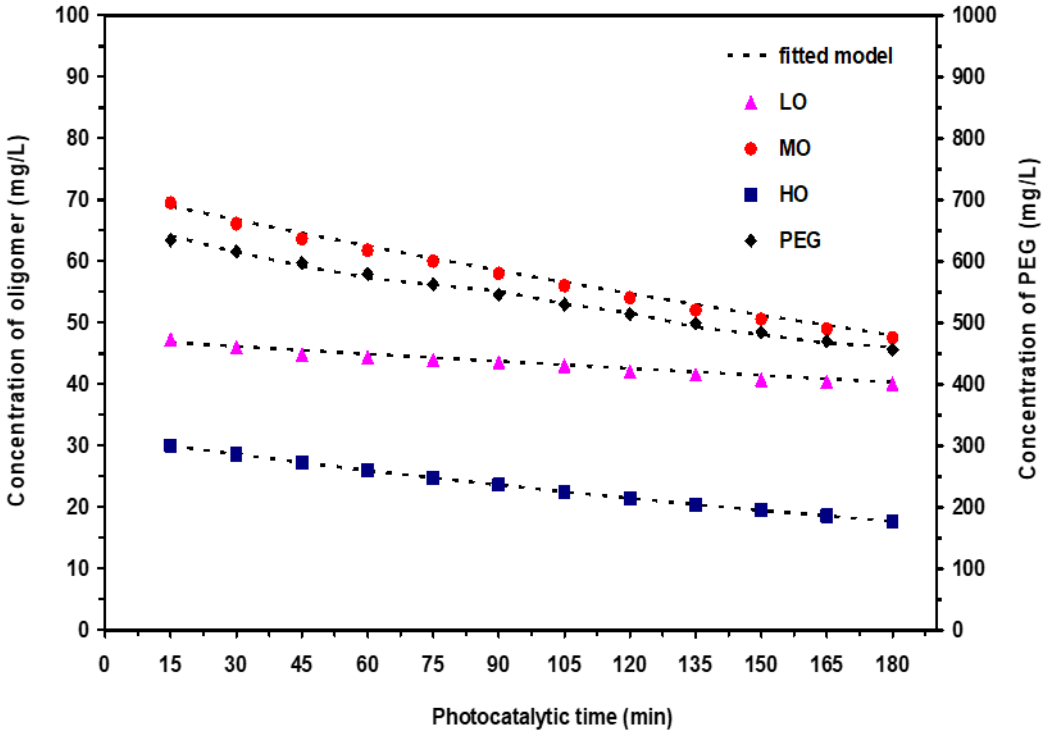

Fig. 4.11: Experimental photocatalytic data of PEG fitted with pseudo-first order model at induction period (15 min), POM loading (0.91 mM), pH (4.66) and oxidant concentration (58.65 mgO_2L^{-1}).

In order to further investigate a reaction kinetics, the rate of reaction (r, $mgL^{-1}.min^{-1}$) was calculated using the integrated rate method **[238]**. Fig. 4.12 shows that for three investigated oligomers, the reaction rate increased almost linearly with the increase in the concentration of each oligomer. A similar trend (a linear relationship) for the total PEG was found. Thus, this relationship confirms exactly the pseudo-first order kinetic model calculated mathematically by Eq. (4.1).

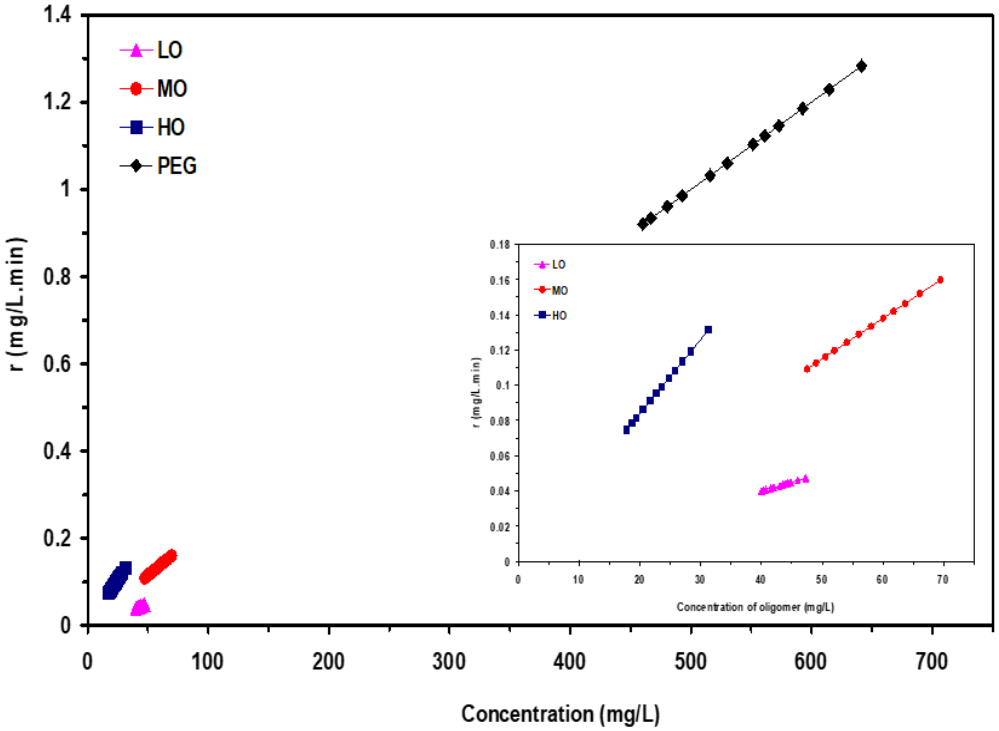

Fig. 4.12: Investigation on the reaction rate as a function of the concentration of selected oligomers and total PEG, POM loading (0.91mM), pH (4.66) and oxidant concentration (58.65 mgO_2L^{-1}) with enlarged view of plot in bottom right hand corner.

Fig. 4.13 shows that the reaction rate of LO, MO, HO and total PEG decreases as the photocatalytic time increases. For example, the initial reaction rates of LO, MO and HO at 15 min were 0.047, 0.160 and 0.131 $mgL^{-1}.min^{-1}$ respectively, while the final reaction rates at 180 min were 0.040, 0.109 and 0.075 $mgL^{-1}.min^{-1}$ respectively. For total PEG, the reaction rate is higher than that of these oligomers and was at 15 min (1.283 $mgL^{-1}.min^{-1}$) and 180 min (0.920 $mgL^{-1}.min^{-1}$).

Generally, the reaction rate was found for each investigated oligomer to be in the following order: MO>HO>LO. The reaction rate constant is independent of the concentration, but the rate of reaction is dependent on the concentration **[238]**. So, this order is expected since the starting individual concentration of each oligomer is not equal as shown in Fig. 4.12, and thus the rates of reaction of each oligomer and total PEG were higher at the start of reaction due to higher concentrations and then decreased with increasing time (Fig. 4.13).

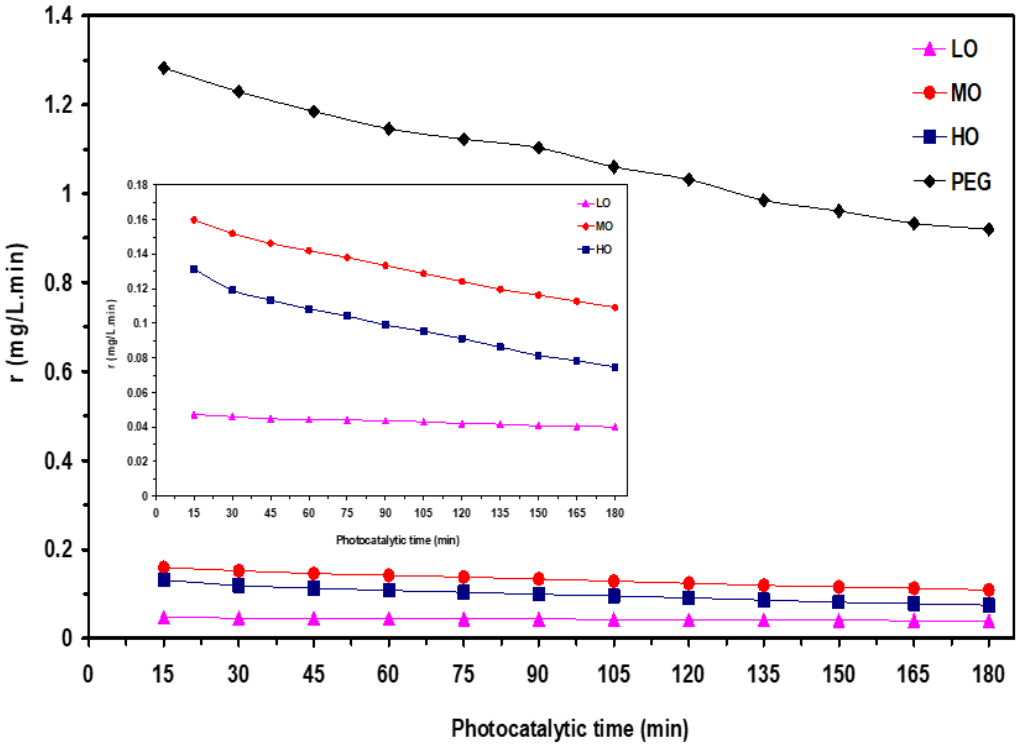

Fig. 4.13: Investigation on the reaction rate as a function of photocatalytic time, POM loading (0.91mM), pH (4.66) and oxidant concentration (58.65 mgO_2L^{-1}) with enlarged view of plot in bottom left hand corner.

The interaction effect of various combined operating parameters on K_{app} was examined for LO, MO, HO and total PEG. One example of this effect, *for total PEG*, is shown in Fig. 4.14. It appears that K_{app} increases with decreasing the POM loading and pH (Fig. 4.14-a), POM loading and oxidant concentration (Fig. 4.14-b) and oxidant concentration and pH (Fig. 4.14-c). Similar observations were found for the effect of these parameters on LO, MO and HO (see Fig. B7 in *Appendix B*).

The general trend of these results is similar to that of primary degradation based on the same effect of these parameters, as a result K_{app} follows the same order of HO > MO > LO as shown in Table 4.2. Similarly, in terms of the saliency analysis, K_{app} for three selected oligomers and total PEG was mainly influenced by the pH and then POM loading, while the oxidant concentration has a less effect.

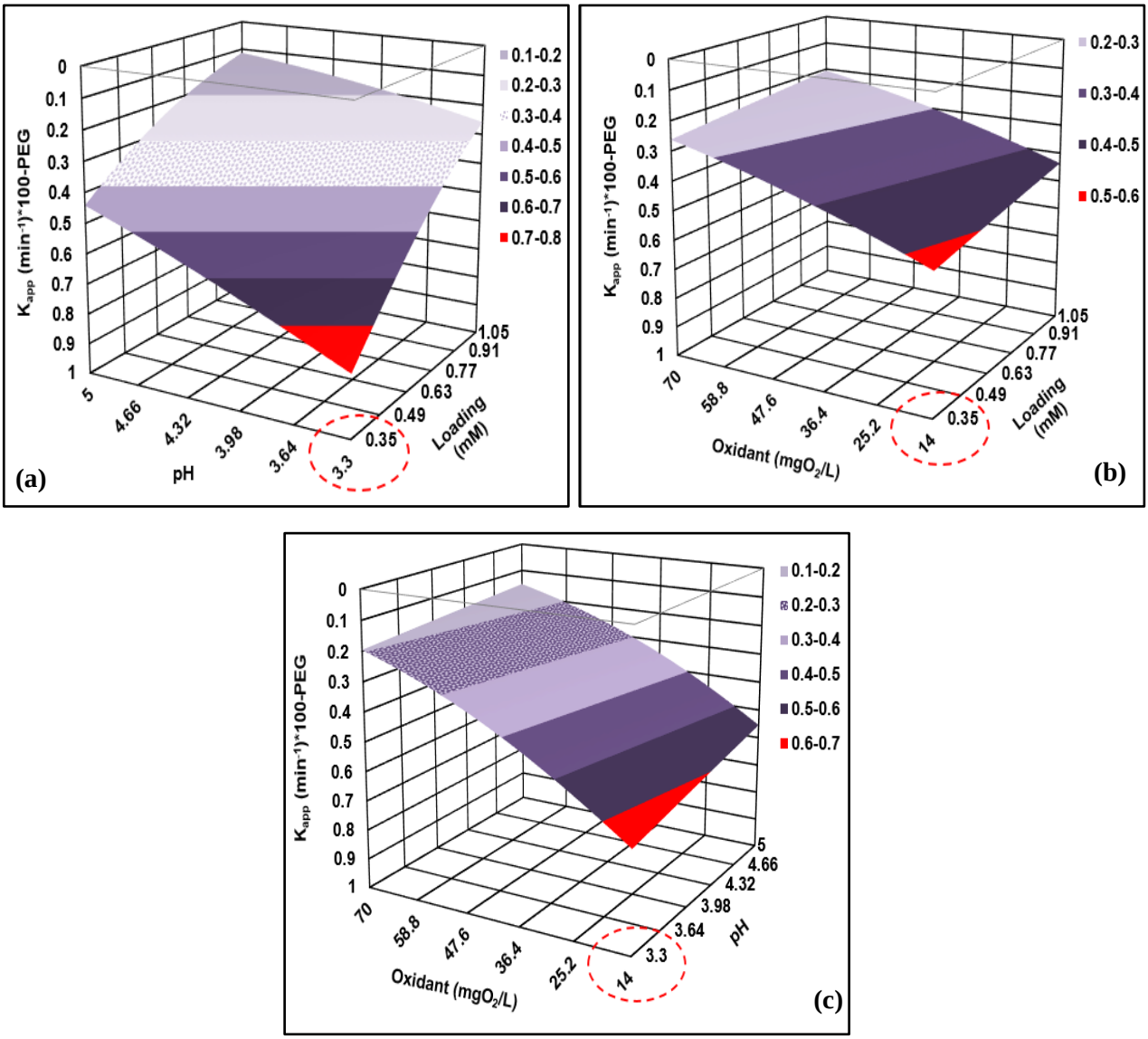

Fig. 4.14: NN simulation of a pseudo-first order reaction constant of the total PEG under various operating conditions: (a) POM loading and pH, (b) POM loading and oxidant concentration and (c) oxidant concentration and pH.

4.3.3 Optimal conditions

1) Prediction of the optimal conditions

In literature, several authors used the dependence of a reaction rate constant on POM loadings to identify the optimal loading **[25, 239, 240]**. In the current investigation, the %PD and K_{app} are used to identify the optimal conditions.

The observable performance of the %PD and K_{app} for the selected oligomers and total PEG in Figs. 4.8-4.10, 4.14 and B5, B7 (*Appendix B*) allowed the optimal operating conditions to be predicted theoretically within the experimental boundaries as POM loading (0.35 mM), pH (3.3) and oxidant (14 mgO_2L^{-1}). Under these conditions, the %PD and K_{app} of the selected oligomers and total PEG

were experimentally investigated (*experiment 19 in Table 4.2*) to verify if these conditions would be optimal. Table 4.2 shows that the results of this experiment based on the %PD and K_{app} are higher than that of the other experiments, indicating that it achieved an optimum performance so far.

2) Confirmation of the optimal conditions

In order to confirm the obtained results at the optimal predictable conditions and validate the model predication, a set of additional experiments were proposed and carried out experimentally based on the following assumptions:

i. *In terms of pH,* it is a crucial factor that was selected to be 3.3 as a minimum stability limit to avoid any acceleration of the non-photocatalytic reaction of POM with PEG.

ii. *In terms of POM loading*, a range of systematic POM loadings, higher (0.49, 0.70, 0.91 and 1.05 mM) and lower (0.17 mM) than that of the optimal predictable POM loading (0.35 mM) was proposed based on their pH effect as stated above and shown in Fig. A8 (*Appendix A*).

iii. *In terms of oxidant,* DO concentration was selected to be 14 mgL^{-1} to avoid the inner filter effect caused by higher concentrations as explained earlier in section 4.3.1 (2).

The experimental results of additional investigating experiments based on the assumption above are shown in Table 4.2 and Fig. 4.15. These results clearly showed that when the POM loading increased from 0.175 to 0.35 mM, the performance of %PD (Fig. 4.15-a) and K_{app} (Fig. 4.15-b) increased for the three oligomers and total PEG. A further increase in POM loading after (0.35 mM) had a negative effect on this performance. This behavior is due to the characteristic phenomenon of POM homogeneous photocatalysis as discussed in section 4.3.1 (1). Thus, the optimal photocatalytic degradation conditions based on the %PD and K_{app} for the LO, MO, HO and total PEG were POM loading (0.35 mM), pH (3.3) and oxidant concentration (14 mgO_2L^{-1}).

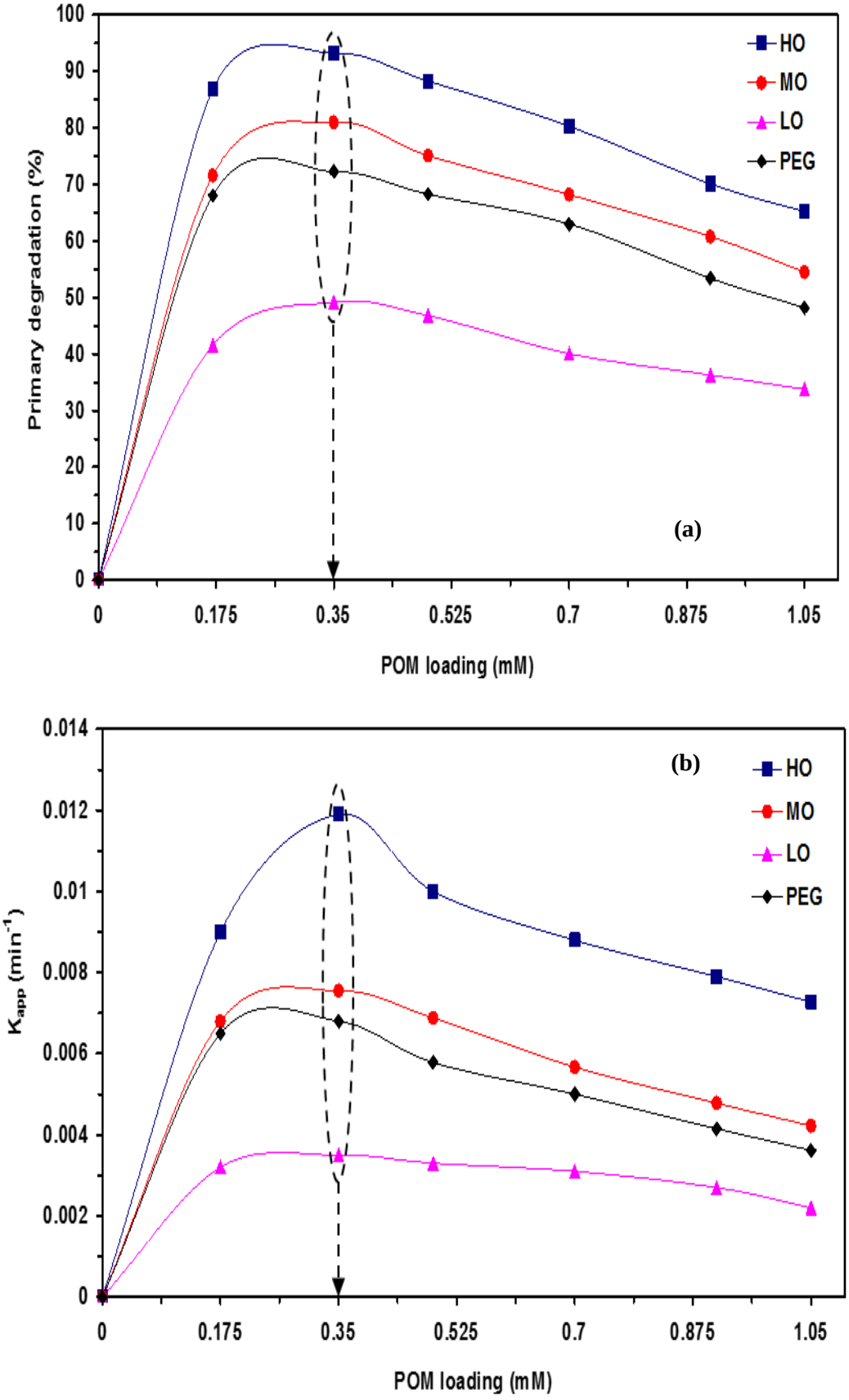

Fig. 4.15: Confirmation on the optimal conditions with various POM loadings and fixed operating parameters of pH (3.3) and oxidant concentration (14 mgO_2L^{-1}) at 180 min photocatalytic treatment time: (a) %PD and (b) K_{app}.

3) Confirmation of the model validity

To confirm the a neural network (*NN*) as a model adequacy for predicting the numeric values of response functions, %PD and K_{app}, under the confirmed optimum conditions (POM loading 0.35 mM, pH 3.3 and oxidant concentration 14 mgO_2L^{-1}), Table 4.4 shows the predicted (model) and experimental results under these conditions. As shown in Table 4.4, there is a good agreement between these results for all investigated response functions, and thus this used model has shown a high validity.

Table 4.4: Comparison between predicted and experimental results under the optimal conditions.

Results	**%PD**				**K_{app} (min^{-1})**			
	LO	***MO***	***HO***	***Total PEG***	***LO***	***MO***	***HO***	***Total PEG***
Predicted (model)	48.84	79.31	91.99	71.49	0.0034	0.0065	0.0115	0.0079
Experimental	49.18	80.98	93.22	72.78	0.0035	0.0076	0.0119	0.0068

4.3.4 POM chemical stability

As shown earlier in section 4.2.3, POM ($H_3PW_{12}O_{40}$) in the form $[PW_{12}O_{40}]^{3-}$ is not chemically stable in PEG reactant solution under different investigated conditions (*no UV*) with and without controlling the pH. It converted partially into various lacunary species of *W*.

Under UV conditions, the chemical stability of POM in the form $[PW_{12}O_{40}]^{3-}$ and other lacunary species of *W* was examined under various experimental design conditions shown in Table 4.2 for 180 min of photocatalytic reaction time. Examination of POM under these conditions showed that there was no significant change in the chemical structure of it in the form $[PW_{12}O_{40}]^{3-}$ as well as other identified lacunary species of *W*. Results of this examination are similar to that of *case* 5 in Fig. 4.6, so they are not shown here.

It is noteworthy that POM in the form $[PW_{12}O_{40}]^{3-}$ is still dominant in all investigating photocatalytic conditions based on the experimental design (Table 4.2). Also, the experimental results under these conditions showed that the total elemental concentration of POM based on the *W* after adsorption period was not significantly changed during all course of photocatalytic reaction conditions. In particular, there was found that a very minor variation of this total elemental concentration of POM, which is relating to the release or desorption of POM from the walls of the components' system (Fig. 3.4, *a* and *b*) to the reactant solution.

Actually, these are interesting results, confirming that POM in the form $[PW_{12}O_{40}]^{3-}$ with other identified lacunary species of W (highly oxidizing species) will play a significant role in the proposed homogeneous PMR (next chapter).

4.3.5 Degradation pathway and formation of intermediates

Photolysis formed malonic, glycolic, formaldehyde, formic, acetic and propionic acids as VFAs intermediates. Their concentrations were generally very limited (< 0.5% of the PEG concentration after adsorption period). This is expected since photolysis showed little effect on the degradation of PEG as explained earlier in section 4.2.1.

The formation of VFAs as a function of the operating parameters (POM loading, pH and oxidant) was investigated based on the *CCED*. An example of this investigation under the confirmed optimal conditions is shown in Fig. 4.16. In Fig. 4.16-a, the non-photocatalytic reaction of POM with PEG formed several VFAs including formaldehyde, formic, acetic and propionic where the total concentration of these formed acids was so limited (< 1% of PEG concentration at 30 min of a non-photocatalytic reaction after adsorption period). While for photocatalytic reaction, the same these acids as well as malonic and glycolic acids were generated. The total concentration of these acids was 15% of PEG concentration after adsorption.

It is important to mention that there are other concentrations of unidentified VFAs (not detected), so the total concentration of produced VFAs will be significantly increased. The total concentration of identified VFAs generated as a function of the investigated operating parameters is shown in Table 4.2. It is clear to see from Table 4.2 that very low mineralization in terms of TOC removal was obtained, concluding that these (identified and unidentified) acids are difficult to be further mineralized under POM photocatalysis. This finding is in agreement with that reported in the literature where *Mantzavinos et al.,* **[6]** showed that oxalic, malonic, formic and acetic acids formed under wet air oxidation process of the treatment of PEG10,000 were resistant to total oxidation. *Giroto et al.,* **[14]** used photo-Fenton and UV/H_2O_2 processes for the degradation of two types of PEG (PEG6000 and PEG20,000) and found that formic and acetic acids were recalcitrant to total oxidation. As shown in Fig. 4.16-a, the VFAs concentrations in (gL^{-1}) were in the following order: formic > acetic > propionic > formaldehyde > glycolic > malonic.

A drop in pH over photocatalytic reaction time (Fig. 4.16-b) is constituent with the formation of VFAs and other unidentified acids. The formation of these acids as intermediates changes pH of PEG reactant solution, concluding that pH gives an indicator for the formation of these reaction intermediates.

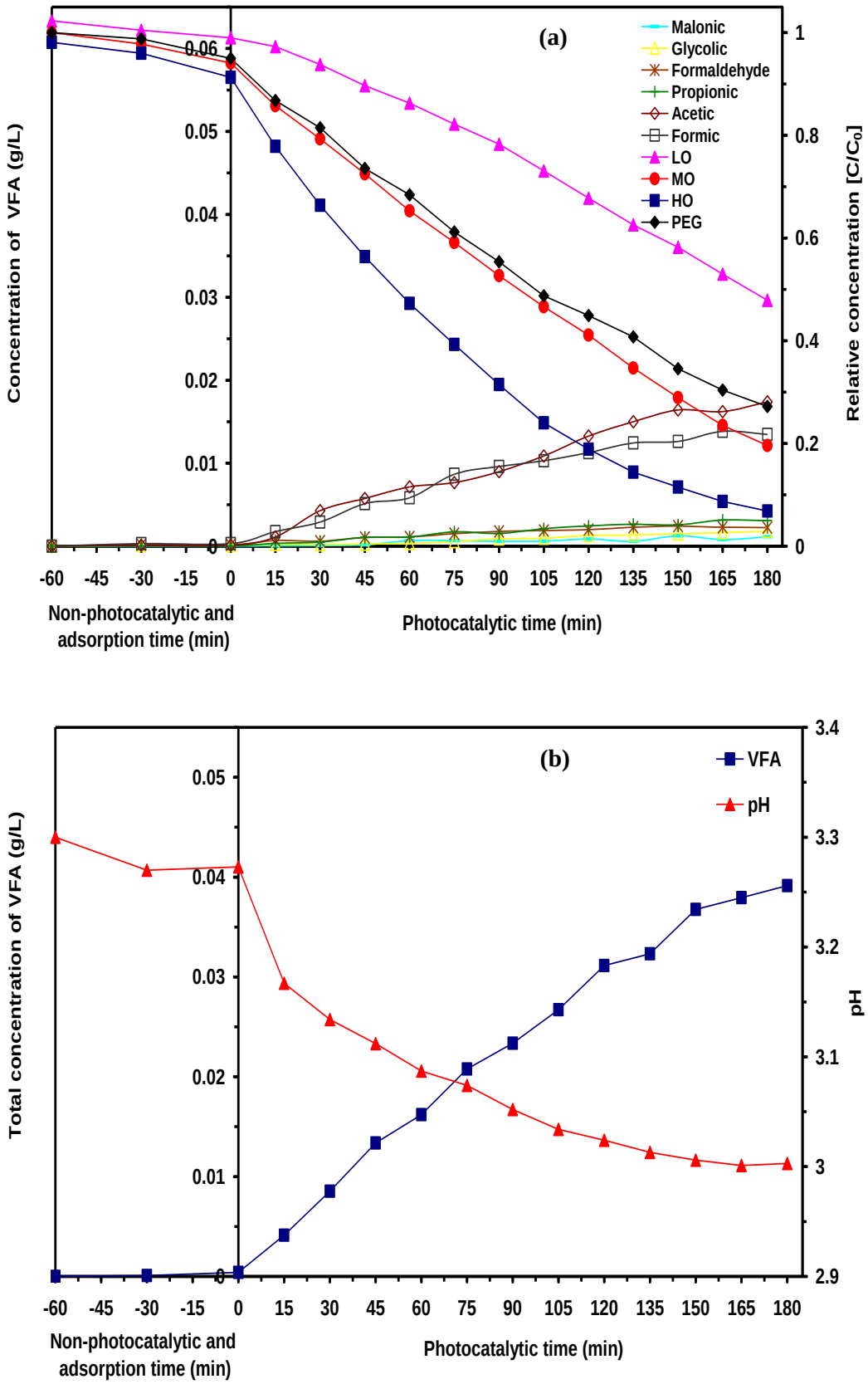

Fig. 4.16: Reaction intermediates formation during non-photocatalytic and photocatalytic reaction of POM with PEG times, loading (0.35 mM), pH (3.3) and oxidant concentration (14 mgO_2L^{-1}): (a) change in concentration of intermediates and relative degradation of PEG, (b) change in total concentration of VFA (gL^{-1}) and pH.

Under the optimal photocatalytic conditions, Fig. 4.16-a, the concentration of formic, acetic and propionic acids increased gradually until 135 min and then remained quite stable to the end course of reaction. While the concentration of glycolic, formaldehyde and malonic acids varied during this period. In literature, this indicates that glycolic acid might be partially oxidized into formic acid **[9]**, formaldehyde acid into formic acid **[10]** and malonic acid into acetic acid **[6]**.

So, the adapted mechanism for POM photocatalytic degradation of reaction intermediates can be proposed in Fig. 4.17.

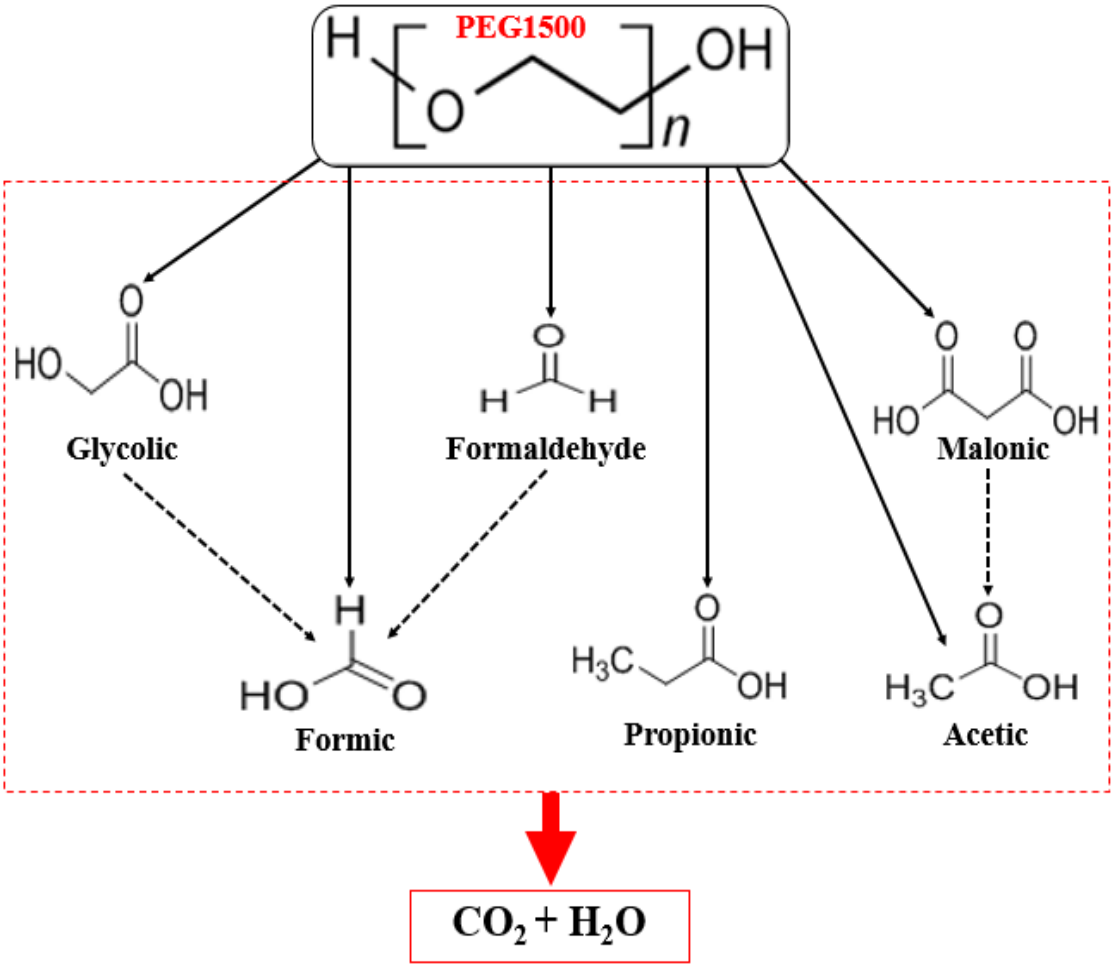

Fig. 4.17: Proposed mechanism of POM photocatalytic degradation of reaction intermediates.

4.3.6 Mineralization of PEG

Direct photolysis process showed a slight reduction in the TOC of PEG over photolytic time of 180 min as shown in Fig. 4.18, indicating that UV alone has an insignificant effect on TOC removal of PEG (1.3%). Fig. 4.18 shows that POM photocatalytic reaction under the optimal conditions achieved lower concentration of TOC of PEG than that of photolytic reaction, with the TOC removal of 3.6%. It is clear to see from Table 4.2 that little photocatalytic mineralization recorded (< 6%) for all investigated conditions.

Several authors concerning the oxidation of VFAs have shown that such acids are very resistant to total mineralization, further mineralization of them to CO_2 is usually the rate-limiting step for TOC in AOPs **[6, 10, 241]**. *In terms of partial mineralization*, one reason for this mineralization is that some of early acids generated may be directly oxidized to total oxidation end-products (CO_2 and H_2O). *Mantzavinos et al.*, **[13]** showed that VFAs as reaction intermediates generated from wet oxidation process of PEG 10,000 either partially oxidized to form stable compounds (like acetic acid) or directly oxidized (like formic acid) to total oxidation end-products.

Overall, the stable concentration of formed (identified and unidentified) VFAs as reaction intermediates by POM homogeneous photocatalysis of PEG explains why TOC remains stable, and thus obtaining a partial mineralization.

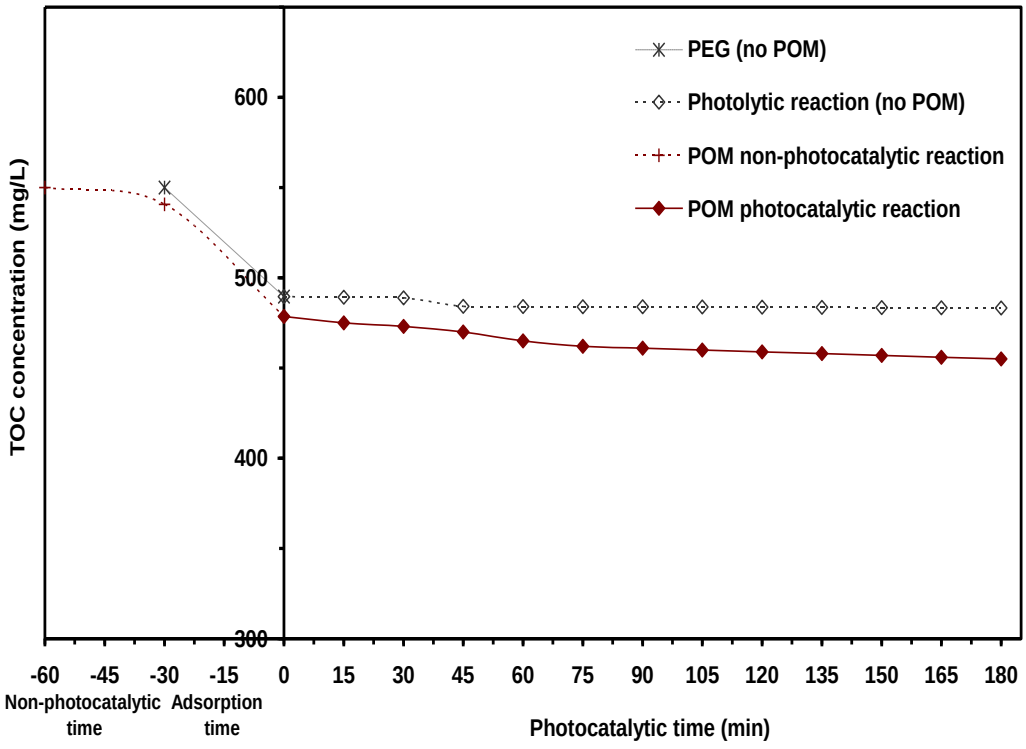

Fig. 4.18: The TOC concentration of PEG under photolysis and POM (non-photocatalytic and photocatalytic reactions at the optimal conditions).

4.4 Chapter conclusions

The main aim of this chapter was done in the two sections (4.2 and 4.3) and the following conclusions for each section were drawn:

- Photolysis process showed a limited photolytic effect on the degradation of PEG.
- POM photocatalyst could react with PEG non-photocatalytically via electron-transfer mechanism and its consumption increased with increasing its applied loading.
- pH played a significant role in accelerating a non-photocatalytic reaction between POM and PEG under pH 1 using HCl condition. While, the conditions of pH using NaOH from 3.3 to 5 did not affect a non-photocatalytic reaction.
- In terms of POM chemical stability, an extensive investigation on this stability at pH 1 showed that POM in the form $[PW_{12}O_{40}]^{3-}$ is not chemically stable under aqueous solution and PEG reactant solution. This finding is totally different from the reported literature in this regard where it decomposed partially into several lacunary species of *W*, which are having an oxidative ability to react with PEG oligomers. This decomposition of POM with regard to chemical stability and total elemental concentration of POM based on *W* were not significantly affected under the examined photocatalytic reaction conditions based on a *CCED*.
- The optimal conditions were theoretically predicted, POM loading (0.35 mM), pH (3.3) and oxidant (14 mgO_2L^{-1}), using *CCED* and *NN* and then experimentally confirmed. Under these optimal conditions, maximum %PD and K_{app} for the three investigated oligomers and total PEG were obtained. *NN* as a model fitting showed a high validity between predicated and experimental results, and allowed to determine the interaction effect of these parameters in terms of saliency analysis to be in the following order: pH > loading > oxidant.
- The selected oligomers based on different MWs showed similar behavior of overall photocatalytic degradation conditions in terms of %PD and K_{app} when compared with that of the total PEG under all examined conditions.
- Several low MW VFAs as reaction intermediates formed under POM homogeneous photocatalysis was highly resistant to further oxidation, and thus little mineralization (TOC removal < 6%) was found. The formation of these intermediates exhibited that there was a variation in their types and concentrations depending on the photolytic and POM homogeneous (non-photocatalytic and photocatalytic) reactions. From the behavior of these formed intermediates, the mechanism of POM photocatalytic degradation pathway was adapted depending on the relevant literature.

Chapter 5

POM Homogeneous Photocatalytic Membrane Reactor

5.1 Introduction

Up to date, it is still challenging to separate and recycle POM homogeneous photocatalyst. Thus, making POM homogeneous photocatalysis is unsuitable for any kind of environmental applications. In order to extend the knowledge and real application of POMs in the field of industrial wastewater treatment, the principal aim of this chapter is to investigate the possibility of using and recycling the POM photocatalyst in a proposed photocatalytic membrane reactor (PMR) for the treatment of PEG. This aim was achieved in three separate sections (5.2, 5.3 and 5.4) where the experimental procedure of these sections described in chapter 3, section 3.4.3.1.

The first section (5.2) discusses the ability of membrane (NF270) to separate a POM homogeneous photocatalyst with PEG reactant using dead-end membrane filtration process (*no UV*) and then using this membrane in the proposed cross-flow PMR later.

The second section (5.3) continues to investigate POM homogeneous photocatalysis of PEG as a control process (*no membrane*) based on the obtained results of investigated operating parameters (POM loading, pH and oxidant concentration) from chapter 4. The pH and oxidant concentration showed a negative impact on photocatalytic degradation activity of PEG. *In this section*, this impact is further confirmed experimentally, and thus these parameters are not controlled, only monitored. This investigation of control photocatalysis (*no membrane*) was carried out at various POM loadings and assessed in terms of the proposed evaluating parameters (primary degradation, reaction kinetics and mineralization). These evaluating parameters will be used as a basis of establishing a comparable performance of this control photocatalysis with cross-flow PMR later (section 5.4).

The third section (5.4) concentrates on applying the cross-flow PMR under batch mode of operation to validate if the concept *'membrane enhanced homogeneous photocatalysis'* is feasible based on the evaluating parameters mentioned above when comparing with that of control photocatalysis (section 5.3). Additionally, this section discusses the possibility to convert batch photocatalysis under an optimal investigated POM loading to a continuous photocatalysis using PMR. Finally, the discussion of these three sections conclude this chapter.

5.2 Investigation on the separation of POM (*no UV*)

Initially, dead-end membrane filtration process was used to examine the ability of membrane (NF270) to reject POM homogeneous photocatalyst and PEG reactant separately and together as feed without using UV light. The membrane rejection gives a primary indictor to retain each of them in the annular photoreactor.

A higher control loading of POM (1 gL^{-1}) with and without PEG as an example of this investigation was chosen. Particularly, apart from separate investigation of POM and PEG since there was a non-photocatalytic reaction of POM with PEG as explained in chapter 4, section 4.2.2 and also is confirmed in coming section (5.3), the membrane could effectively separate POM homogeneous photocatalyst from PEG reactant solution with complete rejection (100%) as shown in Table 5.1. Moreover, PEG based on total concentration and TOC was rejected by > 89.9% and 99.2% respectively. To confirm these results, the SEM images in Fig. 5.1 were used to offer more information about the formation of membrane fouling. Fig. 5.1 shows that the comparison of surface morphology of a new (virgin) membrane with fouled surfaces of PEG, POM and PEG-POM feeds. It is clear to see that the membrane surface was fouled with the presence of these feeds when compared with a new surface one.

The obtained results in terms of the rejection of PEG and in particular with POM are very encouraging results for using the membrane (NF270) in the proposed cross-flow PMR later.

Table 5.1: Membrane characterization of different feeds using dead-end membrane filtration process under POM loading (1 gL^{-1}) and PEG concentration (1 gL^{-1}).

Type			Rejection (%)	Feed concentration (mgL^{-1})	Permeate concentration (mgL^{-1})	Retentate concentration (mgL^{-1})	Mass (%)
POM			100	995.0	-	1572.7	21.0
PEG		C	> 89.9	998.9	< MDL	1551.2	< 22.4
		TOC	86.3	564.3	77.6	776.4	24.3
PEG-POM	*POM*		100	880.4	-	1360.0	22.8
	PEG	C	> 89.9	990.6	< MDL	1531.7	< 17.6
		TOC	99.2	554.2	4.6	924.4	15.3

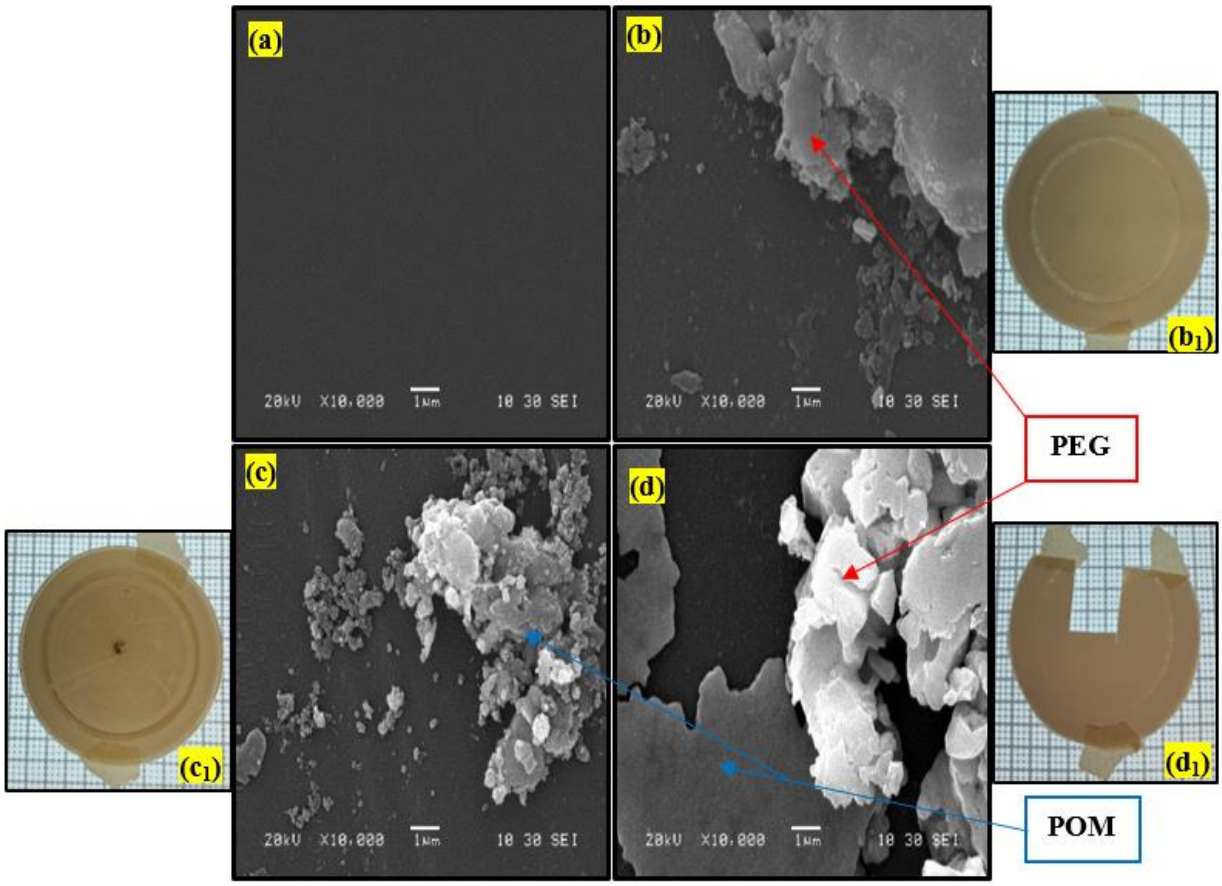

Fig. 5.1: SEM images of the top surface of membrane (magnification: x 10,000 and scale: 1 μm) using dead-end membrane filtration process at POM loading (1 gL^{-1}): (a) new membrane, (b) fouled membrane with PEG, (c) fouled membrane with POM, (d) fouled membrane with PEG-POM. Real photos of the top surface of membrane fouled with: (b_1) PEG, (c_1) POM and (d_1) PEG-POM.

In terms of permeate flux, Fig. 5.2 compares different profiles of permeate fluxes of POM, PEG and (PEG-POM) feeds. It can be observed that typical permeate fluxes of these feeds declined gradually with increasing the filtration time. It is generally accepted that the hydrodynamic conditions at the membrane surface changed with time because of the membrane fouling in terms of cake layer formation **[242]**. The resulting cake layer on the membrane surface increases the hydraulic resistance to permeate flow, and thus decreases permeate flux through the membrane **[243]**. This flux decline is supported by the rejection data shown in Table 5.1 and the SEM images (Fig. 5.1). A rapid reduction of permeate flux for (PEG-POM) feed was observed when compared with a single component feed of PEG or POM. This is expected due to the deposition of a thick foulant cake layer of both PEG and POM on the surface of membrane by the nature of dead-end filtration used, resulting in more significant permeance drop to the initial permeate flux of each of them individually.

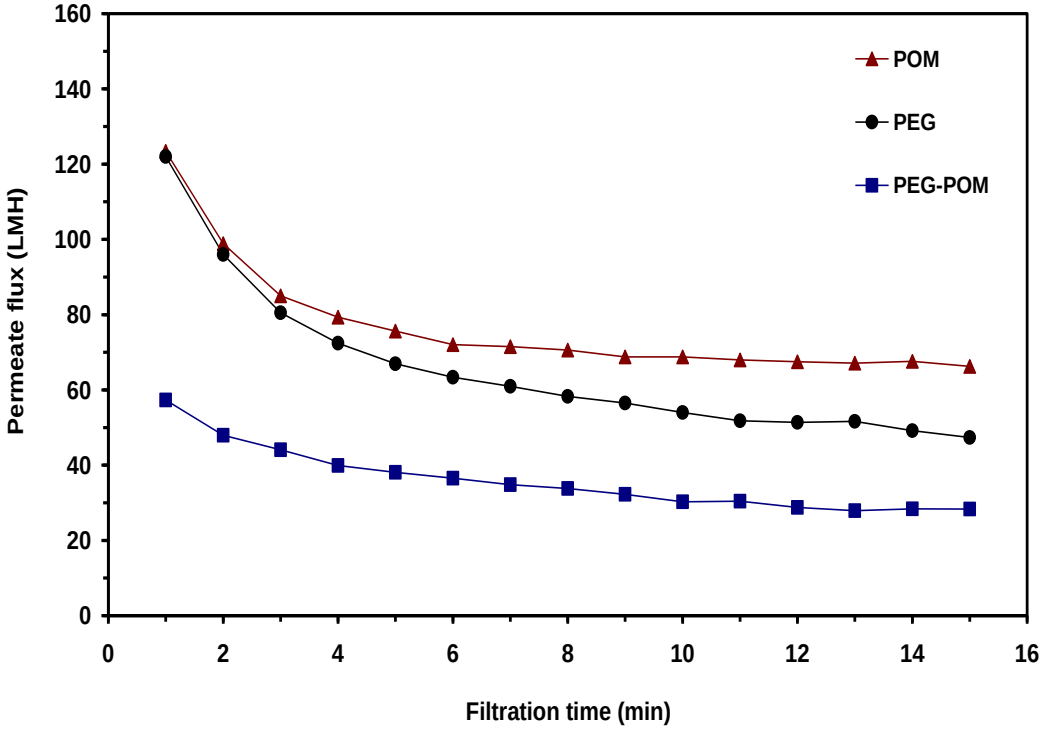

Fig. 5.2: Permeate flux profile of water, PEG, POM and PEG-POM under dead-end membrane filtration process.

5.3 POM homogeneous photocatalysis (*no membrane*)

The aim of this section is to apply POM homogenous photocatalysis of PEG as a control process without using membrane separation process to establish a comparable performance of this control process with proposed PMR (section 5.4) based on the evaluating parameters of primary degradation, reaction kinetics and mineralization.

From previous chapter (4), the optimal confirmed operating conditions are POM loading (0.35 mM), pH (3.3) and oxidant (14 mgO_2L^{-1}). The pH and oxidant concentration showed a negative impact on photocatalytic degradation activity of PEG. In the current section, *to confirm this impact*, one experiment under POM loading (0.35 mM) was carried out without controlling the pH and oxidant. Experimental result of this experiment is shown in Fig. C1 (*Appendix C*) where the %PD of PEG without controlling the pH and oxidant is higher than that of controlling them. This result confirms that pH condition using NaOH affected significantly the photocatalytic degradation of PEG because of the deprotonation of $HO^{\bullet}$ under NaOH conditions **[235]**. Also, DO as conventional oxidant caused an '*inner filter'* effect as explained in chapter 4, section 4.3.1 (2) **[170, 236]**.

Therefore, it was decided that the pH and oxidant were monitored only under different investigating conditions. The aim of this section was achieved by two steps as shown below:

5.3.1 POM consumption under non-photocatalytic reaction with PEG

Initially, *as shown in chapter 4, section 4.2.2*, POM could react with PEG under non-photocatalytic conditions. So, several experiments were done to identify the percentage consumption of different POM control loadings with PEG under these conditions. Fig. 5.3 shows that the percentage consumption of POM as a function of theoretical control loadings. This consumption increased with increasing its applied theoretical loading and followed a non-linear relationship (power model). This behavior of POM consumption is similar to that found in the range of POM loadings from 1 to 3 gL^{-1} under the effect of pH and oxidant concentration (chapter 4, section 4.2.2) for the same reason of the mechanism of electron-transfer reaction **[94]**.

In terms of comparative purposes, it is important to mention that the theoretical expression of POM control loadings (0.25, 0.50, 0.75 and 1.00 gL^{-1}) were used to represent all coming results instead of the actual concentrations of POM (0.23, 0.44, 0.67 and 0.87 gL^{-1}) respectively after the non-photocatalytic reaction conditions with PEG.

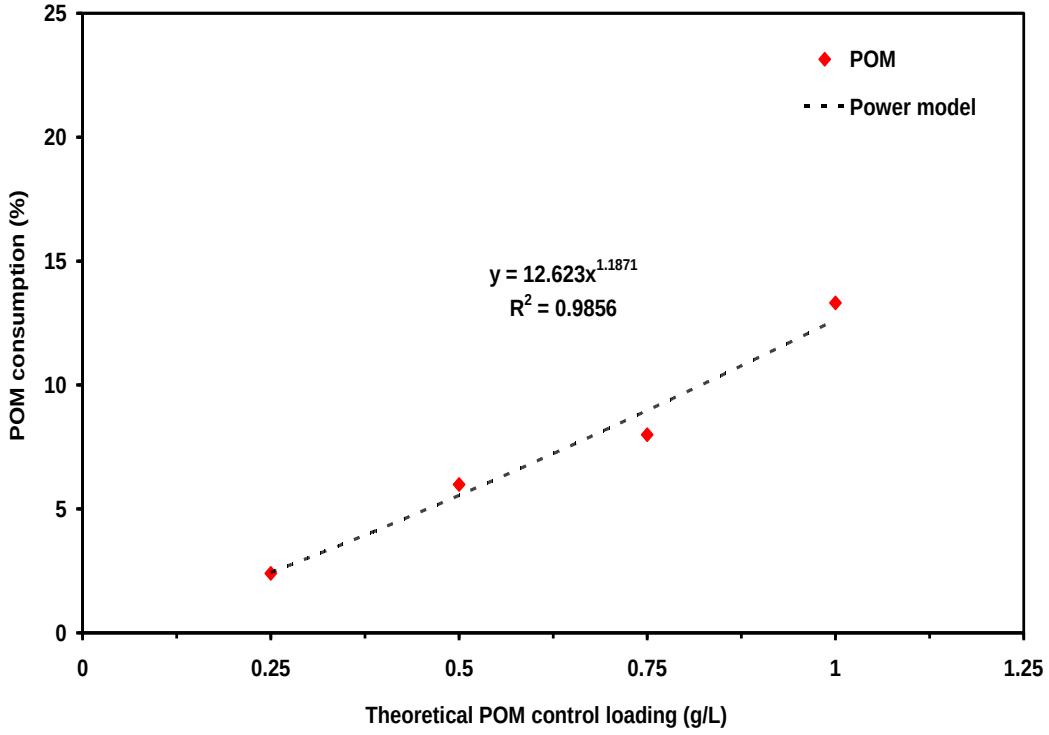

Fig. 5.3: Percentage theoretical POM control consumption under a non-photocatalytic reaction conditions with PEG.

5.3.2 Effect of POM control loading

1) Primary degradation

The effect of POM control loadings in the range of 0.25 to 1.00 gL^{-1} on the %PD of PEG as a function of photocatalytic time was examined in Fig. 5.4. It is clear to see that when POM loading increased from 0.25 to 0.75 gL^{-1}, the %PD increased significantly. A further increase in POM loading at 1.00 gL^{-1} had a negative effect on the %PD. This indicates that POM photocatalytic activity reached the critical level of photon capture at 0.75 gL^{-1} **[24, 25, 38]**.

It becomes evidence that the POM loading of 0.75 gL^{-1} is an optimal control loading of photocatalysis of PEG under no membrane conditions.

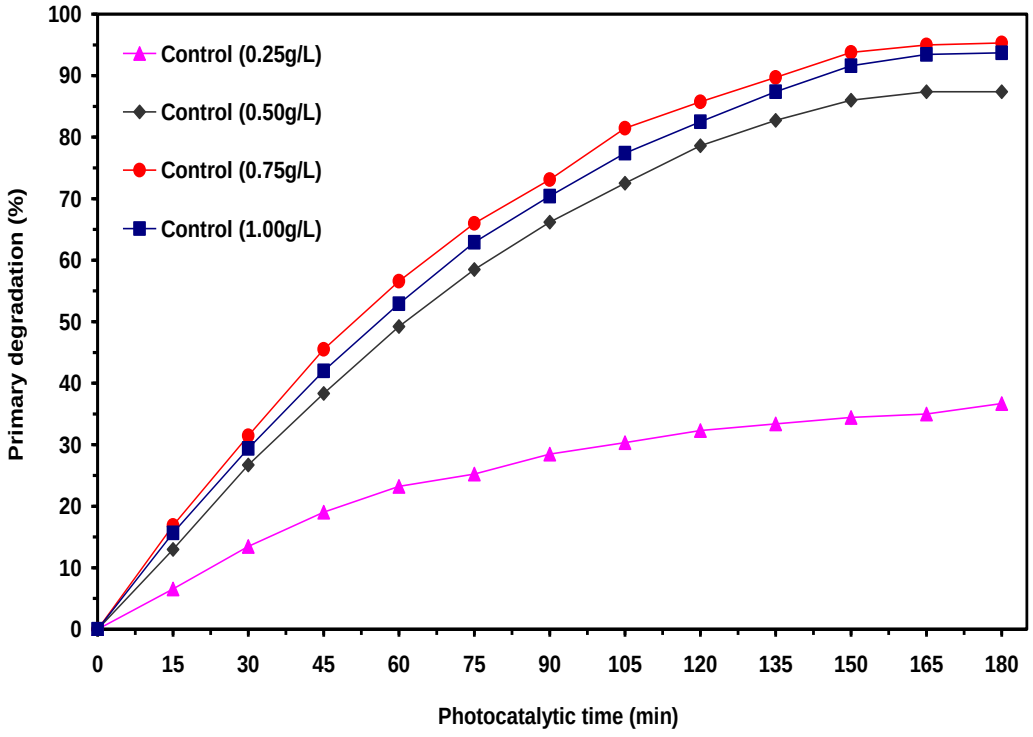

Fig. 5.4: Effect of POM control loadings on the percentage primary degradation of PEG.

2) Reaction kinetics

Based on the extensive investigation of reaction kinetics shown in chapter 4, section 4.3.2 in terms of reaction rate for each selected oligomer (LO, MO and HO) and total PEG, *in order to simplify the reaction analysis*, so it was decided to follow the reaction rate constant (K_{app}) as an evaluating parameter for the assessment of control photocatalysis performance.

The dependence of K_{app} on the POM loadings is shown in Fig. 5.5. It shows that the maximum K_{app} corresponds to the POM loading of 0.75 gL^{-1}.

The general trend of these results is similar to that of primary degradation based on the same effect of POM loading, as a result K_{app} gives a further support that POM loading (0.75 gL^{-1}) is an optimal control loading to be used as an evaluating parameter for the performance of proposed PMR later in coming section (5.4).

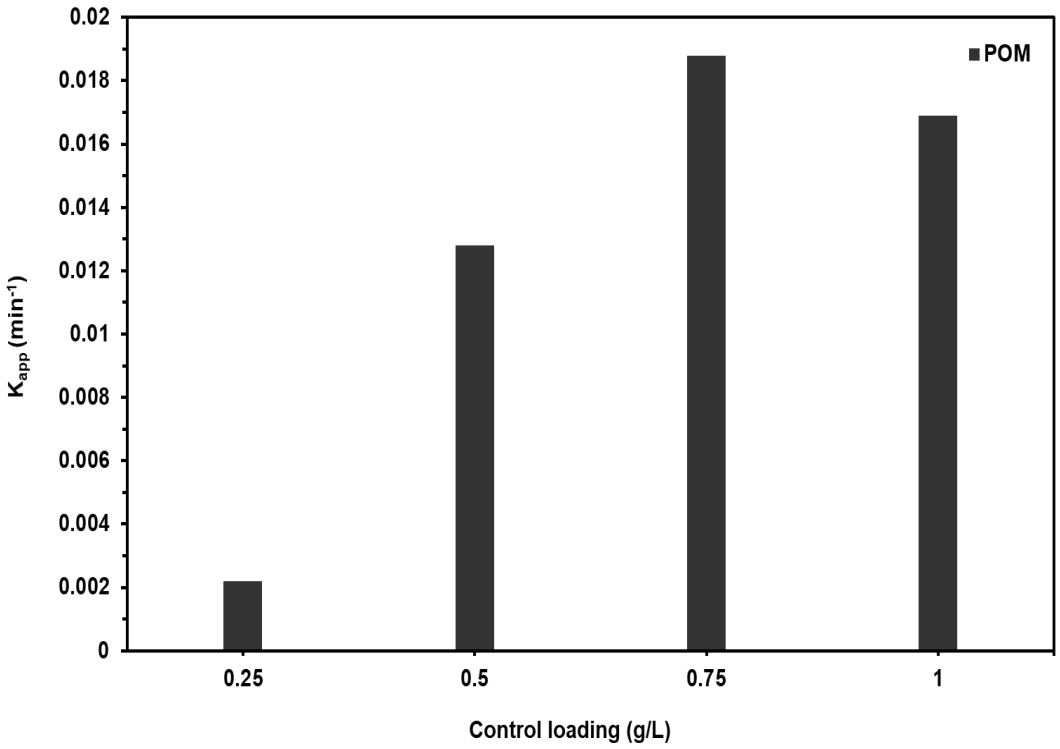

Fig. 5.5: Effect of POM control loadings on the K_{app} of PEG.

3) Mineralization

POM photocatalytic mineralization of PEG in terms of the %TOC removal under various POM loadings were investigated in Fig. 5.6. It shows that a partial mineralization of PEG was found to be less than 3% TOC removal. This is attributable to the resistance of formed VFAs (malonic, glycolic, formaldehyde, formic, acetic and propionic) to further oxidation under these conditions. The total concentration of these formed VFAs as a function of photocatalytic time is shown in Fig. 5.7. This result of partial mineralization of PEG is similar to that obtained and explained earlier with more detail in chapter 4, section 4.3.6.

In order to better understand the photocatalytic mineralization of PEG, *instead of %TOC*, the TOC concentration in relation with formed VFAs will be used as an evaluating parameter for the performance of control photocatalysis of PEG with proposed PMR later.

In terms of degradation pathway, the same observation of intermediate products as VFAs identified in chapter 4, section 4.3.5 was found, so it is not shown in the current section.

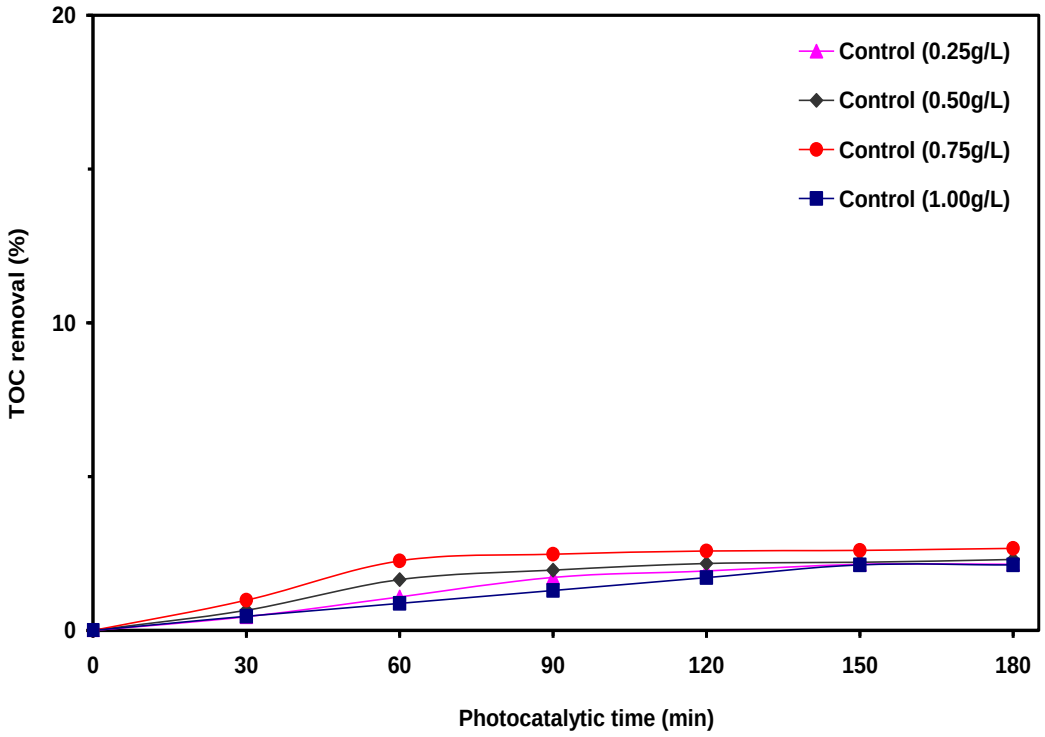

Fig. 5.6: %TOC removal over a photocatalytic time at various POM control loadings.

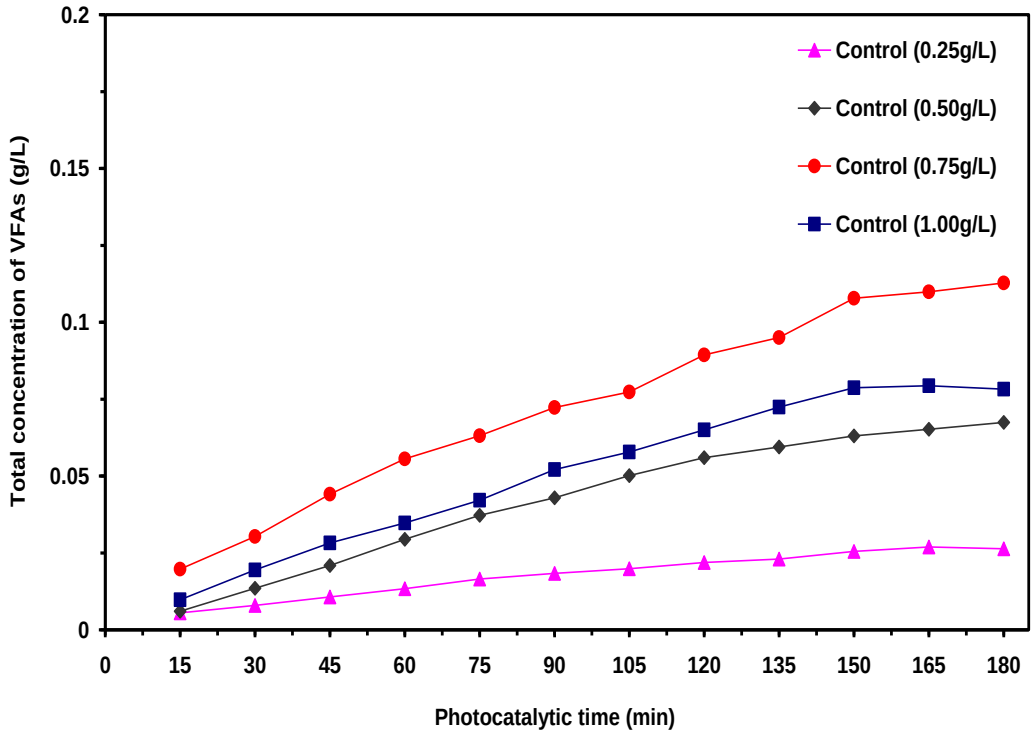

Fig. 5.7: Total concentration of formed VFAs over a photocatalytic time at various POM control loadings.

5.4 Cross-flow homogeneous PMR

5.4.1 Batch PMR operation

The aim of this section is to validate if the concept *'membrane enhanced homogeneous photocatalysis under batch mode of cross-flow PMR operation'* is feasible when comparing with control photocatalysis (*no membrane*) shown in section 5.3 based on the evaluating parameters (primary degradation, reaction kinetics and minimization). The hydrodynamic conditions, TMP (15 bar) and CFV (1.3 cms^{-1}), were initially selected for carrying out batch PMR experiments and then the influence of other hydrodynamic conditions on batch PMR performance will be examined later.

1) Primary degradation

The performance of cross-flow PMR based on the %PD of PEG with various POM loadings was examined in Fig. 5.8 and compared with control photocatalysis. As shown in Fig. 5.8, at POM loading (0.75 gL^{-1}), which was an optimal control loading of photocatalysis of PEG, the %PD of PEG using PMR decreased when compared with control photocatalysis.

Similar results of PMR were observed under POM loading of 1.00 gL^{-1} (data not shown in Fig. 5.8 to avoid the inference between the lines) as compared to control photocatalysis. On the other hand, at POM loadings of 0.25 and 0.50 gL^{-1}, a clear increase in the %PD of PEG was found in comparison with their control photocatalysis loadings.

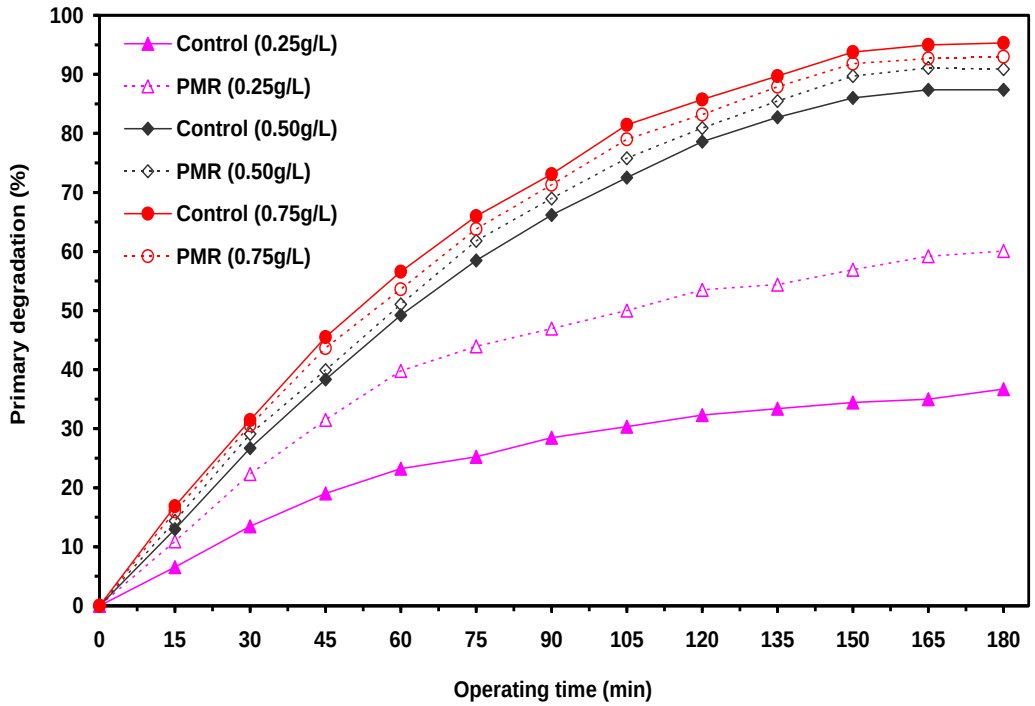

Fig. 5.8: Comparative performance of %PD of PEG between control photocatalysis and batch PMR mode of operation at different POM loadings.

Comparing this performance of PMR with control photocatalysis could be explained by the rejection of POM and PEG, and permeate flux characteristics of the membrane.

In terms of POM rejection, the membrane could successfully separate POM homogeneous photocatalyst from PEG reactant solution with complete rejection (100%). More details about this rejection with POM chemical stability are shown in section 5.4.1.2.

This complete rejection cannot explain the relationship in terms of the retentate POM concentration inside the BSR (*or in the photoreactor*) as a function of the permeate flux over 180 min operating time. This relationship can significantly affect the performance of PMR based on the %PD of PEG. Therefore, instead of this complete rejection, the retentate POM concentration would be used for this.

Fig. 5.9 shows that as the time of cross-flow filtration progressed, the retentate POM concentration increased for all investigated POM loadings to be higher than that of original control loadings. This increase in POM concentration played a significant role in the photocatalytic performance of PMR. For example, at POM loadings of 0.25 and 0.50 gL^{-1}, the increases in concentration of POM in the retentate (or photoreactor) were 61 and 34% respectively at a 180 min operating time resulted in increasing the %PD of PEG by 64 and 4% respectively under PMR when comparing with control photocatalysis (Fig. 5.8). Similarly, the POM concentration increased in the retentate by 20% at POM loading (0.75 gL^{-1}) and 11% at POM loading (1.00 gL^{-1}) in comparison with their original control loadings. This increase in POM concentration led to decrease the %PD of PEG by 2 and 5% respectively under PMR due to the fact that a significant decrease in photon capture as explained in section 5.3.2, (1).

It is interesting to note that the performance of PMR at POM loading of 0.50 gL^{-1} showed a comparable photocatalytic activity to that of control photocatalysis (*no membrane*) at the optimum POM loading (0.75 gL^{-1}) as shown in Fig. 5.8. This was achieved by increasing the retentate POM concentration under PMR to be close to an optimum concentration of control photocatalysis as shown in dashed line in Fig. 5.9. Therefore, the POM loading of 0.50 gL^{-1} would be selected to be an optimum loading of cross-flow PMR so far and be used to further investigation later.

The obtained results confirm exactly that the membrane separation process enhanced POM homogeneous photocatalysis and then the concept of proposed cross-flow homogeneous PMR is feasible under only the loadings (0.25 and 0.50 gL^{-1}), which are below the optimal control loading of photocatalysis process (no membrane), 0.75 gL^{-1}.

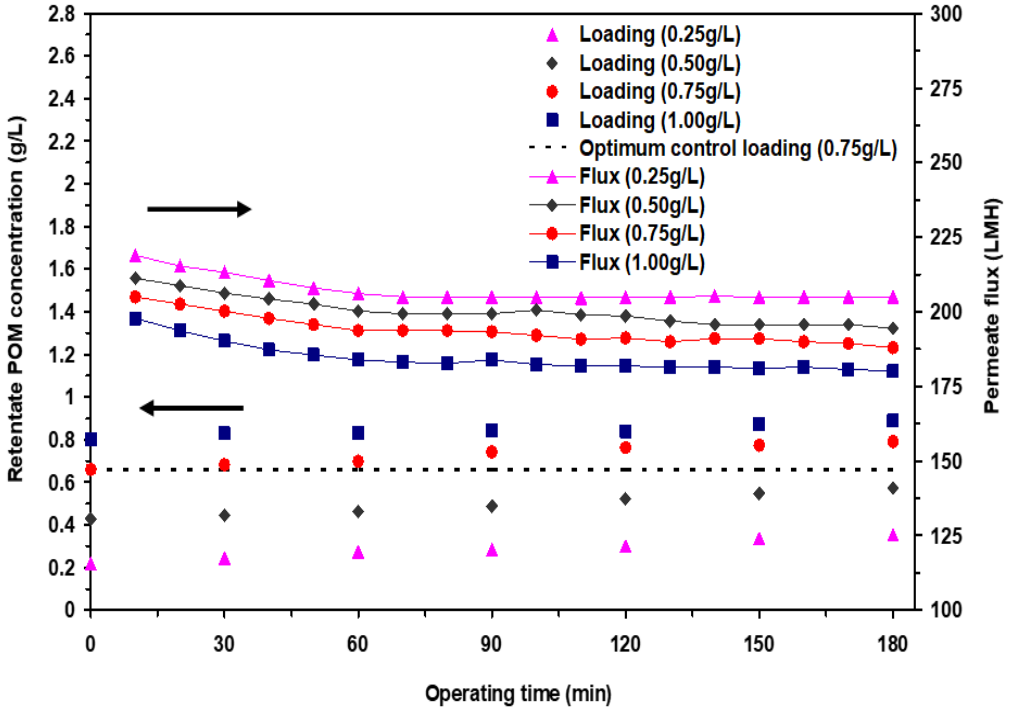

Fig. 5.9: Retentate POM concentration and permeate flux as a function of operating time of batch PMR mode of operation.

In terms of PEG rejection, PEG as feed consists of 23 oligomers with low, medium and high ranges of MWs as shown in Fig. 5.10-a (after adsorption). Under all examined PMR conditions, it was found that as the operating time (photocatalytic reaction time in conjunction with cross-flow filtration time) proceeded, the concentration of each oligomer within medium and high MW ranges (their MWs > LO MW) in the retentate decreased significantly depending on the photocatalytic reaction conditions (concentrating the POM concentration in the photoreactor due to filtration as shown earlier). At the end of course of photocatalytic reaction (180 min), for example a POM loading of 0.50 gL^{-1}, no peaks of PEG oligomers in terms of HPLC chromatograms were detected at medium and high MW ranges (Fig. 5.10-b), and thus their concentrations could not be determined. *In this regard, there are two possible scenarios, with each of them completing the other.*

The first scenario assumes that the concentrations of these oligomers were to be less than the MIDL of HPLC methodology and calibration. This decrease in concentration is thought to be because these oligomers based on their MWs were greatly oxidized to be below the MWCO of used membrane (200-400 $gmol^{-1}$), thus potentially passing through the membrane to the permeate. Investigation on these oligomers in the permeate confirmed this thought exactly where no chromatographic peaks (oligomers) could be identified (Fig. 5.10-c) since the detector baseline of HPLC appeared to drift and showed an excessive noise. Based on this result, the total concentration of PEG (*the sum of all expected oligomers in the permeate*) could be predicated to be significantly below the MDL of HPLC methodology and calibration (100 mgL^{-1}). While, the concentrations of LO MW range in the retentate

were obviously identified by HPLC chromatograms (Fig. 5.10-b). These oligomers behaved quite differently from other oligomers of medium and high MW ranges where their concentrations increased and then decreased as operating time increased as shown in Fig. 5.11. As a consequence of this behaviour, the second scenario is assumed.

The second scenario is built based on the mechanism of PEG oligomers degradation where high MW oligomers degraded to medium MW oligomers, which in turn degraded to low MW oligomers in sequential order. This sequential order, in terms of %PD of PEG, has been confirmed earlier in chapter 4, section 4.3.1, (1) on the basis of HO > MO > LO. As a result, the concentrations of oligomers with low MW range would increase due to an increase in the number of new degraded oligomers from high and medium MW ranges. In literature, *Mantzavinos et al.,* **[6, 13]** showed that the wet air oxidation of PEG 10,000 produced polymeric (oligomeric) fractions and non-polymeric fractions as short chain organic acids. They reported that these oligomeric fractions could fragment down to new oligomers with MW lower than that of original oligomeric fragments. *Guo et al.*, **[7]** and *Santos et al.,* **[9]** showed that the UV/H_2O_2 process could degrade PEG3550 molecules to oligomers with different ranges of MWs and then these oligomers gradually degraded to lower MW oligomers. Experimental results of the retentate in Fig. 5.12 showed that the concentration of PEG after a 180 min operating time in terms of remaining identified oligomers (seven oligomers only within LO MW range, excluding the oligomers that reached the MIDL) was 58.1 mgL^{-1} when compared with the initial concentration of PEG (23 oligomers) after adsorption (783.4 mgL^{-1}).

Therefore, this scenario assumes that these identified oligomers with LO MW range in the retentate were to be partially (lightly) oxidized and the membrane could successfully reject them from passing through the membrane and return them to the photoreactor for further oxidation. This rejection is assumed to be attributable to their MWs > MWCO. Unfortunately, literature concerning a combination of an oxidative and seperative process of treatment of PEG based on oligomeric investigation is still unavailable. However, *Hellenbrand et al.*, **[244]** used wet oxidation and nanofiltration process as an integrated system for the treatment of PEG 10,000 as a model compound feed. They used TOC and chemical oxygen demand (COD) as lumped parameters in evaluating the process. Higher rejections of COD and TOC were obtained by using the standard polymeric NF membrane (polyamide, AFC40). They suggested that this membrane could retain untreated (partially) oxidized molecules with higher MW and then recycle them into the wet oxidation reactor for further oxidation, while highly oxidized molecules could pass through the membrane to the permeate.

Note that, in terms of total PEG rejection, the concentration of permeate was much below the MDL (< 100 mgL^{-1}) and the concentration of each oligomer in retentate was being changed depending on the operating time, affecting the total concentration of PEG. Therefore, the calculation of true

rejection of PEG is not accurate. However, this rejection can be calculated based on the results of TOC investigation later.

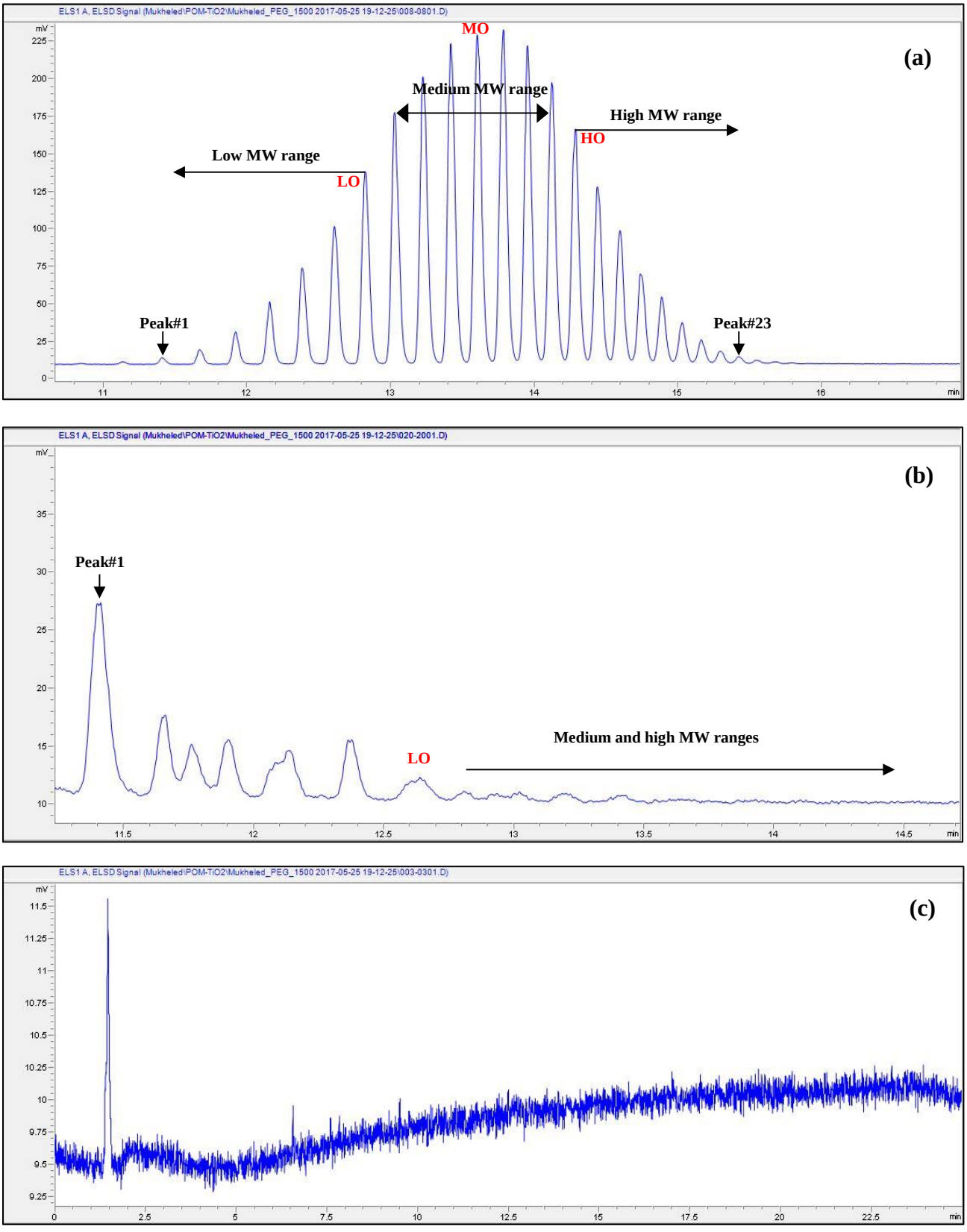

Fig. 5.10: RP-HPLC/ELSD chromatograms of PEG oligomers under batch PMR mode of operation (POM loading of 0.50 gL^{-1}), (a) feed after adsorption, (b) retentate and (c) permeate.

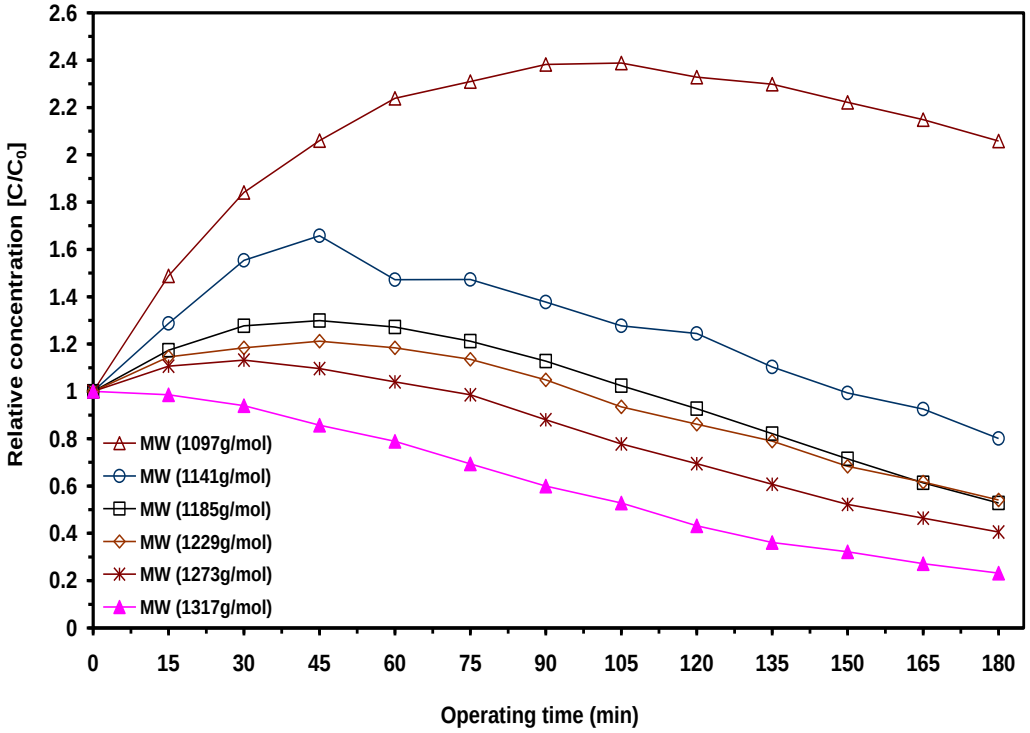

Fig. 5.11: Relative concentration profile of PEG oligomers of LO MW range as a function of operating time of batch PMR mode of operation (POM loading of 0.50 gL^{-1}).

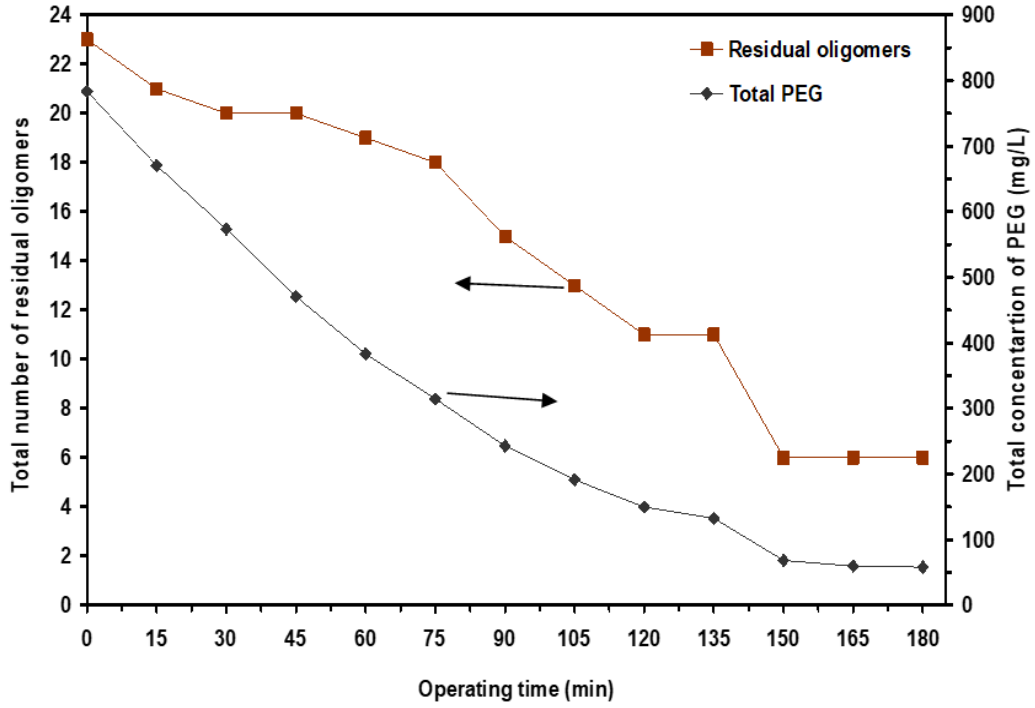

Fig. 5.12: Residual oligomers and total concentration of PEG as a function of operating time of batch PMR mode of operation (POM loading of 0.50 gL^{-1}).

In terms of permeate flux, Fig. 5.9 describes the experimental permeate flux profile for various POM loadings as a function of cross-flow filtration time. There was a gradual decline of permeation flux under all examined POM loadings for 90 min. After that, the permeate flux was nearly stable. The steady fluxes under POM loadings of 0.25, 0.50, 0.75 and 1.00 gL^{-1} were 205, 195, 188 and 180 LMH respectively, which accounted for the proportion of pure water flux of 10, 14, 17 and 21% respectively. The systematic decline in the permeate flux relative to pure water indicates that the membrane surface was fouled **[242, 245]**. This fouling can be explained with more details by SEM images.

The SEM images in Fig. 5.13 show that the membrane surface was fouled. This fouling is due to the *'solute-solute interaction'* between completely rejected POM homogeneous photocatalyst and partially oxidized PEG oligomers together or individually with the surface of membrane, leading to the adsorption of them onto the surface of membrane. Thus, the fouling in terms of concentration polarization was initially developed and then the formation of cake layer **[243, 246]**. This resulting layer had an impact on permeate flux behaviour where a gradual permeate flux decline was observed as shown in Fig. 5.9.

It should be noted that several authors have reported that a sharp decline in permeate flux was observed under conventional separation processes at the beginning of filtration followed by a gradual flux decline. They attributed this to the adsorption of solutes onto the surface of membrane with rapid pore blocking and then the resulting development of cake layer formation **[157, 243, 245-247]**.

In the current flux investigation under all examined conditions, Fig. 5.9, a gradual permeate flux decline was observed instead of a sharp flux. Moreover, the used membrane showed a continuous ability to promote a significant rate of permeate fluxes. *Since there is no literature available into the behaviour of POM homogeneous photocatalyst with PEG oligomers under membrane separation process*. This is thought because the effect of the partially oxidized PEG oligomers on the development of concentration polarization layer over the surface of membrane. The concentrations of these oxidized oligomers were being changed during the photocatalytic reaction time, consequently this layer was significantly changed in its nature. This change in the concentration of PEG oligomers might be a possible explanation for why the behaviour of obtained permeate flux was gradually declined (not sharply). In addition, the continuous permeate fluxes gave an indicator about there was no complete pore blocking. Generally, these are interesting results that will be useful when converting homogenous photocatalysis to continuous photocatalysis later.

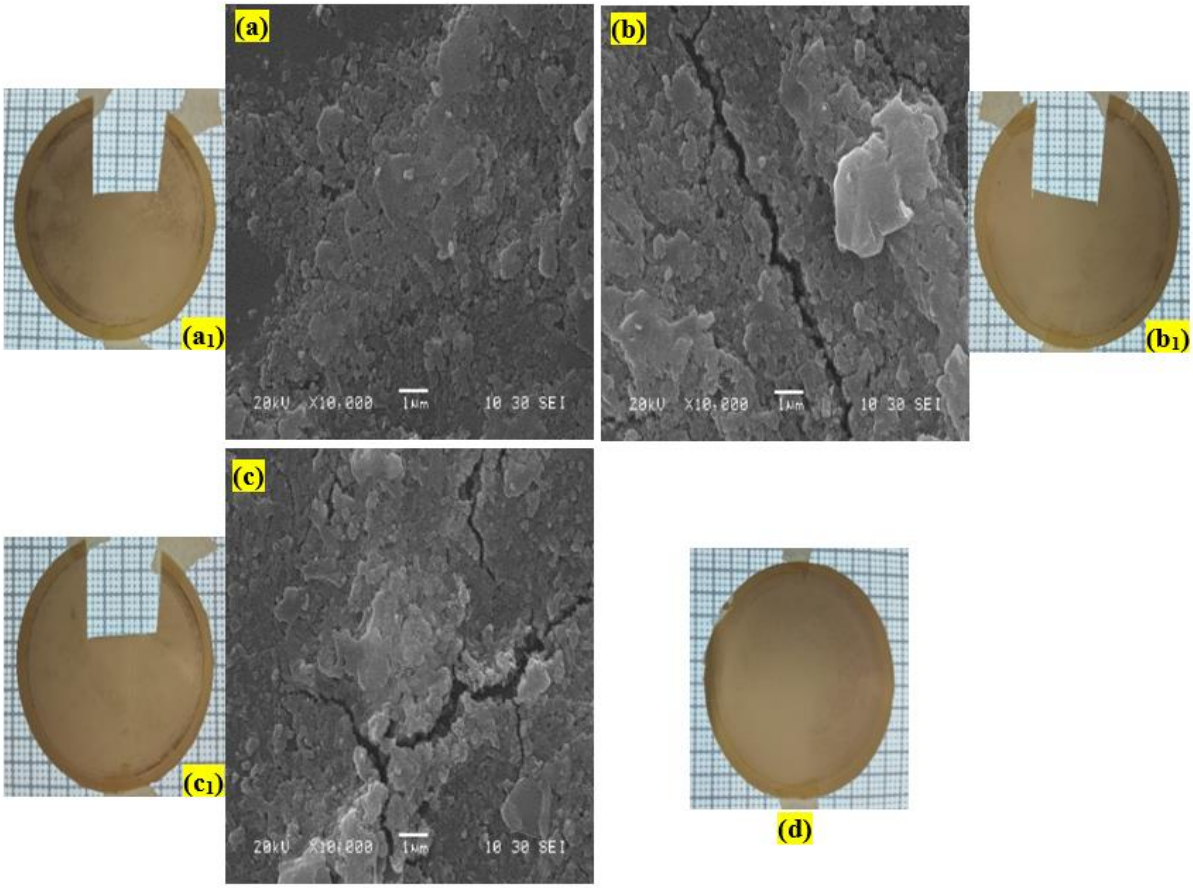

Fig. 5.13: SEM images of the top surface of a fouled membrane with PEG and various POM loading using cross-flow PMR, magnification: x 10,000 and scale: 1 µm: (a) POM loading 0.25 gL^{-1}, (b) POM loading 0.50 gL^{-1} and (c) POM loading 0.75 gL^{-1}. Real photos of the top surface of membrane fouled with: (a_1) POM loading 0.25 gL^{-1}, (b_1) POM loading 0.50 gL^{-1}, (c_1) POM loading 0.75 gL^{-1} and (d) POM loading 1.00 gL^{-1}.

2) Reaction kinetics

The comparative performance in terms of K_{app} between cross-flow PMR and control photocatalysis under various POM loadings is shown in Fig. 5.14. At lower POM loadings of 0.25 and 0.50 gL^{-1}, the values of K_{app} under PMR increased by 86 and 17% when compared with control photocatalysis. While, at higher POM loadings of 0.75 and 1.00 gL^{-1}, they decreased under PMR by 11 and 15% when compared with control photocatalysis. The general trend of these results is similar to that obtained with %PD of PEG under the same comparable conditions due to the characteristic phenomenon of POM homogeneous photocatalysis as discussed in section 5.3.

Based on these obtained results, it becomes evident that the cross-flow homogeneous PMR enhanced POM homogeneous photocatalysis under the POM loadings (0.25 and 0.50 gL^{-1}) lower than the optimal control loading of photocatalysis process (no membrane).

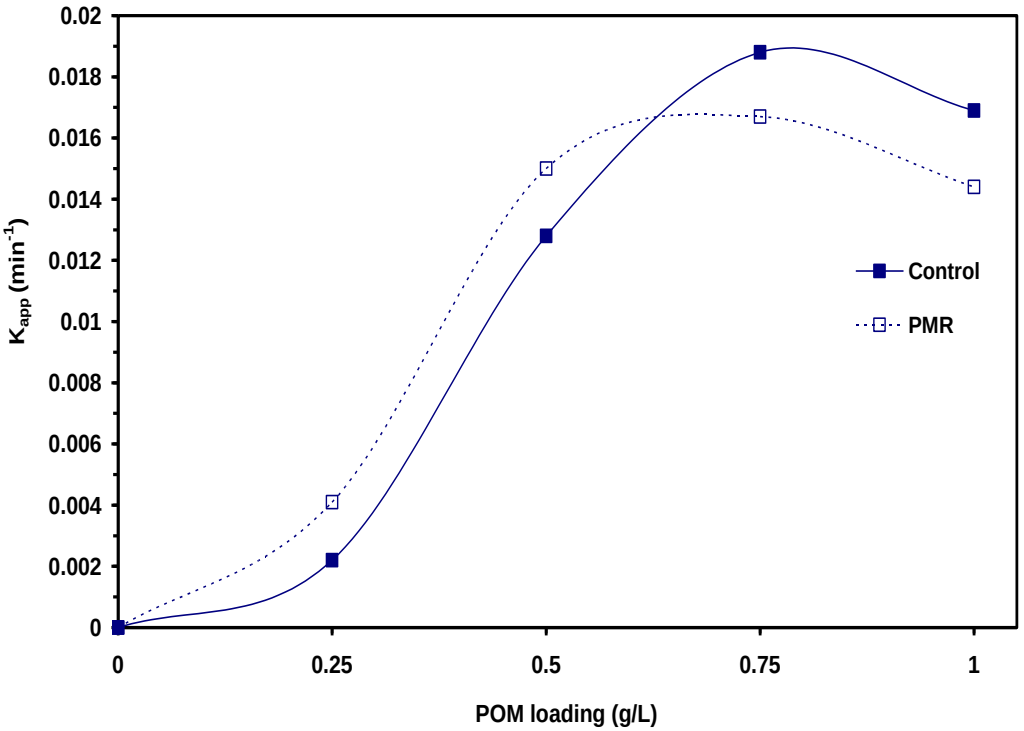

Fig. 5.14: Comparative performance of K_{app} between control photocatalysis and batch PMR mode of operation under various POM loadings.

3) Mineralization

The photocatalytic mineralization performance of PMR compared with control photocatalysis (no membrane) could be explained by the TOC concentration of PEG in the retentate over a 180 min operating time in Fig. 5.15. *Note that the control photocatalysis data in Fig. 5.15 and Fig. 5.16 are for comparison purposes*. As seen in Fig. 5.15 that as the operating time increases, the concentration of TOC in the retentate increases significantly under all examined conditions when compared with control photocatalysis. This increase is because of two reasons:

The first reason, several VFAs (malonic, glycolic, formaldehyde, formic, acetic and propionic) were generated in the retentate and the total concentration of these acids increased significantly with increasing the operating time in comparison with control photocatalysis under all examined conditions (Fig. 5.16). As shown in Fig. 5.16, the rejection (R%) of these VFAs by the membrane for example at POM loading (0.50 gL^{-1}) was 95%. Surprisingly, this higher VFAs rejection is unexpected since the MW of these acids is generally less than the MWCO of used membrane and should be passing through the membrane to the permeate stream. This unexpected result can be possibly explained by the adsorption of these formed VFAs on the formed cake layer, which acts as a *'secondary dynamic membrane'* in controlling the adsorbed VFAs in terms of rejection and selectivity **[248, 249]**. As a result of the accumulation of these adsorbed VFAs on the membrane surface, the shear forces by a cross-flow filtration might be leading to push these adsorbed acids from the surface

of membrane or formed cake layer and return them to the retentate stream, and then to the photoreactor. The nature of these acids generally are so resistant to total mineralization (complete conversion in the photoreactor into CO_2 and water) as explained earlier with more details in chapter 4, section 4.3.6. Consequently, the TOC concentration in the retentate increased significantly under these conditions.

The second reason, it is expected that there was a wide range of unidentified compounds (*not detected in the current research*), including lightly (partially) oxidized PEG oligomers (these were not included in the 23 identified oligomers of the original PEG based on the used HPLC methodology), polymeric fractions like ethylene glycol and reaction intermediates like VFAs. The TOC concentration can give an indictor about all these organic compounds in the reactant solution. It is assumed that these compounds were completely rejected by the membrane leading to increase significantly the TOC concentration in the retentate. This assumption can be supported by the experimental results of the permeate when comparing with retentate where for example at a POM loading of 0.50 gL^{-1} with 180 min operating time, the TOC concentration in the permeate was 14 mgL^{-1} corresponding to the identified VFAs of 5 mgL^{-1}. While, for the retentate, it was 702 mgL^{-1} (TOC) corresponding to the identified VFAs of 100 mgL^{-1}. Similar results were found for the other investigated POM loadings. This big difference, in particular for the retentate, between the concentrations of identified VFAs and TOC confirms this assumption.

On the basis of these obtained results, the cross-flow membrane separation process could not enhance the photocatalytic mineralization of PEG. Consequently, the mineralization of PEG cannot be used as an evaluating parameter for further investigation of membrane operating conditions in the coming section (5.4.1.1).

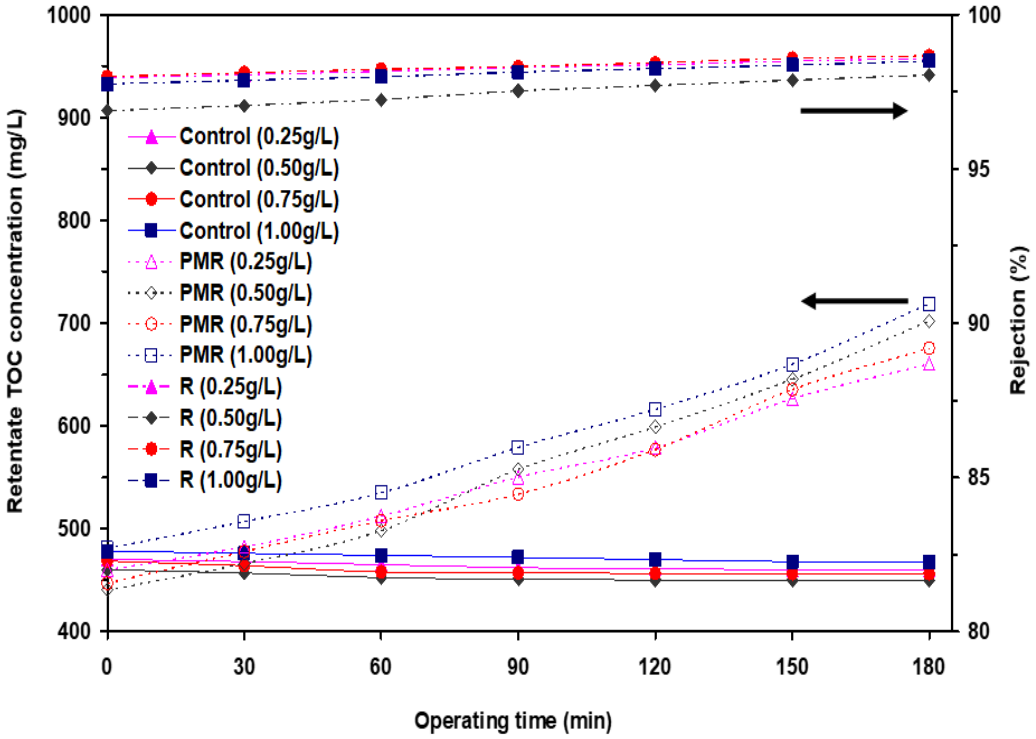

Fig. 5.15: Comparative performance of TOC concentration between control photocatalysis and batch PMR mode of operation at various POM loadings.

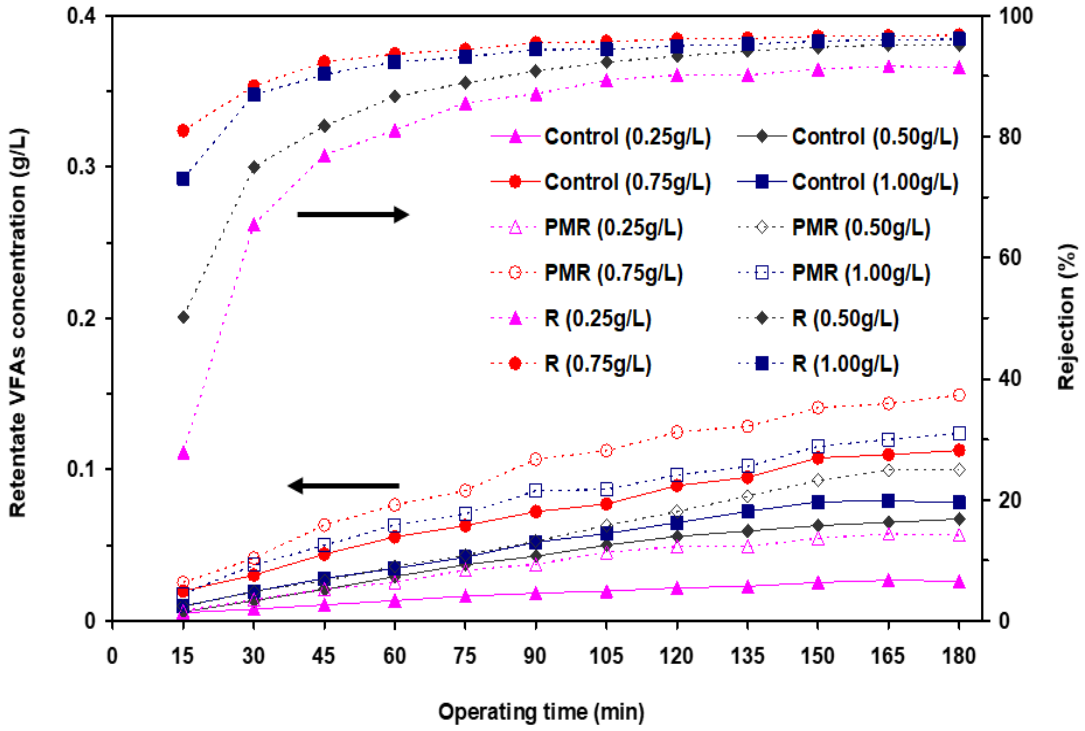

Fig. 5.16: Comparative performance of VFAs between control photocatalysis and batch PMR mode of operation at various POM loadings.

5.4.1.1 Influence of hydrodynamic conditions on batch PMR performance

The hydrodynamic conditions (membrane operating conditions) such as transmembrane pressure, TMP and cross-flow velocity, CFV have been shown to significantly affect the efficiency of separation and the quality of permeate **[61]**. The experimental results obtained have shown clearly that the cross-flow homogeneous PMR enhanced homogeneous photocatalysis in terms of the %PD and K_{app} evaluating parameters at lower POM loadings (0.25 and 0.50 gL^{-1}).

In this section, a 0.50 gL^{-1} POM loading was selected to investigate the effect of these membrane operating conditions on the performance of batch PMR mode of operation. This performance was evaluated on the basis of the %PD and K_{app} of PEG. The retentate POM concentration and permeate flux were considered to achieve this evaluation.

Note that, due to the technical limitations of used pump 2 (Fig. 3.4) in this project, a higher limit of TMP (25 bar) and a lower limit of CFV (0.65 cms^{-1}) were selected to compare their performance with previous results, which were done under TMP (15 bar) and CFV (1.3 cms^{-1}).

1. Effect of TMP

The effect of TMPs on the permeate flux and retentate POM concentration as a function of operating time was examined at constant CFV in Fig. 5.17. Examination of Fig. 5.17 reveals that the higher the TMP the greater the permeate flux. This result is expected since with increase in TMP, the driving force across the membrane increases, and thus increasing the permeate flux **[245, 246, 250]**. This increase in the TMP in relation with permeate flux had a positive impact on the increase of retentate POM concentration inside the BSR and then in the photoreactor. This is also expected due to the effect of filtration process. As seen in Fig. 5.17, the concentration of POM in the retentate increased significantly with increasing the TMP from 15 to 25 bar and reached nearly the optimum concentration of POM control photocatalysis (no membrane) as shown in dashed line. This is an interesting result that the %PD of PEG at TMP (25 bar) should be increased to be similar to that of the optimum control photocatalysis.

On the contrary, it decreased significantly when comparing with TMP (15 bar) as shown in Fig. 5.18 despite the concentration of POM at 25 bar increased considerably to be higher than that of 15 bar (Fig. 5.17). This unexpected result is due to a technical problem related to a damper component in PMR system (chapter 3, Fig. 3.4), which was being used to stabilize the produced pressure by pump 2. This damper was not working appropriately in stabilization of this pressure leading to generate huge quantities of air bubbles as like thick foam inside the BSR and these bubbles were being continuously pumped by pump 1 to the photoreactor. As a consequence, these bubbles played a negative impact on the photocatalytic degradation activity at 25 bar in comparison with that of 15

bar, *inducing an inner filter effect*, and thus reducing the UV light intensity **[2, 170]**. This finding was supported by the measurements of oxidant concentration (mgO_2L^{-1}) as shown in Fig. 5.19 in which the concentration of oxidant under TMP (25 bar) increased greatly with increasing the operating time. Consequently, leading to decrease the %PD of PEG. This effect of oxidant concentration (DO) is explained earlier with more details in chapter 4, section 4.3.1, (2).

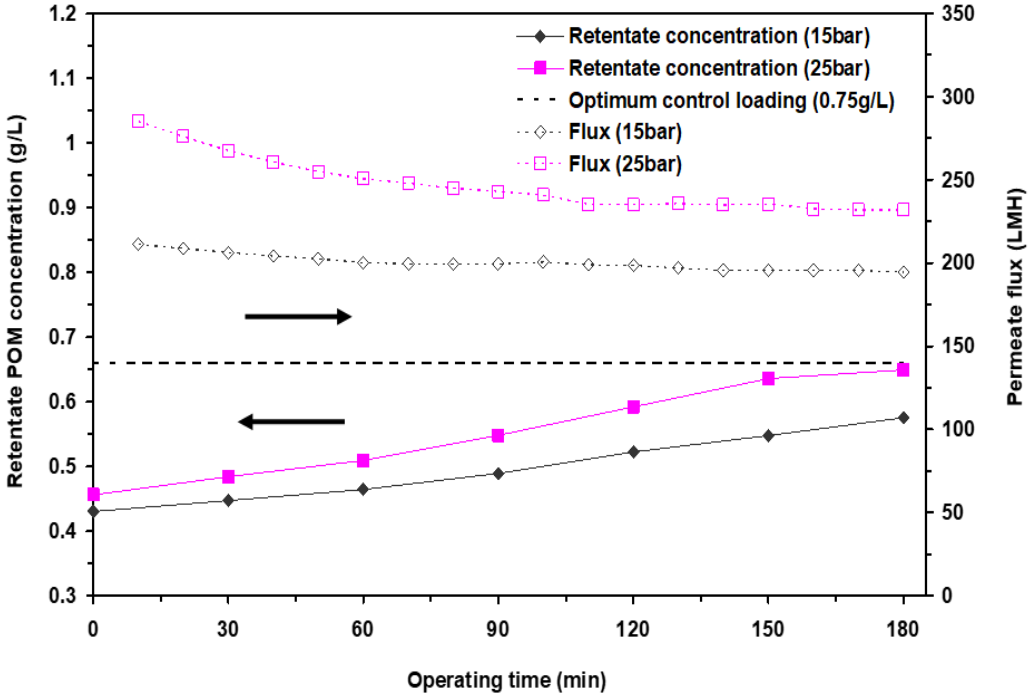

Fig. 5.17: Retentate POM concentration and permeate flux as a function of operating time of batch PMR mode of operation under a constant CFV (1.3 cms^{-1}), a POM loading (0.50 gL^{-1}) and different TMPs.

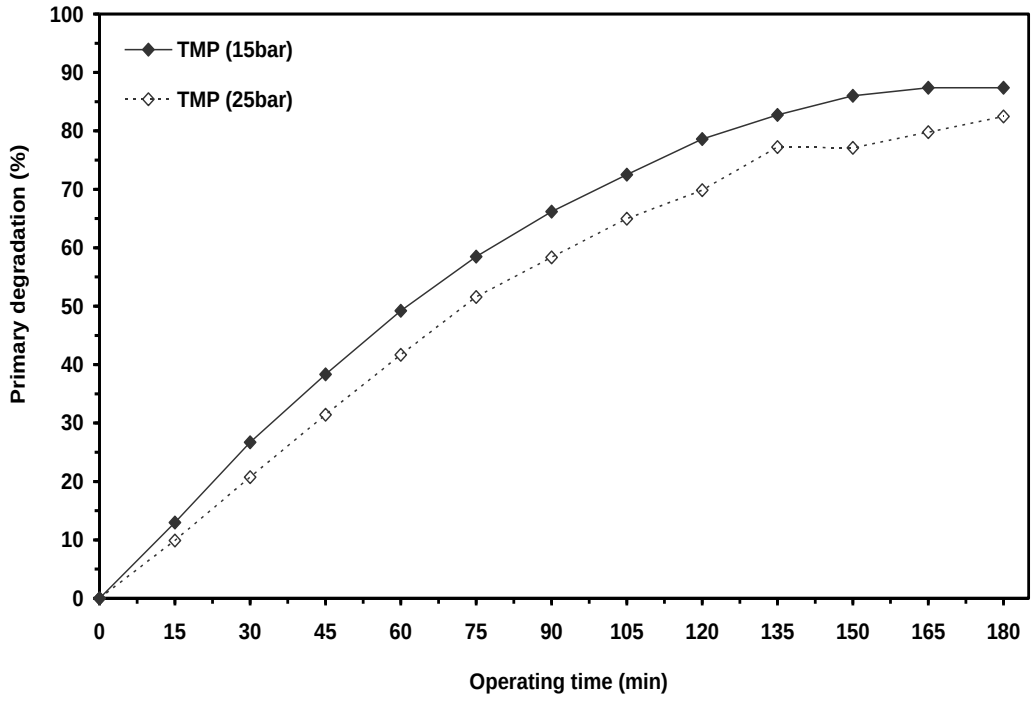

Fig. 5.18: Effect of different TMPs on the %PD of PEG using batch PMR operation with a constant CFV (1.3 cms^{-1}) and a POM loading (0.50 gL^{-1}).

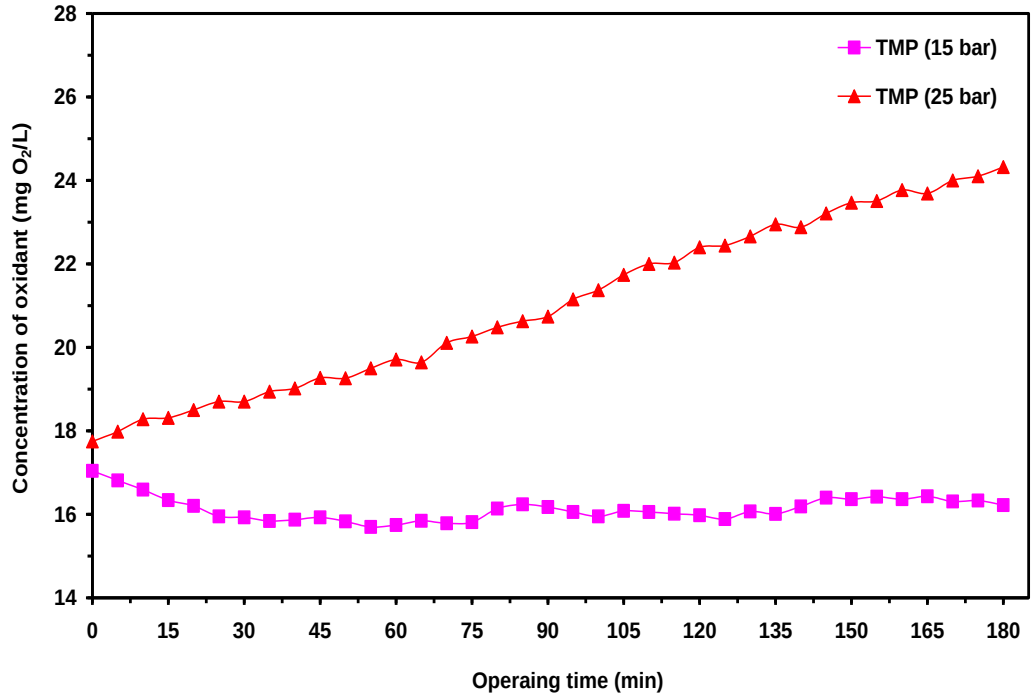

Fig. 5.19: The oxidant concentration monitoring as a function of operating time of batch PMR operation under a constant CFV (1.3 cms^{-1}), a POM loading (0.50 gL^{-1}) and different TMPs.

In terms of reaction kinetics, the effect of TMPs on K_{app} is shown in Fig. 5.20. It appears that the increase in TMP from 15 to 25 bar caused the decrease in the K_{app} by 31%. The general trend of this result is similar to that of the %PD due to the same inner filter effect as explained above.

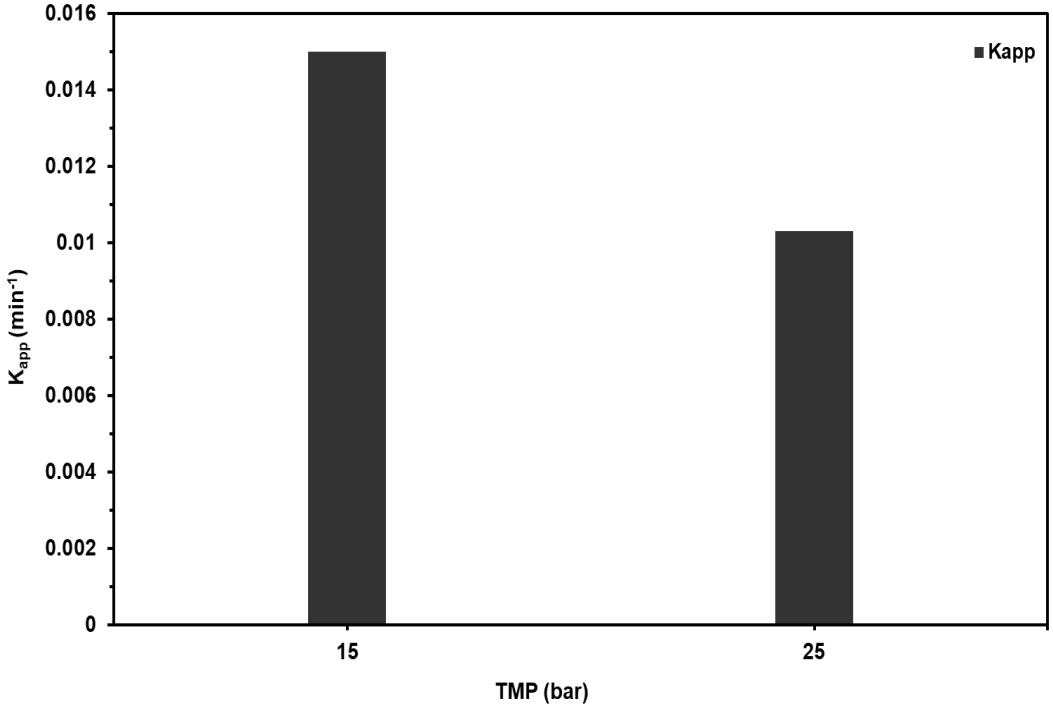

Fig. 5.20: Effect of different TMPs on the K_{app} using batch PMR mode of operation with a constant CFV (1.3 cms^{-1}) and a POM loading (0.50 gL^{-1}).

In Fig. 5.21, the SEM images show that the fouling on the surface of membrane at TMP of 25 bar is lower than that of 15 bar. This finding is unexpected since as reported in literature increasing the TMP can lead to more severe fouling due to an increase in the initial flux by increasing the pressure drop across the membrane **[242]**. The permeate flux data, Fig. 5.17, confirmed this SEM finding where the permeate flux at 25 bar is higher than that of 15 bar. A possible explanation for this is that an increase in TMP led to increase the resulting development of the cake layer (POM photocatalyst and partially oxidized PEG oligomers) onto the membrane surface and then this developed layer was compressed (foulant compaction) by this higher TMP to produce foulant agglomeration as suggested by several authors in literature **[61, 243, 251]**. As a result, this higher TMP causing many of the lightly fouled regions between these compressed agglomeration as shown in Fig. 5.21-b, which allowed to increase greatly the permeate flux at 25 bar through them as compared with 15 bar.

Although a higher TMP (25 bar) showed a significant performance in increasing the retentate POM concentration inside the BSR and permeate flux, there was a clear effect of inner filter under this condition resulting in decreasing the %PD of PEG.

Therefore, TMP of 15 bar was selected to further investigation in the coming section (effect of CFV).

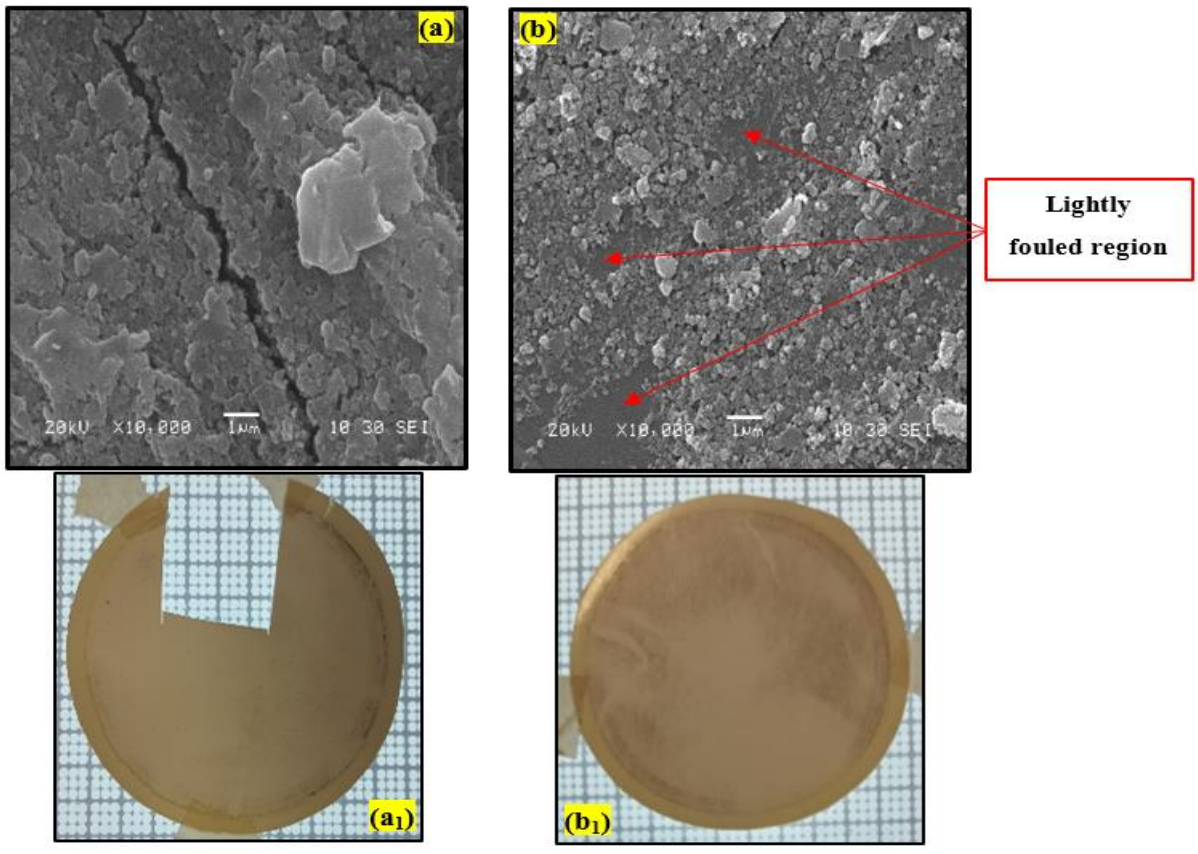

Fig. 5.21: SEM images of the top surface of a fouled membrane with PEG and POM loading (0.50 gL^{-1}) using batch PMR operation under a constant CFV (1.3 cms^{-1}) and different TMPs, magnification: x 10,000 and scale: 1 µm: (a) 15 bar and (b) 25 bar. Real photos of the top surface of a membrane: (a_1) 15 bar and (b_1) 25 bar.

2. Effect of CFV

The effect of two CFVs on the performance of batch PMR mode of operation in terms of the retentate POM concentration and permeate flux as a function of operating time was examined in Fig. 5.22 under a selected TMP of 15 bar. As seen in Fig. 5.22, as operating time proceeded, in terms of the retentate POM concentration inside the BSR, it increased systematically under a higher CFV of 1.3 cms^{-1}, while it decreased dramatically under lower CFV of 0.65 cms^{-1} despite the permeate flux under 0.65 cms^{-1} is higher than that of 1.3 cms^{-1}. A possible explanation for this decrease in POM concentration under 0.65 cms^{-1} is that POM showed a strong tendency to adsorb on, the surface of membrane and the developed cake layer, due to a weak effect of exerted shear force under this CFV to push the adsorbed POM molecules towards the bulk solution. This explanation could be confirmed by SEM images (Fig. 5.23) where a very thick deposition layer under 0.65 cms^{-1} was found in Fig. 5.23-b as compared to that of 1.3 cms^{-1} (Fig. 5.23-a). Also, a real photo of membrane at 0.65 cms^{-1} is visually shown this thick deposition comparing with that of 1.3 cms^{-1}. This thick deposition is to be assumed relating to adsorbed POM molecules.

On the other hand, under 1.3 cms^{-1}, the effect of shear force was so enough to push the adsorbed POM molecules towards the bulk solution and so the POM concentration increased with increasing CFV in the retentate as shown in Fig. 5.22. In this regard, this finding is consistent with the literature by which an increase in CFV increases the applied shear forces, and thus decreasing the effect of the developed cake layer due to sweeping deposited foulants away from the surface of membrane and so increasing the permeate flux **[61, 204, 245, 246, 251]**.

The obtained results of the retentate POM concentration played an influential role in the %PD of PEG under examined CFV conditions as shown in Fig. 5.24, where the %PD of PEG at 1.3 cms^{-1} is greatly higher than that of 0.65 cms^{-1}. A similar trend of these results was found in Fig. 5.25 based on $K_{app,}$ where the decrease in CFV from 1.3 to 0.65 cms^{-1} resulted in decrease in the $K_{app,}$ by 81%. These obtained results of the %PD of PEG and K_{app} confirmed the above explanation in terms of the tendency of POM adsorption.

Based on the experimental results above, a CFV of 1.3 cms^{-1} showed a better performance as compared with 0.65 cms^{-1}. *Therefore, in terms of hydrodynamic conditions, a TMP and CFV of 15 bar and 1.3 cms^{-1} respectively were selected for further investigation later.*

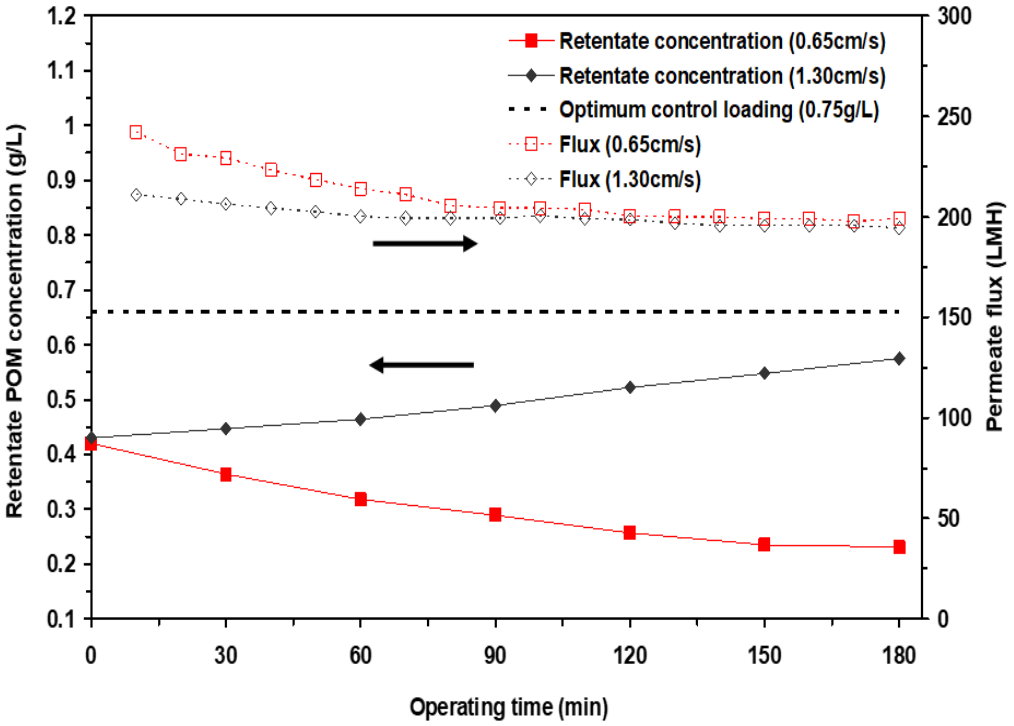

Fig. 5.22: Retentate POM concentration and permeate flux as a function of operating time of batch PMR mode of operation under a constant TMP (15 bar), a POM loading (0.50 gL^{-1}) and different CFVs.

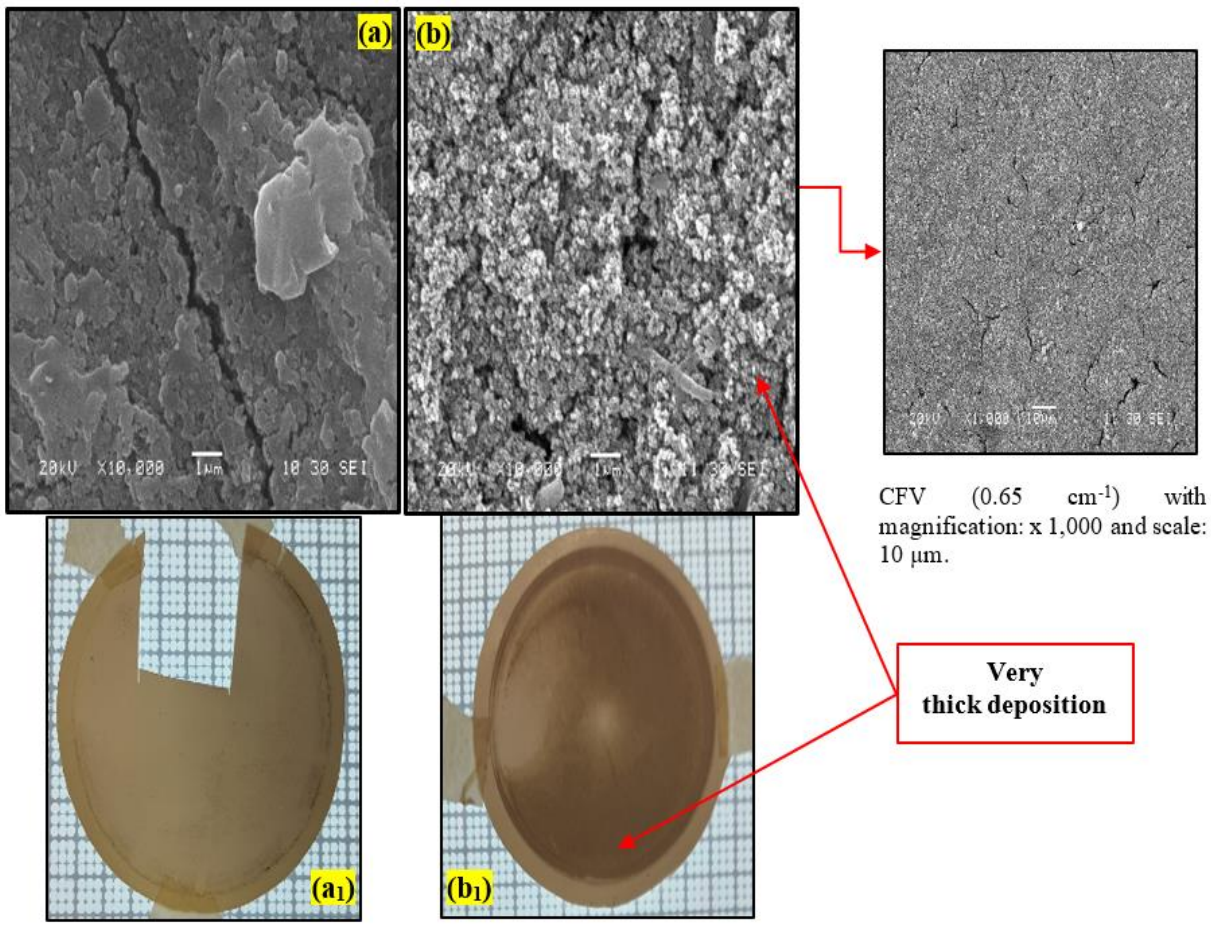

Fig. 5.23: SEM images of the top surface of a fouled membrane with PEG and POM loading (0.50 gL^{-1}) using batch PMR operation under a constant TMP (15 bar) and different CFVs, magnification: x 10,000 and scale: 1 µm: (a) 1.30 cms^{-1} and (b) 0.65 cms^{-1}. Real photos of the top surface of a membrane: (a_1) 1.30 cms^{-1} and (b) 0.65 cms^{-1}.

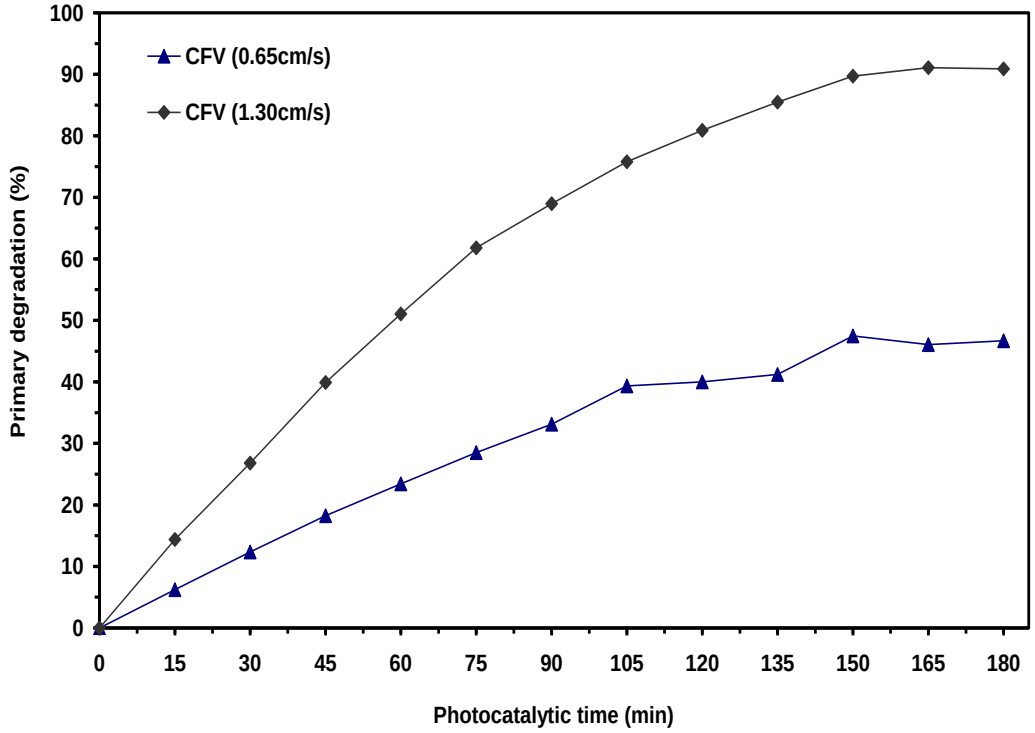

Fig. 5.24: Effect of different TMPs on the %PD of PEG using batch PMR mode of operation with a constant TMP (15 bar) and a POM loading (0.50 gL^{-1}).

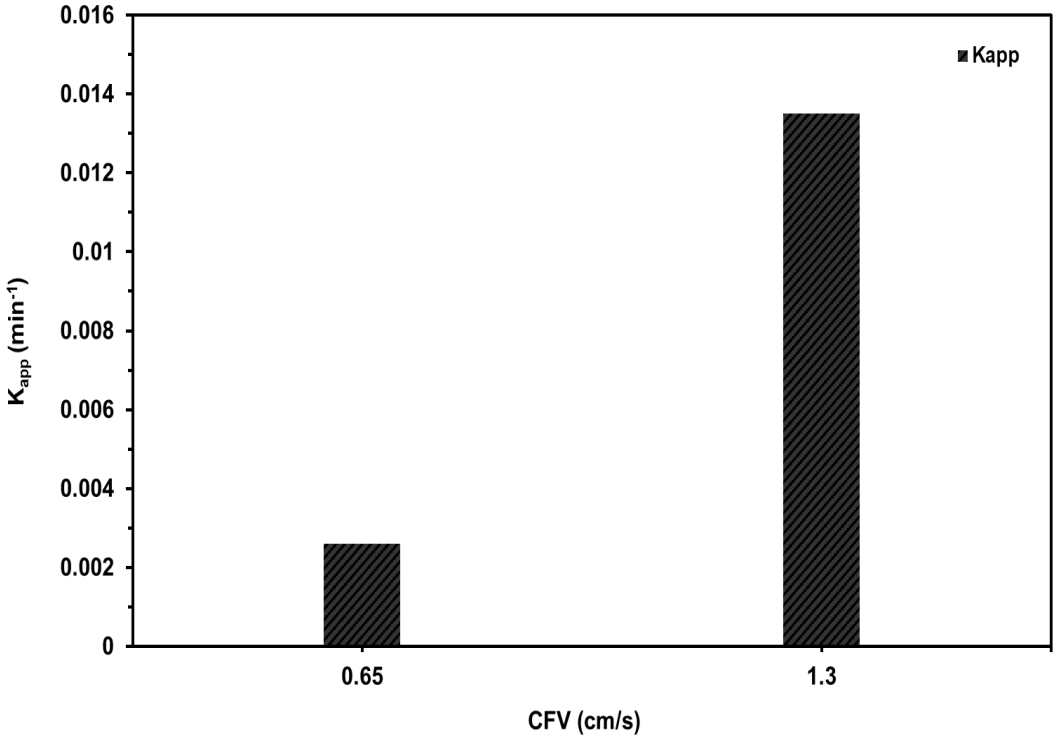

Fig. 5.25: Effect of different CFVs on the K_{app} using batch PMR mode of operation with a constant TMP (15 bar) and a POM loading (0.50 gL^{-1}).

5.4.1.2 POM chemical stability

The chemical stability of POM ($H_3PW_{12}O_{40}$) in the form $[PW_{12}O_{40}]^{3-}$ was examined under different investigating conditions of batch PMR mode of operation. One example of this investigation at POM loading (1 gL^{-1}) is shown in Fig. 5.26.

Fig. 5.26-a shows that POM-$H_3PW_{12}O_{40}$ in the form $[PW_{12}O_{40}]^{3-}$ is not chemically stable in PEG reactant solution as feed under a non-photocatalytic reaction condition (no UV light). It converted partially into various lacunary species of *W*.

Fig. 5.26-b shows that there is no significant change in the chemical structure of POM in the form $[PW_{12}O_{40}]^{3-}$ as well as other identified lacunary species of *W* in the retentate for 180 min of photocatalytic reaction time. These results in terms of POM chemical stability under UV conditions are similar to that found in chapter 4, section 4.3.4.

While in Fig. 5.26-c, POM in the form $[PW_{12}O_{40}]^{3-}$ was not detected in the permeate when comparing with feed (Fig. 5.26-a) and retentate (Fig. 5.26-b). This result confirms that the used membrane could reject POM in the form $[PW_{12}O_{40}]^{3-}$ completely (100%). However, some lacunary species were detected in the permeate. This finding possibly suggests that these lacunary species could pass through membrane with very limited concentration, which their total elemental concentration based on *W* may be expected to be less the minimum detection limit of an *AAS* methodology (3 mg W L^{-1}). However, further investigation in this regard is required to confirm the individual concentration of these lacunary species in the permeate below this limit, *this will be part of future work.*

Overall, POM in the form $[PW_{12}O_{40}]^{3-}$ was completely rejected by the used membrane with a full chemical stability for 3 h operating time under the batch PMR mode of operation. This complete rejection in conjunction with full chemical stability played a significant role in the degradation of PEG oligomers effectively.

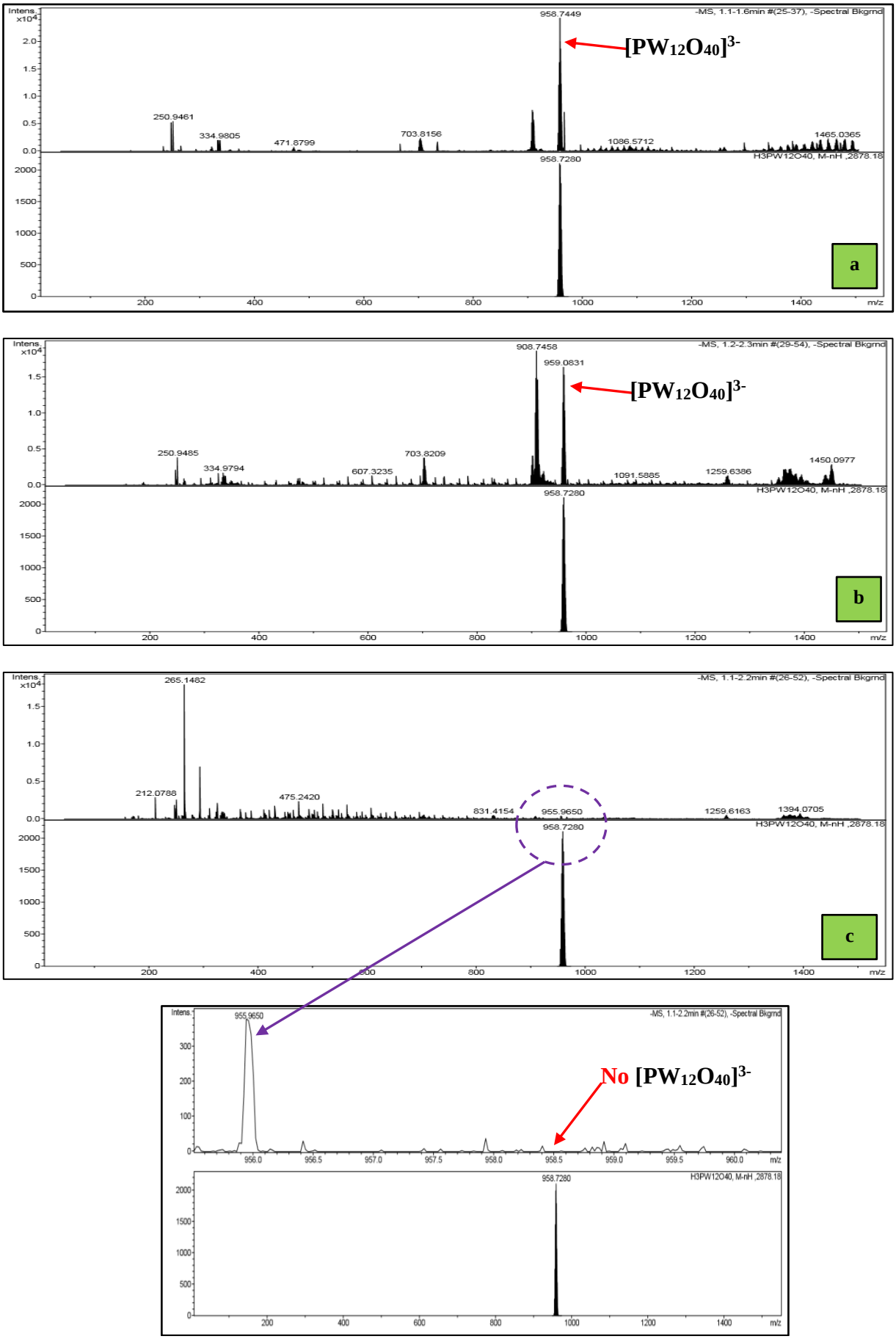

Fig. 5.26: HPLC-ESI-TOF chromatograms for the investigation of chemical stability of POM under batch PMR mode of operation, POM loading (1 gL^{-1}): (a) 30 min of non-photocatalytic reaction of POM with PEG (feed), (b) 180 min photocatalytic reaction of POM with PEG (retentate) and (c) permeate with enlargement view of scale.

5.4.2 Continuous PMR operation (*Continuous photocatalysis*)

The aim of this section is to convert batch homogeneous photocatalysis (control process no-membrane) under the optimal loading of POM photocatalyst (0.75 gL^{-1}) to a continuous photocatalysis using continuous mode of PMR operation. *To achieve this*, a continuous fresh PEG feed was added to the original PEG reactant solution inside the BSR. The PMR was continuously operated under a TMP (15 bar) and CFV (1.3 cms^{-1}) for 9 h. The performance of continuous photocatalysis was evaluated according to the percent primary degradation, reaction kinetics and mineralization, and compared with batch control photocatalysis. *Note that, batch photocatalysis (no membrane), continuous photocatalysis (continuous PMR operation) and batch PMR operation are referred to as control, CPMR and BPMR respectively.*

In Fig. 5.27, a photocatalytic performance based on the %PD of PEG between batch photocatalysis under a 3 h photocatalytic reaction time and continuous photocatalysis under a 9 h operating time (photocatalytic reaction time in conjunction with cross-flow filtration time) was examined. As seen in Fig. 5.27, the continuous photocatalysis showed a similar overall %PD of PEG as the batch photocatalysis. At 3 h, there was a slight decrease in the %PD of PEG under continuous photocatalysis by 10% as compared to batch photocatalysis. This is because the concentration of POM under continuous photocatalysis decreased when comparing with that of batch photocatalysis as shown in Fig. 5.27. Thus, the overall photocatalytic degradation activity of PEG deceased. This decrease in retentate POM concentration under continuous photocatalysis is expected and can be explained by the dilution effect of the added fresh PEG feed to the original PEG reactant solution inside the BSR as shown earlier with more detail in chapter 3, section 3.4.4.

This dilution effect can be generally described in terms of permeate flux under BPMR and CPMR operations as shown in Fig. 5.28. It shows that the permeate flux under BPMR is higher than that of CPMR, indicating that the constant rate of addition (fresh PEG feed) is higher than the rate of filtration under CPMR. Thus, reducing the concentration of POM inside the BSR as shown in Fig. 5.27 and then affecting the %PD of PEG. *In this respect and for future work, this point should be considered.*

Further investigation on the permeate flux under continuous photocatalysis for a 9 h operating time is shown in Fig. 5.28. As the operating time processed, the permeate flux declined. This behaviour indicaes that the surface of membrane was fouled. This fouling can be confirmed by SEM images. The SEM images in Fig. 5.29 show that fouled agglomerations on the surface of membrane where there are huge spaces of lightly fouled regions in the membrane surface (Fig. 5.29), which allowed the permeate flux to be continued gradually. *These fouled agglomeration could be explained by the rejection of POM and PEG oligomers.*

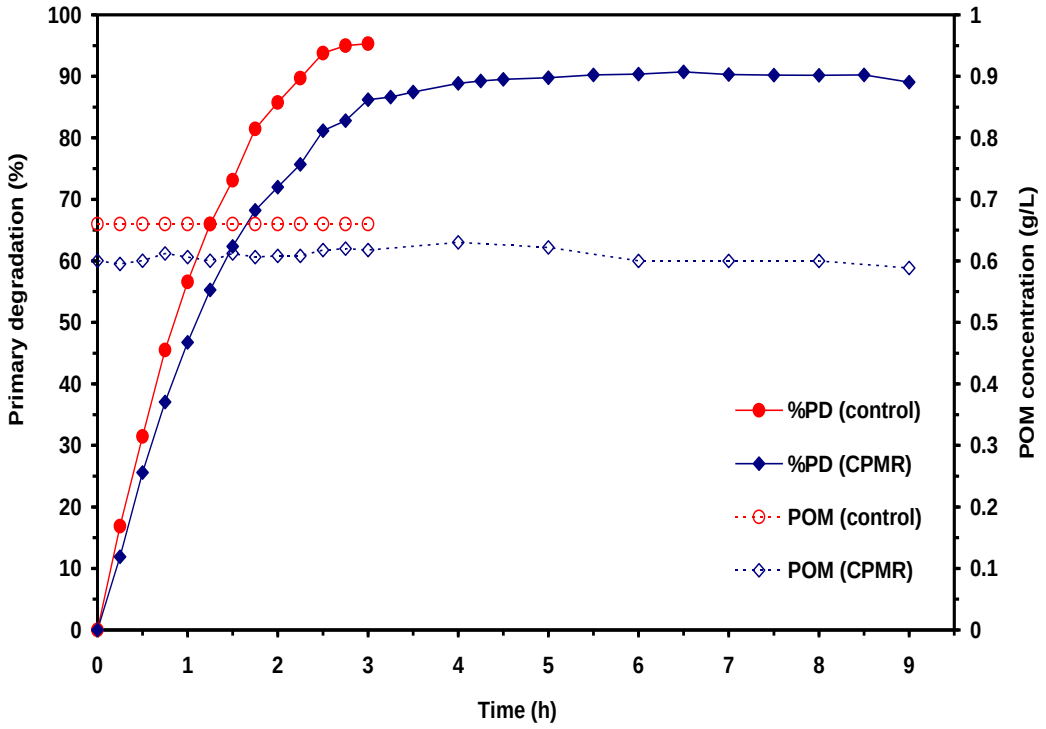

Fig. 5.27: Comparative performance of %PD of PEG and POM concentration as a function of time between batch photocatalysis and continuous photocatalysis under the optimal POM loading (0.75 gL^{-1}).

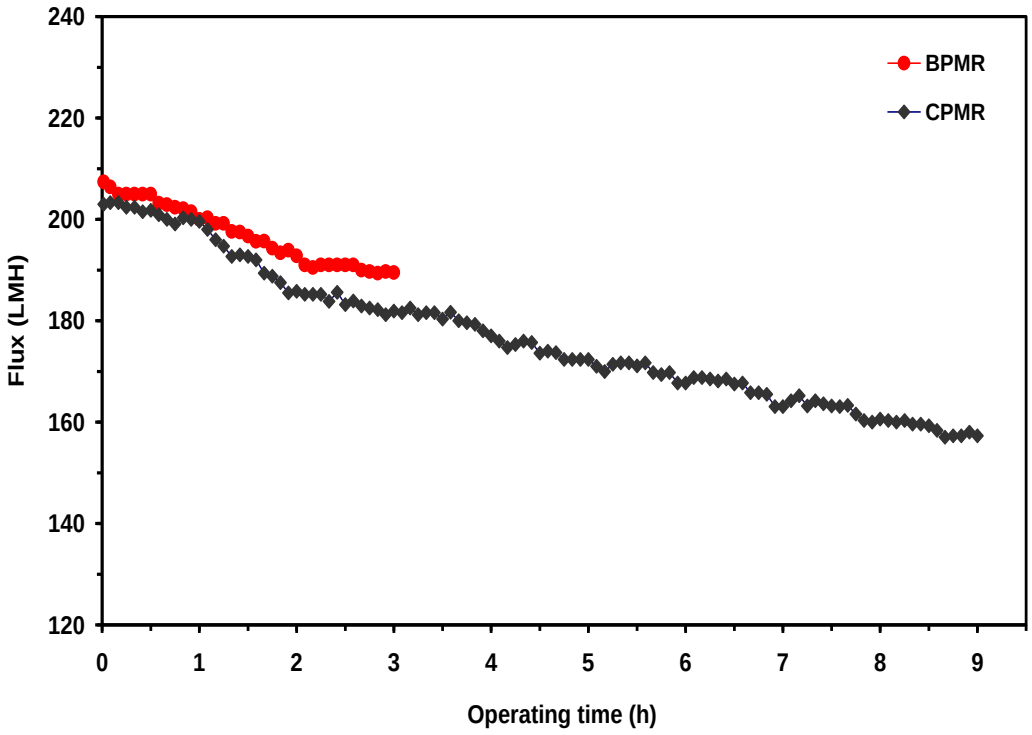

Fig. 5.28: Permeate flux as a function of operating time for batch and continuous PMR modes of operation at POM loading (0.75 gL^{-1}).

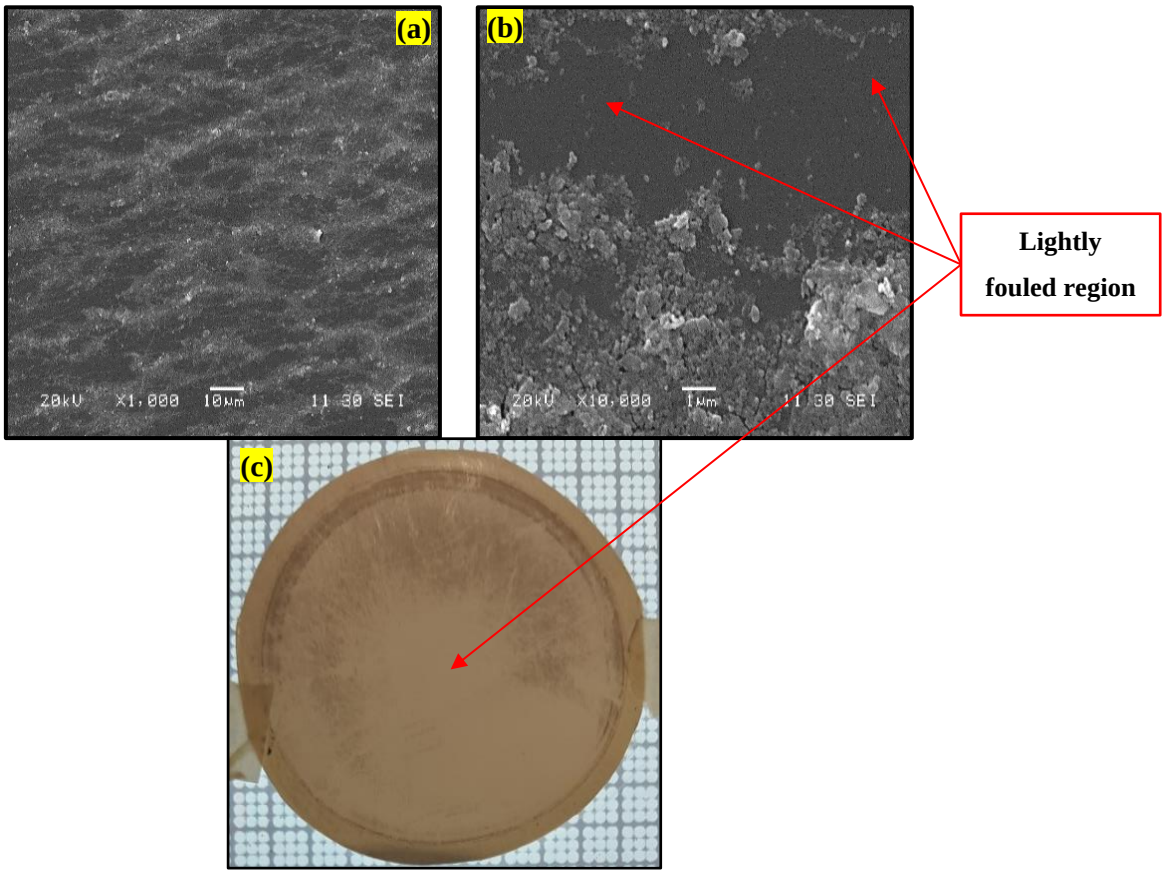

Fig. 5.29: SEM images (a-b) and a real photo (c) of the top surface of a fouled membrane with PEG and POM loading (0.75 gL^{-1}) under continuous photocatalysis, magnification: (a) x 1,000 and scale: 10 µm and (b) x 10,000 and scale: 1 µm.

In terms of POM rejection, the membrane showed a continuous ability for a 9 h operating time to reject POM in the form $[PW_{12}O_{40}]^{3-}$ completely as similar to that of batch PMR mode of operation with a full chemical stability under UV examined conditions as explained in section 5.4.1.2.

In terms of PEG rejection, this could be explained by the two assumed scenarios shown in section 5.4.1, 1 because the similar trend of experimental data was obtained for low, medium and high ranges of MWs of PEG as feed in the retentate and permeate. For permeate investigation, the permeate experimental results are in agreement with the first scenario. Whilst for retentate, Fig. 5.30 shows that at 3 h, the total number of residual PEG oligomers was 11 oligomers located at LO and MO ranges of MWs under continuous photocatalysis. Based on the second scenario, these identified residual oligomers were partially (lightly) oxidized and the membrane could successfully reject them from passing through the membrane to the permeate and return them to the photoreactor for further oxidation. At 9 h, the partially oxidized oligomers were found to be 10 oligomers and potentially they were rejected by the membrane, and thus agglomerated on the surface of membrane as shown in SEM images (Fig. 5.29). Also, Fig. 5.30 shows the comparison of residual oligomers and total concentration of PEG under batch and continuous photocatalysis. It can be observed that the total

number of residual PEG oligomers was 6 oligomers within LO range of MW only under batch photocatalysis when comparing with 11 oligomers under continuous photocatalysis. Consequently, the total concentration of PEG was affected. This result was expected since batch photocatalysis showed higher %PD of PEG than continuous photocatalysis (Fig. 5.27).

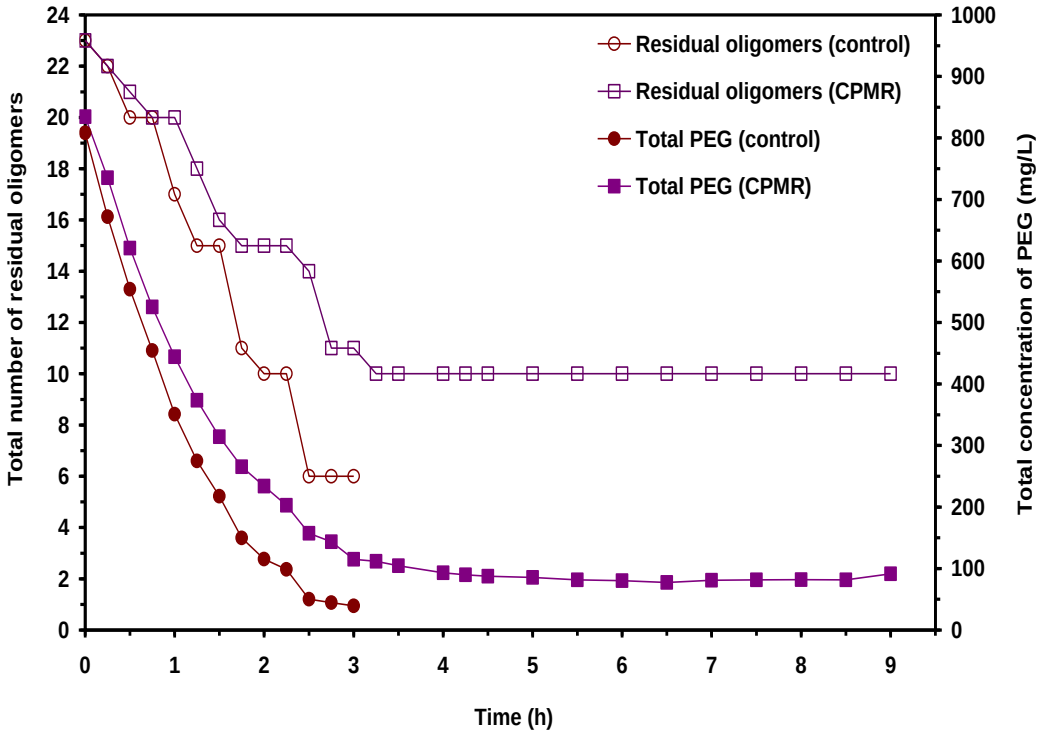

Fig. 5.30: Comparison of residual oligomers and total concentration of PEG as function of operating time in the retentate between batch photocatalysis and continuous photocatalysis under the optimal POM loading (0.75 gL^{-1}), TMP (15 bar) and CFV (1.3 cms^{-1}).

The photocatalytic mineralization performance of batch photocatalysis as compared to continuous photocatalysis could be explained by the TOC concentration in relation to VFAs formation as a function of time in Fig. 5.31. It was found that at 3 and 9 h operating times of continuous photocatalysis, the concentration of TOC increased by 48 and 132% respectively and the concentration of VFAs increased by 61 and 343% respectively when compared with that of batch photocatalysis. This is due to two reasons as explained with more details in section 5.4.1, 3. The rejection data in Fig. 5.32 confirmed these possible reasons in which at 3 and 9 h operating times, the rejection of TOC was 94 and 96% respectively, while the rejection of VFAs was 95 and 96% respectively.

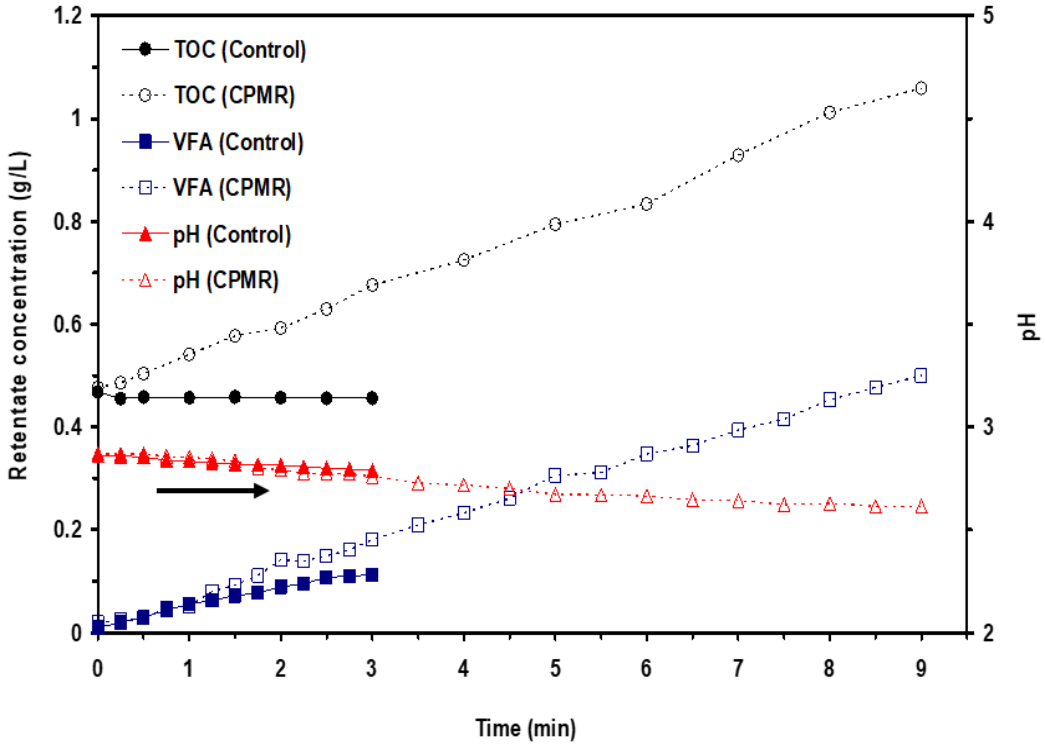

Fig. 5.31: Comparative performance of TOC, VFAs and pH over time between batch photocatalysis and continuous photocatalysis under the optimal POM loading (0.75 gL^{-1}).

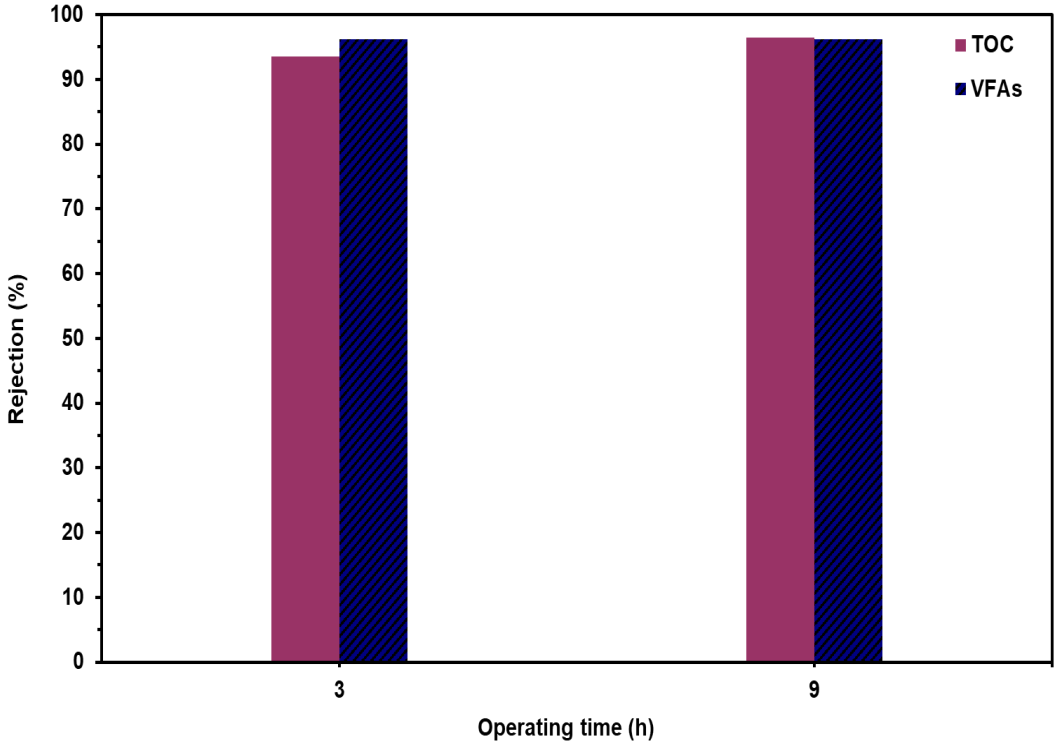

Fig. 5.32: Comparison of the rejection of TOC and VFAs between batch photocatalysis and continuous photocatalysis under the optimal POM loading (0.75 gL^{-1}).

In terms of monitoring the pH, the formation of VFAs as reaction intermediate compounds under batch photocatalysis was associated with the drop of pH values as shown in Fig. 5.31. While, for continuous photocatalysis, the pH gave an indicator about the formation and rejection of these acids. These acids were greatly rejected by the membrane as shown in Fig. 5.32, thus their concentrations increased significantly in spite of the dilution effect of added fresh PEG feed as explained earlier.

In terms of monitoring the oxidant concentration (DO), it is important to mention that the concentration of DO in the BSR after the adsorption period was 17±1 mgL^{-1}. This concentration was achieved by the recirculation of (PEG-POM) solution through PMR system using pump 1 and pump 2 (Fig. 3.4) together without supplying a continuous oxygen feed. Under this condition, the solution was oxygenated through a mass transfer from ambient air only for a 9 h operating time. The concentration of DO under continuous photocatalysis is monitored in Fig. 5.33. As shown in Fig. 5.33, there is no significant change in the concentration of DO during the continuous photocatalysis. The same results were nearly found under control photocatalysis (no membrane) and batch PMR where the consumption of DO was not more than 2 mgO_2L^{-1}. *This gave evident that the concentration of generated DO from ambient air was so enough to sustain the POM photocatalytic reactions for a 9 h operating time. This result is interesting in terms of economic considerations.*

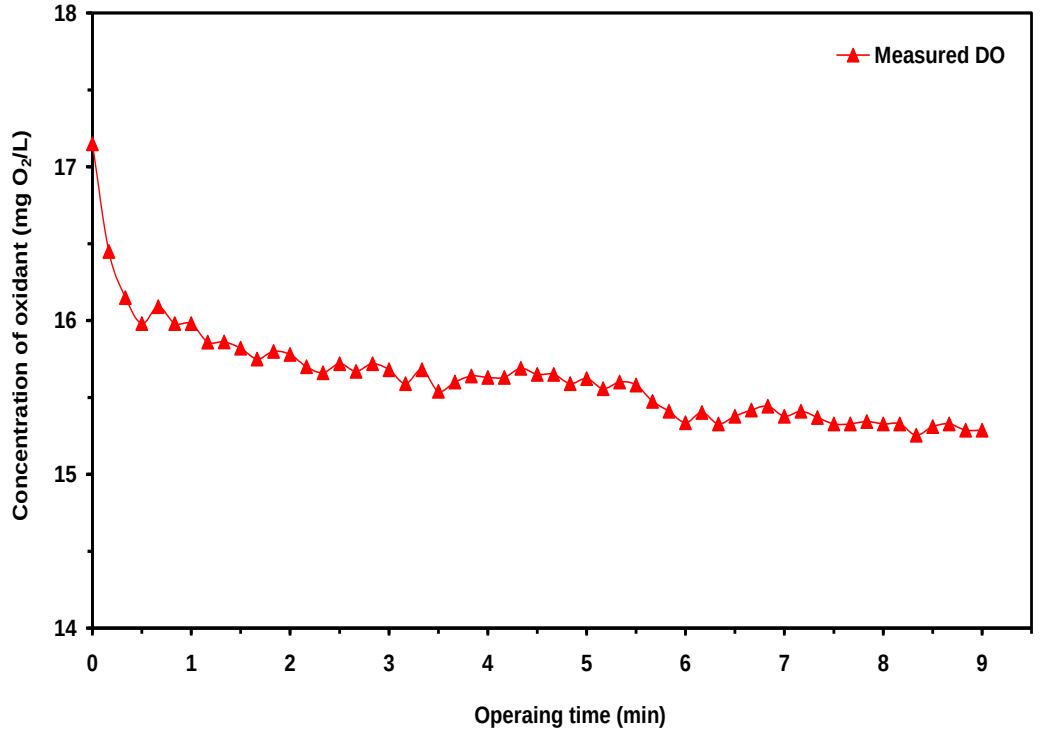

Fig. 5.33: Concentration of oxidant (DO) as a function of operating time for continuous photocatalysis at optimal POM loading (0.75 gL^{-1}).

In terms of reaction kinetics, a simplified Langmuir-Hinshelwood (L-H) kinetic model was successfully used to describe the reaction kinetics of PEG under batch PMR mode of operation for a 3 h operating time (section 5.4.1, 2) and also for homogeneous photocatalysis-no membrane (section 5.3.2, 2). Under these examined conditions the primary photocatalytic degradation of PEG was dominant, so the expression of a single pseudo-first order reaction (L-H) model fitted well the degradation data. However, under POM continuous photocatalysis of PEG using PMR, examination of a kinetic reaction analysis for a 9 h operating time (data not shown) reveals that the semi log data does not produce a single straight line, and thus does not fit a simplified (L-H) kinetic model for the total course of photocatalytic reaction time. Therefore, to elucidate more about this reaction analysis, a series of three first order reaction kinetic models was proposed in Fig. 5.34.

In literature, this is an accepted kinetic modelling strategy for the reactions of AOPs. In particular for the heterogeneous photocatalysis, *Shariffuddin et al.,* **[252]** used a three step series of first order reaction (L-H) kinetic models to describe the overall photocatalytic reaction data of hydroxyapatite derived from mussel shells as a heterogeneous photocatalyst for the degradation of methylene blue (MB). They reported that the photocatalytic degradation of MB consisted of three different reaction steps including fast primary degradation, slower secondary degradation of intermediates and finally mineralization.

The three pseudo-first order reaction constants for three kinetic steps from Fig. 5.34 are shown in Fig. 5.35. It is clear to see from Fig. 5.35 that the trend of these reaction constants represents the photocatalytic reaction mechanism of PEG under continuous photocatalysis where fast primary photocatalytic degradation of original PEG oligomers (region *a*), slower secondary photocatalytic degradation of reaction intermediate compounds (region *b*) and finally the photocatalytic degradation of these intermediates into complete mineralization (region *c*). The obtained results reflect the photocatalytic reaction pathway of PEG under continuous photocatalysis. However, the reaction of intermediates like VFAs need to be accounted for the reaction kinetics of PEG. Therefore, a full kinetic analysis of these reaction intermediates will be part of future work.

Overall, a proposed PMR could successfully convert batch photocatalysis to continuous photocatalysis with an interesting performance of photocatalytic degradation of PEG for a 9 h operating time due to the excellent ability of used membrane to retain the POM photocatalyst and recycle it to the photoreactor as well as a continuous ability to promote good membrane flux until the end time of operation.

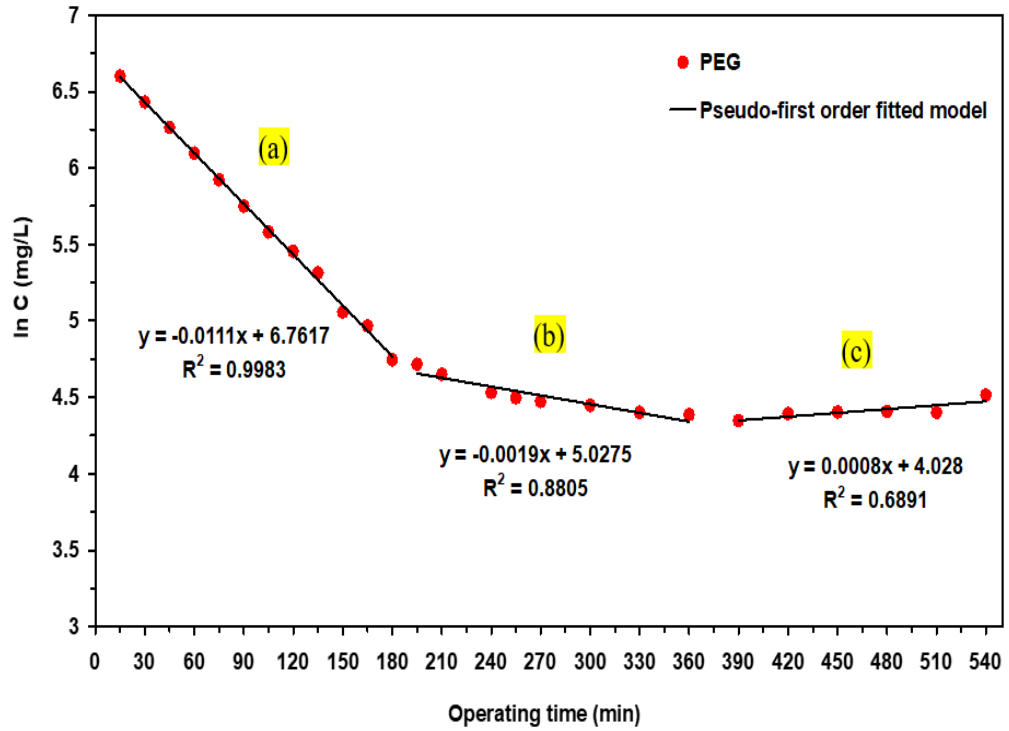

Fig. 5.34: Three stage pseudo-first order reaction constants plot for the kinetic photocatalytic degradation of PEG under continuous photocatalysis using PMR.

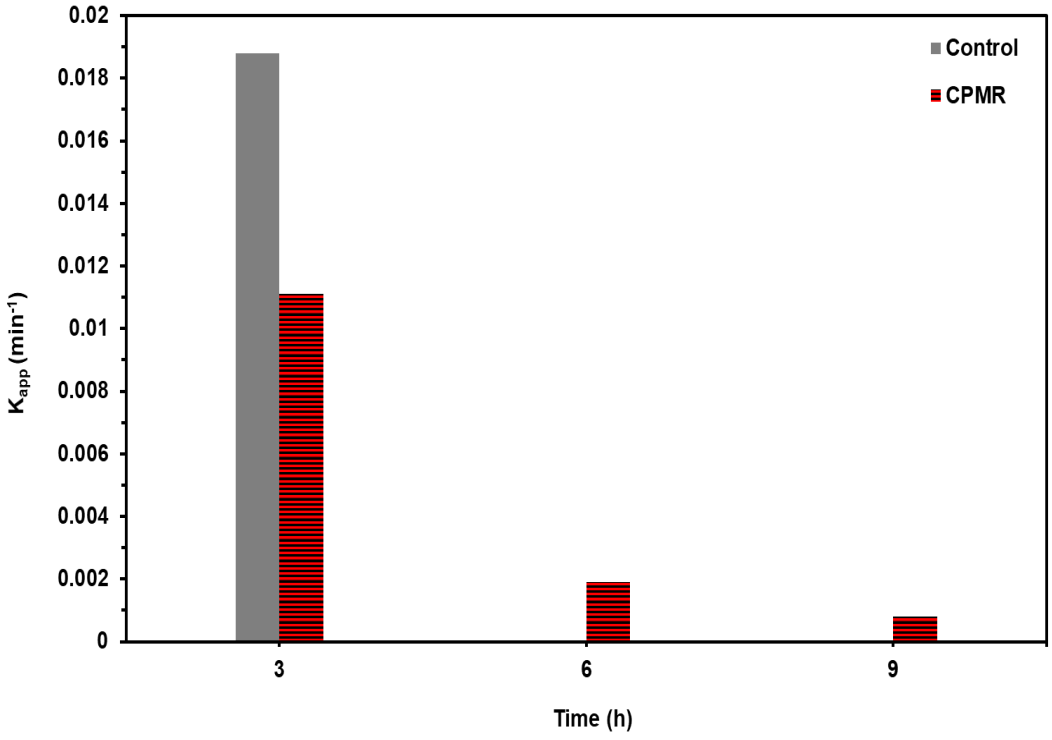

Fig. 5.35: Comparative performance of K_{app} as a function of time between batch photocatalysis and continuous photocatalysis under the optimal POM loading (0.75 gL^{-1}).

5.5 Chapter conclusions

The main aim of this chapter was to use and recycle POM homogeneous photocatalyst in a proposed PMR for the treatment of PEG under batch and continuous modes of operation. This aim was carried out in the three sections (5.2, 5.3 and 5.4) and the following conclusions for each part were drawn:

1) Investigation on the separation of POM (no UV)

- A complete separation of POM homogeneous photocatalyst from PEG reactant solution was achieved by the membrane (NF270) under the examined condition of dead-end membrane filtration process. This interesting result led to use this membrane in the proposed cross-flow PMR.
- The same membrane could reject PEG with total concentration (> 90%) and TOC with (99%) from (PEG-POM) reactant solution. This result confirms that this membrane could be used for retain PEG in the photoreactor of proposed cross-flow PMR.

2) POM homogeneous photocatalysis (no membrane)

- POM could react with PEG non-photocatalytically and its consumption increased with increasing its applied loading.
- The optimal control loading of POM was found at 0.75 gL^{-1}, achieving the maximum %PEG of PEG, which was selected to convert batch photocatalysis to continuous photocatalysis.
- A simplified Langmuir-Hinshelwood (L-H) kinetic model was successfully used to express the photocatalytic degradation data of PEG under control photocatalysis and also batch PMR operation.
- Low mineralization as expressed in TOC removal < 3% was found. This is due to the formation of several low MW VFAs as reaction intermediates such as malonic, glycolic, formaldehyde, formic, acetic and propionic acids that were highly resistant to further oxidation.

3) Cross-flow homogeneous photocatalytic membrane reactor

A. Batch PMR operation:

- The concept of membrane enhanced homogenous photocatalysis is feasible at lower POM loadings of 0.25 and 0.50 gL^{-1}, which are below the optimal POM control loading of photocatalysis (0.75 gL^{-1}). This concept has been proven depending on the suggested evaluating parameters of %PD and K_{app}. Due to filtration, the membrane could concentrate the lower POM

loadings to be comparable to that of an optimal POM loading, and thus increasing the values of these parameters to be comparable to that of an optimum control photocatalysis.

- For POM rejection, the PMR could completely retain the POM photocatalyst in the form $[PW_{12}O_{40}]^{3-}$ based on HPLC-ESI-TOF methodology and return it successfully to the photoreactor.
- For PEG rejection, the PMR could retain the PEG oligomers that are higher than the MWCO of membrane and return them to the photoreactor for further oxidation. At the end of course of operating time (3 h), lightly oxidized oligomers were identified in the retentate within low range of MWs. While, the greatly oxidized oligomers within medium and high ranges of MWs were not detected in the permeate based on the MIDL of HPLC methodology and calibration. So, the calculation of true PEG rejection in terms of individual oligomers or total PEG is not accurate.
- For mineralization, the PMR could not enhance the photocatalytic mineralization of PEG due to the resistance of formed VFAs to total mineralization and also these VFAs could not considerably pass through the membrane to the permeate because of the effect of a secondary dynamic membrane by the adsorbed VFAs on the membrane surface.
- The TMP (25 bar) increased greatly the permeate flux and as a result, increasing the POM concentration in the retentate. However, the %PD of PEG decreased significantly due to an inner filter effect caused by bubbles of air (technical problem in used damper) and then reducing the UV light intensity. While, this inner filter effect was minor under the TMP (15 bar) in terms of the %PD of PEG when compared with TMP (25 bar) and therefore it was selected for further investigation of continuous PMR operation.
- The higher CFV (1.3 cms^{-1}) increased the applied shear forces to push the POM molecules towards the annular photoreactor and consequently increasing the %PD of PEG when comparing with lower CFV (0.65 cms^{-1}).
- POM in the form $[PW_{12}O_{40}]^{3-}$ was chemically stable for 180 min of operating time (under UV conditions). This chemical stability played a significant role in the degradation of PEG oligomers.

B. Continuous PMR operation:

- The proposed cross-flow PMR could successfully convert batch photocatalysis to continuous process for a 9 h operating time with high photocatalytic efficiency in the degradation of PEG, indicating that under this examined condition, POM photocatalyst showed a high photocatalytic performance.

- The membrane could retain POM photocatalyst in the form $[PW_{12}O_{40}]^{3-}$ with a complete rejection as similar to the batch PMR mode of operation. Similarly, it could retain the identified lightly oxidized oligomers within low range of MWs as well as TOC in relation with the formed VFAs in the retentate and return them for photoreactor for further degradation. Despite this complete rejection of POM and higher rejection of PEG oligomers with formed VFAs by the used membrane (NF270), this membrane showed a continuous ability to promote good membrane flux until the end of operation. This indicates that there was no complete pore blocking caused by using the POM homogeneous photocatalyst.
- Monitoring the pH gave an indication relating to the formation and rejection of VFAs since these acids could partially pass through the membrane, so their concentrations increased in the retentate in spite of the condition of dilution effect of added fresh PEG feed.
- Monitoring the DO showed that the consumption of POM photocatalytic reactions for the end of course of operation was so limited (< 2 mgO_2L^{-1}) and the formed DO concentration inside the PMR system from ambient air was sufficient to sustain these reactions. This is very interesting result in terms of economical point of view, reflecting positively in real wastewater treatment applications when using POM homogenous PMR under batch and continuous operations.
- The overall photocatalytic reaction pathway of PEG under continuous photocatalysis for a 9 h operating time was represented well by three steps of first order reaction (L-H) kinetic models. The obtained reaction rate constants reflected the photocatalytic reaction mechanism of PEG, which included fast photocatalytic degradation of original PEG oligomers, slower secondary degradation of intermediates and complete mineralization.

Chapter 6

TiO_2 Heterogeneous Photocatalytic Membrane Reactor

6.1 Introduction

As shown earlier in chapter 2, there is no literature available into the application of TiO_2 heterogeneous photocatalysis on PEG. Therefore, the principal aim of this chapter is to use and recycle the TiO_2 heterogeneous photocatalyst in a proposed cross-flow PMR for the treatment of PEG. The results of this chapter obtained will be used later as benchmark for comparing with a POM homogeneous cross-flow PMR. This chapter is divided into three main sections where the experimental procedure of these sections were performed in chapter 3, section 3.4.3.2.

The first section (6.2) investigates the ability of membrane (NF270) to separate a TiO_2 photocatalyst using dead-end membrane filtration process (*no UV*), giving that the possibility of using this membrane later in a proposed cross-flow PMR.

The second section (6.3) discusses several preliminary experiments that identified the best conditions to be used in a TiO_2 heterogeneous photocatalysis of PEG as control process (*no membrane*). This control process was assessed based on the evaluating parameters of primary degradation, reaction kinetics and minimization.

The last section (6.4) concentrates on applying the cross-flow PMR under batch mode of operation to validate if the concept *'membrane enhanced heterogeneous photocatalysis'* is feasible based on the evaluating parameters mentioned above in comparison with that of control photocatalysis (section 6.3). Additionally, this section discusses the possibility to convert batch heterogeneous photocatalysis under an optimal investigated TiO_2 loading to a continuous heterogeneous photocatalysis. Finally, the discussion of these three sections conclude this chapter.

6.2 Investigation on the separation of TiO_2 (*no UV*)

Based on the comparative purposes with POM homogenous photocatalyst, *in the current investigation*, the same membrane (NF270) was used in dead-end membrane filtration process under dark conditions (*no UV*) to examine its ability to reject a TiO_2 heterogeneous photocatalyst with and without PEG reactant as feed. A TiO_2 loading (1 gL^{-1}) with and without PEG as an example of this investigation was chosen similar to that of POM homogeneous photocatalyst investigated in chapter 5, section 5.1.

The experimental results of this investigation are shown in Table 6.1where the used membrane could completely reject TiO_2 photocatalyst (100%) from PEG reactant solution and also from aqueous solution (*no PEG*). While for total PEG rejection, a poor rejection from (PEG-TiO_2) solution was found to be 33.7% in comparison with that of > 89.9% from PEG reactant solution only (*no TiO_2*). Similarly, for TOC rejection, it was 43.8% at (PEG-TiO_2) solution when comparing with 86.3% at PEG reactant solution.

It is interesting to note there is a significant difference between two rejections based on total PEG and TOC. This difference could be explained by a non-photocatalytic reaction between TiO_2 and PEG, changing the oligomeric structure of PEG with regard to MW, and thus some oligomers could pass through the membrane to the permeate. The results in the permeate in terms of the individual concentration of each PEG oligomer (Fig. 6.1) based on RP-HPLC/ELSD chromatograms (not shown here) as a function of PEG oligomer MW confirmed this a non-photocatalytic reaction of TiO_2 with PEG, which is discussed in further detail later in section 6.3.1.1.

Table 6.1: Membrane characterization of different feeds using dead-end membrane filtration method under TiO_2 loading (1 gL^{-1}) and PEG concentration (1 gL^{-1}).

Type			Rejection (%)	Feed concentration (mgL^{-1})	Permeate concentration (mgL^{-1})	Retentate concentration (mgL^{-1})	Mass (%)
TiO_2			100	969.9	-	1745.8	10.1
PEG		C	>89.9	998.9	<MDL	1551.2	<22.4
		TOC	86.3	564.3	77.6	776.4	24.3
PEG-TiO_2	*TiO_2*		100	930.1	-	1682.1	10.3
	PEG	C	33.7	913.6	605.9	1229.4	0.5
		TOC	43.8	551.5	309.7	651	12.9

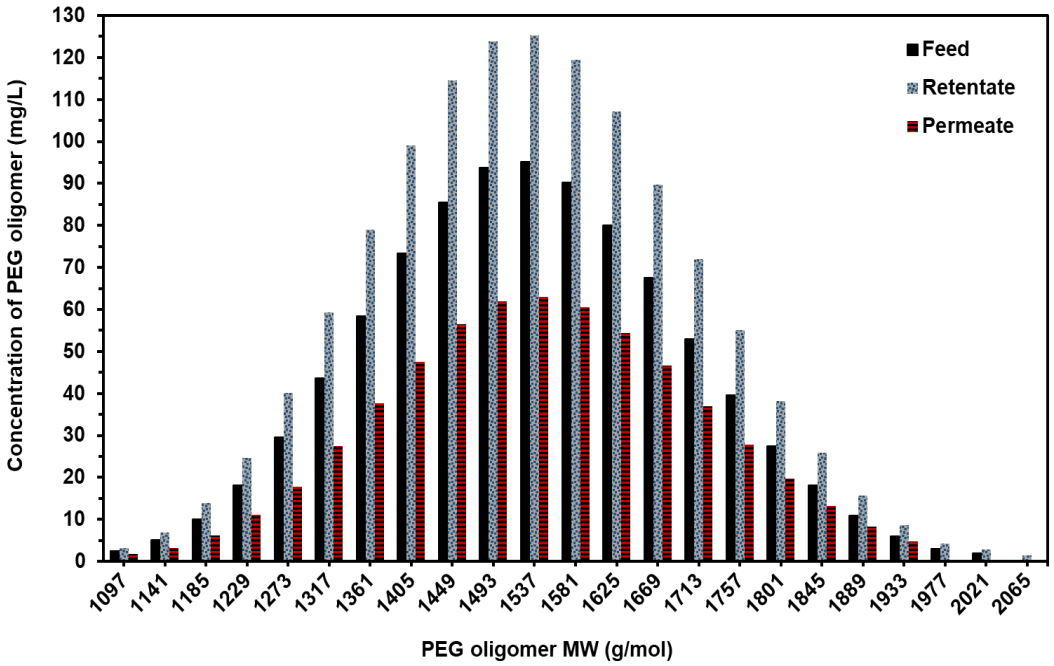

Fig. 6.1: The concentration of PEG oligomer in feed (after a non-photocatalytic reaction), retentate and permeate as a function of PEG oligomer MW under dead-end membrane filtration process with TiO_2 loading (1 gL^{-1}).

In terms of permeate flux, the comparison of different profiles of permeate fluxes for PEG, TiO_2 and (PEG-TiO_2) feeds is shown in Fig. 6.2. It is clear to see that a single component feed of TiO_2 showed a higher permeate flux compared with other feeds. This can be attributed to the repulsive forces between the TiO_2 particles, opening the pores in the resulted cake layer to be a porous layer, and thus increasing the permeate flux **[253, 254]**. On the other hand, a rapid reduction of permeate flux for (PEG-TiO_2) feed was found when comparing with that of each single component feed of TiO_2 or PEG. This is expected and could be explained by the fact that the interaction between the TiO_2 particles and the PEG oligomers, forming a dense developed cake layer and then decreasing the permeate flux significantly. This finding is agreement with a study by *Lee et al.*, **[254]** who investigated UF fluxes for humic acid, powdered TiO_2 and a mixture of them under dark conditions (no UV). The flux of mixture was lower than that of humic acid or TiO_2. They explained that due to the interaction of humic acid and TiO_2 particles, leading to form a dense cake layer when compared with that of TiO_2 and then reducing the permeate flux.

The obtained flux decline in Fig. 6.2 is supported by the rejection data shown in Table 5.1 and the SEM images (Fig. 6.3). The SEM images in Fig. 6.3 provided more information about the formation of membrane fouling. It can be seen that the membrane surface was fouled with the presence of TiO_2, PEG and (PEG-TiO_2) feeds when compared with a new surface one. A thick deposited layer of (PEG-TiO_2) feed (Fig. 6.3-d) was formed with agglomeration effect as shown in Fig. 6.3 (d-1 and d-2). This agglomeration effect led to decrease the permeate flux accordingly.

In conclusion, the obtained results based on the rejection of TiO_2 are very encouraging results for using the membrane (NF270) in the proposed cross-flow PMR later. However, in terms of PEG rejection, since there was a non-photocatalytic reaction of TiO_2 with PEG leading to change the oligomeric profile of PEG, and thus passing some oligomer MW through the membrane. In this respect, in the coming work under PMR, this point should be considered.

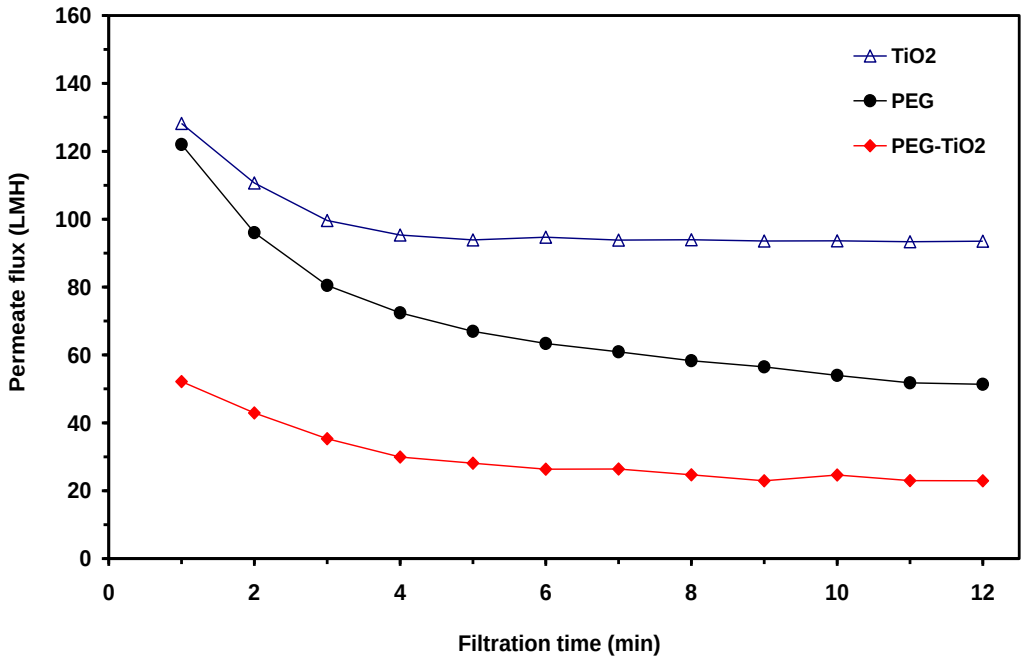

Fig. 6.2: Permeate flux profiles under dead-end membrane filtration process.

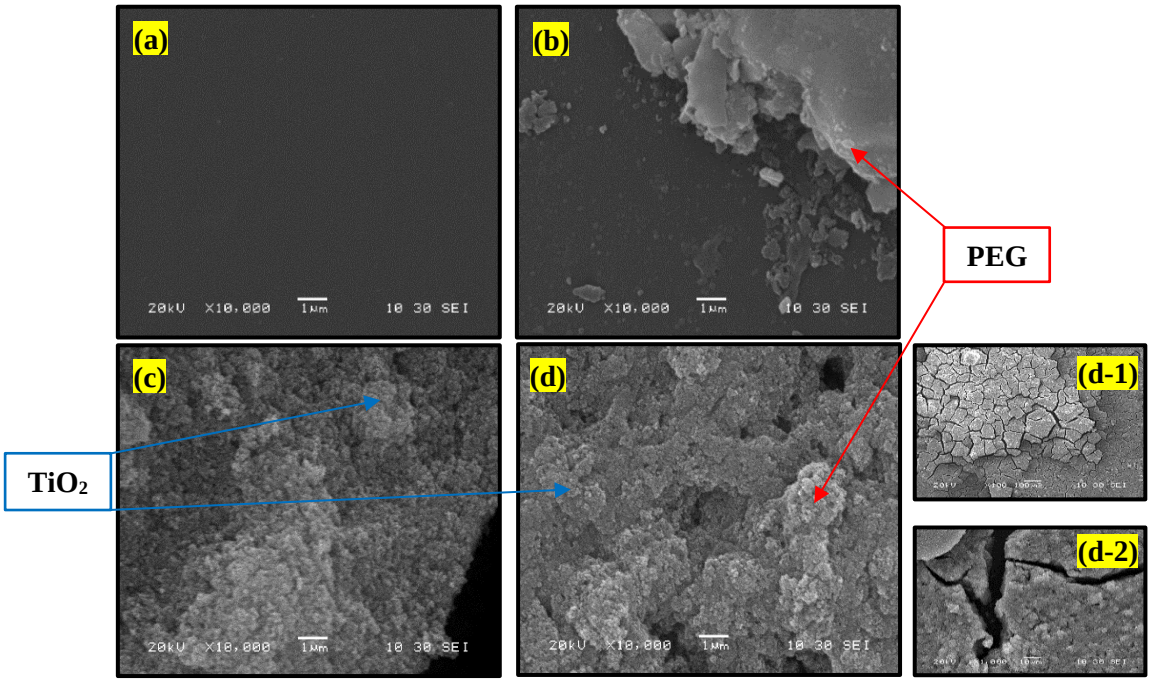

Fig. 6.3: SEM images of the top surface of a membrane (magnification: x 10,000 and scale: 1 µm) using dead-end membrane filtration process at TiO_2 loading (1 gL^{-1}): (a) new membrane, (b) fouled membrane with PEG, (c) fouled membrane with TiO_2 and (d) fouled membrane with (PEG-TiO_2) feed with two magnifications, (d-1): x 1000 and scale: 10 µm and (d-2): x 100 and scale: 100 µm.

6.3 TiO_2 heterogeneous photocatalysis (*no membrane*)

6.3.1 Preliminary experiments

6.3.1.1 Non-photocatalytic reaction of TiO_2 with PEG

When adding a suspended loading of TiO_2, for example 0.50 gL^{-1}, to PEG reactant solution and mixing for 180 min under the examined conditions (*no UV* and *no circulation*), it was found that there was a clear reduction in the concentrations of PEG oligomers when compared with an initial PEG (*no TiO_2*) as shown in Fig. 6.4. In terms of the total concentration of PEG, it was reduced by 13%. One possible explanation for this reduction so far is due the effect of adsorption of PEG oligomers on the surface of TiO_2 photocatalyst, leading to decrease the concentrations of these oligomers in the reactant solution. However, Fig. 6.5 shows that during monitoring the pH under a dark period, it decreased sharply at first minute and then increased gradually to be nearly stable at 25 min. Afterward there is no significant change in pH until the end of experiment (180 min), so pH data is not presented in Fig. 6.5. This sharply reduction in pH would not support a claim shown above (*the decrease in the concentrations of PEG oligomers is due to the effect of adsorption only*). This implies that there is another principal reason for this reduction in the pH. This principal reason is probably due to a non-photocatalytic reaction between TiO_2 and PEG oligomers that occurred first, leading to the sharp reduction in pH because of the generation of reaction intermediate compounds (like short chain acids) and then the adsorption of PEG oligomers would occur on the surface of TiO_2, thus increasing the pH.

In order to confirm this principal reason, further investigation is required before any conclusive reason can be given. Therefore, the investigation of intermediate compounds formation would play a crucial confirmation in this regard. This investigation confirmed exactly that various types of short chain acids-volatile fatty acids (VFAs) like malonic, glycolic, formaldehyde, acetic and propionic were formed as shown in RID-HPLC chromatograms (Fig. 6.6) with total concentration of 0.02 gL^{-1}. As seen from Fig. 6.6, among these formed VFAs, formaldehyde acid was dominant. This finding in conjunction with pH monitoring gives a strong evidence that there was a non-photocatalytic reaction between TiO_2 and PEG oligomers. These observations were also found with other investigated TiO_2 loadings including 0.1, 0.3, 0.75, 1.00 and 1.5 gL^{-1}. This non-photocatalytic reaction of TiO_2 with PEG oligomers is unexpected and very tricky issue since there is no literature available specifically pertaining to report the ability of TiO_2 to react with pollutants under dark conditions.

As shown earlier in Table 6.1, there was a clear difference of the obtained results in the permeate based on the concentrations of total PEG and TOC where for (PEG-TiO_2) solution, they were 605.6 and TOC 309.7 mgL^{-1} respectively when comparing with that of 77.6 and < MDL (100 mgL^{-1})

respectively of PEG reactant solution only (*no TiO_2*). This a big difference resulted significantly in changing the obtained rejections. These findings are due to a non-photocatalytic reaction of TiO_2 with PEG, which changed the oligomeric structure of PEG based on MW, and thus some PEG oligomers could pass through the membrane to the permeate.

Overall, this non-photocatalytic reaction between TiO_2 and PEG has been experimentally proven. Therefore, 30 min of non-photocatalytic reaction of TiO_2 with PEG was selected prior to carrying out the adsorption period (60 min). The scientific explanation of this reaction is beyond the scope of this PhD study and will be part of future work.

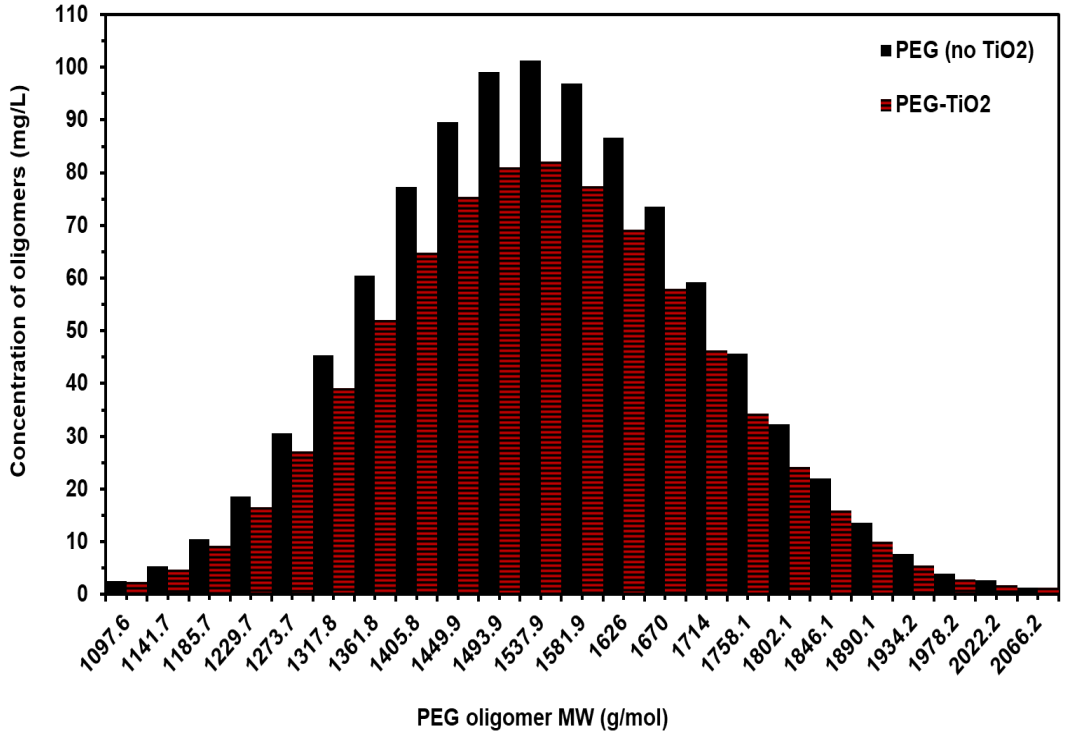

Fig. 6.4: A non-photocatalytic reaction of TiO_2 with PEG at loading (0.50 gL^{-1}) for 180 min.

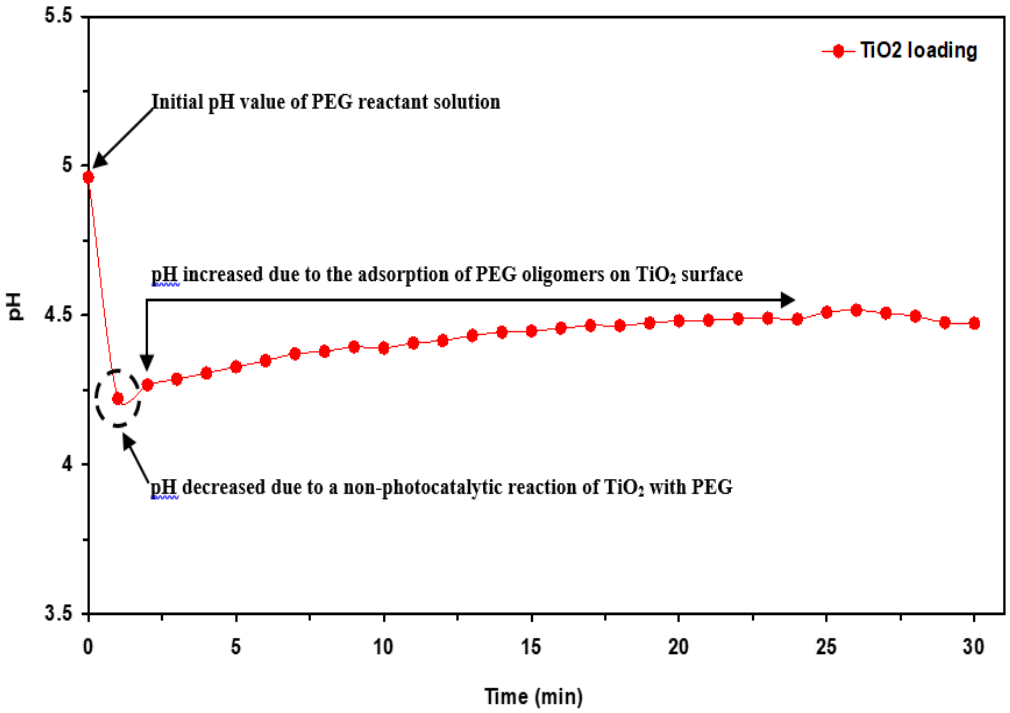

Fig. 6.5: pH monitoring during a non-photocatalytic reaction of TiO_2 with PEG and adsorption of PEG oligomers on the surface of TiO_2 at loading (0.50 gL^{-1}) for 30 min.

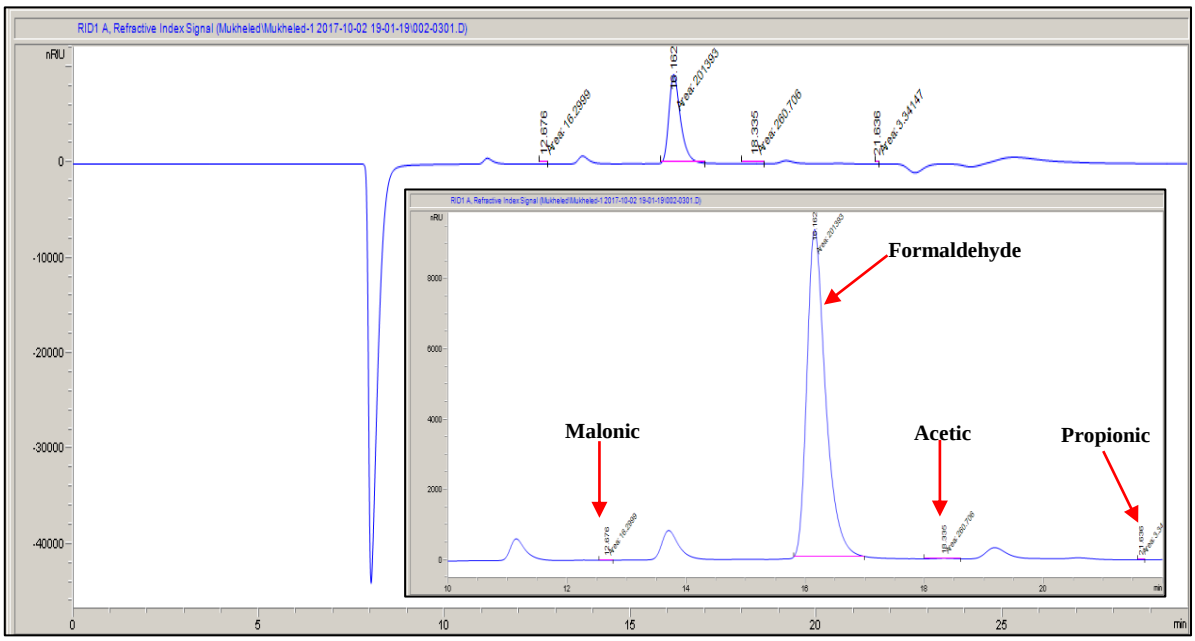

Fig. 6.6: RID-HPLC chromatograms of intermediate compounds formation during a non-photocatalytic reaction between TiO_2 (loading 0.50 gL^{-1}) and PEG with enlarged view of plot in bottom right hand corner.

6.3.1.2 Effect of pH on the adsorption of PEG oligomers onto TiO_2 particles

Several experiments were executed to examine the effect of pH conditions on the adsorption of PEG oligomers onto the TiO_2 particles. One example of these experiments was run at a TiO_2 loading (0.5 gL^{-1}) with an initial pH~4.8 of prepared (PEG-TiO_2) solution under either acidic condition using HCl (pH 3) or basic condition using NaOH (pH 11).

Fig. 6.7 shows that the concentrations of PEG oligomers decreased generally due to a non-photocatalytic reaction of TiO_2 with these oligomers as explained in last section (6.3.1.1) in conjunction with the adsorption of these oligomers onto the surface of TiO_2 particles. On the other hand, the concentrations of these oligomers increased significantly under the effect of pH conditions to be higher than that of (PEG-TiO_2) solution and also comparable to that of initial PEG solution (*no TiO_2*). This could be explained by the liberation (release) or desorption of PEG oligomers from the surface of suspended TiO_2 photocatalyst to the bulk solution phase because of the strong effect of pH change. Based on this result, it is expected that the performance of TiO_2 heterogeneous photocatalytic reaction will be significantly affected since the adsorption of the reactants like (PEG oligomers) onto the active sites of heterogeneous photocatalyst like (TiO_2) plays a fundamental step in heterogeneous photocatalytic reaction mechanism. Several studies have shown that pH has a strong influence on the rate of adsorption of pollutants onto the surface of photocatalyst particles, aggregation (particle attraction) and band energy. Consequently, affecting significantly the efficiency of photocatalysis process **[64, 67, 255, 256]**.

From the obtained results above and also in terms of the aim of the current project, to use and recycle TiO_2 heterogeneous photocatalyst as benchmarking with a POM homogeneous photocatalyst in a PMR, the pH operating parameter was not controlled in the current chapter to get a fair comparison with POM homogenous PMR work (chapter 5) on the same comparable basis in monitoring pH only.

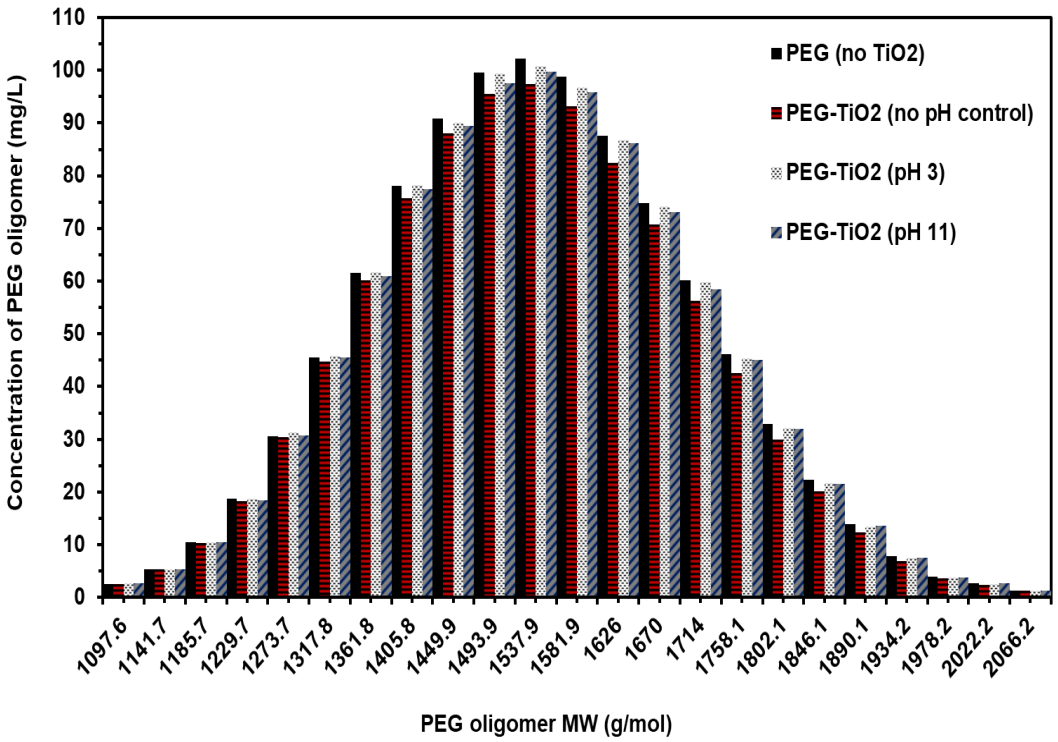

Fig. 6.7: Effect of pH conditions on the adsorption of PEG oligomers onto PEG oligomers under TiO_2 loading (0.5 gL^{-1}) for 30 min of non-photocatalytic reaction of TiO_2 with PEG.

6.3.1.3 Effect of adsorption on TiO_2 concentration

The aim of this investigation was to specify the adsorption equilibrium time for TiO_2 to take place in the whole parts of PMR system (*no membrane*). The adsorption effect on TiO_2 concentration with respect to time is shown in Fig. 6.8. This effect shows that a significant reduction in the initial concentration of TiO_2 by 36±3% for all investigating experiments during 30 min. After that a gradual reduction in its concentration was observed until the end of course of experiments (210 min). This investigation (Fig. 6.8) confirmed that TiO_2 suffers from a higher rate of adsorption where the effect of adsorption on TiO_2 was clearly observed in the BSR wall (Fig. 6.9).

Therefore, to ensure a minimum effect for adsorption to take place, an adsorption equilibrium time of 60 min was used prior to carrying out any reactions later.

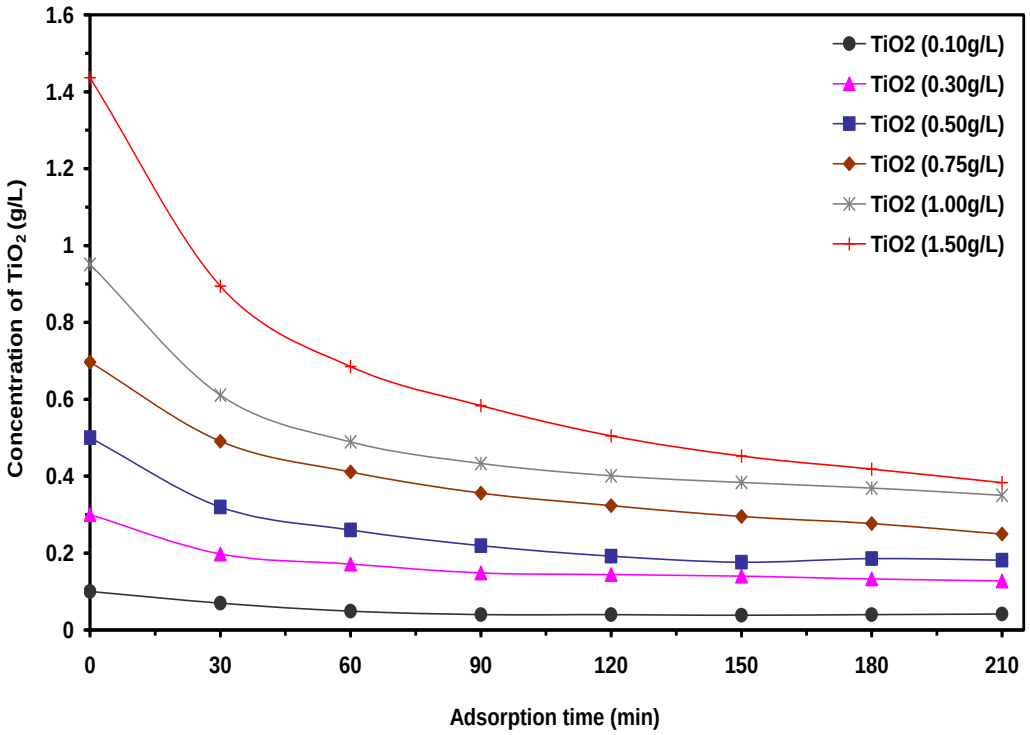

Fig. 6.8: Effect of adsorption on the TiO_2 concentration inside a PMR system.

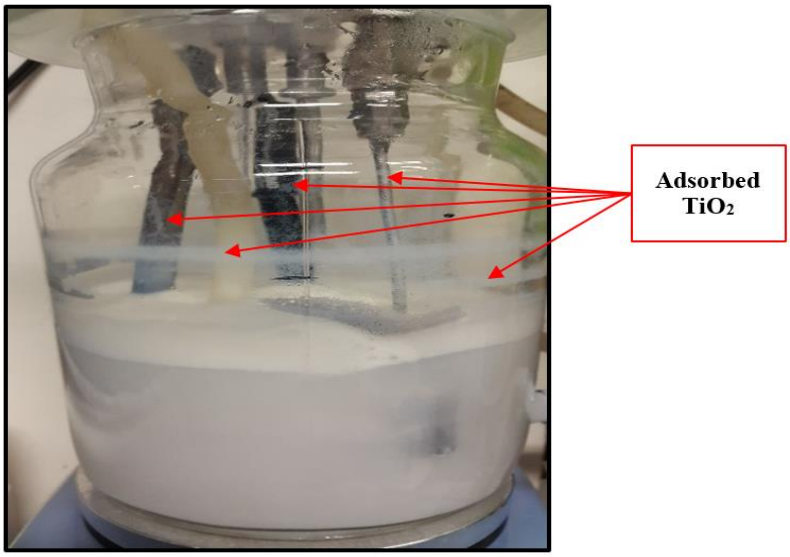

Fig. 6.9: Picture showing the adsorption of TiO_2 on the wall of BSR.

6.3.2 Photocatalytic reaction of TiO_2 with PEG

6.3.2.1 Effect of oxidant concentration

The effect of oxidant concentration (dissolved molecular oxygen, DO) on the photocatalytic reaction of TiO_2 was initially investigated under monitoring DO only to examine whether the concentration of oxidant (mgO_2L^{-1}) in (PEG-TiO_2) reactant solution inside the BSR is enough to ensure the best conditions for photocatalytic reaction of TiO_2 with PEG. Note that, the concentration of oxidant during the circulation of reactant solution in the PMR system (*no membrane*) by pump 1 and pump 2 shown in Fig. 3.4 (natural oxygenation of the solution through mass transfer from ambient air) was 17±1 mgO_2L^{-1}. This effect of oxidant concentration was examined under TiO_2 loading of 0.25 gL^{-1}.

Fig. 6.10 shows that as the photocatalytic reaction proceeded, the oxidant concentration deceased significantly to be stable nearly at 6.5 mgO_2L^{-1}. This finding is totally different from POM homogeneous photocatalysis shown earlier in chapter 4 where there was insignificant decrease in the oxidant concentration (< 2 mgO_2L^{-1}). It can be concluded that the oxidant concentration should be continuously supplied to sustain a TiO_2 heterogeneous photocatalysis of PEG. Therefore, two experiments were carried out at 20 and 75 mgO_2L^{-1} to examine the effect of oxidant concentration on the %PD of PEG and then to identify the best oxidant concentration to be used later in the next section (6.3.2.2).

In Fig. 6.11, the %PD of PEG increased significantly at the oxidant concentration of 20 mgO_2L^{-1} in comparison with that of control (*no oxidant*). This implies that the oxidant concentration (DO) plays a significant role as an electron acceptor to form the superoxide radical ions ($O_2^{\cdot-}$), which are able to further react with PEG oligomers, thus increasing the overall primary degradation in TiO_2 heterogeneous photocatalysis **[18, 81, 181, 232, 257]**. However, the %PD of PEG decreased with increasing the oxidant concentration from 20 to 75 mgO_2L^{-1}. This could be explained due to the *'inner filter effect'* (this reason is explained with more detail for POM homogeneous photocatalysis of PEG in chapter 4, section 4.3.1, 2). Furthermore, since heterogeneous photocatalysis is a surface photocatalytic reactions, the DO bubbles could attach on the surface of photocatalyst particles, thus hindering these reactions **[233]**.

Based on the obtained results, the oxidant concentration of 20-25 mgO_2L^{-1} was selected for all coming TiO_2 photocatalytic reactions.

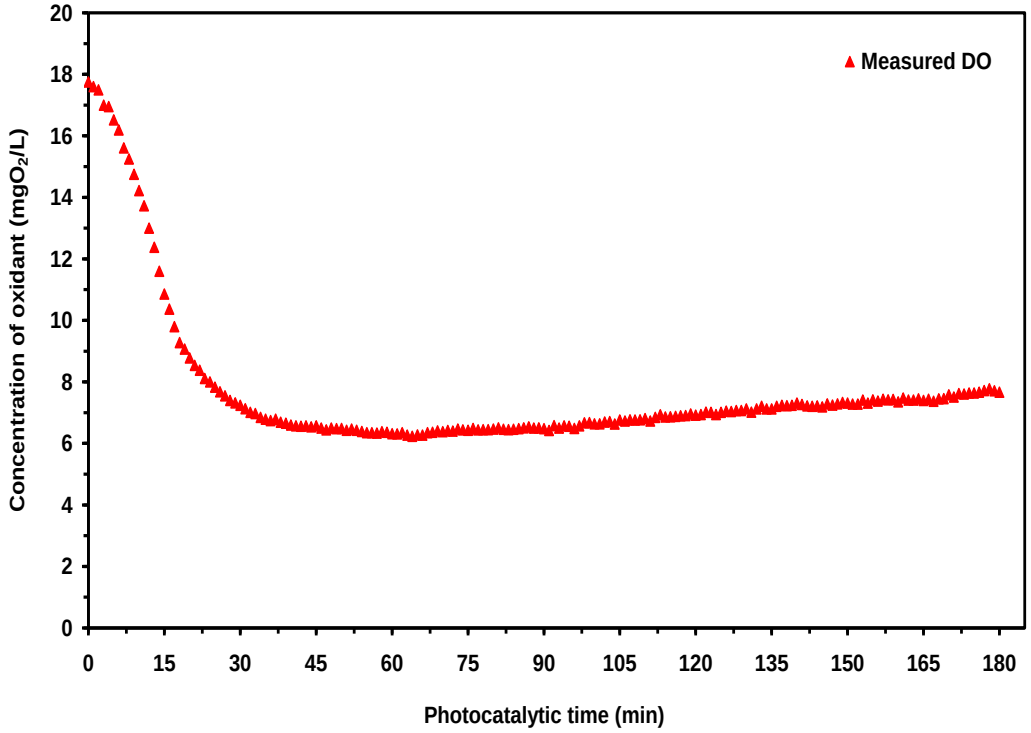

Fig. 6.10: Oxidant concentration monitoring over a photocatalytic reaction time, TiO_2 loading (0.25 gL^{-1}).

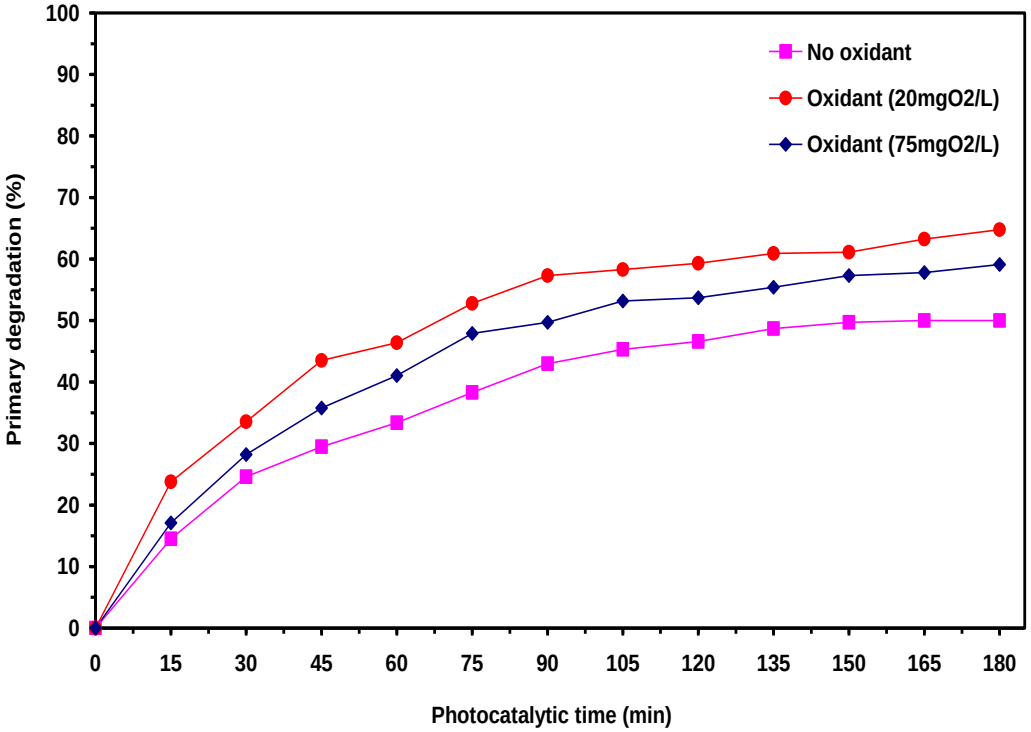

Fig. 6.11: Effect of oxidant concentration on the primary degradation of PEG, TiO_2 loading (0.25 gL^{-1}).

6.3.2.2 Effect of TiO_2 loading

The aim of this section is to investigate the TiO_2 heterogeneous photocatalysis of PEG as a control process (*no membrane*) under various TiO_2 loadings. This investigation was assessed with primary degradation, reaction kinetics and mineralization as proposed evaluating parameters. These evaluating parameters will be used as a basis of establishing the comparable performance of control photocatalysis with TiO_2 heterogeneous PMR later.

This investigation was achieved based on the obtained results from the last sections (6.3.1.2 and 6.3.2.1) where the pH was not controlled and the oxidant concentration was controlled in the range 20-25 mgO_2L^{-1}.

1) Primary degradation

The effect of TiO_2 control loadings on the %PD of PEG is shown in Fig. 6.12. This effect under various photocatalytic reaction times showed that the %PD of PEG increased with increasing TiO_2 loading from 0.125 to 0.250 gL^{-1} due to increasing the amount of active site on the surface of TiO_2 photocatalyst particles. After this loading (0.250 gL^{-1}) as expected for heterogeneous photocatalysis, the PD% of PEG decreased significantly because of light scattering effects **[64, 79, 166]**.

It is important to mention that TiO_2 as heterogeneous photocatalyst benchmarking showed a poor photocatalytic activity (63%) when compared with POM homogeneous photocatalyst (95%) based on the total concentration of PEG at the end course of reaction time (180 min). This result gave evidence that TiO_2 photocatalytic activity is lower than that of POM. One direct explanation for this poor photocatalytic activity of TiO_2 is attributable to the effect of adsorption on the TiO_2 particles under the examined conditions. The presented results in Fig. 6.13 confirms this adsorption effect by decreasing the concentration of TiO_2 over a photocatalytic reaction time, and thus lowering the photocatalytic activity.

Based on the obtained results (Fig. 6.12), the loading of 0.250 gL^{-1} is an optimal control loading of TiO_2 heterogeneous photocatalysis of PEG and would be used to evaluate the performance of proposed PMR later.

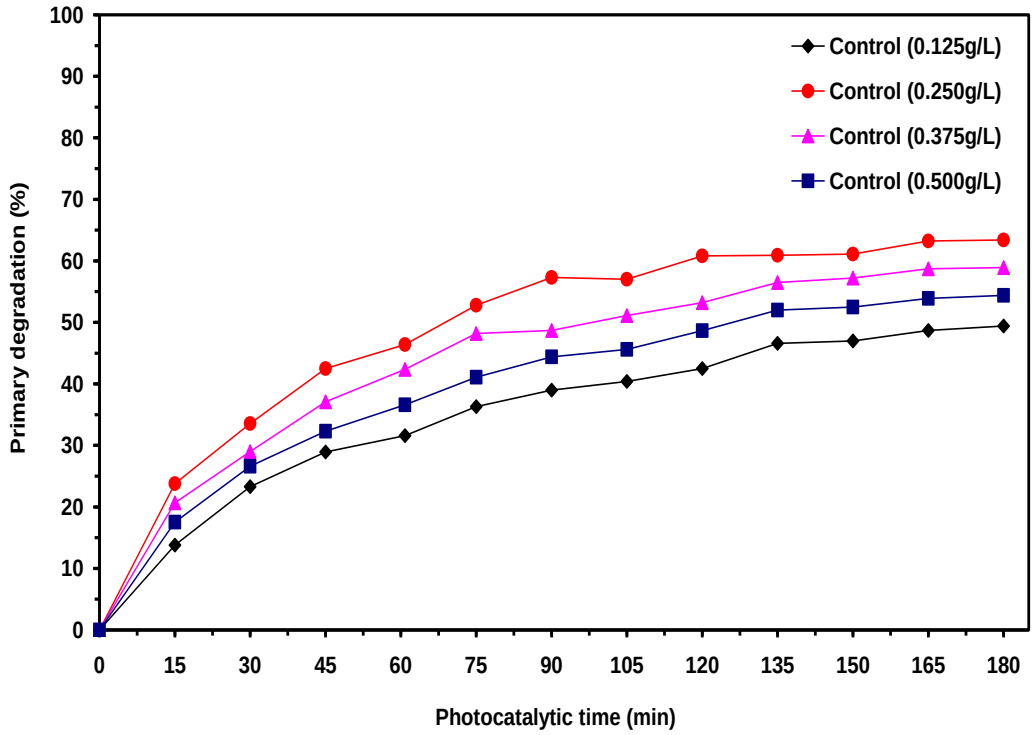

Fig. 6.12: Effect of various TiO_2 control loadings on the percentage primary degradation of PEG.

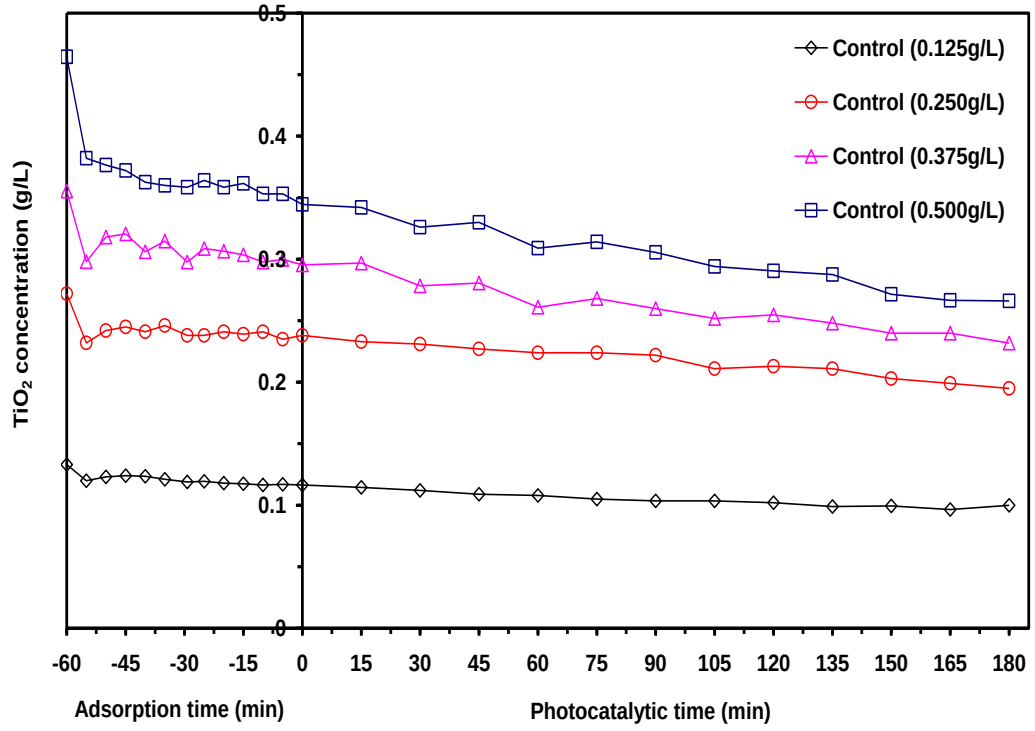

Fig. 6.13: Effect of adsorption on the TiO_2 concentration inside the BSR as a function of time.

2) Reaction kinetics

Kinetic analysis of the total concentration of PEG versus photocatalytic reaction time under TiO_2 heterogeneous photocatalysis showed that the primary degradation of PEG mainly followed a simplified Langmuir-Hinshelwood (L-H) kinetic model (pseudo-first order reaction constant, K_{app}), which is commonly used for heterogeneous photocatalysis **[86, 87]**.

The Eq. 4.1 was used for fitting the photocatalytic data, one example concentration of TiO_2 (0.25 gL^{-1}) versus photocatalytic time, is shown in Fig. 6.14. The fitted reaction rate constants for various TiO_2 loadings are shown in Fig. 6.15. The presented results in Fig. 6.15 show that a 0.25 gL^{-1} loading has a maximum K_{app} in comparison with that of other loadings. These results give further support that a loading (0.25 gL^{-1}) is an optimal TiO_2 control loading.

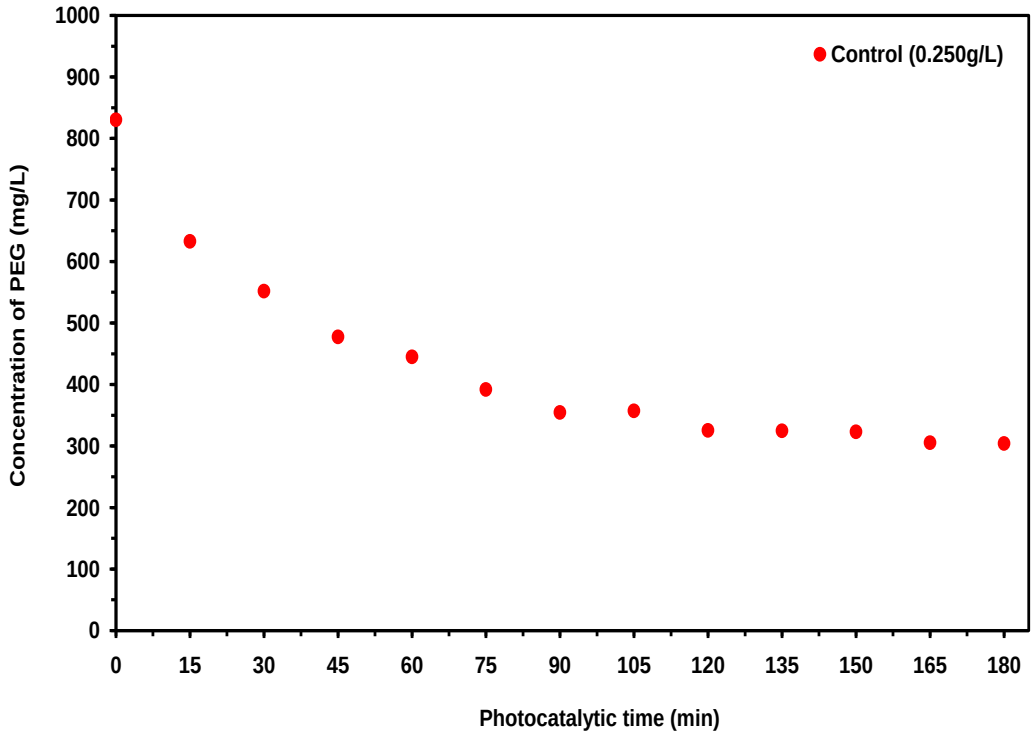

Fig. 6.14: Experimental photocatalytic data of PEG under TiO_2 control loading (0.25 gL^{-1}).

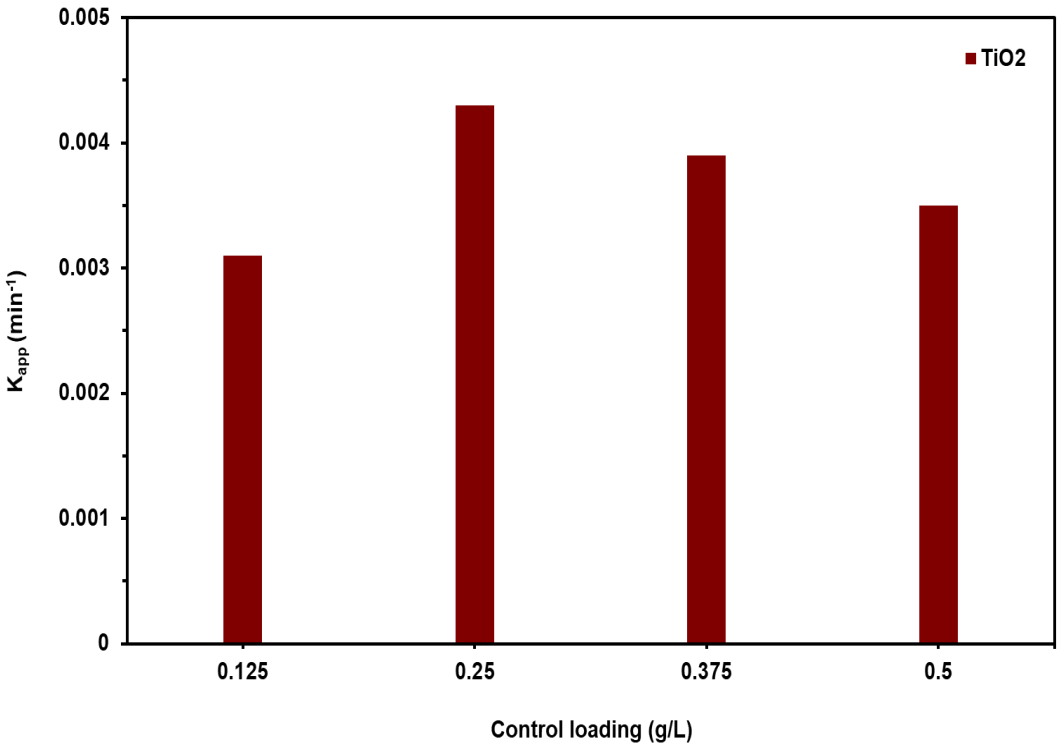

Fig. 6.15: Effect of TiO_2 control loadings on the K_{app} of PEG.

3) Mineralization

TiO_2 photocatalytic mineralization of PEG (%TOC removal) as a function of various TiO_2 loadings were investigated. This investigation in Fig. 6.16 showed that a partial mineralization of PEG was found to be < 2% TOC removal. As reported in literature **[6, 10, 241]**, *in terms of PEG oxidation based on AOPs*, this partial mineralization is attributed to the formation of lower carboxylic acids, which are so resistant to complete mineralization. More details about this partial mineralization are shown in chapter 4, section 4.3.6. The lower carboxylic acids (VFAs) formed as reaction intermediate compounds were malonic, glycolic, formaldehyde, formic, acetic and propionic. The total concentration of these formed VFAs as a function of photocatalytic time is shown in Fig. 6.17.

In order to a better understanding of the photocatalytic mineralization of PEG, *instead of %TOC*, the TOC concentration in relation with formed VFAs will be used as an evaluating parameter for the performance of TiO_2 control photocatalysis of PEG with proposed PMR later.

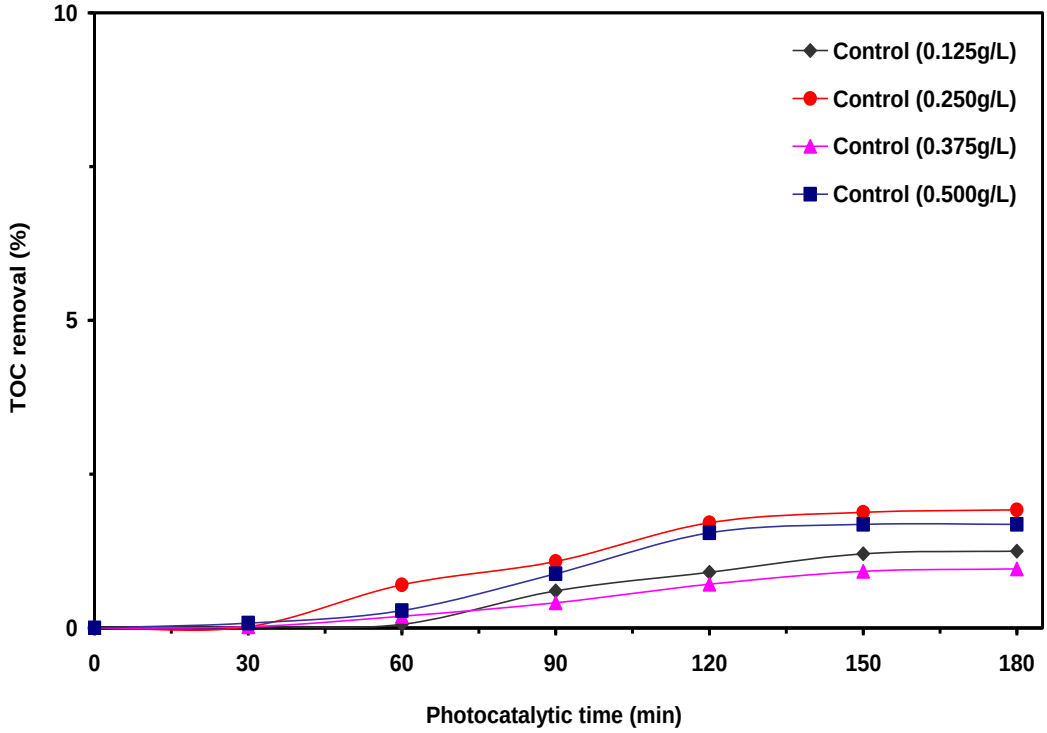

Fig. 6.16: %TOC removal over a photocatalytic time at various TiO_2 control loadings.

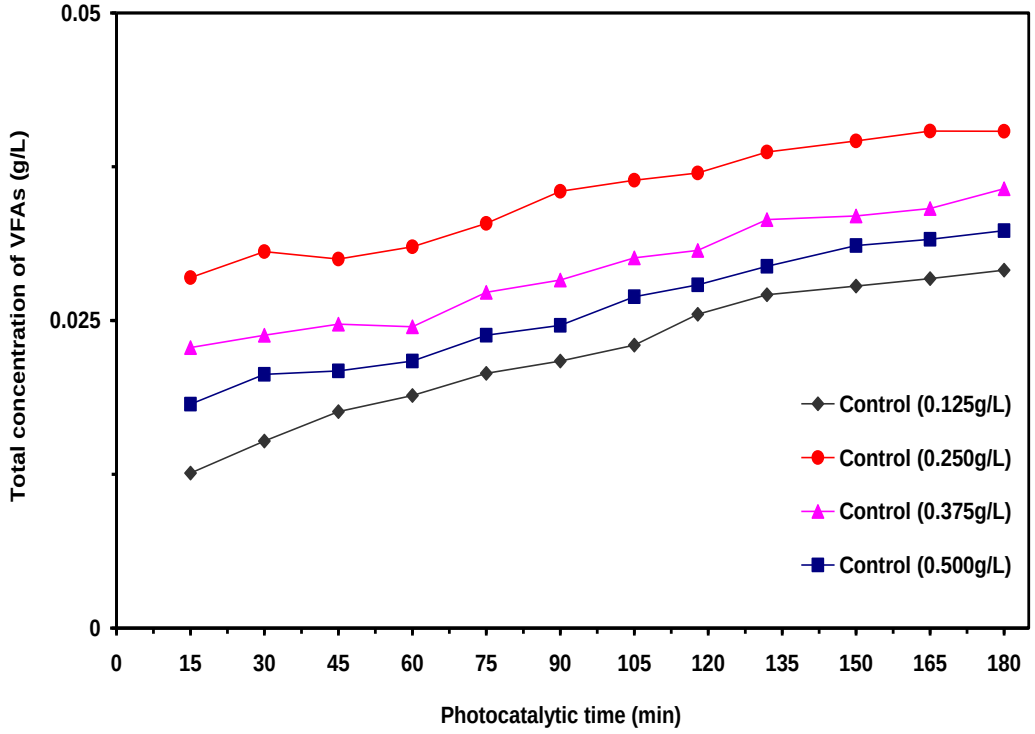

Fig. 6.17: Total concentration of formed VFAs over a photocatalytic time at various TiO_2 control loadings.

In terms of degradation pathway, the concentrations of identified VFAs over a photocatalytic reaction time are shown in Fig. D1 (*Appendix D*). It can be seen that the concentrations of malonic, and formaldehyde acids varied in increasing and decreasing during the course of reaction. This means that, according to literature based on the oxidation of PEG using AOPs shown earlier in chapter 4, section 4.3.5, malonic might be partially oxidized to acetic acid and formaldehyde to formic acid. As shown in Fig. Fig. D1 (*Appendix D*), formic acid was not formed from the beginning of photocatalytic reaction time, it started to form after at least 30 min of reaction. This result gives a confirmation about its formation from oxidation of formaldehyde acid as mentioned above.

On the other hand, the concentrations of glycolic, acetic and propionic acids increased systematically until the end of reaction, indicating that the difficulty of these acids to be mineralized under the examined conditions. Similar results were observed under other investigated TiO_2 loadings (0.125, 0.375 and 0.50 gL^{-1}).

From the obtained results, the adapted mechanism for TiO_2 photocatalytic degradation of reaction intermediates can be proposed in Fig. 6.18.

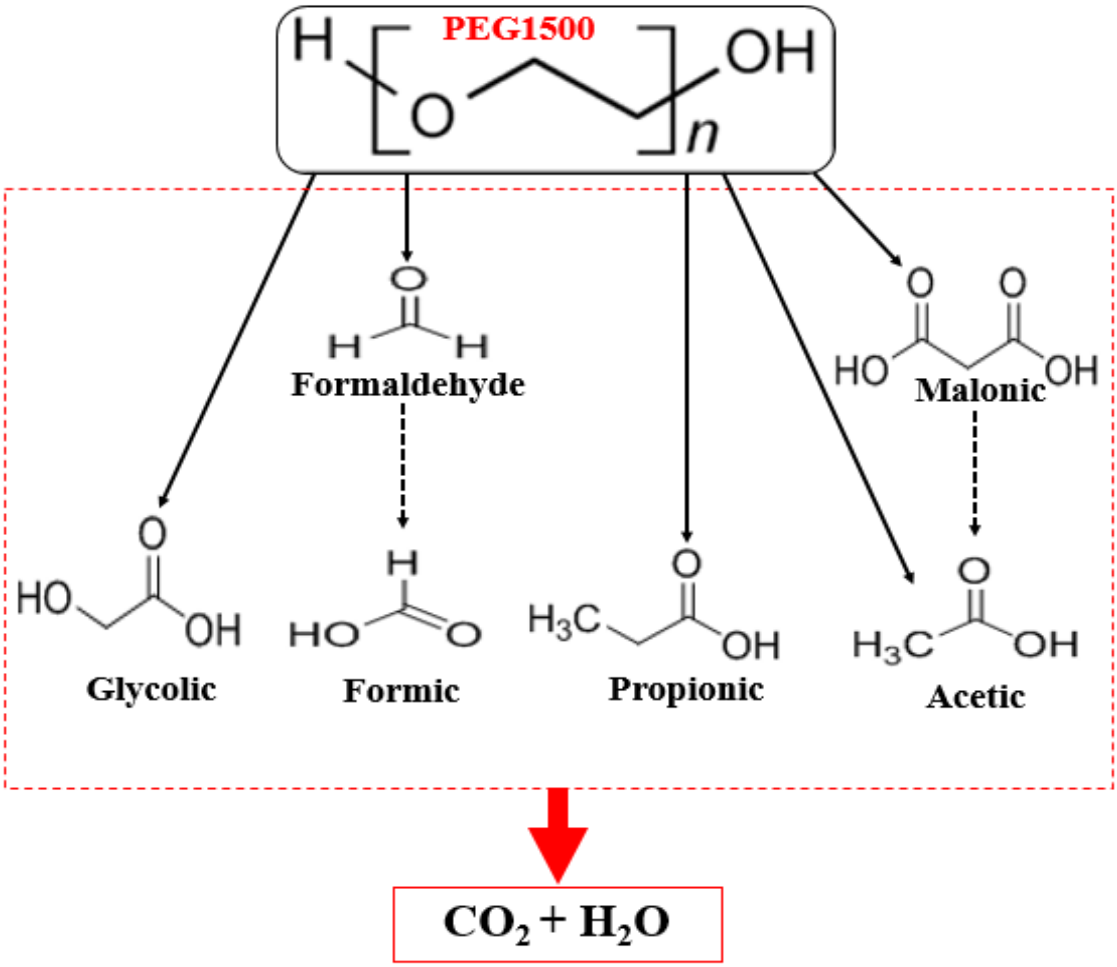

Fig. 6.18: Proposed mechanism of TiO_2 photocatalytic degradation of reaction intermediates.

6.4 Cross-flow heterogeneous PMR

6.4.1 Batch PMR operation

The aim of this section is to validate if the concept *'membrane enhanced heterogeneous photocatalysis under batch mode of cross-flow PMR operation'* is feasible when comparing with control photocatalysis (*no membrane*) shown in section 6.3 based on the evaluating parameters (primary degradation, reaction kinetics and minimization).

The hydrodynamic conditions, TMP (15 bar) and CFV (1.3 cms^{-1}), were initially selected for carrying out batch PMR experiments and then the influence of other hydrodynamic conditions on batch PMR performance will be examined later. The evaluation of batch PMR performance is shown below:

1) Primary degradation

As shown earlier in chapter 5, the concept of membrane enhanced homogeneous photocatalysis is feasible at lower POM loading of 0.25 and 0.50 gL^{-1}, which are below the optimal POM control loading of photocatalysis (0.75 gL^{-1}). The optimal control loading of TiO_2 for control photocatalysis of PEG (no membrane) was found to be 0.25 gL^{-1} (section 6.3.2.2, 1). In order to get a better understanding of the performance of cross-flow heterogeneous PMR with control heterogeneous photocatalysis based on the %PD of PEG, two proposed TiO_2 loadings of 0.125 and 0.25 gL^{-1} were selected to examine this performance since TiO_2 suffered from the effect of adsorption as shown earlier (section 6.3.1.3).

Examination of Fig. 6.19 reveals that under an optimal control loading (0.25 gL^{-1}), the %PD of PEG using PMR decreased significantly compared with that of control photocatalysis. In the same way, under TiO_2 loading of 0.125 gL^{-1}, the same results were obtained. This unexpected performance of PMR under the examined conditions could be explained by the relationship between the rejection of TiO_2 and permeate flux.

In terms of TiO_2 rejection, TiO_2 photocatalyst was successfully rejected with 100% by the membrane. This complete TiO_2 rejection cannot explain the relationship between the retentate TiO_2 concentration inside the BSR (or in the photoreactor) and the permeate flux through the membrane over a 180 min operating time. So, instead of it, the retentate TiO_2 concentration was used to explain the performance of PMR with regard to %PD of PEG.

Fig. 6.20 shows that as the operating time proceeded, there was a gradual decline in the permeate flux for both TiO_2 loadings, expecting that the concentration of TiO_2 in the retentate and

then in the photoreactor should be increased accordingly. *Conversely*, the retentate TiO_2 concentration inside the BSR decreased significantly when using PMR under two proposed TiO_2 loadings to be lower than that of original control photocatalysis (the control photocatalysis data shown in Fig. 6.20 are for comparison purposes only). It becomes evident that the membrane could not concentrate the TiO_2 concentration inside the BSR and then in the photoreactor by the cross-flow filtration. *This is thought to be because of two reasons:*

Firstly, the tendency of TiO_2 particles to adsorb on the surface of membrane where the rate of adsorption increased with increasing the rate of separation. This is discussed in further detail later in relation to the SEM investigation. Also, the adsorption of TiO_2 was visually observed on the wall inside the BSR and on the other components of PMR.

Secondly, possibly the presence of PEG oligomers and formed VFAs would adsorb onto the surface of TiO_2 particles and then these particles would bind together to form a dense layer of TiO_2 on the surface of membrane. This observation was reported by *Song et al.*, **[253]** who used a TiO_2 heterogeneous PMR (similar to PMR used in this project) for the treatment of humic acid. They reported that humic acid could adsorb onto the surface of TiO_2 particles and filled the gap between these particles, forming a dense cake layer.

Consequently, the retentate TiO_2 concentration inside the BSR decreased significantly by 21 and 23% with TiO_2 loadings of 0.125 and 0.25 gL^{-1} respectively at the end of course of operating time, and thus decreasing the %PD of PEG by 20 and 19% under PMR as compared to control photocatalysis. This finding is in contrast to the case of POM homogeneous PMR by which the concentration of POM inside the BSR increased with increasing the rate of separation, thus increasing the %PD of PEG.

Based on this negative influence of the effect of adsorption on TiO_2 concentration, the membrane separation process using batch PMR mode of operation could not enhance heterogeneous photocatalysis process.

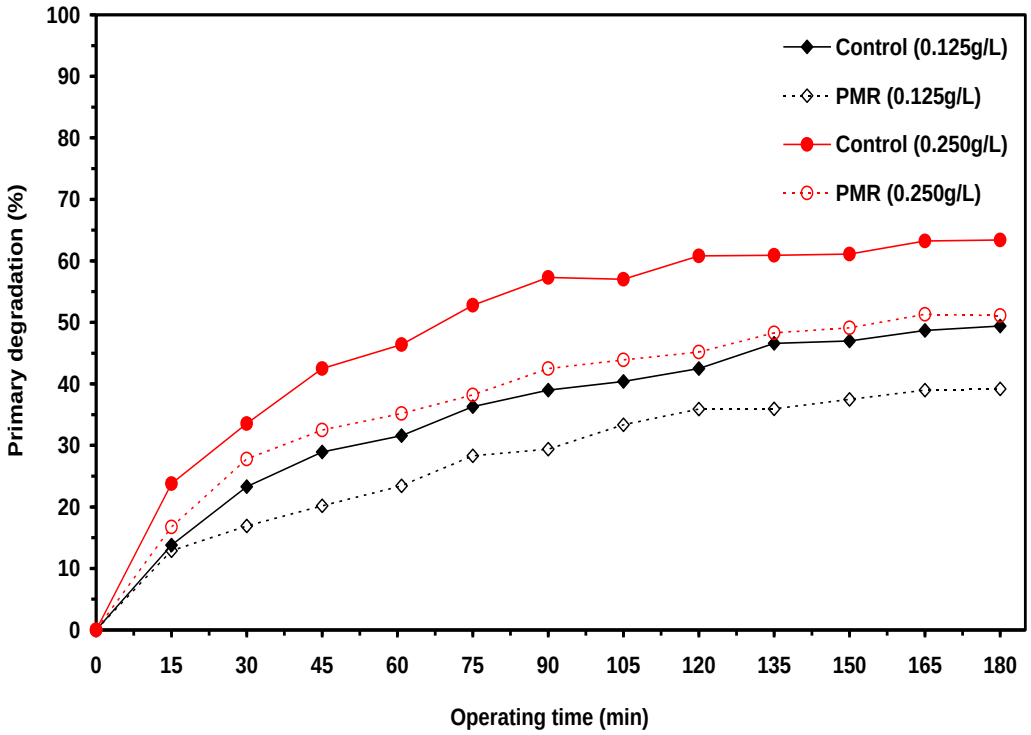

Fig. 6.19: Comparative performance of %PD of PEG between control photocatalysis and batch PMR mode of operation at different TiO_2 loadings.

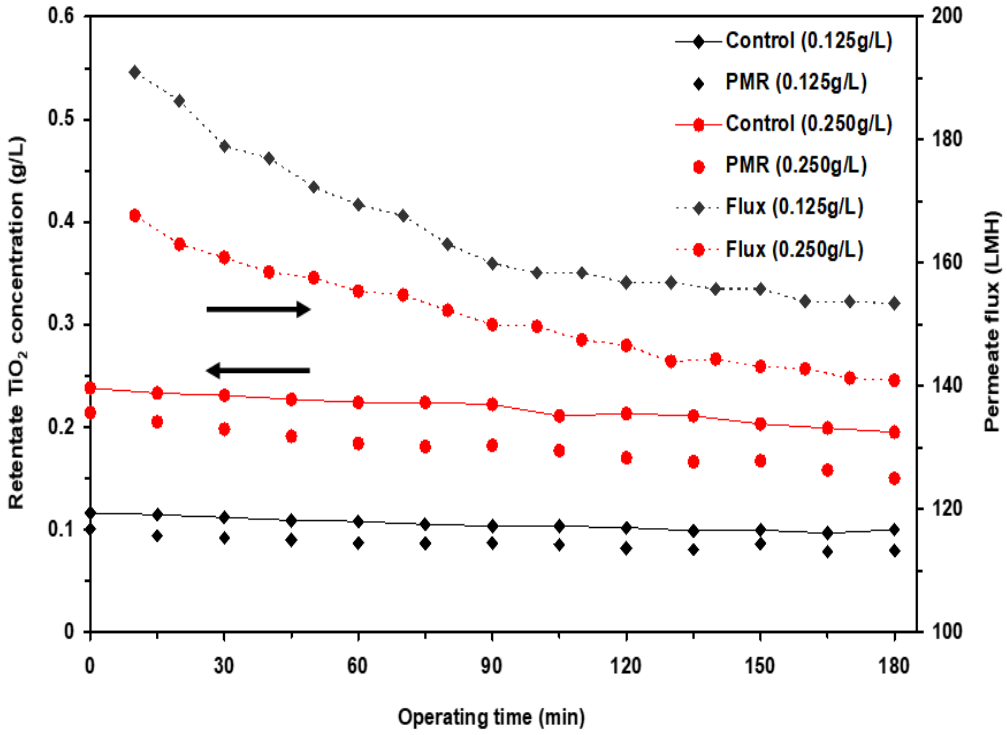

Fig. 6.20: Retentate TiO_2 concentration and permeate flux as a function of operating time of batch PMR mode of operation.

In order to further investigate the performance of TiO_2 heterogeneous PMR, the PEG rejection was studied at TiO_2 loadings of 0.125 and 0.25 gL^{-1}. An example of this investigation, a 0.25 gL^{-1} TiO_2 loading was selected.

As the operating time (photocatalytic reaction time in conjunction with cross-flow filtration time) proceeded, the %PD of PEG increased gradually in combination with decreasing the PEG rejection as shown in (Fig. 6.21). This result could be explained by RP-HPLC/ELSD chromatograms shown in Fig. 6.22 at the end course of operation.

From these chromatograms, each concentration of PEG oligomers in the retentate and permeate was obtained as shown in Fig. 6.23 based on MW of each oligomer identification ranging from 1097 to 1889 $gmol^{-1}$. This MW identification in Fig. 6.23 shows clearly that the same identified MW oligomers were found in the retentate and permeate.

This finding is puzzling especially with regard to MWCO mechanism of membrane separation. It should be noted that the MW of each PEG oligomer was experimentally identified using MALDI TOF under the initial conditions of prepared PEG (*no reaction* and *no separation*) to support the developed RP-HPLC/ELSD method. Therefore, the identified MW of each PEG oligomer in Fig. 6.23 is only for comparative purposes and cannot be taken into consideration for explaining the true individual oligomer rejection. However, *based on the MWCO mechanism of membrane separation*, there are two possible scenarios that can be assumed for explaining this:

The first scenario for the permeate assumes that the greatly oxidized oligomers could pass through the membrane (their MWs < MWCO), and thus their concentrations were actually identified by HPLC analysis. While the second scenario for retentate assumes that since the photocatalytic degradation of PEG oligomers continued for 180 min, expecting that as reported in literature **[6, 7, 9, 13]**, new oxidized PEG oligomers based on the sequential order of oligomeric degradation were being generated where high MW oligomers degraded to medium MW oligomers, which in turn degraded to low MW oligomers as explained earlier with more detail in chapter 5, section 5.4.1 (1). These new oxidized PEG oligomers having (MWs > MWCO) were rejected by the membrane and returned them to the photoreactor for further oxidation.

In this respect, from practical point of view, each identified PEG oligomer MW in the retentate (Fig. 6. 22-b) is totally different from that identified in the permeate (Fig. 6.22-c). Thus, it becomes necessary to further investigate the real MW of each PEG oligomer during the photocatalytic degradation times. *This investigation will be part of future work*.

From the above presented results, *instead of the individual oligomer rejection*, the total PEG concentration in the permeate and retentate was used to calculate the total PEG rejection where at the end course of operation, it was found that the %PD of total PEG was 51% corresponding to the total PEG rejection of 56%. These obtained results can be more confirmed by TOC investigation later.

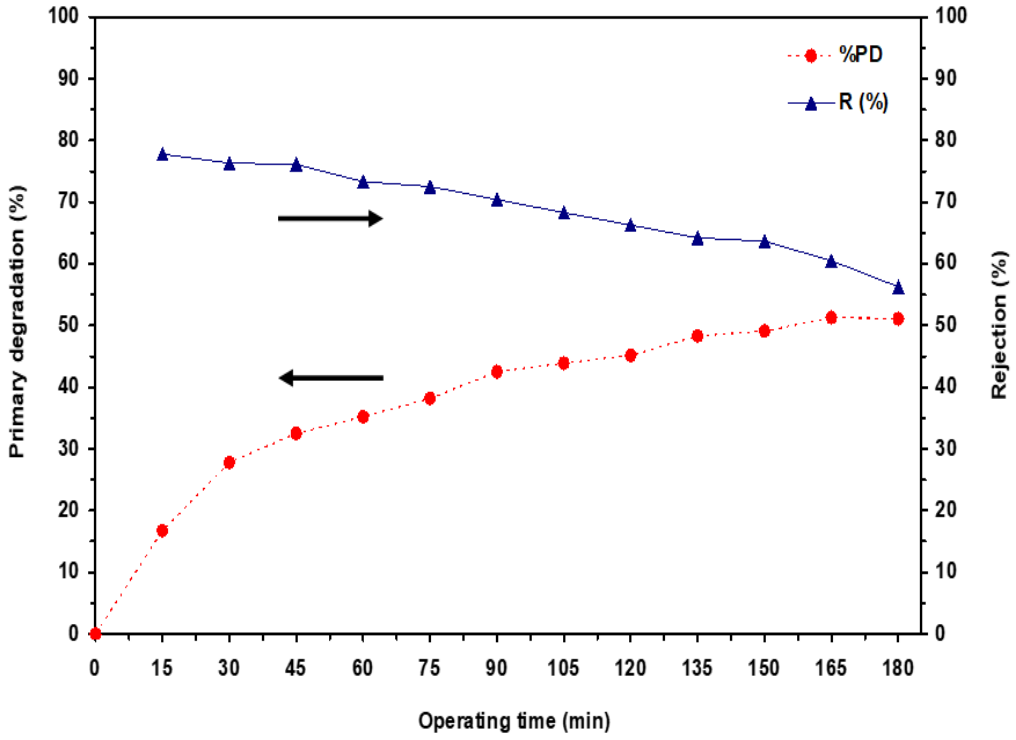

Fig. 6.21: Evaluation of PMR at TiO_2 (0.25 gL^{-1}) in terms of percentage primary degradation of PEG and PEG rejection (%) based on the total concentration of PEG.

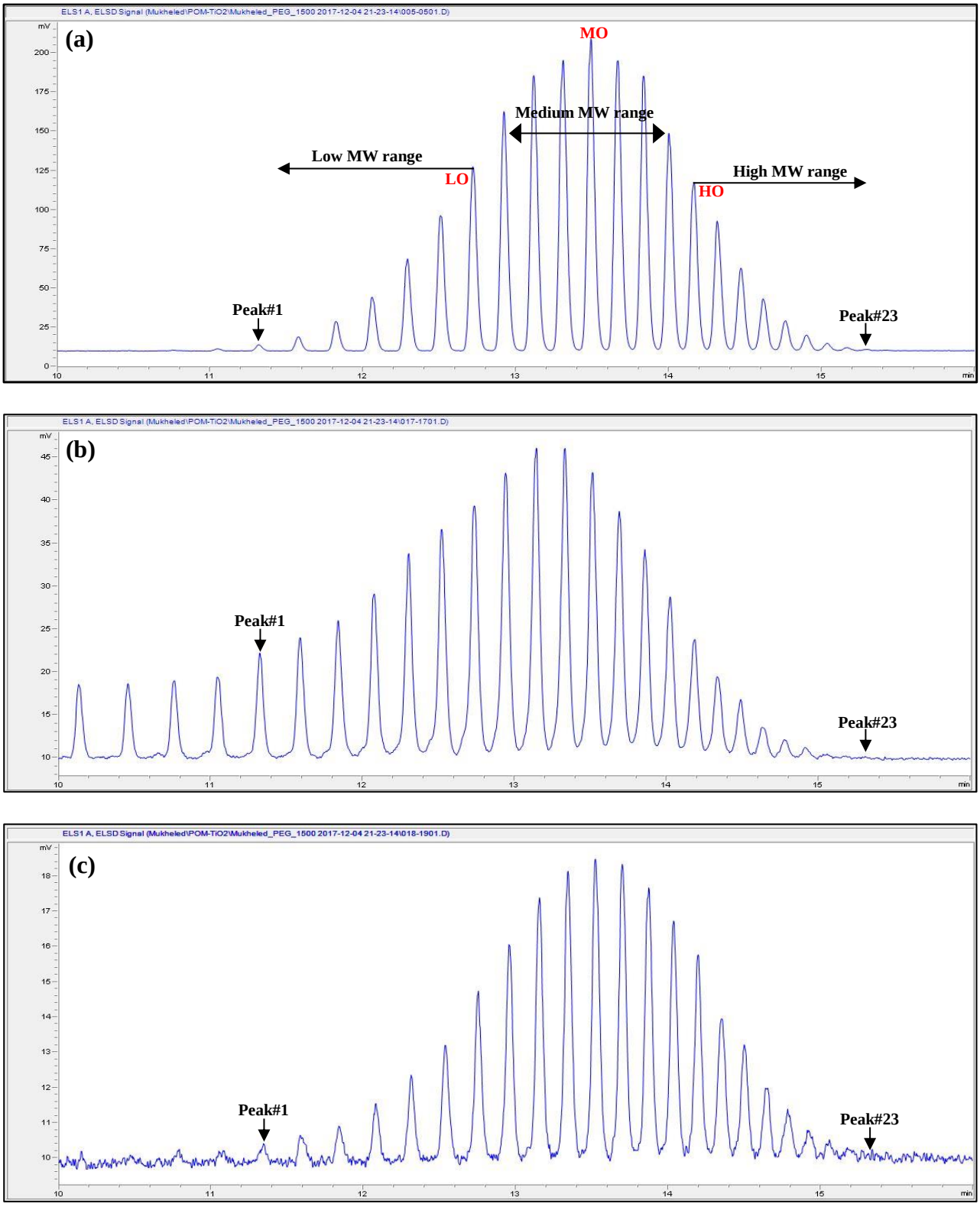

Fig. 6.22: RP-HPLC/ELSD chromatograms of PEG oligomers under batch PMR operation (TiO_2 loading of 0.25 gL^{-1}), (a) feed after adsorption, (b) retentate, (c) permeate.

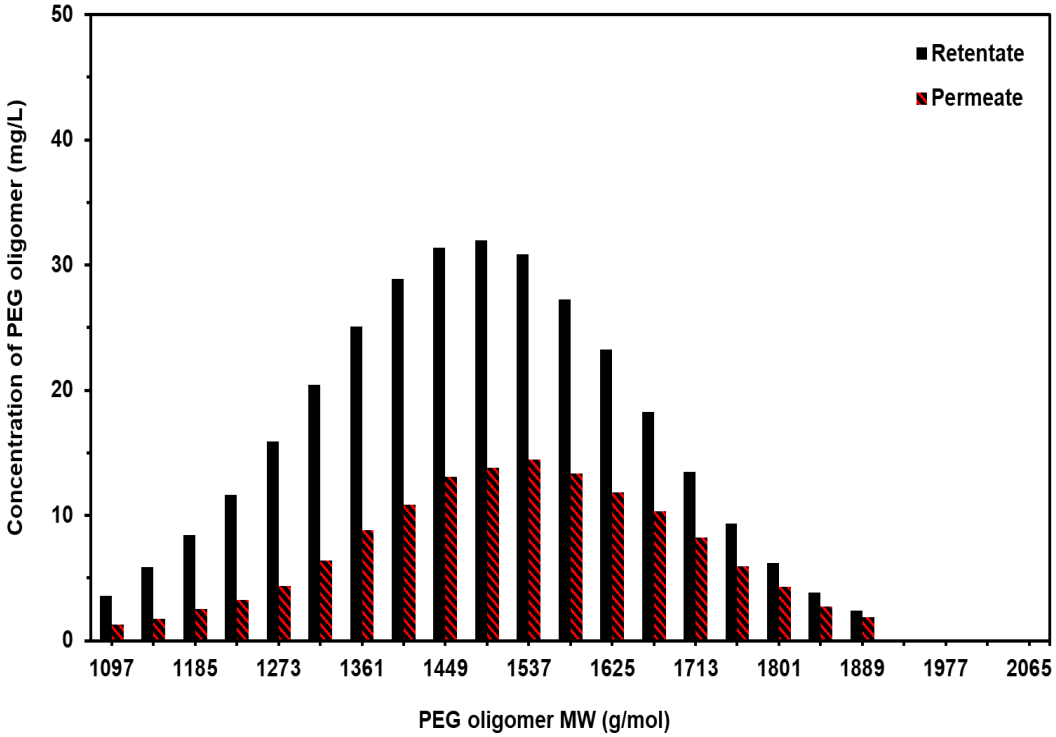

Fig. 6.23: The concentration of PEG oligomers in the retentate and permeate as a function of PEG oligomer MW under batch heterogeneous photocatalysis with TiO_2 loading (0.25 gL^{-1}) at the end of operation.

In terms of permeate flux, as shown in Fig. 6.20, a permeate flux decreased gradually during 135 min of operating time up to reach a steady state value of 153 and 141 LMH at TiO_2 loadings of 0.125 and 0.25 gL^{-1} respectively (corresponding to a relative reduction of pure water by 32 and 38% respectively). The gradual diminution in the permeate flux could be explained by the deposition of TiO_2 particles on the surface of membrane as reported in literature **[255, 258]**. This deposition of TiO_2 was studied using the SEM images (Fig. 6.24 a, c). A thick cake layer of TiO_2 was formed on the surface of membrane at loading of 0.25 gL^{-1} (Fig. 6.24-c) when compared with that of loading of 0.125 gL^{-1} (Fig. 6.24-a). The same result was found by the observation of the surface of membrane with the naked eye (Fig. 6.24 b, d) where the formation of deposited layer is proportional to the used TiO_2 loading. As a result, the permeate flux decreased by 8% when TiO_2 increased from 0.125 to 0.25 gL^{-1}. This result is expected in terms of TiO_2 heterogeneous photocatalyst separation as explained in the literature **[161]**.

The presented results in Fig. 6.24 show that the tendency of TiO_2 to adsorb on the membrane surface under two investigated loadings, and thus decreasing its concentration inside the BSR and then in the photoreactor. This finding gave additional support about the effect of adsorption on TiO_2 concentration as shown earlier where the rate of adsorption on the surface of membrane as well as on the other parts of PMR system increased significantly with increasing the rate of separation. The SEM results in Fig. 6.24 and also in Fig. D2 (*Appendix D*) confirm that the effect of adsorption of TiO_2 on

the surface of membrane was predominant when comparing this effect with that on the other components of PMR system.

One possible solution is that increasing the CFV may lead to push the adsorbed TiO_2 particles from the surface of membrane towards the bulk solution. Under this condition, potentially the membrane can concentrate the TiO_2 concentration inside the BSR and then in the photoreactor, thus increasing the %PD of PEG. In the current project, in terms technical point of view, there was a technical limitation with using pump 2 (Fig. 3.4) where a higher CFV was 1.3 cms^{-1} that used in above investigation, therefore this solution will be part of future work.

In terms of the investigation of hydrodynamic conditions (TMP and CFV) on batch heterogeneous PMR mode of operation, expecting that increasing the TMP will play a negative impact on the %PD of PEG due to the effect of inner filter as shown in chapter 4, section 4.3.1 (2). While for CFV, as shown above, a higher CFV was investigated. Considering a lower CFV (0.65 cms^{-1}) can lead to increasing the effect of TiO_2 adsorption on the surface of membrane.

Therefore, a TMP (15 bar) and CFV (1.3 cms^{-1}) were selected for further investigation later.

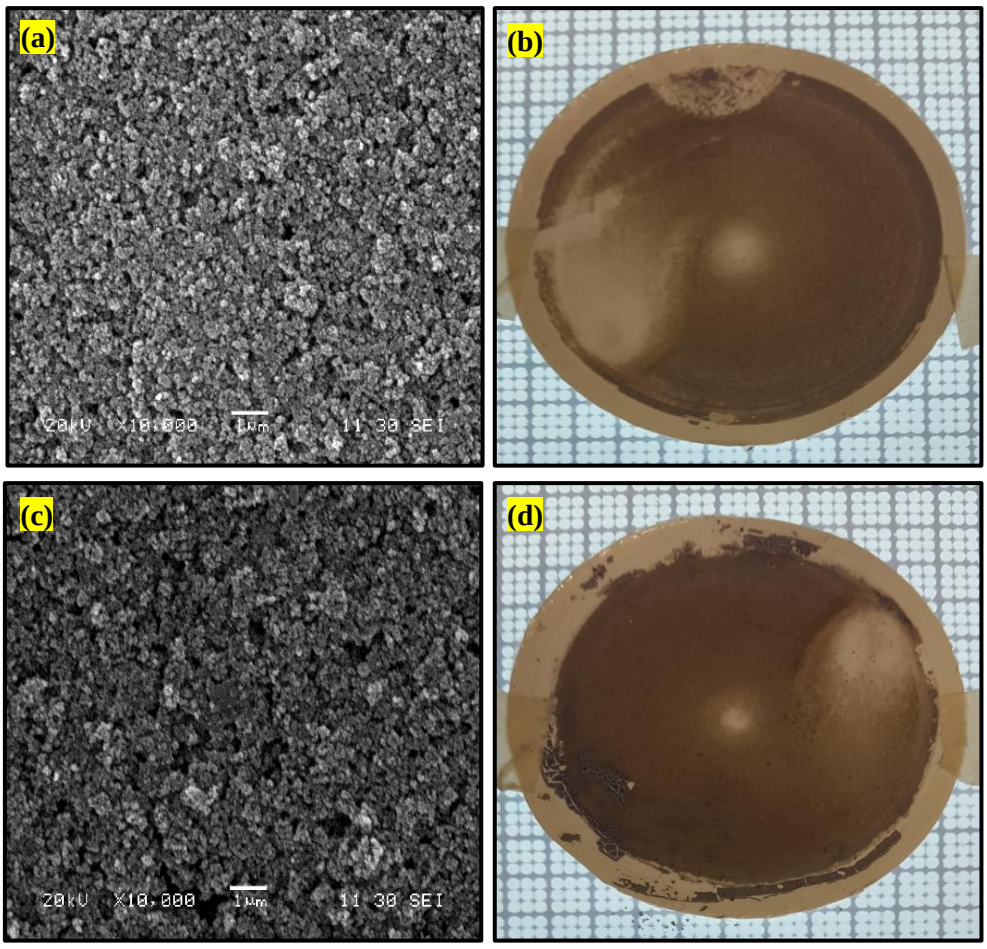

Fig. 6.24: SEM images (a, c) and real photos (b, d) of the top surface of a fouled membrane with PEG and two TiO_2 loadings using batch PMR, magnifications: x 10,000 and scale 1 µm: (a, b) TiO_2 loading 0.125 gL^{-1} and (c, d) TiO_2 loading 0.250 gL^{-1}.

2) *Reaction kinetics*

The dependence of K_{app} on the TiO_2 loadings under batch PMR mode of operation and TiO_2 control photocatalysis is shown in Fig. 6.25. The reaction kinetic data, K_{app}, confirmed that under two investigated TiO_2 loadings (0.125 and 0.25 gL^{-1}) the values of K_{app} decreased by 26 and 31% respectively in comparison with that of control photocatalysis. This result is expected and the general trend is similar to that of the %PD of PEG due to the same reasons explained earlier relating to the effect of adsorption on the TiO_2 photocatalyst.

From the obtained results, it becomes evident that the concept of membrane enhanced TiO_2 heterogeneous photocatalysis under batch PMR mode of operation is not feasible at the examined conditions.

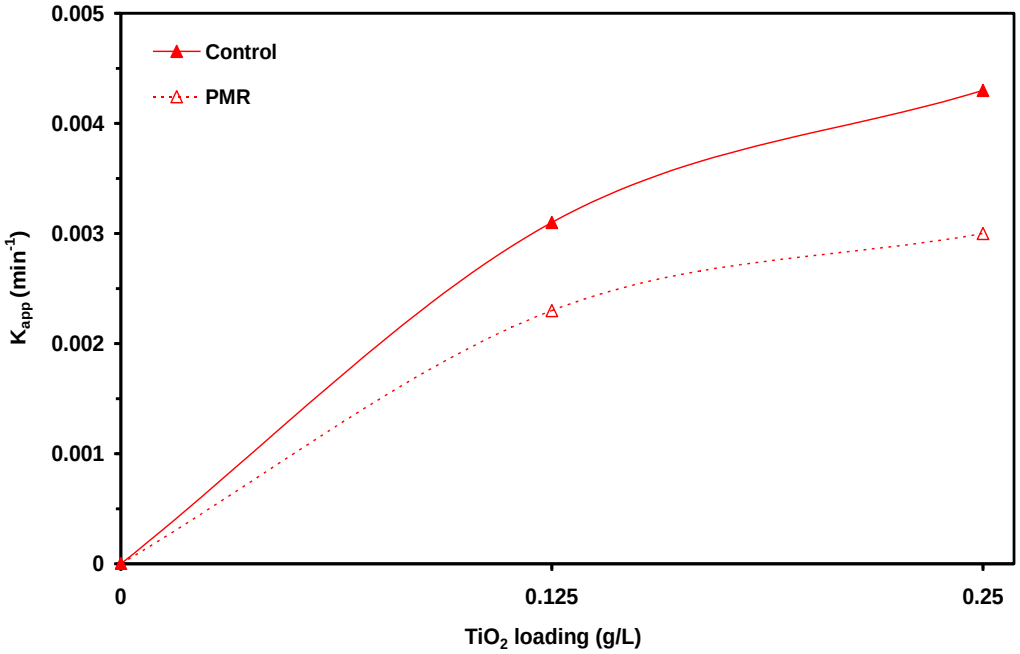

Fig. 6.25: Comparative performance of K_{app} between control photocatalysis and batch PMR mode of operation under various TiO_2 loadings.

3) *Mineralization*

The performance of batch PMR mode of operation based on the photocatalytic mineralization and intermediates formation under two TiO_2 loadings was examined in Fig. 6.26 and Fig. 6.27 respectively, and compared with TiO_2 control photocatalysis. This photocatalytic mineralization was expressed by the TOC concentration in the retentate over a 180 min operating time. The presented results of control photocatalysis in these Figs. are only for comparison purposes.

In Fig. 6. 26, it can be seen that the concentration of TOC in the retentate increased significantly with increasing the operating time for two investigated loadings of TiO_2 in comparison with control photocatalysis. *This increase in the TOC concentration can be explained by two possible reasons:*

One possible reason is that TiO_2 control photocatalysis showed a partial mineralization of PEG (< 2% TOC removal) because of the resistance of formed VFAs (malonic, glycolic, formaldehyde, formic, acetic and propionic) for total mineralization as explained earlier in section 6.3.2.2, (3). The total concentration of these VFAs in the retentate (Fig. 6.27) increased with increasing the operating time when comparing with control photocatalysis under all examined conditions. This could be further expressed by the rejection of the membrane for these acids as shown in Fig. 6.27 where it was 86.7 and 57.4% at TiO_2 loadings of 0.125 and 0.25 gL^{-1} respectively. This rejection of VFAs is still higher and unexpected since the MW of these acids is generally less than the MWCO of used membrane and should be passing through the membrane to the permeate stream. This unexpected result can be attributed to the adsorption of these formed VFAs on the surface of TiO_2 particles, forming a dense developed layer with other lightly oxidized PEG oligomers onto the surface of membrane and then this layer acts as a *'secondary dynamic membrane'* in controlling the adsorbed VFAs in terms of rejection and selectivity **[248, 249, 258]**. The same findings were found by *Song et al.,* **[253]** and *Xi et al.,* **[259]** who reported that humic acid could adsorb on the surface of TiO_2 particles and also on the surface of membrane, filling the pores between TiO_2 particles and then binding these particles to form a dense cake layer with high resistance to the permeate flux.

Another possible reason is that there were unidentified compounds (*not detected in the current project*), including lightly (partially) oxidized PEG oligomers (these were not included in the 23 identified oligomers of the original PEG based on the used HPLC methodology), polymeric fractions like ethylene glycol and reaction intermediates like VFAs. The TOC concentration can give an indictor about all these organic compounds in the retentate and permeate. It is assumed that these compounds were completely rejected by the membrane, leading to increase significantly the TOC concentration in the retentate. This assumption can be supported by the experimental results of TOC in the retentate when comparing with permeate.

At the end course of operating time (180 min), *for the retentate*, it was 685 mgL^{-1} (corresponding to the identified VFAs of 53.3 mgL^{-1}) at TiO_2 loading (0.125 gL^{-1}) and 655.6 mgL^{-1} (corresponding to the identified VFAs of 64.5 mgL^{-1}) at TiO_2 loading (0.25 gL^{-1}). *While for the permeate*, it was 54.1 mgL^{-1} (TOC) with 7.1 mgL^{-1} (VFAs) and 136.6 mgL^{-1} (TOC) with (27.5 mgL^{-1}) at TiO_2 loadings of 0.125 and 0.25 gL^{-1} respectively. The TOC rejection in Fig. 5.23 was found to be 92.3 and 79.2% at TiO_2 loadings of 0.125 and 0.25 gL^{-1} respectively. These results show that that there is a significant difference, in particular for the retentate, between the concentrations of identified VFAs and TOC confirms this assumption.

From the results presented above, it can be concluded that the membrane could not enhance the mineralization of PEG and consequently, the mineralization of PEG cannot be considered as an evaluating parameter for further investigations.

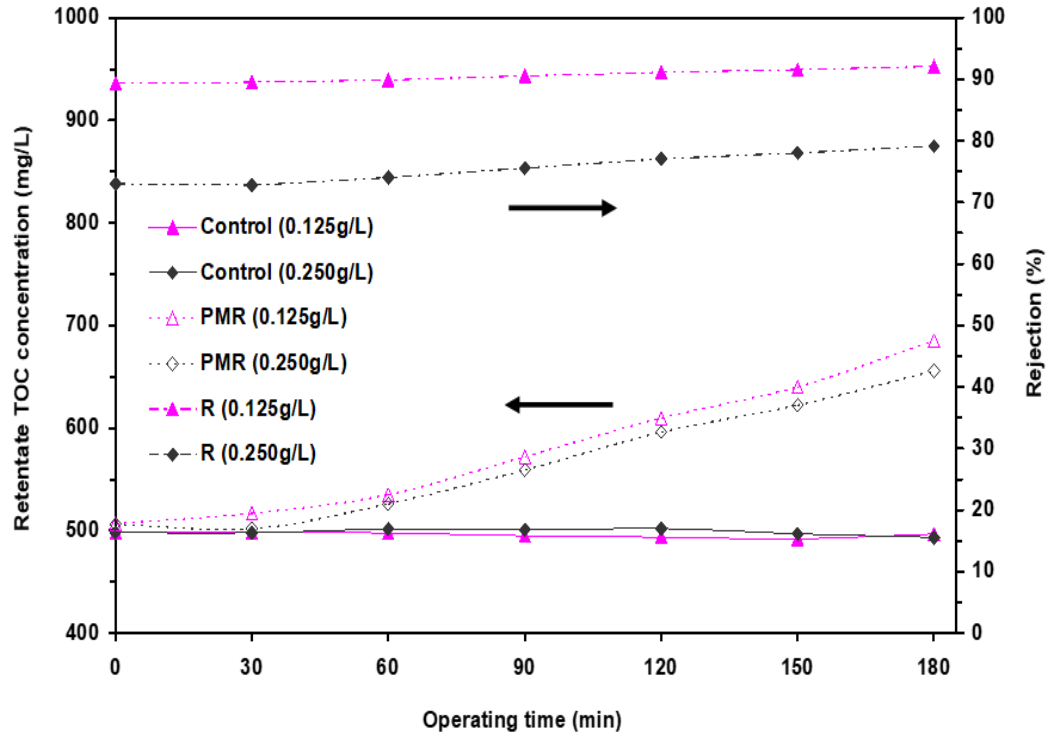

Fig. 6.26: Comparative performance of TOC concentration between control photocatalysis and batch PMR mode of operation at various TiO_2 loadings.

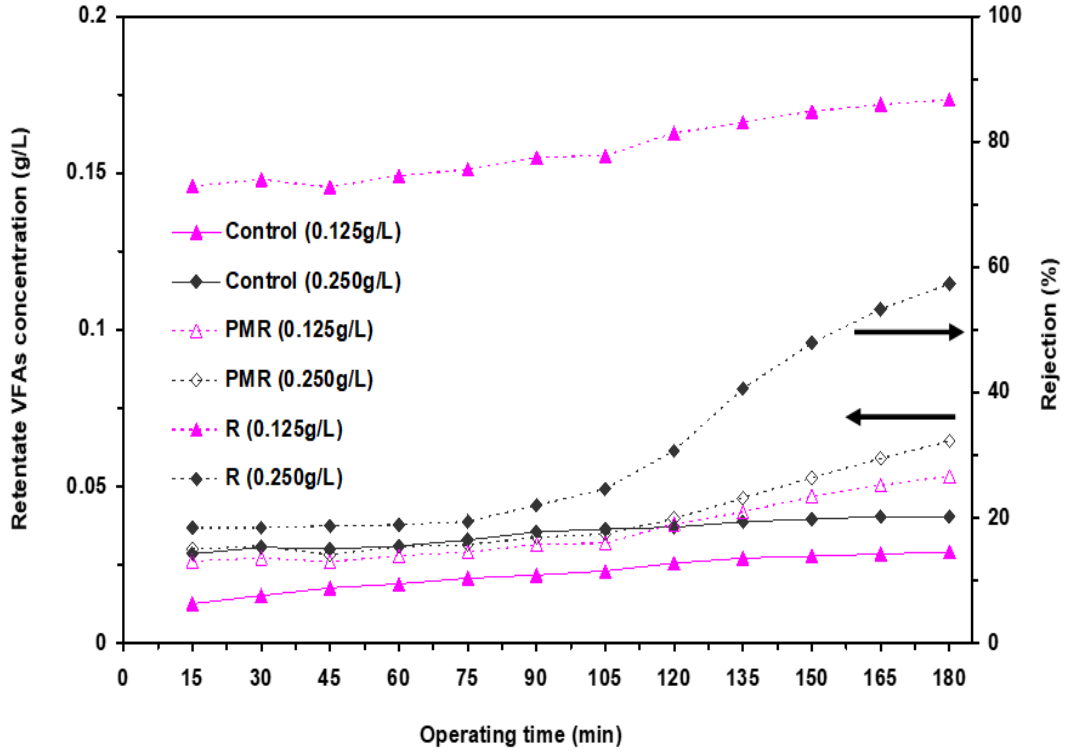

Fig. 6.27: Comparative performance of VFAs between control photocatalysis and batch PMR mode of operation at various TiO_2 loadings.

6.4.2 Continuous PMR operation (*Continuous photocatalysis*)

The aim of this work is to convert batch heterogeneous photocatalysis (control process-no membrane) to a continuous photocatalysis mode of operation by using PMR. *To achieve this*, a continuous fresh PEG feed was added to the BRS and the cross-flow PMR was continuously operated at the optimal TiO_2 loading (0.25 gL^{-1}) for 9 h. The performance of continuous PMR operation was evaluated according to the percent primary degradation, reaction kinetics and mineralization, and compared with batch control photocatalysis. *Note that, batch photocatalysis (no membrane), continuous photocatalysis (continuous PMR operation) and batch PMR operation are referred to as control, CPMR and BPMR respectively.*

In Fig. 6.28, the continuous photocatalysis showed a similar overall %PD of PEG as batch photocatalysis. For example, at a 3 h operating time, the %PD of PEG decreased by 22% under continuous photocatalysis in comparison with the batch photocatalysis. This decrease in %PD of PEG is expected to be due to three reasons:

The first and second reasons are similar to that explained in batch PMR operation in section 6.4.1, (1) leading to increase the tendency of TiO_2 to adsorb significantly on the surface of membrane and other components of PMR system. The third reason can be explained by the effect of addition of fresh PEG feed to the original PEG reactant solution in terms of permeate flux under BPMR and CPMR operations as shown in Fig. 6.29. It shows that the permeate flux under CPMR is greater than that of BPMR, indicating that the constant rate of addition (fresh PEG feed) is lower than the rate of filtration by CPMR. In this respect, *there is no dilution effect*, thus significantly increasing the tendency of TiO_2 to adsorb on the surface of membrane and other components of the PMR system and then reducing the concentration of TiO_2 in the BSR (and later in the photoreactor) for a 9 h operating time as shown clearly in Fig. 6.28 and affecting the %PD of PEG.

Further investigation on the permeate flux under continuous photocatalysis for a 9 h operating time is shown in Fig. 6.29. The behavior of permeation flux was a gradual decline over investigated time, indicating that the surface of membrane was fouled. The SEM images in Fig. 6.30 confirmed this fouling, and thus decreasing the permeate flux. This fouling could be explained by the rejection of TiO_2 and PEG oligomers.

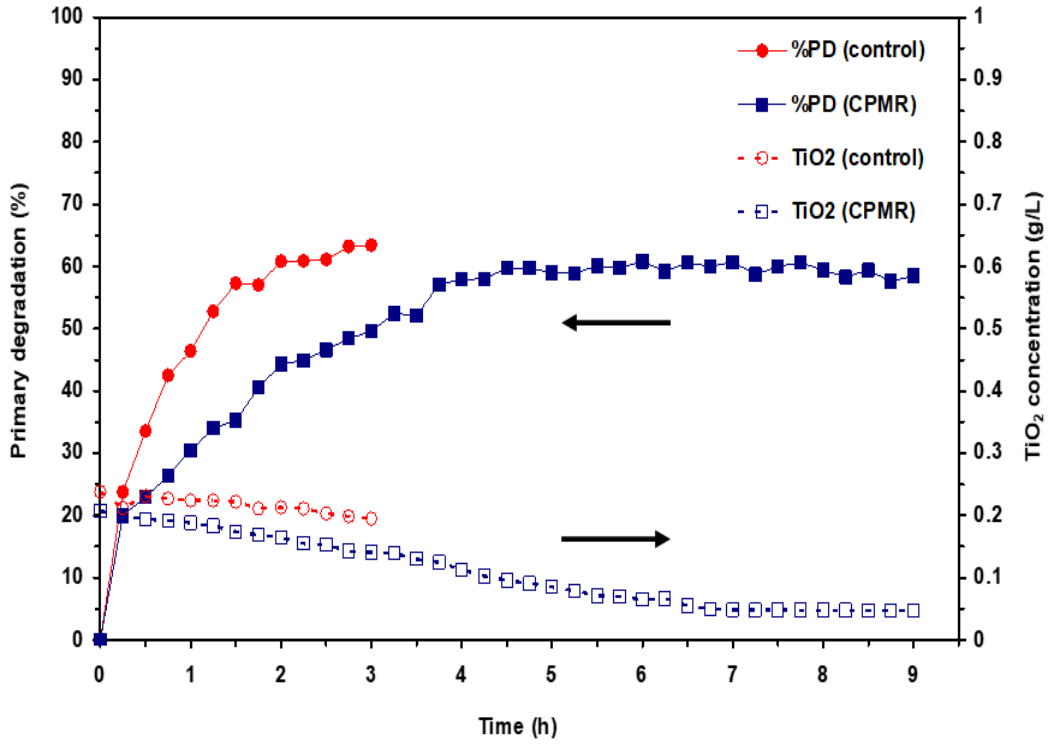

Fig. 6.28: Comparative performance of %PD of PEG and TiO_2 concentration as a function of time between batch photocatalysis and continuous photocatalysis under the optimal TiO_2 loading (0.25 gL^{-1}).

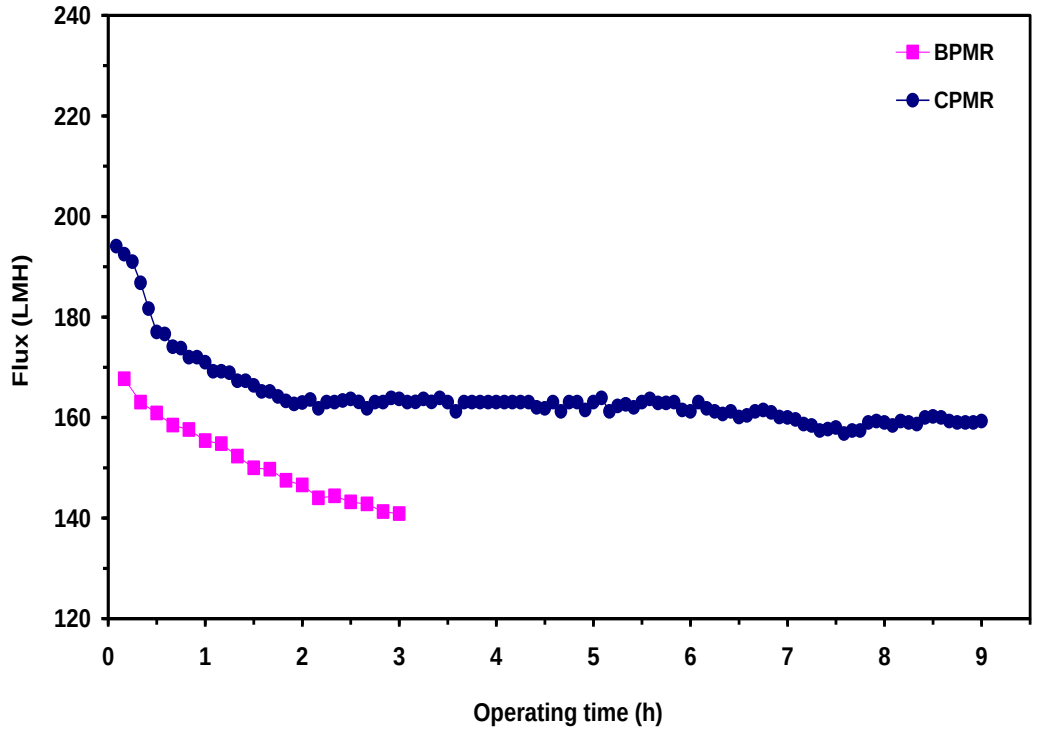

Fig. 6.29: Permeate flux as a function of operating time for batch and continuous PMR modes of operation at TiO_2 loading (0.25 gL^{-1}).

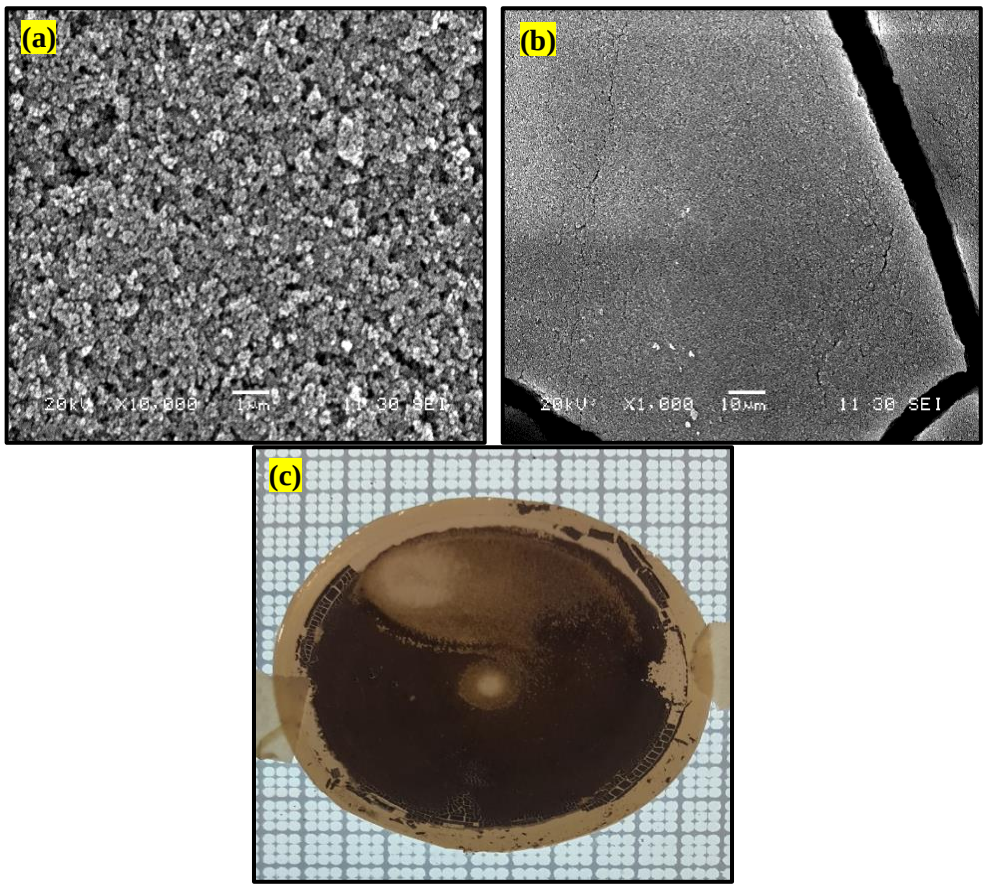

Fig. 6.30: SEM images (a-b) and a real photo (c) of the top surface of a fouled membrane with PEG and TiO_2 loading (0.25 gL^{-1}) under continuous heterogeneous photocatalysis (CPMR), magnification: (a) x 10,000 and scale: 1 µm and (b) x 1,000 and scale: 10 µm.

In terms of TiO_2 rejection, for a 9 h operating time, TiO_2 photocatalyst was continuously rejected with 100% by the membrane.

In terms of PEG rejection, the behavior of individual PEG oligomers under continuous PMR mode of operation (continuous photocatalysis) was found to be similar to that of batch PMR mode of operation where for example at a 9 h operating time (Fig. 6.31), the same identified MW oligomers were found in the retentate and permeate, and thus the true individual oligomer rejection cannot be valid for the same reasons explained in section 6.4.1, (1). However, *in terms of total PEG*, it was rejected by 33% where the concentrations in the retentate and permeate (Fig. 6.31) were 310 and 209 mgL^{-1} respectively.

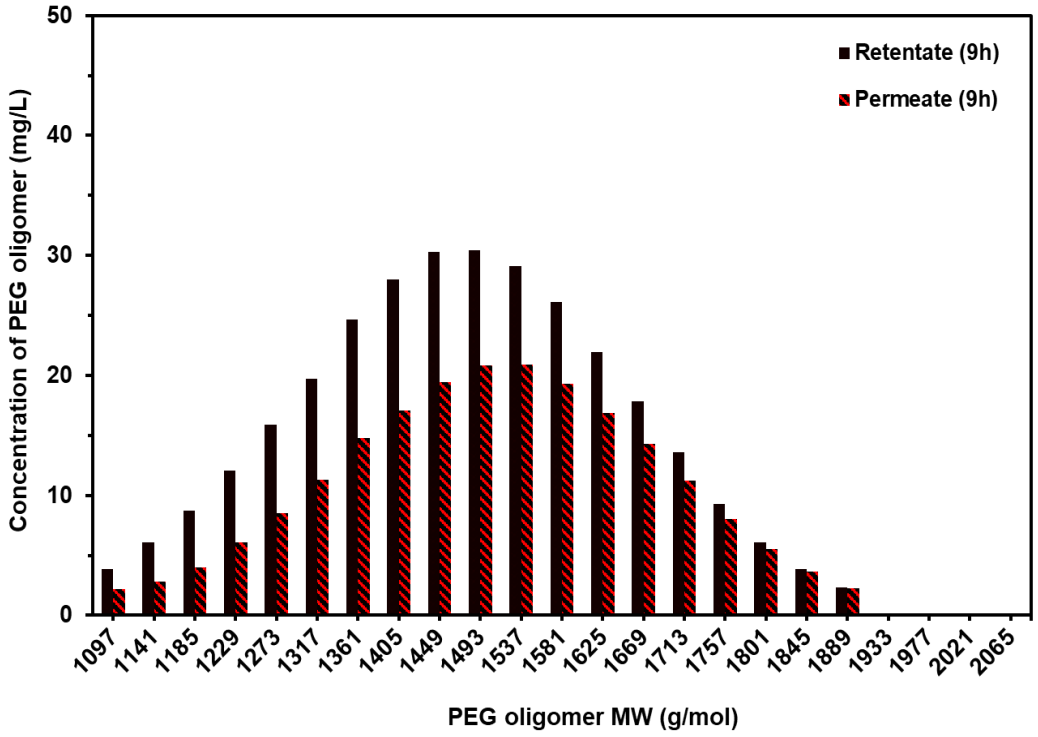

Fig. 6.31: The concentration of PEG oligomers in the retentate and permeate as a function of PEG oligomers MW under a continuous heterogeneous photocatalysis with TiO_2 loading (0.25 gL^{-1}) for a 9 h operating time.

In Fig. 6.32, the photocatalytic mineralization performance of batch photocatalysis in comparison with continuous photocatalysis based on the TOC concentration in relation to VFAs formation as a function time was examined. This examnination under continuous photocatalysis showed that the concentration of TOC and formation of VFAs in the retentate increased when comapring with the batch photocataysis. This increase is expected according to the two possible reasons explained in section 6.4.1, (3). These reasons can be supported by rejection data of TOC and VFA formation as shown in Fig. 6.33. For TOC rejection, it was 59, 62 and 63% at 3, 6 and 9 h operating times respectively, while for VFAs rejection was 80, 83 and 85% at 3, 6 and 9 h operating times respectively.

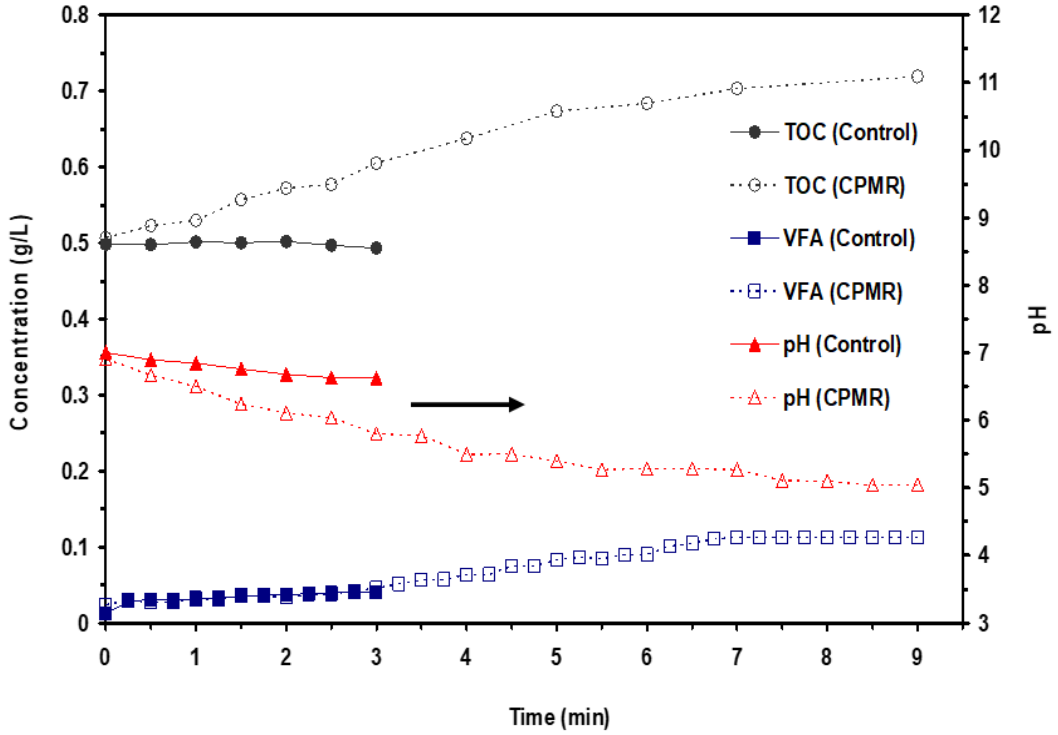

Fig. 6.32: Comparative performance of TOC, VFAs and pH over time between batch photocatalysis and continuous photocatalysis under the optimal TiO_2 loading (0.25 gL^{-1}).

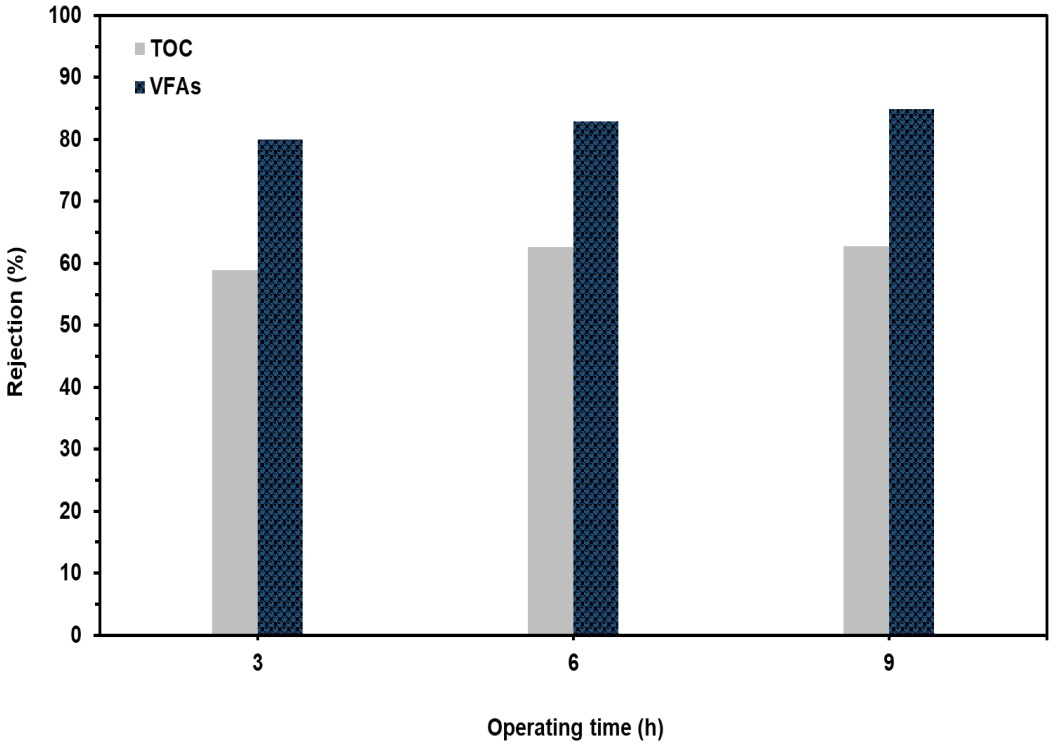

Fig. 6.33: Comparison of the rejection of TOC and VFAs between batch photocatalysis and continuous photocatalysis at TiO_2 loading (0.25 gL^{-1}) for various operating time intervals.

In terms of monitoring the pH, Fig. 6.32 shows the formation of identified VFAs as reaction intermediates under batch and continuous photocatalysis was associated with the drop of pH. It was found that the pH decreased significantly at continuous photocatalysis in comparison with that of batch photocatalysis. This is due to the higher rejection for these formed VFAs by the membrane (Fig. 6.33) and there was no dilution effect of added fresh PEG feed on the concentrations of these rejected acids in the retentate (Fig. 6.29), thus significantly decreasing the pH during the course of reaction.

In terms of reaction kinetics, a simplified Langmuir-Hinshelwood (L-H) kinetic model was successfully used to describe the reaction kinetics of PEG under batch PMR operation for a 3 h operating time (section 6.4.1, 2) and also for heterogeneous photocatalysis (section 6.3.2.2, 2). However, under continuous photocatalysis, examination of this model for a 9 h operating time (data not shown) reveals that the semi log data does not produce a single straight line, and thus does not fit this model for the total course of photocatalytic reaction time. This finding is similar to that found for POM continuous photocatalysis (chapter 5, section 5.4.2). Therefore, to elucidate more about this reaction analysis, a series of three first order reaction kinetic models was proposed in Fig. 6.34.

The three pseudo-first order reaction constants for three kinetic steps obtained from Fig. 6.34 are shown in Fig. 6.35. As shown in Fig. 6.35, the trend of these reaction constants represents the photocatalytic reaction mechanism of PEG under continuous photocatalysis where fast primary photocatalytic degradation of original PEG oligomers (region *a*), slower secondary photocatalytic degradation of reaction intermediate compounds (region *b*) and finally the photocatalytic degradation of these intermediates into complete mineralization (region *c*). These obtained results reflect the photocatalytic reaction pathway of PEG under continuous photocatalysis. However, the reaction of intermediate compounds like VFAs need to be accounted for the reaction kinetics of PEG. Therefore, a full kinetic analysis of these intermediate reactions will be part of future work.

Overall, the proposed heterogeneous cross-flow PMR could successfully convert batch photocatalysis to continuous process for the 9 h operating time. The membrane retained the TiO_2 photocatalyst completely and showed a continuous ability to promote a stable membrane flux until the end time of operation.

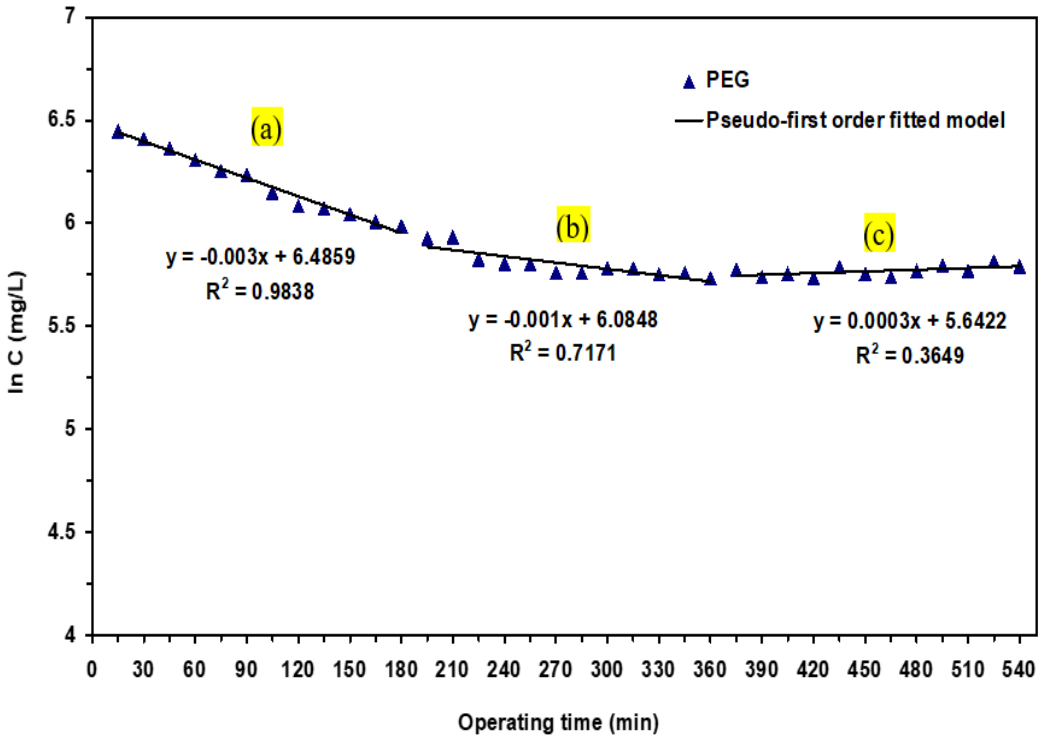

Fig. 6.34: Three stage pseudo-first order reaction constants plot for the kinetic photocatalytic degradation of PEG under continuous photocatalysis using PMR.

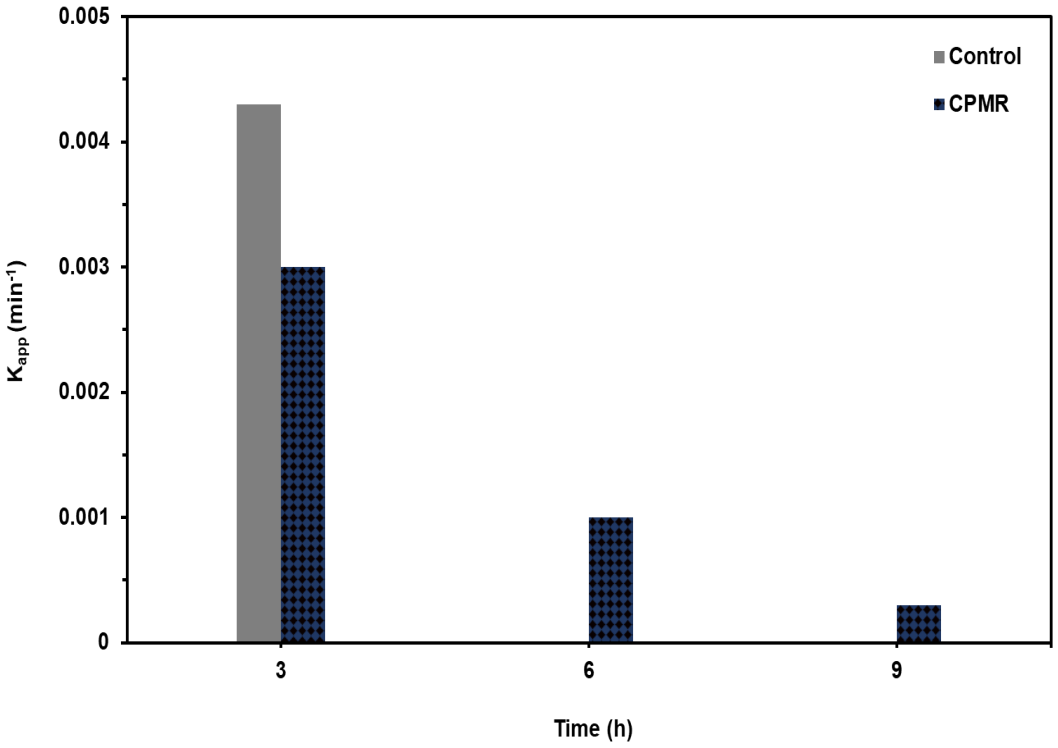

Fig. 6.35: Comparative performance of K_{app} as a function of time between batch photocatalysis and continuous photocatalysis under the optimal TiO_2 loading (0.25 gL^{-1}).

6.5 Chapter conclusions

The main aim of this chapter was to use and recycle the TiO_2 heterogeneous photocatalyst in a PMR for the treatment of PEG under batch and continuous modes of operation. This chapter was achieved in three sections (6.2, 6.3 and 6.4) and the following conclusions for each section were drawn:

1) *Investigation on the separation of TiO_2 (no UV)*

- A complete separation (100%) of the TiO_2 heterogeneous photocatalyst from the PEG reactant solution was achieved by the membrane (NF270) under the examined condition of dead-end membrane filtration process. Based on this interesting result, the membrane was used in the proposed cross-flow heterogeneous PMR.
- The used membrane could reject PEG based on total concentration with 34% and TOC with 44% from (PEG-TiO_2) solution when compared with that of PEG reactant solution (*no TiO_2*). This poor rejection is due to a non-photocatalytic reaction of TiO_2 with PEG, changing the MWs of PEG oligomers, and then these oxidized oligomers passing through the membrane to the permeate.

2) *TiO_2 heterogeneous photocatalysis (no membrane)*

- Preliminary experiments showed that the best adsorption equilibrium time of TiO_2 to take place in the system was 60 min prior to carrying out any reactions later. The experimental results of these experiments confirmed that there was a non-photocatalytic reaction of TiO_2 with PEG, generating several low MW VFAs intermediates and changing suddenly the pH of reactant solution. The pH played a crucial role in identifying this non-photocatalytic reaction. Examination of the effect of pH parameter under acidic (pH 3) and basic (pH 11) conditions on the adsorption of PEG oligomers onto the surface of TiO_2 particles showed that the adsorption of these oligomers was strongly affected under these pH conditions by releasing these adsorbed oligomers from the active sites of TiO_2 particles to the bulk solution. This will significantly affect the TiO_2 photocatalytic reactions. Therefore, the pH parameter was not controlled in photocatalysis and PMR experiments.

3) Cross-flow heterogeneous photocatalytic membrane reactor

A. Batch PMR operation:

- Investigation of the effect of oxidant (DO) concentration on the %PD of PEG showed that it played a significant role in increasing the %PD at 20 mgO_2L^{-1} as compared to that of without using DO (17±1 mgO_2L^{-1} from natural oxygenation of the solution through mass transfer from ambient air). However, a higher oxidant concentration of 75 mgO_2L^{-1} showed a negative impact on %PD due to the inner filter effect. So, the oxidant concentration in the range 20-25 mgO_2L^{-1} was used for TiO_2 photocatalytic reactions.
- A simplified Langmuir-Hinshelwood (L-H) kinetic model was successfully used to express the photocatalytic degradation data of PEG under heterogeneous photocatalysis (no-membrane) and batch PMR operation.
- The membrane separation process under cross-flow heterogeneous PMR operation could not enhance heterogeneous photocatalysis because of the tendency of TiO_2 photocatalyst to greatly adsorb on the membrane surface and also on the other components of PMR system. This adsorption rate increased significantly with the increase in the rate of separation, reducing the concentration of TiO_2 inside the BSR and then in the photoreactor, thus decreasing the %PD of PEG. Therefore, the concept of membrane enhanced heterogeneous photocatalysis is not feasible under the examined conditions.
- For TiO_2 rejection, the cross-flow PMR could successfully separate the TiO_2 photocatalyst (100%) from (PEG-TiO_2) solution and recycled it back into the photoreactor.
- For PEG rejection, the total PEG rejection was 56% at the end of course of operation. This rejection is due to the greatly oxidized PEG oligomers with MWs < MWCO of membrane could pass through the membrane to the permeate. While the lightly oxidized PEG oligomers with MWs > MWCO could not pass through the membrane and recycled for further oxidation.
- For mineralization, the cross-flow heterogeneous PMR could not enhance the photocatalytic mineralization of PEG due to the resistance of formed VFAs to total mineralization and also these VFAs could not considerably pass through the membrane to the permeate because of the effect of a secondary dynamic membrane by the adsorbed VFAs on the TiO_2 particles and on the surface of membrane.

B. Continuous PMR operation:

- The proposed cross-flow PMR could successfully convert batch heterogeneous photocatalysis to continuous process for a 9 h operating time at comparable photocatalytic degradation efficiency of PEG to control heterogeneous photocatalysis under the optimal control loading of TiO_2 (0.25 gL^{-1}).
- The membrane could completely retain the TiO_2 photocatalyst. Also, it could retain the identified lightly oxidized oligomers within low range of MWs as well as TOC in relation with the formed VFAs in the retentate and return them for photoreactor for further degradation. Despite the complete rejection of POM and higher rejection of PEG oligomers with formed VFAs by the membrane (NF270), this used membrane showed a continuous ability to promote good membrane flux until the end of operation.
- Monitoring the pH gave an indication about the rejection of VFAs since these acids could partially pass through the membrane and also there was no dilution effect of fresh PEG feed, so their concentrations increased in the retentate.
- The overall photocatalytic reaction pathway of PEG under continuous photocatalysis for a 9 h operating time was represented well by three steps of first order reaction (L-H) kinetic models. The obtained reaction rate constants reflected the photocatalytic reaction mechanism of PEG, which included fast photocatalytic degradation of original PEG oligomers, slower secondary degradation of intermediates and complete mineralization.

Chapter 7

Combined Homogeneous and Heterogeneous Photocatalytic Membrane Reactor

7.1 Introduction

In literature, up to now, the separation and recycle of POM homogeneous photocatalyst is still a big challenge. This challenge, *in the current project*, was successfully resolved in a proposed homogeneous cross-flow PMR for the treatment of PEG as shown extensively in chapter 5. This successful achievement allowing this chapter considerable breath of investigation.

The main aim of this chapter is to investigate the use and recovery of combined (POM-TiO_2) photocatalysts in a proposed cross-flow PMR for the treatment of PEG. This investigation was assessed based on the synergetic effect of combined photocatalysts as compared with separate photocatalyst. The experimental procedure of this chapter was performed in chapter 3, section 3.4.3.3.

This chapter is divided into two main sections, with the first (7.2) discussing the combined (POM-TiO_2) photocatalysis of PEG as control (*no membrane*). In this section, a new concept of synergistic effect of combined (POM-TiO_2) photocatalysts is proposed based on two scenarios, which the first scenario uses POM as a primary photocatalyst and TiO_2 as a secondary photocatalyst while second scenario uses TiO_2 as a primary photocatalyst and POM as a secondary photocatalyst. Both scenarios are tested with the %PD of PEG to identify which of them is better to be used in exploring the optimum loadings of these combined photocatalysts. These optimum loadings are assessed based on the evaluating parameters of primary degradation, reaction kinetics and minimization and will be used as a basis of control photocatalysis. While, the second section (7.3) comparing the performance of cross-flow combined (POM-TiO_2) PMR under batch mode of operation with investigated control photocatalysis based on the evaluating parameters (section 7.2) to validate if the concept *'membrane enhanced combined (POM-TiO_2) photocatalysis'* is to be feasible. Furthermore, this section discusses the possibility to convert batch photocatalysis under an optimal combined (POM-TiO_2) loadings to a continuous photocatalysis. Finally, the discussion of these two sections conclude this chapter.

It is import to mention the examination of ability of membrane (NF270) to separate combined (POM-TiO_2) photocatalysts using a dead-end membrane filtration process (*no UV*) has not been done since each photocatalyst was completely separated as shown in chapters (5-6).

7.2 Combined (POM-TiO_2) photocatalysis (*no membrane*)

7.2.1 Concept of synergistic effect development

As known in literature, a synergistic effect of combined processes or materials, producing a higher effect than that of each of them separately. Since there is no literature available into studying the effect of combined photocatalysts of POM and TiO_2 on PEG. A new synergistic effect concept was proposed depending on the combination of POM homogeneous and TiO_2 heterogeneous photocatalysts. *This proposed concept was adopted based on two scenarios:*

The first scenario assumed that POM is a primary photocatalyst and TiO_2 is a secondary photocatalyst. While second scenario assumed that TiO_2 is a primary photocatalyst and POM is a secondary photocatalyst, detailed information about the experimental procedure of these scenarios is shown in chapter 3, section 3.4.3.3.1, (A).

Several experiments, *to investigate which proposed scenario in terms of the %PD of PEG is better to be adopted in the examination of synergistic combination of POM and TiO_2,* were carried out. An example of this investigation was done at predetermined synergistic effect loadings of POM (0.25 gL^{-1}) and TiO_2 (0.125 gL^{-1}). The effect of first and second scenarios on the %PD of PEG is shown in Fig. 7.1. The photocatalytic performance (%PD of PEG) of the first scenario is higher than the second scenario. This finding implies that the selection process of POM or TiO_2 as primary or secondary photocatalysts plays an essential role in affecting the photocatalytic degradation activity of PEG. *This can be explained as follows:*

For second scenario, TiO_2 was added first as a primary photocatalyst and PEG oligomers were adsorbed on the surface of TiO_2 particles. When adding POM as a secondary photocatyst, the pH of prepared (PEG-TiO_2) solution changed suddenly to be more acidic conditions. This sudden change in pH led to liberate (release) the adsorbed PEG oligomers from the surface of active sites of TiO_2 to the bulk solution. Thus, decreasing the %PD of PEG. The conditions of second scenario are similar to that explained in chapter 6, section 6.3.1.2 (effect of pH on the adsorption of PEG oligomers onto TiO_2 particles).

While for first scenario, POM was added first and the pH of PEG reactant solution changed to be more acidic conditions and then when adding TiO_2, the PEG oligomers could potentially be adsorbed onto the active sites of TiO_2 particles under these acidic conditions, thus increasing the %PD of PEG (Fig. 7.1).

It is important to mention that as reported earlier, there was a non-photocatalytic reaction between POM with PEG (chapter 5) and TiO_2 with PEG (chapter 6). Under the examined conditions

of both scenarios, it was found that this non-photocatalytic reaction was not significantly affected. Therefore, the first scenario was used in all coming experiments.

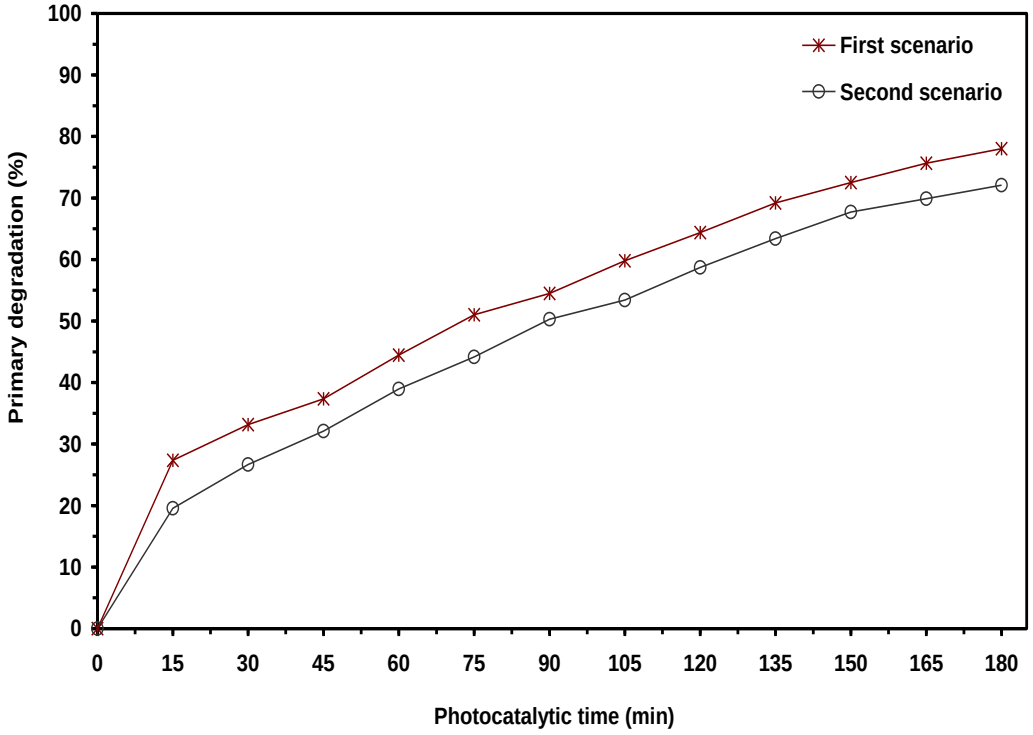

Fig. 7.1: Synergistic effect of first and second scenarios on the %PD of PEG.

7.2.2 Exploration of the optimal synergistic effect loadings

The aim of this section is to explore the optimal synergistic effect loadings of combined (POM-TiO_2) photocatalysts. This exploration was assessed with the evaluating parameters of primary degradation, reaction kinetics and mineralization. These evaluating parameters will be used as a basis of control photocatalysis when comparing with combined (POM-TiO_2) PMR later.

1) Primary degradation

Initially, the synergistic effect of combined (POM-TiO_2) photocatalysts on the PD% of PEG under their predetermined optimal loadings was investigated. As found earlier in chapters (5-6), the optimal loadings of separate POM and TiO_2 photocatalysts were 0.75 and 0.25 gL^{-1} respectively. Fig. 7.2 shows that a poor photocatalytic performance of combined photocatalysts when compared with each separate photocatalyst of POM and TiO_2. This could be explained by the reflection of incident light intensity caused by an excessive loading of combined (POM-TiO_2) photocatalysts despite of the presence of large number of active sites, thus decreasing the %PD of PEG.

Based on this result, it seems that there is no synergistic effect of combined (POM-TiO_2) photocatalysts under these examined conditions compared separately with POM and TiO_2.

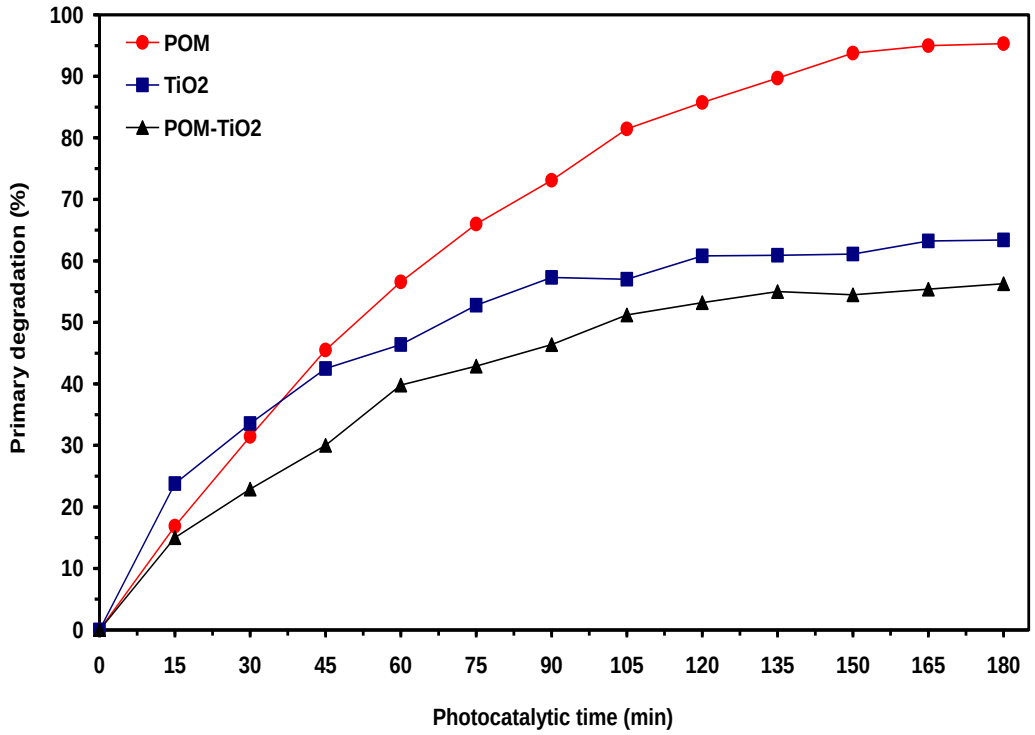

Fig. 7.2: Investigation on the synergistic effect of combined (POM-TiO_2) photocatalysts with separate POM and TiO_2 at their optimal loadings (POM-0.75 gL^{-1}, TiO_2-0.25 gL^{-1}) based on the %PD of PEG.

In order to further investigate the synergistic effect of combined photocatalysts in terms of examined photocatalyst loadings, several preliminary experiments were carried out to examine these loadings. It was found that the best range of systematic POM loadings was 0.25 and 0.125 gL^{-1} in conjunction with various TiO_2 loadings since this POM range showed a poor photocatalytic activity when used alone. Thus, two sets of experiments referred to as Set 1 and Set 2 were carried out to investigate the optimum loadings for combined (POM and TiO_2) photocatalysts, which will be used later as a basis of control photocatalysis (*no membrane*) and compared with combined (POM-TiO_2) PMR later.

To achieve this investigation, POM loadings as a primary photocatalyst in Set 1 and Set 2 were selected to be 0.25 and 0.125 gL^{-1} respectively in combination with systematic TiO_2 loadings as a secondary photocatalyst in the range from 0.125 to 0.625 gL^{-1} for each set.

Investigation on Set 1 and Set 2 in Fig. 7.3 and Fig. 7.4 shows that the maximum %PD of PEG was found at TiO_2 loading of 0.5 and 0.25 gL^{-1} respectively. A further increase in TiO_2 loading at 0.625 gL^{-1} (Fig. 7.3) and 0.375 gL^{-1} (data not shown in Fig. 7.4 to avoid interference with 0.50 gL^{-1} line) decreased the %PD of PEG due to light scattering effects **[64, 79, 255]**. A synergistic effect of combined photocatalysts based on the %PD of PEG under Set 1 and Set 2 as compared with separate photocatalysts of POM and TiO_2 is shown in Fig. 7.5. The synergistic effect of the PD% of PEG at Set 1 and Set 2 was greater than that of the separate POM and TiO_2 photocatalysts. Concluding that

the concept of combined photocatalysts based on synergistic effect is confirmed at two different conditions of Set 1 and Set 2.

Therefore, the optimal conditions for Set 1 (POM-0.25 gL^{-1} and TiO_2-0.5 gL^{-1}) and Set 2 (POM-0.125 gL^{-1} and TiO_2-0.25 gL^{-1}) will be used for batch combined (POM-TiO_2) PMR mode of operation later. As shown in Fig. 7.5, under these optimal conditions, the %PD of PEG of Set 2 is greater than that of Set 1. So, it will be used for continuous photocatalysis using PMR later.

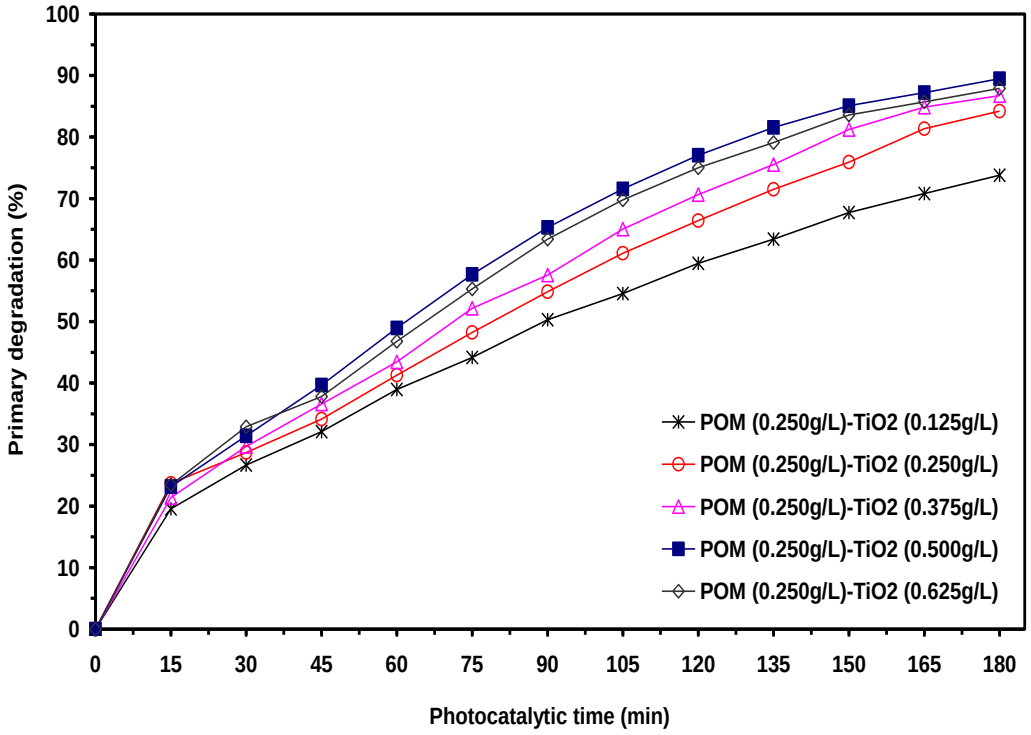

Fig. 7.3: Investigation on the optimal synergistic effect loadings of combined (POM-TiO_2) photocatalysts at Set 1 based on the %PD of PEG over photocatalytic reaction time.

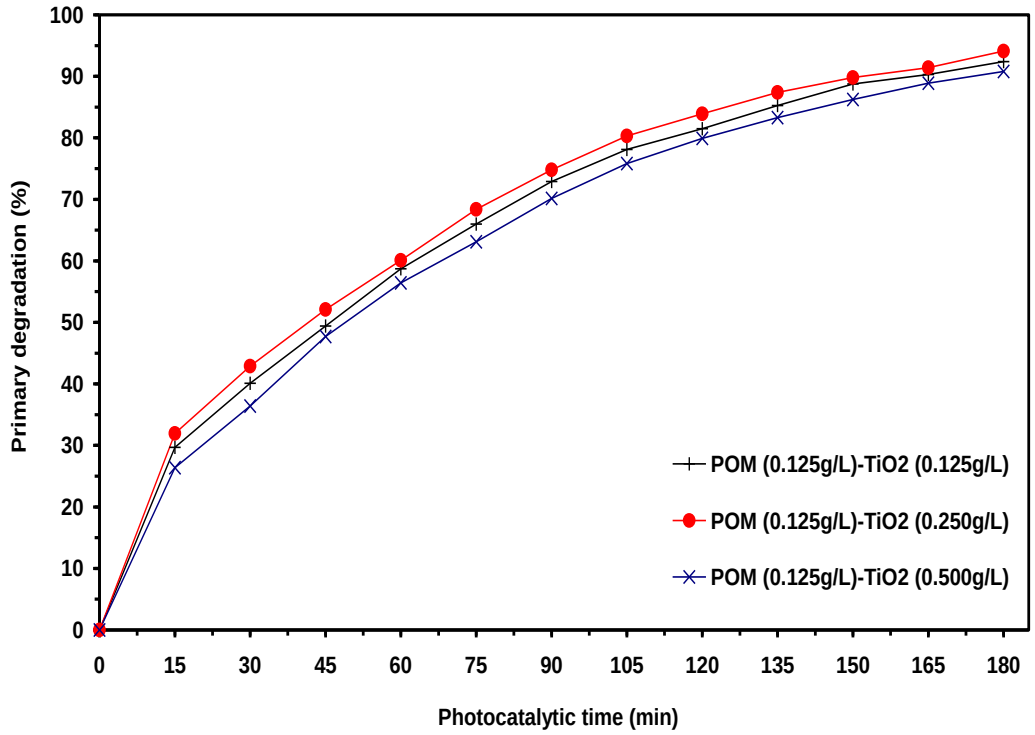

Fig. 7.4: Investigation on the optimal synergistic effect loadings of combined (POM-TiO_2) photocatalysts at Set 2 based on the %PD of PEG over photocatalytic reaction time.

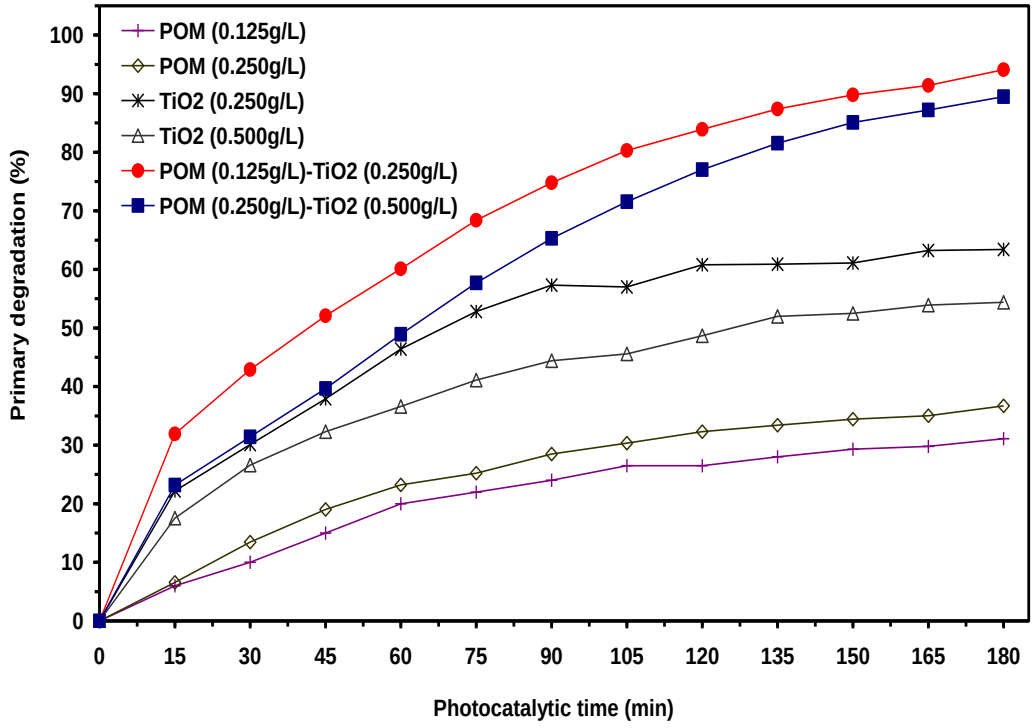

Fig. 7.5: A comparison of synergistic effect of combined (POM-TiO_2) photocatalysts at the optimal loadings of Set 1 and Set 2 with separate POM and TiO_2 photocatalysts based on the %PD of PEG over photocatalytic reaction time.

The effect of adsorption on the TiO_2 concentration under Set 1 and Set 2 conditions as compared with each separate TiO_2 photocatalyst was examined. An example of this examination for set 1 is shown in Fig. 7.6. It is clear to see from Fig. 7.6 that the concentration of separate TiO_2 photocatalyst (loading 0.50 gL^{-1}) decreased by 48% at the end time of operation. While, this concentration decreased by 13% only under the optimal conditions of Set 1 (POM-0.25 gL^{-1} and TiO_2-0.5 gL^{-1}) at the end time of operation. This is due to the presence of POM photocatalyst (0.25 gL^{-1}) where it changed the pH of the bulk solution since POM in aqueous solution is acidic **[38, 93]**, and thus reducing the effect of adsorption on the TiO_2 concentration. Similar behavior was found under all investigated TiO_2 photocatalyst of Set 1 and Set 2.

These are very encouraging results for potentially proving the concept of the membrane enhanced combined (POM-TiO_2) PMR later.

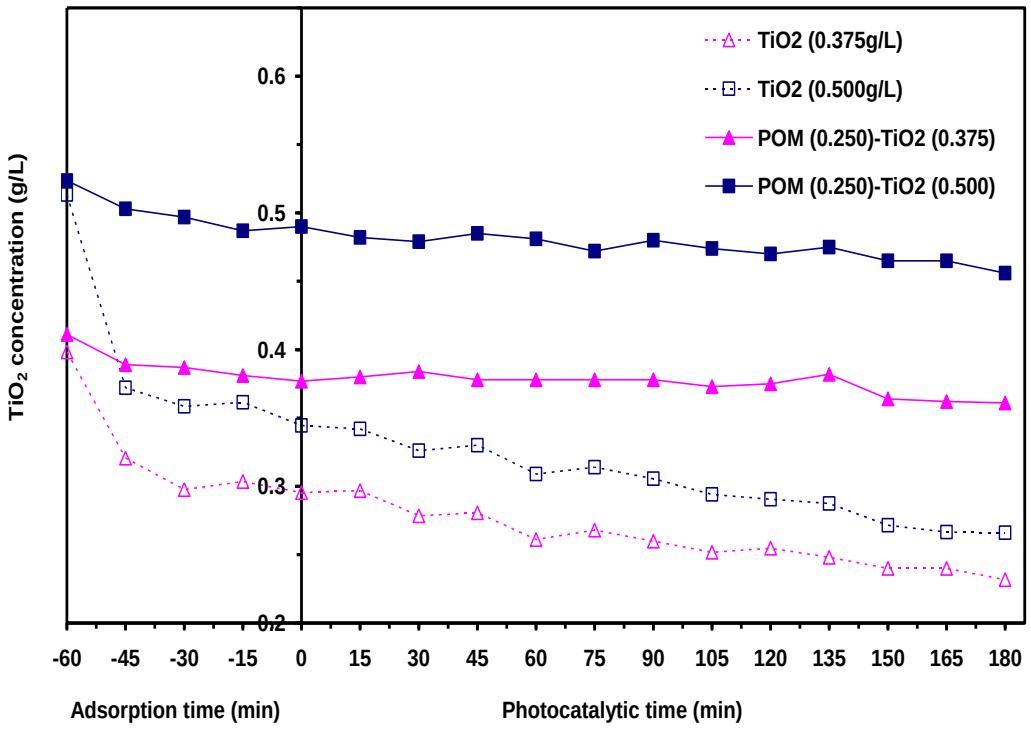

Fig. 7.6: A comparison of the concentration of TiO_2 during adsorption and photocatalytic reaction times at the synergistic effect of combined (POM-TiO_2) photocatalysts of Set 1 with separate TiO_2 photocatalyst.

2) Reaction kinetics

A simplified Langmuir-Hinshelwood (L-H) kinetic model in terms of K_{app} fitted well the photocatalytic data of combined (POM-TiO_2) photocatalysts under examined synergistic effect conditions of Set 1 and Set 2. To simplify this examination, the optimal conditions of Set 1 and Set 2 were selected in comparison with separate POM and TiO_2 photocatalysts as shown in Fig. 7.7.

The presented results in Fig. 7.7 show that the synergistic effect of combined (POM-TiO_2) photocatalysts based on K_{app} at the optimal loadings of Set 1 and Set 2 is greater than that of separate POM and TiO_2 photocatalysts. These results in Fig. 7.7 gave further support to confirm the proposed concept of synergistic effect between POM primary photocatalyst and TiO_2 secondary photocatalyst.

In literature, several authors used different types of AOPs to study the synergism of these individual processes on the overall degradation of various pollutants based on kinetic reaction **[229, 230, 260, 261]**. *In the current section*, the Eq. 7.1 was proposed to determine the synergistic effect of combined (POM-TiO_2) photocatalysts with their individual photocatalysts on the basis of K_{app}:

$$\text{Synergy}\ (\%) = \left[\frac{K_{\text{POM}-\text{TiO}_2} - \left(K_{\text{POM}} + K_{\text{TiO}_2}\right)}{K_{\text{POM}-\text{TiO}_2}}\right] * 100 \qquad (7.1)$$

Where $K_{\text{POM}-\text{TiO}_2}$, K_{POM} and K_{TiO_2} are the pseudo-first order reaction constant for combined (POM-TiO_2), POM and TiO_2 photocatalysts respectively.

The synergy of Set 1 and Set 2 under the optimal conditions was mathematically calculated using Eq. (7.1) and found to be 55 and 63% respectively, confirming the proposed concept of combined photocatalysts.

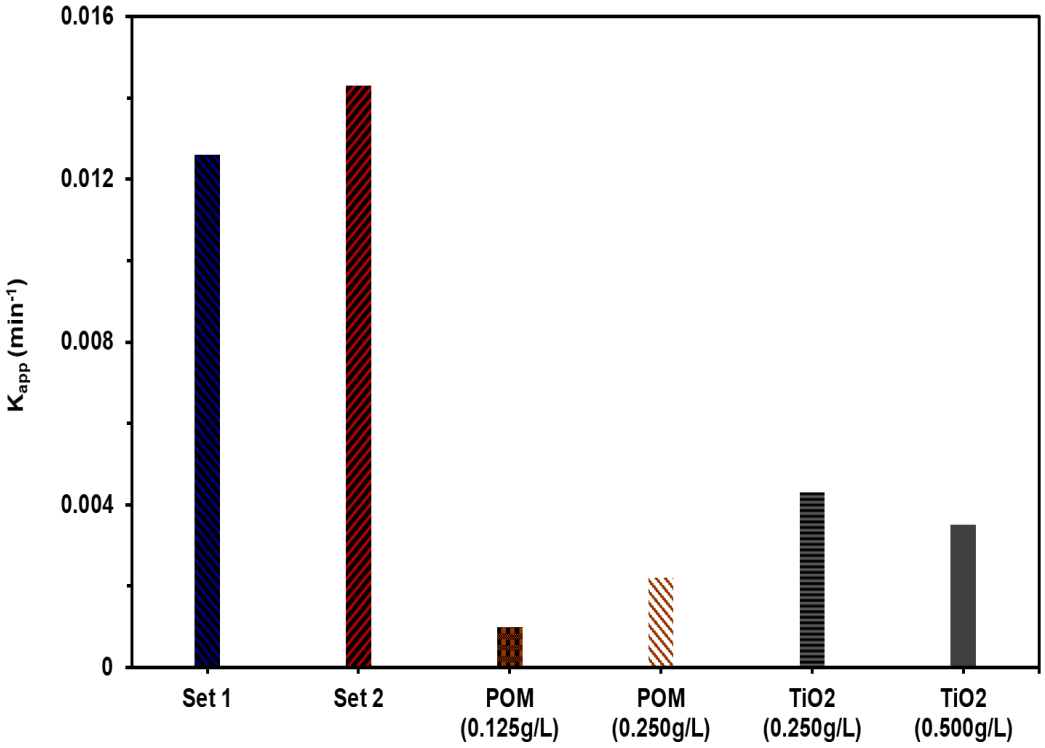

Fig. 7.7: A comparison of K_{app} between synergistic effect of combined (POM-TiO_2) photocatalysts at the optimal loadings of Set 1 and Set 2 with their individual photocatalysts.

3) Mineralization

The effect of photocatalytic mineralization of combined (POM-TiO_2) photocatalysts on PEG (%TOC removal) under the optimal conditions of Set 1 and Set 2 was investigated in Fig. 7.8. This investigation showed that a partial mineralization of PEG was found to be less than 2% TOC removal. This partial mineralization is attributable to the formation of several VFAs. These VFAs are so resistant to total mineralization as explained earlier in Chapters 4-6. Under these investigated conditions, the VFAs formed as reaction intermediates were malonic, glycolic, formaldehyde, acetic and propionic. The total concentration of these formed VFAs as a function of photocatalytic time is shown in Fig. 7.9. In order to better understanding the photocatalytic mineralization of PEG, *instead of %TOC*, the TOC concentration in relation with formed VFAs, will be used as an evaluating parameter for the performance of combined (POM-TiO_2) PMR later.

In terms of degradation pathway, it was found to be similar to that of TiO_2 heterogeneous photocatalysis shown in chapter 6, section 6.3.2.2, (3).

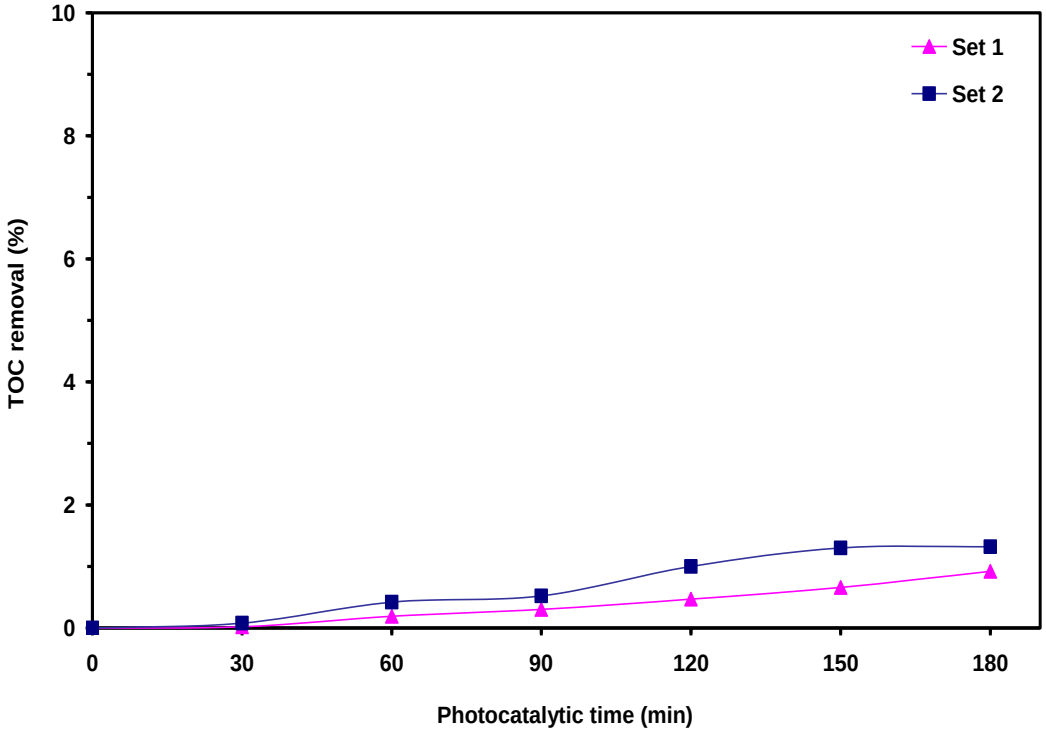

Fig. 7.8: %TOC removal over a photocatalytic time at the optimal conditions of Set 1 and Set 2.

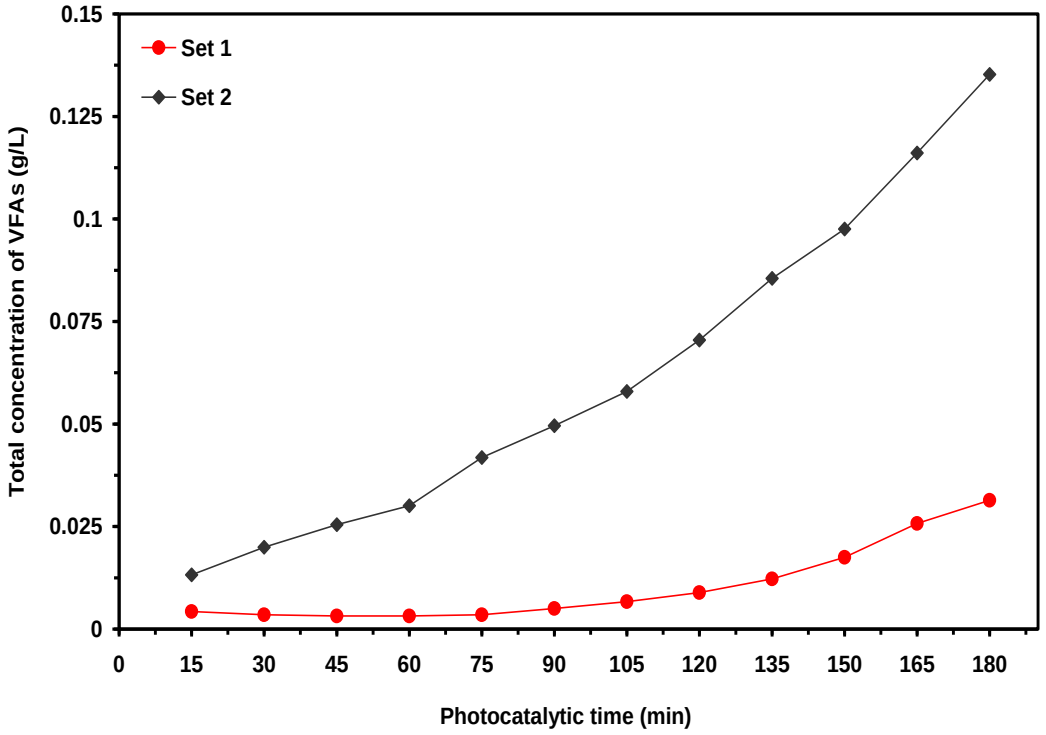

Fig. 7.9: Total concentration of formed VFAs over a photocatalytic time at the optimal conditions of Set 1 and Set 2.

7.3 Cross-flow combined (POM-TiO_2) PMR

7.3.1 Batch PMR operation

The concept '*membrane enhanced photocatalysis under batch mode of cross-flow PMR operation*' was extensively investigated in chapter 5 for POM homogeneous PMR and in chapter 6 for TiO_2 heterogeneous PMR. This concept was successful only for POM homogenous photocatalyst. The aim of this section is to validate if this concept in terms of a synergistic effect of combined (POM-TiO_2) photocatalysts under PMR is feasible when comparing with combined (POM-TiO_2) control photocatalysis (*no membrane*) shown in section 7.2.2 based on the evaluating parameters (primary degradation, reaction kinetics and minimization). The evaluation of combined (POM-TiO_2) PMR performance is shown below:

1) Primary degradation

In order to establish a fundamental understanding of the separation and recycle of combined (POM-TiO_2) photocatalysts under batch PMR mode of operation, the optimal synergistic effect conditions of these photocatalysts at Set 1 (POM-0.25 gL^{-1} and TiO_2-0.5 gL^{-1}) and Set 2 (POM-0.125 gL^{-1} and TiO_2-0.25 gL^{-1}) was initially investigated. Investigation of Fig. 7.10 reveals that the %PD of PEG under Set 1 and Set 2 using PMR decreased significantly by 54 and 24% respectively when compared with that of combined (POM-TiO_2) control photocatalysis. This decrease in the %PD of PEG using PMR could be explained by the rejection of combined photocatalysts and the permeate flux.

In terms of POM and TiO_2 rejections, the used membrane could successfully reject these photocatalysts with 100%. This complete rejection cannot explain the relationship in terms of the retentate concentration of POM and TiO_2 inside the BSR (or in the photoreactor) as a function of the permeate flux over operation time. This relationship can significantly affect the performance of PMR based on the %PD of PEG. Therefore, instead of this complete rejection, the retentate concentration of POM and TiO_2 inside the BSR were used for this.

In Fig. 7.11, as the operating time (photocatalytic reaction time in conjunction with cross-flow filtration time) proceeded, there was a gradual decline in the permeate flux for both Set 1 and Set 2 in relation with increasing the retentate POM concentration by 102 and 53% respectively. This behaviour is similar to that obtained by POM homogeneous PMR (chapter 5).

In Fig. 7.12, the retentate TiO_2 concentration increased by 78 and 110% respectively. This is very interesting result that is in contrast to that obtained by TiO_2 heterogeneous PMR (chapter 6) where as shown in section 7.2.2, the presence of POM photocatalyst at examined loadings of Set 1

(0.25 gL^{-1}) and Set 2 (0.125 gL^{-1}) played a significant role in changing the pH of the bulk solution, and thus reducing the effect of adsorption on the TiO_2 concentration.

It becomes evident that the membrane could effectively concentrate the concentration of POM and TiO_2 together inside the BSR to be significantly higher than the optimal concentrations of combined photocatalysts. Consequently, decreasing the %PD of PEG due to light scattering effect.

Really, these are very encouraging results for proving the concept of the membrane enhanced combined (POM-TiO_2) PMR mode of operation.

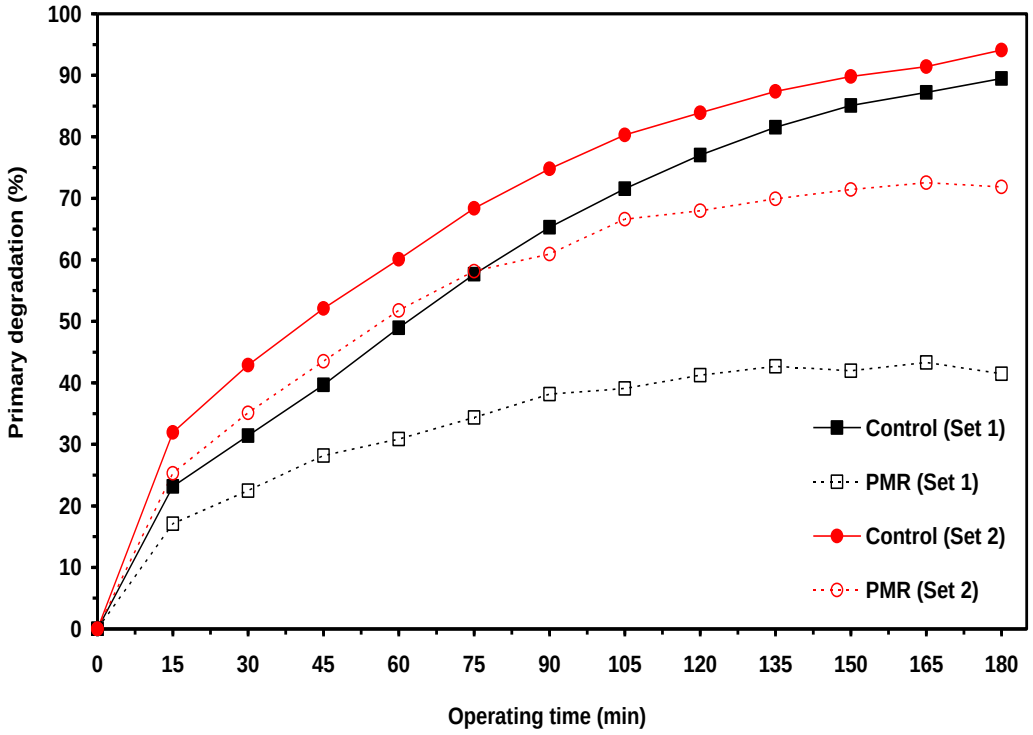

Fig. 7.10: Comparison of the %PD of PEG over operating time between control photocatalysis and batch PMR mode of operation at the optimal conditions of Set 1 and Set 2.

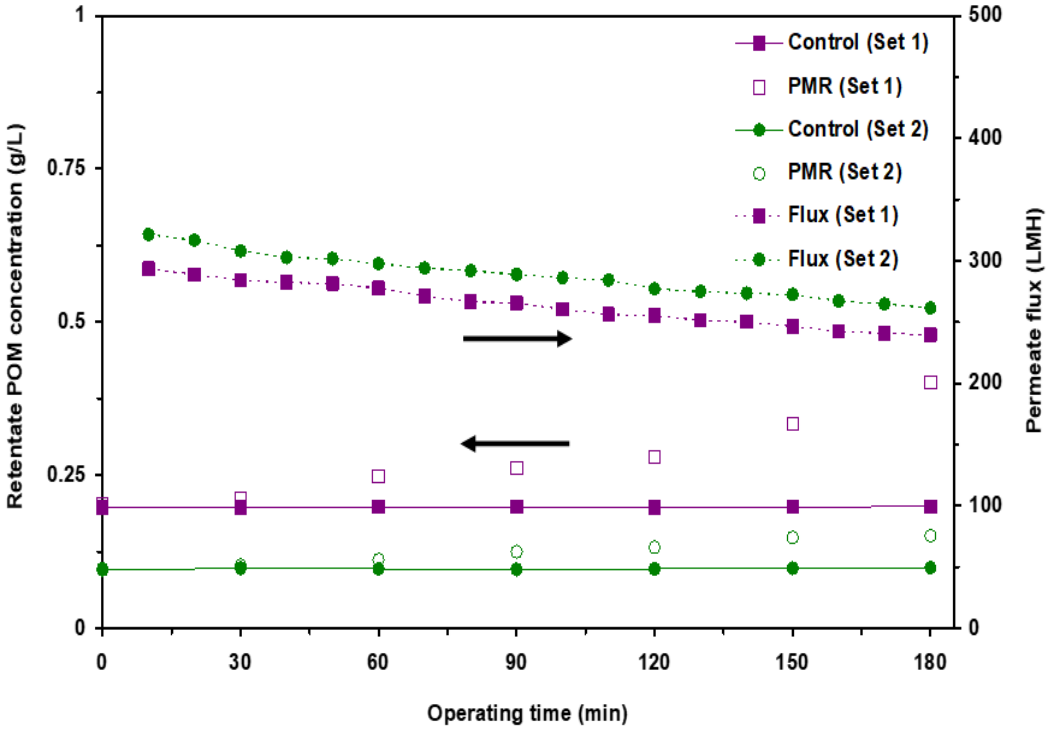

Fig. 7.11: Retentate POM concentration and permeate flux as a function of operating time of batch PMR mode of operation at the optimal conditions of Set 1 and Set 2.

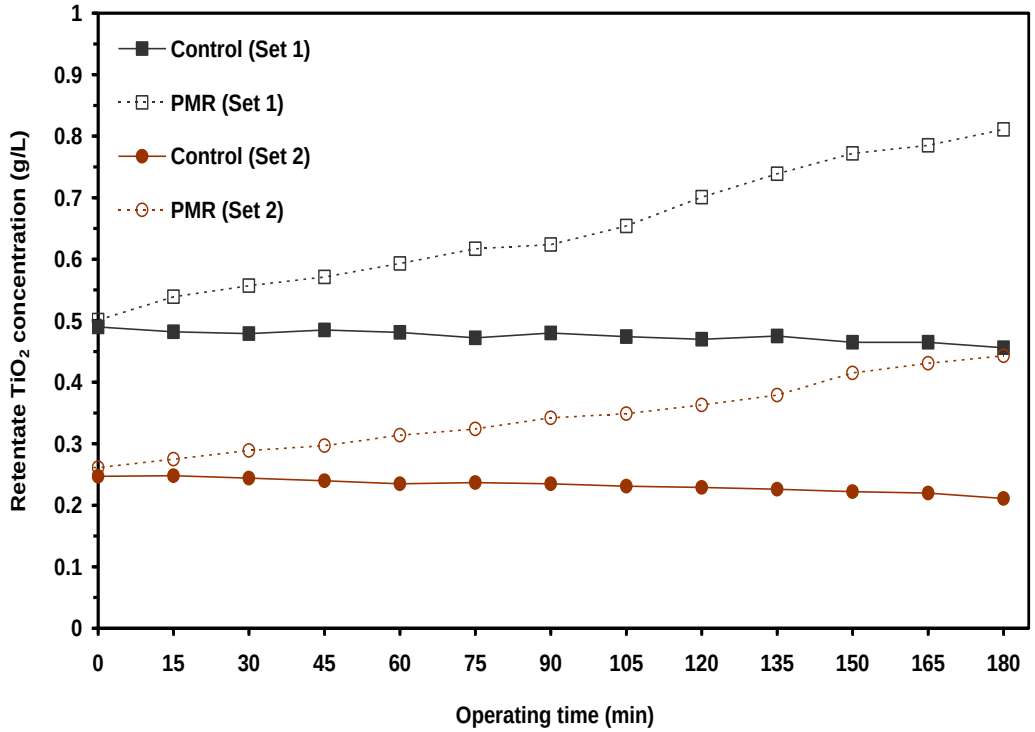

Fig. 7.12: Retentate TiO_2 concentration as a function of operating time of batch PMR mode of operation at the optimal conditions of Set 1 and Set 2.

In order to further investigate about the proof of this concept, as shown earlier for POM PMR (*this concept is feasible below the optimal photocatalyst loading*), so equal POM and TiO_2 photocatalyst loadings of 0.03 gL^{-1} *referred to as Set 3* were selected and examined in Fig. 7.13. Under these examined loadings, Fig. 7.13 shows the %PD of PEG increased using PMR as compared with control photocatalysis. This increase in the %PD of PEG is attributed to increasing the loadings of both photocatalysts as shown in Fig. 7.14 where the retentate concentration of POM and TiO_2 increased significantly by 76 and 215% respectively resulted in increasing the %PD of PEG under the synergistic effect conditions of using PMR (Fig. 7.13) to be comparable to that of control combined (POM-TiO_2) photocatalysis at their predetermined optimal loadings of Set 1 and Set 2 as shown in Fig. 7.15.

Based on these obtained results, it can be concluded that the membrane separation process could effectively enhance combined (POM-TiO_2) photocatalysis and then the concept of proposed cross-flow combined (POM-TiO_2) PMR mode of operation is feasible.

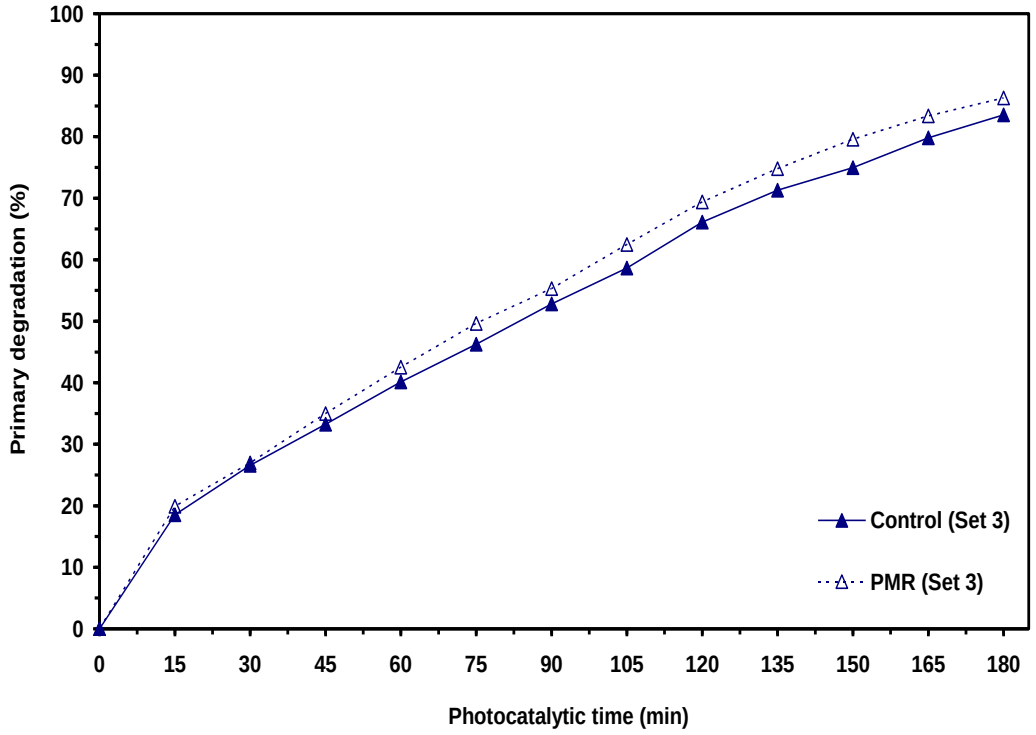

Fig. 7.13: Comparison of the %PD of PEG over a photocatalytic reaction time between control photocatalysis and batch PMR mode of operation at Set 3.

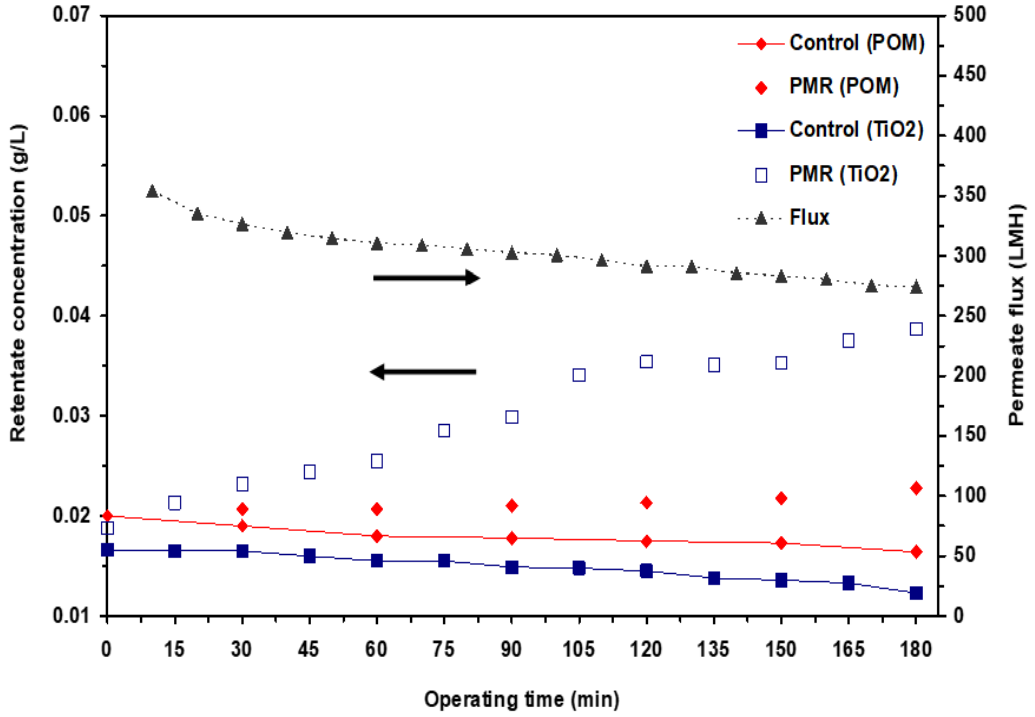

Fig. 7.14: Retentate concentrations of POM and TiO_2 and the permeate flux as a function of operating time of batch PMR mode of operation at Set 3.

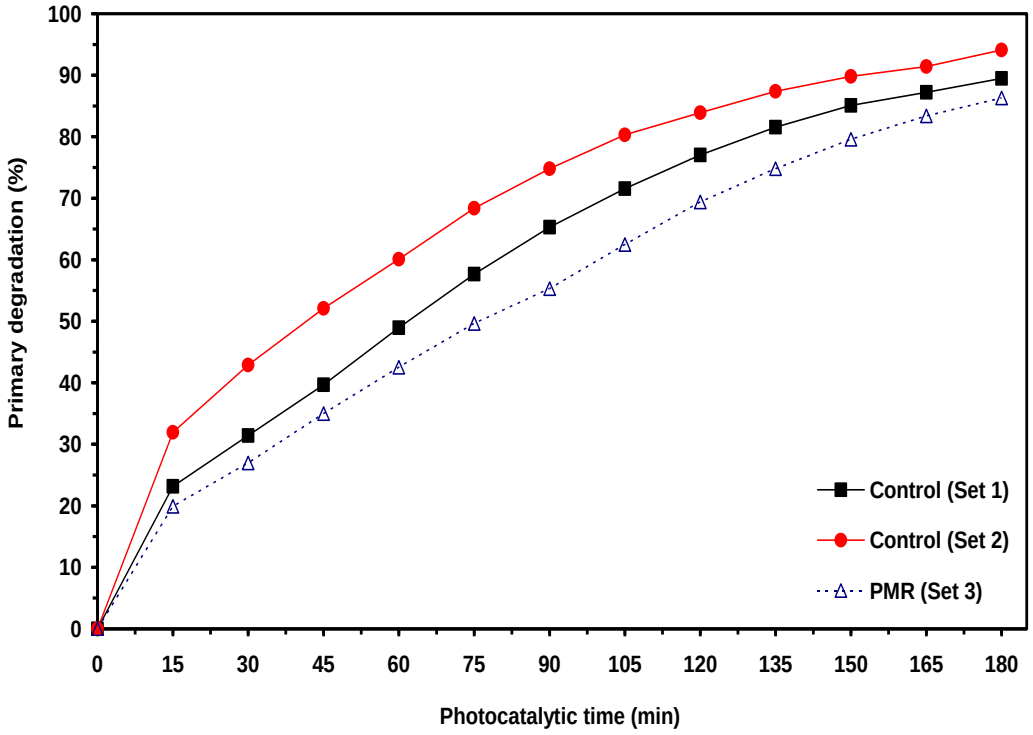

Fig. 7.15: Comparison of the %PD of PEG over a photocatalytic reaction time between control photocatalysis at the optimal loadings of Set and Set 2 and batch PMR mode of operation at Set 3.

Further investigation of the performance of combined (POM-TiO_2) PMR at Set 3 is achieved with regard to PEG rejection. As the operating time progressed, *in the retentate*, the concentrations of PEG oligomers MWs ranging from 1097.6 to 1185.7 $gmol^{-1}$ (corresponding to peak#1 and peak#3 respectively) increased gradually. While the concentrations of PEG oligomers MWs ranging from 1229.7 to 2066.2 $gmol^{-1}$ (corresponding to peak#4 and peak#23 respectively) decreased gradually. At 180 min operating time, it was found that in terms of HPLC chromatograms (Fig. 7.16-b), the concentrations of PEG oligomers (their MW $\geq$ 1934.2 $gmol^{-1}$, corresponding to peak#20) decreased greatly to be less the MIDL of HPLC methodology and calibration (*no peaks of PEG oligomers were detected and thus their concentrations could not be determined*).

For the permeate, no chromatographic peaks (oligomers) could be identified as shown in Fig. 7.16-c in which the detector baseline of HPLC appeared to drift and showed an excessive noise, indicating that the total concentration of PEG is less than 100 mgL^{-1} depending on HPLC methodology and calibration. These results are generally similar to that obtained and explained relating to two suggested scenarios in chapter 5 for POM homogeneous PMR and entirely different from TiO_2 heterogeneous PMR (chapter 6).

Therefore, the calculation of true rejection of PEG is not accurate. However, this rejection can be calculated based on the results of TOC investigation later.

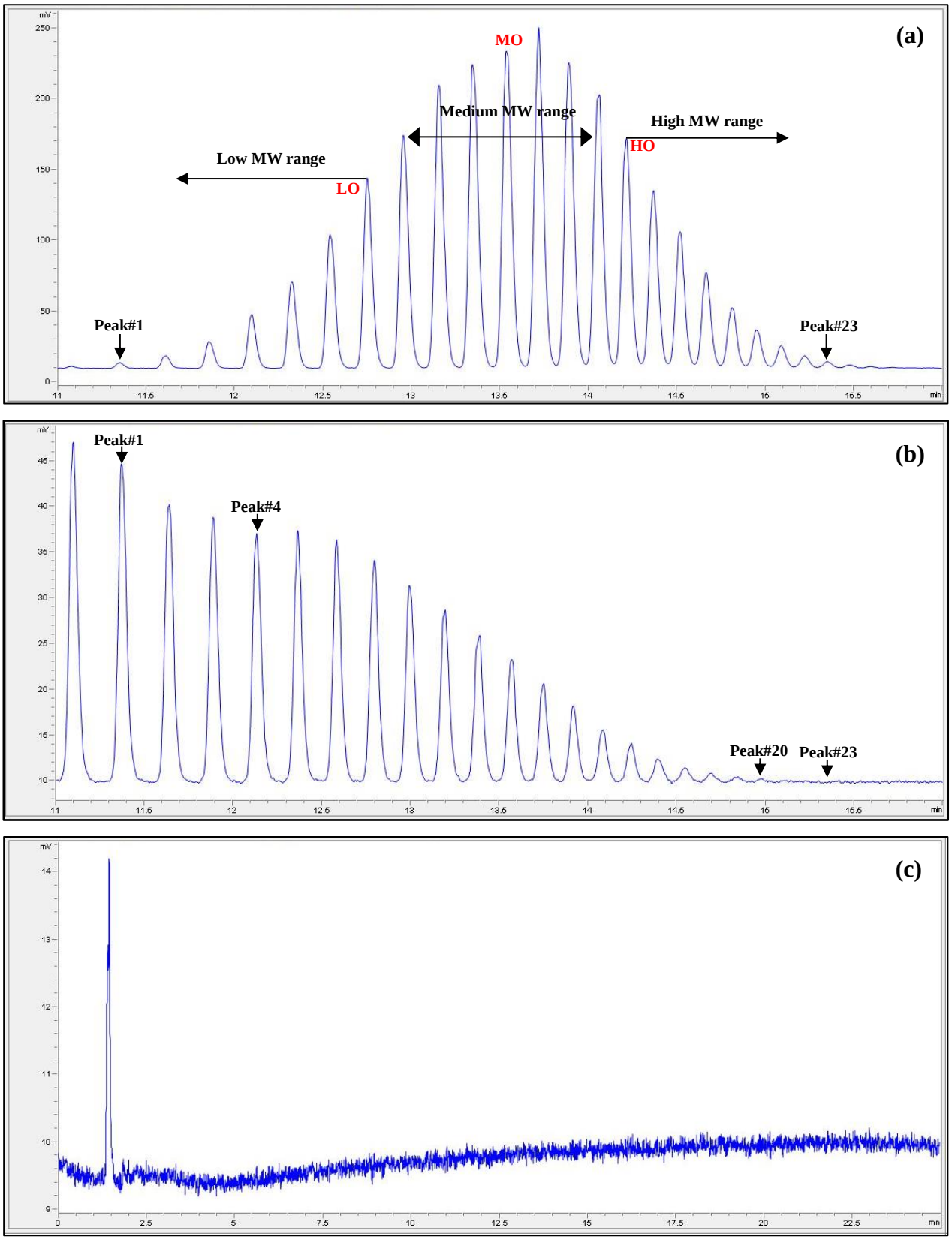

Fig. 7.16: RP-HPLC/ELSD chromatograms of PEG oligomers under combined (POM-TiO_2) PMR mode of operation with Set 3, (a) feed after adsorption, (b) retentate and (c) permeate.

In terms of permeate flux, Fig. 7.14 describes the experimental permeate flux profile for combined (POM-TiO_2) photocatalysts over a cross-flow operating time. A permeate flux decreased gradually during this period to be 274 LMH at 180 min (corresponding to a relative reduction of pure water by 24%). The gradual decrease in the permeate flux could be explained by the deposition of POM and TiO_2 photocatalysts as well as lightly oxidized PEG oligomers on the surface of membrane. This deposition was confirmed by the SEM images (Fig. 7.17-a and Fig. E1 (a, c), *Appendix E*) and also by the observation of real photos (Fig. 7.17-b and Fig. E1 (b, d), *Appendix E*).

Further comparison of permeate fluxes between synergistic effects (Set 1, Set 2 and Set 3) and a single photocatalyst of POM and TiO_2 is shown in Fig. 7.18. It can be seen that the permeate fluxes under the synergistic effects are higher than that of a single photocatalyst where the permeate flux at Set 3 was maximum. This is thought to be relating to a wide range of the interfacial interaction effects of POM, TiO_2, lightly oxidized PEG oligomers and formed VFAs with each other together and/or with the surface of membrane where these interfacial effects can be potentially classified into three groups including *'particle-particle'* interactions **[161]**, *'solute-solute'* interactions **[243]** and *'solute-particle'* interactions **[86]**.

The first group describes the interactions between the particles of TiO_2 heterogeneous photocatalyst. The second group describes the interactions between the molecules of POM homogeneous photocatalyst and/or POM molecules with lightly oxidized PEG oligomers and/or POM molecules with formed VFAs and/or lightly oxidized PEG oligomers with formed VFAs. The last group describes the interactions based on the adsorption effect between lightly oxidized PEG oligomers with TiO_2 particles and/or POM molecules with TiO_2 particles and/or formed VFAs with TiO_2 particles.

These groups of interactions based on combined physiochemical effect played a significant role in developing the concentration polarization layer, and thus affecting the permeate flux as shown in Fig. 7.18 as well as the concentrations of POM and TiO_2 as rejected homogeneous and heterogeneous photocatalysts in the retentate. This effect on the retentate concentration of POM and TiO_2 under different synergistic effect conditions of Set 1 (POM-0.25 gL^{-1} and TiO_2-0.5 gL^{-1}), Set 2 (POM-0.125 gL^{-1} and TiO_2-0.25 gL^{-1}) and Set 3 (POM-0.03 gL^{-1} and TiO_2-0.03 gL^{-1}) was studied at the end of operating time in Fig. 7.19.

As shown in in Fig. 7.19, as POM primary photocatalyst increased from 0.03 to 0.25 gL^{-1} the percent retentate concentration increased from 20 to 102%. While in Fig. 7.20, as TiO_2 secondary photocatalyst increased from 0.03 to 0.5 gL^{-1} the percent retentate concentration decreased from 215 to 78% respectively. *Concluding that concentrating the POM and TiO_2 as combined photocatalysts by the membrane are entirely different due to very complex phenomenon of the interfacial interaction*

effects as shown above. In addition, these interactions effects played a significant role in producing a stable membrane flux until the end time of operation, meaning that in terms of membrane fouling there is no complete pore blocking under these examined conditions.

In literature **[161]**, the understanding of fouling mechanism by reaction of photocatalyst with membrane under PMRs system is not obviously understood. *This fouling mechanism will be part of future work.*

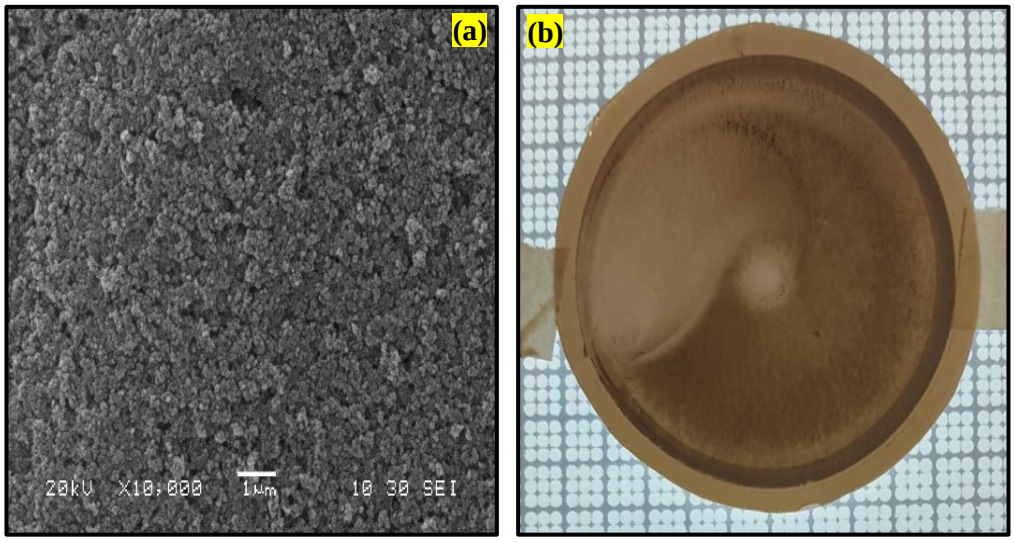

Fig. 7.17: SEM image (a) and real photo (b) of the top surface of a fouled membrane with PEG and combined (POM-TiO_2) photocatalysts with equal loadings of 0.03 gL^{-1} using a cross-flow PMR mode of operation, magnifications: x 10,000 and scale 1 µm.

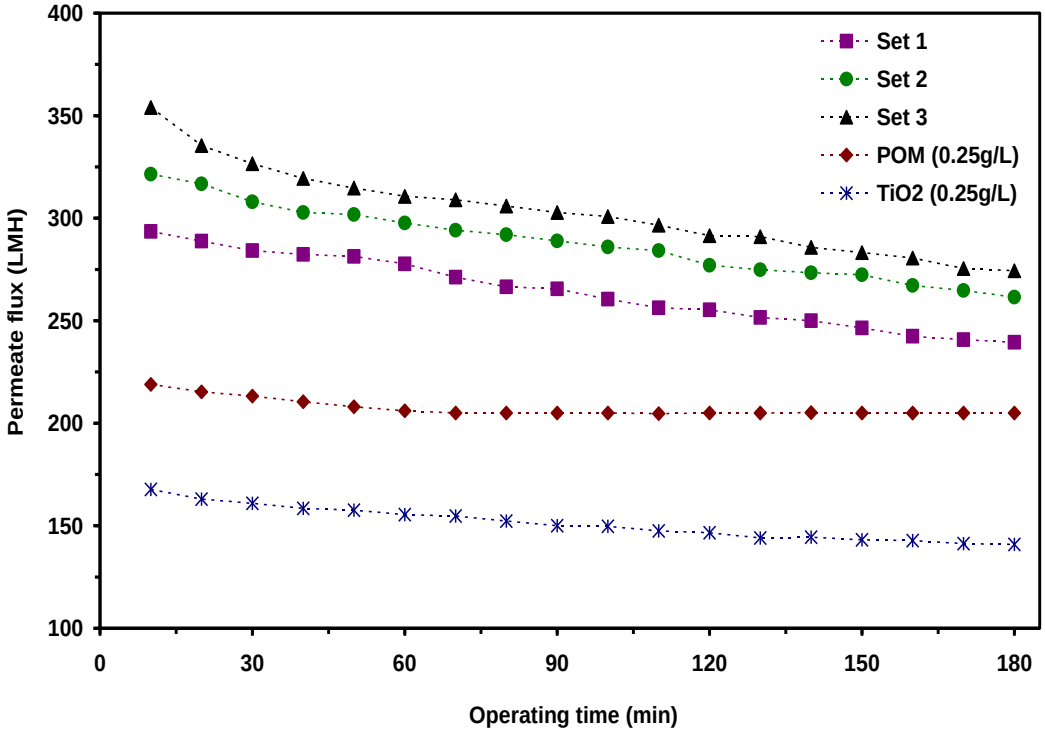

Fig. 7.18: Comparison of the permeate flux between the combined (POM-TiO_2) photocatalysts and a single photocatalyst of POM and TiO_2 at batch PMR mode of operation.

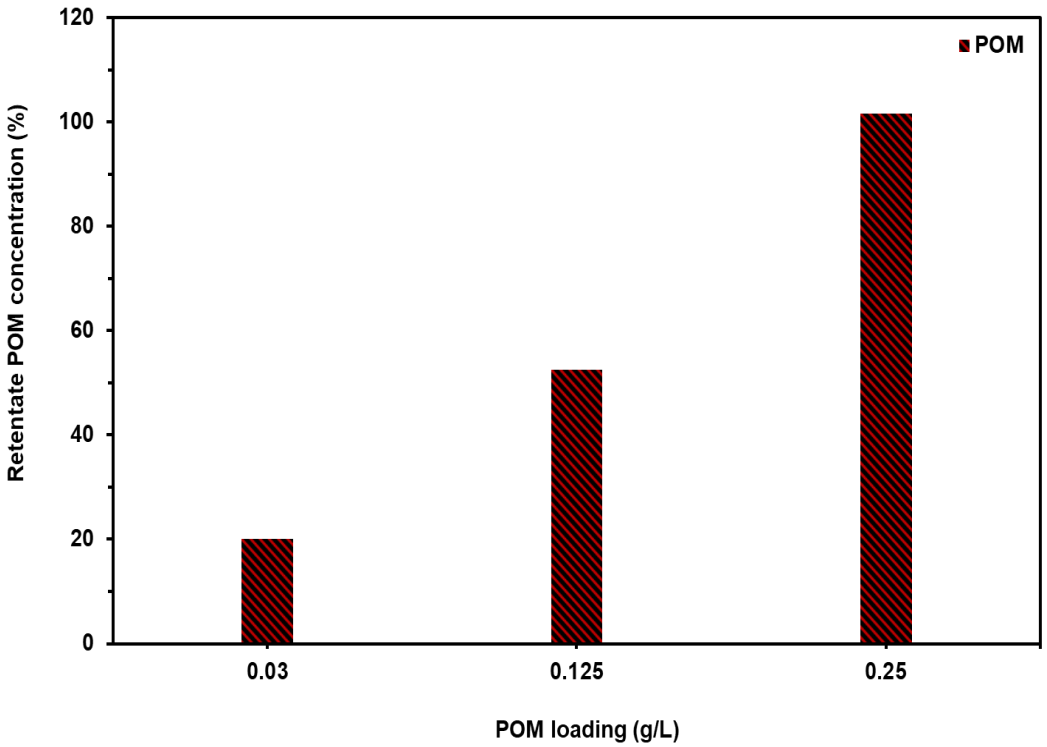

Fig. 7.19: Retentate POM concentration (%) as a function of POM loading under the combined (POM-TiO_2) PMR mode of operation.

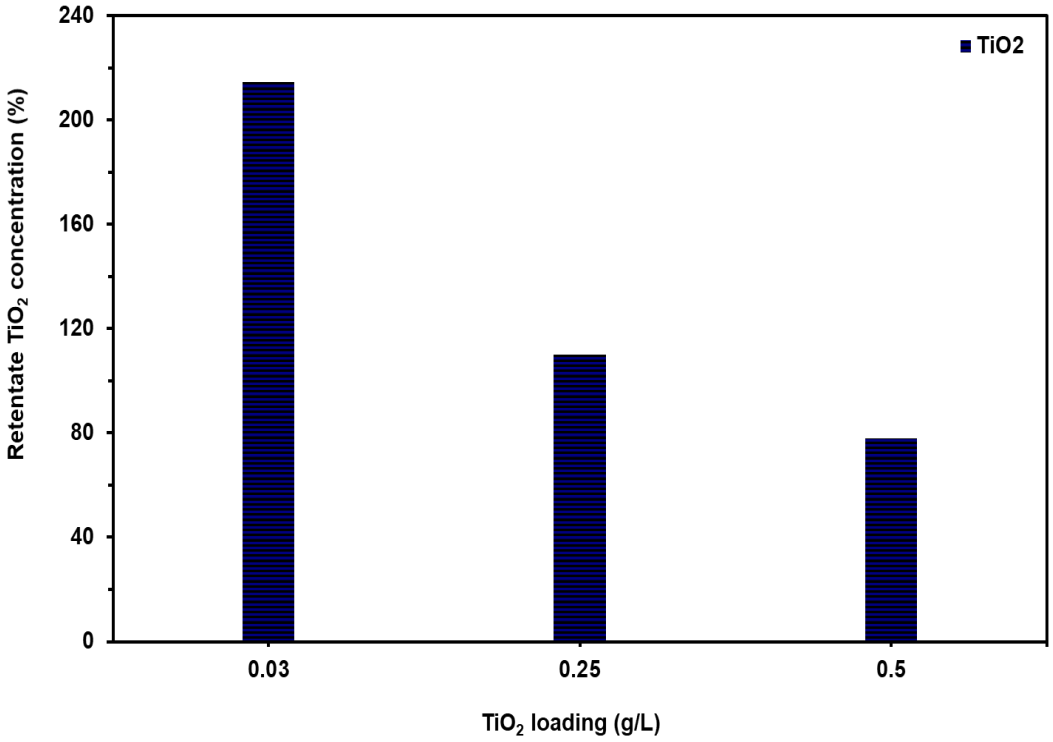

Fig. 7.20: Retentate TiO_2 concentration (%) as a function of TiO_2 loading under the combined (POM-TiO_2) PMR mode of operation.

2) Reaction kinetics

A synergistic effect of combined (POM-TiO_2) photocatalysts with Set 1, Set 2 and Set 3 was investigated in Fig. 7.21 based on a simplified Langmuir-Hinshelwood (L-H) kinetic model in terms of K_{app} under control photocatalysis and PMR. The presented results in Fig. 7.21 show that at Set 1 and Set 2, the K_{app} values decreased greatly under PMR as compared with control photocatalysis. While for Set 3, the K_{app} value increased significantly when comparing to that of control photocatalysis.

These results in Fig. 7.21 are in agreement with that found in the %PD of PEG and gave further support to confirm the validity of the concept of proposed cross-flow combined (POM-TiO_2) PMR to be feasible.

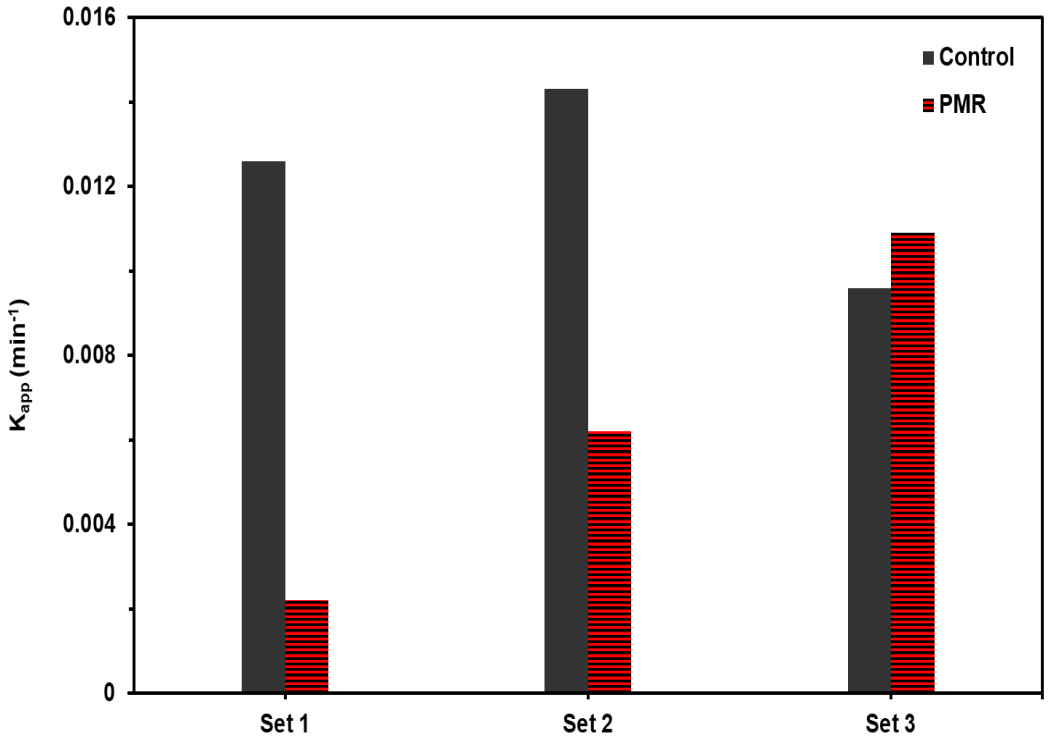

Fig. 7.21: Comparison of K_{app} between control photocatalysis and batch PMR mode of operation under the combined (POM-TiO_2) photocatalysts of Set, Set 2 and Set 3.

3) Mineralization

The performance of combined (POM-TiO_2) PMR based on the photocatalytic mineralization and intermediates formation under the synergistic effect conditions of Set 1, Set 2 and Set 3 was examined in Fig. 7.22 and Fig. 7.23, and compared with control photocatalysis. This photocatalytic mineralization was expressed by the TOC concentration in the retentate over a 180 min operating time. The presented results of control photocatalysis in these Figs. are only for comparison purposes.

For three investigated sets of combined (POM-TiO_2) photocatalysts in the retentate, it was found that the concentration of TOC (Fig. 7.22) in relation with formed VFAs (Fig. 7.23) increased significantly with increasing the operating time when compared with control photocatalysis. Similarly, the higher rejections of the membrane at Set 1, Set 2 and Set 3 for TOC (Fig. 7.22) and formed VFAs (Fig. 7.23) were found to be 98, 96, 95% and 92, 89 and 85% respectively. These findings are in agreement with that obtained earlier by POM homogeneous PMR (chapter 5) and TiO_2 heterogeneous PMR (chapter 6), so the reasons behand these results are not explained here.

It can be concluded that the membrane could not enhance the mineralization of PEG and consequently, the mineralization of PEG cannot be considered as an evaluating parameter for further investigation.

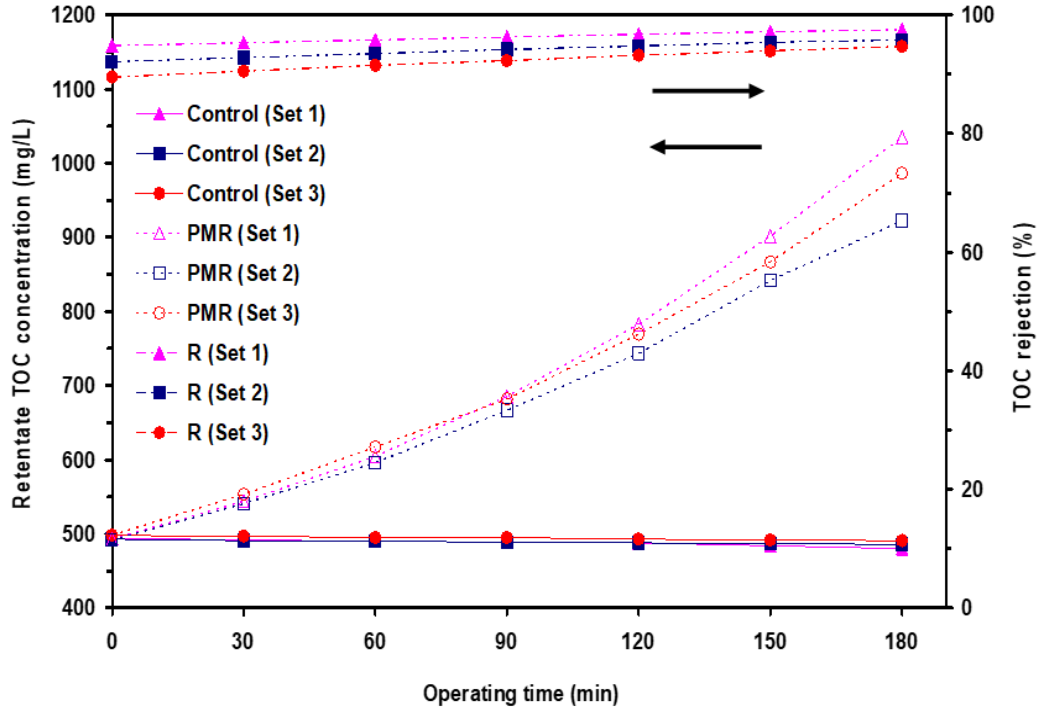

Fig. 7.22: Comparative performance of TOC concentration between control photocatalysis and batch PMR mode of operation at the combined (POM-TiO_2) photocatalysts of Set 1, Set 2 and Set 3.

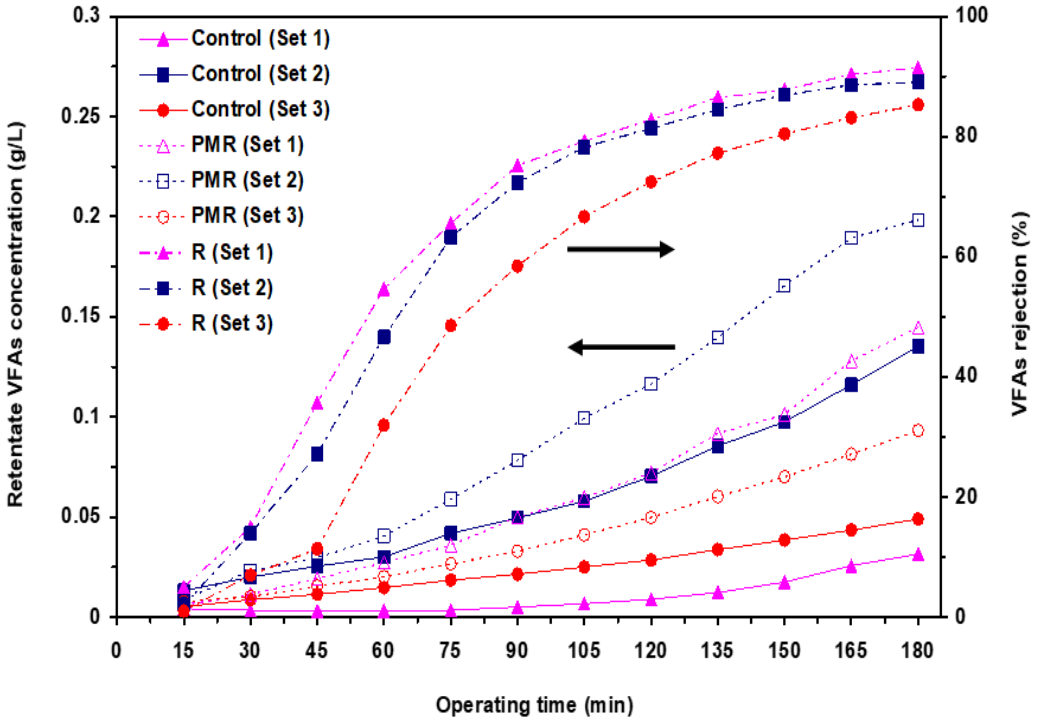

Fig. 7.23: Comparative performance of VFAs concentration between control photocatalysis and batch PMR mode of operation at the combined (POM-TiO_2) photocatalysts of Set 1, Set 2 and Set 3.

7.3.2 Continuous PMR operation (*Continuous photocatalysis*)

The aim of this work is to convert batch combined (POM-TiO_2) photocatalysis (control process-no membrane) to a continuous photocatalysis mode of operation by using PMR. *To achieve this*, a continuous fresh PEG feed was added to the BRS and the cross-flow PMR was continuously operated at the optimal synergistic effect conditions of combined (POM-TiO_2) photocatalysts of Set 2 (POM-0.125 gL^{-1} and TiO_2-0.25 gL^{-1}) for 12 h. The performance of continuous photocatalysis was evaluated according to the percent primary degradation, reaction kinetics and mineralization, and compared with batch control photocatalysis. *Note that, batch photocatalysis (no membrane), continuous photocatalysis (continuous PMR operation) and batch PMR operation are referred to as control, CPMR and BPMR respectively.*

In Fig. 7.24, the %PD of PEG under continuous photocatalysis decreased generally in comparison with batch photocatalysis. For example, at 3 and 12 h, it decreased significantly by 37 and 51% respectively. This decrease in the %PD of PEG could be explained by the dilution effect of continuous addition of fresh PEG feed to the original PEG reactant solution inside the BSR as shown earlier with more detail in chapter 3, section 3.4.4.

This dilution effect can be generally described in terms of permeate flux under BPMR and CPMR operations as shown in Fig. 7.25. It shows that the permeate flux under BPMR is higher that of CPMR, meaning that the constant rate of adding fresh PEG feed is higher than the rate of filtration by CPMR, and thus reducing the concentration of combined photocatalysts of POM and TiO_2 inside the BSR as shown in Fig. 7.24.

The presented results in Fig. 7.24 confirms this dilution effect where the concentration of POM and TiO_2 decreased by 78 and 62% respectively over the operating time of continuous photocatalysis. *As a result, significantly decreasing the overall photocatalytic degradation activity of PEG when compared with batch control photocatalysis.*

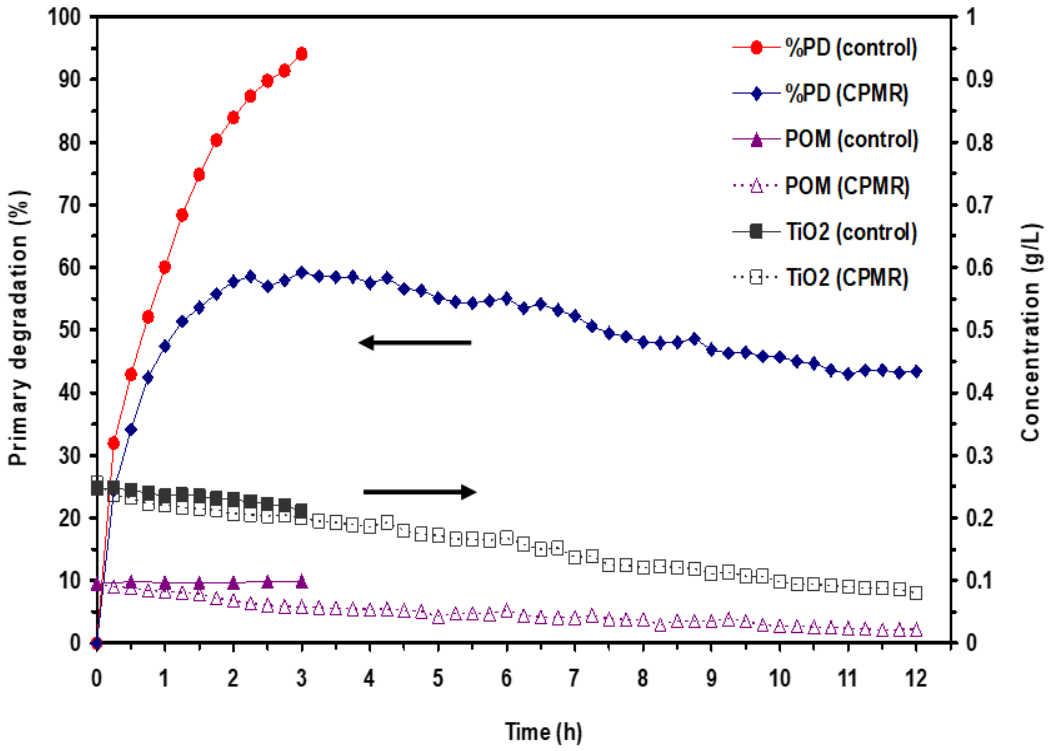

Fig. 7.24: Comparison of the %PD of PEG between batch photocatalysis and continuous photocatalysis using PMR under the optimal conditions of combined (POM-TiO_2) photocatalysts (Set 2).

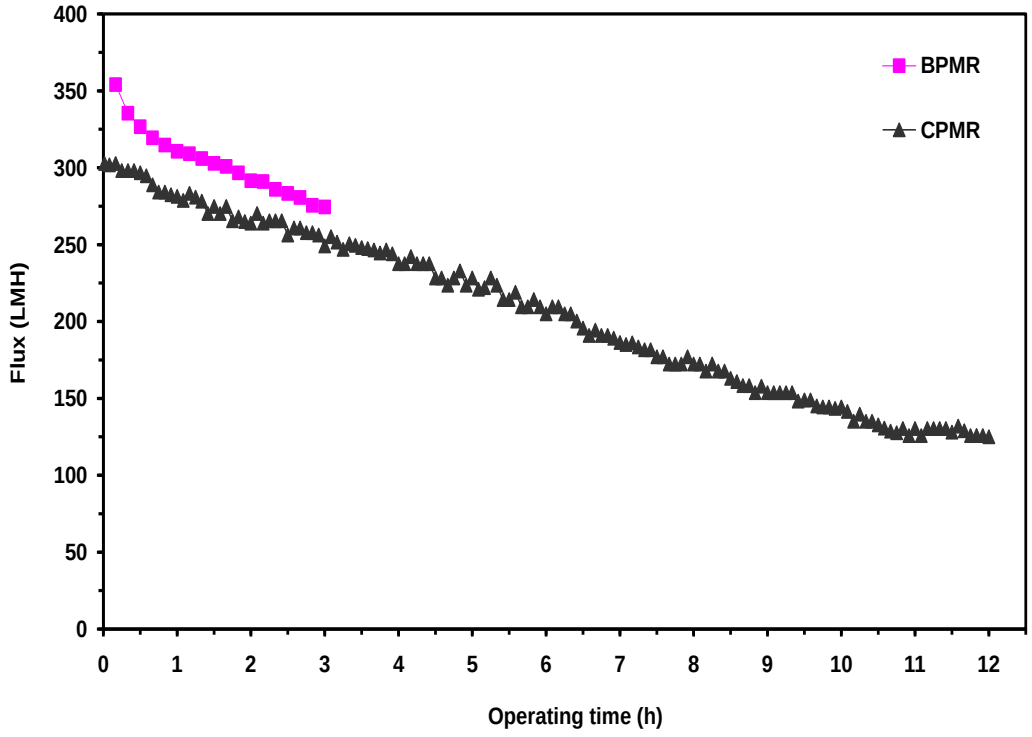

Fig. 7.25: Permeate flux as a function of operating time for batch and continuous PMR modes of operation under combined (POM-TiO_2) photocatalysts (Set 2).

Further investigation on the permeate flux under continuous photocatalysis for a 12 h operating time is shown in Fig. 7.25. The behavior of permeation flux was a sharp decline over 11 h of investigated time and then nearly stable. This behavior is attributed to the fouling in terms of the concentration polarization. The SEM images in Fig. 7.26 confirmed this fouling. It can be seen from Fig 7.26 (b-c) that there is a clear agglomeration effect. In literature, this agglomeration effect is due to particle-particle interactions **[161]**. In addition to particle-particle interactions, as explained earlier in section 7.3.1, 1 under the combined (POM-TiO_2) photocatalysts, there are two additional interactions in terms of solute-solute and solute-particle. These three types of interactions played a significant role in developing the concentration polarization layer in the form of agglomeration, and thus affecting the permeate flux to be sharp. The interesting point is that despite of this complex fouling in terms of three types of interactions, the used membrane showed a continuous ability to produce a higher rate of permeate flux until the end time of operation. Indicating that there is no complete pore blocking under this fouling condition.

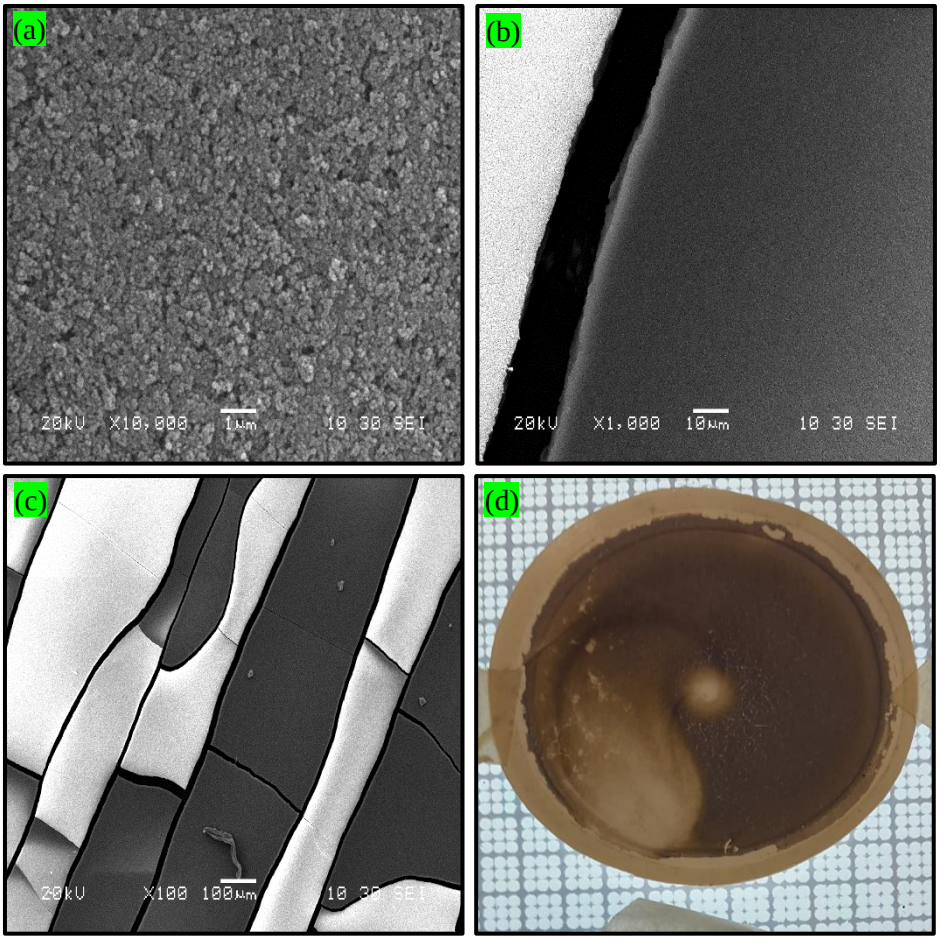

Fig. 7.26: SEM images (a-c) and a real photo (d) of the top surface of a fouled membrane with PEG and combined (PEG-TiO_2) photocatalysts with the optimal conditions (Set 2) under continuous photocatalysis, magnification: (a) x 10,000 and scale: 1 µm, (b) x 1,000 and scale: 10 µm and (c) x 100 and scale: 100 µm.

In terms of rejection, for a 12 h operating time, POM and TiO_2 photocatalysts were continuously rejected with 100% by the membrane.

In terms of PEG rejection, it was found that the trend of experimental rejection with total PEG and individual PEG oligomers under combined (POM-TiO_2) photocatalysts are in agreement with two proposed scenarios of POM continuous photocatalysis shown in chapter 5, section 5.4.2 where at 12 h, it was found that the total number of residual PEG oligomers was 6 oligomers within LO range of MW only under batch photocatalysis when comparing with 21 oligomers under continuous photocatalysis. Consequently, the total concentration of PEG was affected. This result was expected since batch photocatalysis showed higher %PD of PEG than continuous photocatalysis (Fig. 7.24).

The photocatalytic mineralization performance of combined (POM-TiO_2) photocatalysts in terms of TOC concentration in relation with VFAs formation between batch and continuous photocatalysis was examined in Fig. 7.27 and Fig. 7.28. The presented results of control photocatalysis in these Figs. are only for comparison purposes. This examination under continuous photocatalysis (Fig. 7.27) showed that the concentration of TOC and formation of VFAs in the retentate increased with increasing the operating time as compared to batch photocatalysis. This increase is expected for the possible reasons explained earlier in chapters (5 and 6) in terms of resistance of formed VFAs to total mineralization, the ability of these acids to adsorb on the formed cake layer that acts as secondary dynamic membrane to prevent partially passing them through the membrane. These possible reasons can be supported by rejection data of TOC and VFA formation as shown in Fig. 7.28. For TOC rejection, it was 96, 95 and 88 and 81% at 3, 6, 9 and 12 h operating times respectively, while for VFAs rejection was 88, 86, 61 and 50% respectively. It is interesting to note that the VFAs rejection at 9 and 12 h are low, indicating that these VFAs could successfully pass through the membrane to the permeate and their concentrations were found to be 0.2 and 0.3 gL^{-1} respectively.

In terms of monitoring the pH, Fig. 7.27 shows that initially the pH increased during 3 h operating time and then gradually decreased to be stable at 12 h. The pH result does not give an accurate indicator about the formation of these VFAs under the examined conditions of continuous photocatalysis, although a clear increase in these formed VFAs is shown in Fig. 7.27 and higher rejection in particular within 6 h as shown in Fig. 7.28. This is mainly due to the higher effect of dilution by adding fresh PEG feed to the original PEG reactant solution in the BSR (Fig. 7.25), affecting significantly the pH values during the reaction conditions.

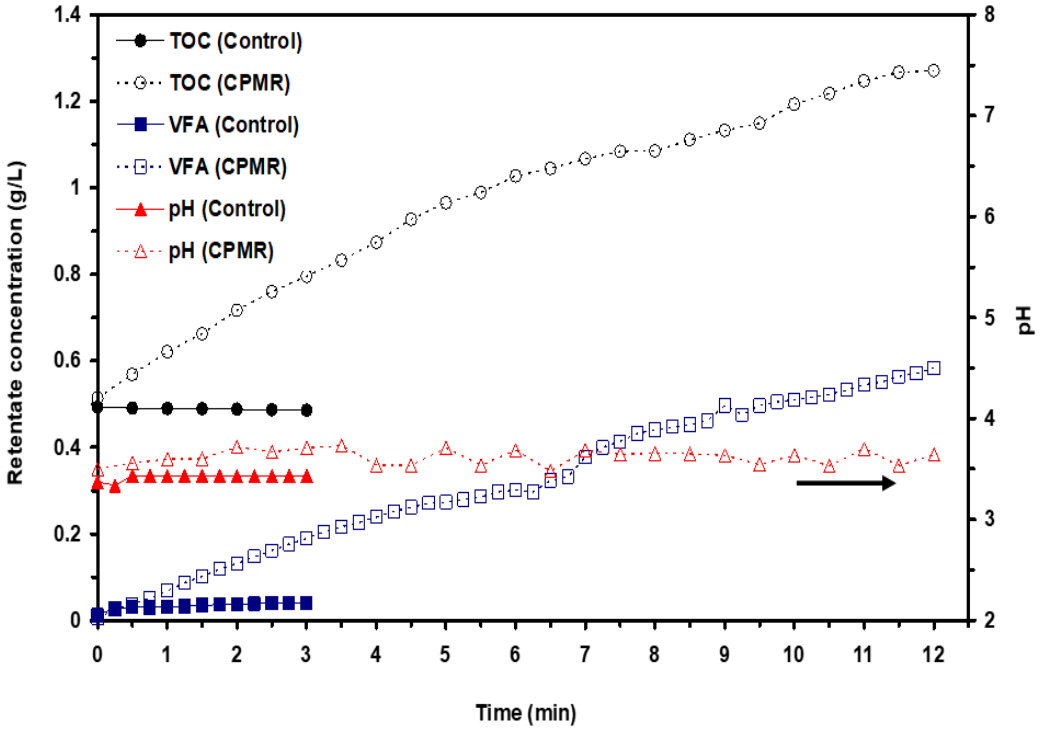

Fig. 7.27: Comparison of retentate concentration, intermediates formation and pH as function of operating time between batch photocatalysis and continuous photocatalysis under the optimal conditions of combined (POM-TiO_2) photocatalysts (Set 2).

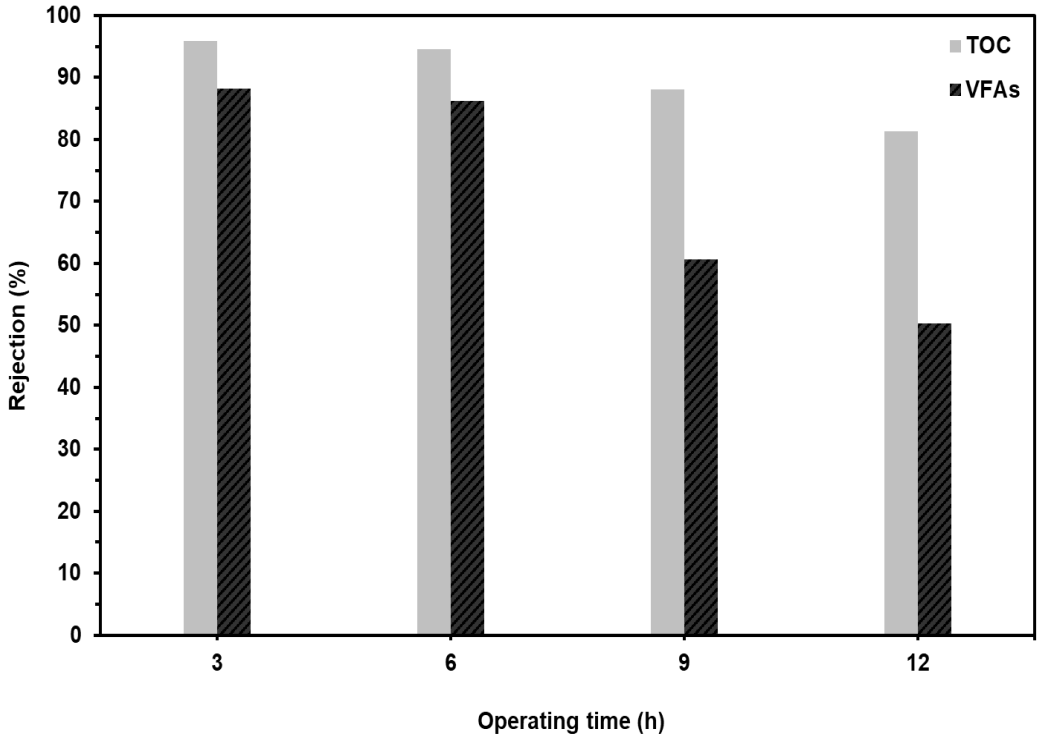

Fig. 7.28: Comparison of the rejection of TOC and VFAs between batch photocatalysis and continuous heterogeneous photocatalysis for various operating time intervals under the optimal conditions of combined (POM-TiO_2) photocatalysts (Set 2).

In terms of reaction kinetics, as explained earlier in chapter 5 for POM and chapter 6 for TiO_2, a series of three first order reaction kinetic models was proposed in Fig. 7.29 to describe the overall photocatalytic reaction data under continuous photocatalysis. The comparative performance based on K_{app} between control photocatalysis and continuous photocatalysis was investigated in Fig. 7.30.

Investigation of K_{app} for 3 h in Fig. 7.30 confirms that the values of K_{app} under continuous photocatalysis decreased significantly by 76% when compared with control photocatalysis. This finding is in agreement with that found in the %PD of PEG (Fig. 7.24). Further investigation of K_{app} for 12 h is shown in Fig. 7.29. The trend of these reaction constants represents the photocatalytic reaction mechanism of PEG under combined (POM-TiO_2) continuous photocatalysis where fast primary photocatalytic degradation of original PEG oligomers (region *a*), slower secondary photocatalytic degradation of reaction intermediate compounds (region *b*) and finally the photocatalytic degradation of these intermediates into complete mineralization (region *c*).

These results reflect the photocatalytic reaction pathway of PEG under continuous photocatalysis. However, the reaction of intermediate compounds like VFAs need to be accounted for the reaction kinetics of PEG. Therefore, a full kinetic analysis of these intermediate reactions will be part of future work.

Overall, the proposed combined (POM-TiO_2) cross-flow PMR could successfully convert batch photocatalysis to continuous process for a 12 h operating time with a comparable rate of the %PD of PEG and a complete rejection (100%) of both photocatalysts as well as a significant rate of permeate flux.

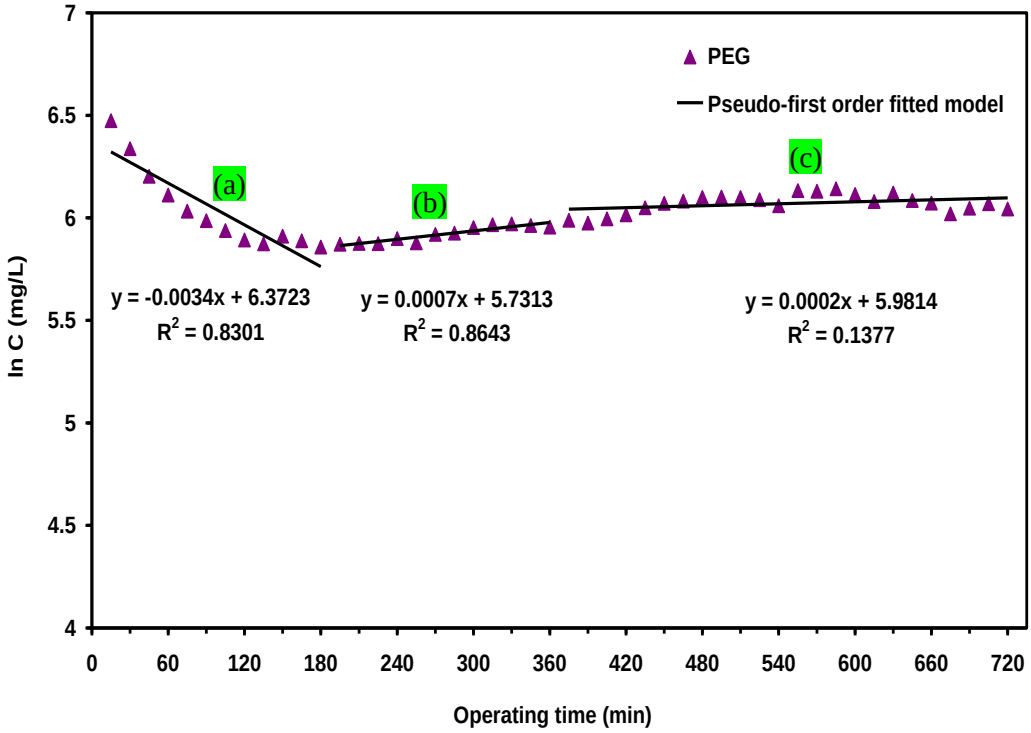

Fig. 7.29: Three stage pseudo-first order reaction constants plot for the photocatalytic degradation of PEG under combined (POM-TiO_2) continuous photocatalysis.

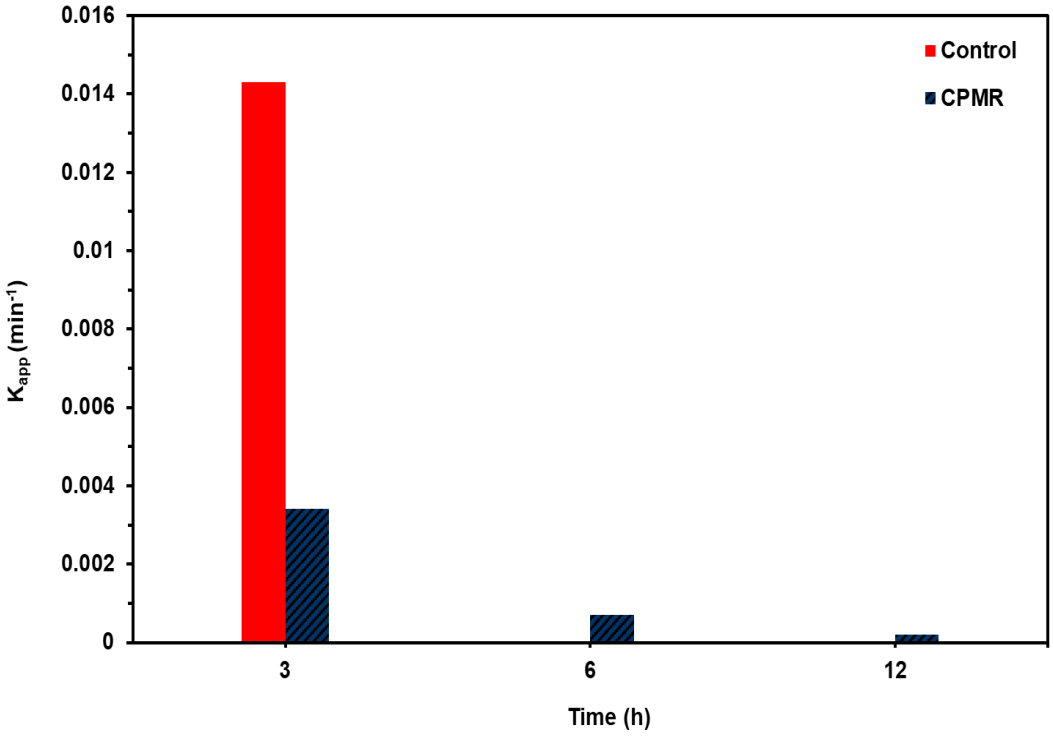

Fig. 7.30: Comparative performance of K_{app} between batch photocatalysis and continuous photocatalysis under the optimal conditions of combined (POM-TiO_2) photocatalysts (Set 2).

7.4 Chapter conclusions

The main aim of this chapter was to use and recycle the combined (POM-TiO_2) photocatalysts in a proposed PMR for the treatment of PEG. This chapter was achieved in two sections (7.2 and 7.3) and the following conclusions for each section were drawn:

1) Combined (POM-TiO_2) photocatalysis (no membrane)

- The concept of synergistic effect of combined (POM-TiO_2) photocatalysts was investigated based on two scenarios where the first scenario used POM as a primary photocatalyst and TiO_2 as a secondary photocatalyst while the second scenario used TiO_2 as a primary photocatalyst and POM as a secondary photocatalyst. Experimental results of the first scenario in terms of the %PD of PEG is higher than the second scenario. So, the first scenario was used in control photocatalysis and PMR experiments.

- Several experiments under Set 1 and Set 2 were carried out to identify the optimum loadings of synergistic effect of combined (POM-TiO_2) photocatalysts based on the %PD of PEG. The optimal loadings were found at Set 1 (POM-0.25 gL^{-1} and TiO_2-0.5 gL^{-1}) and Set 2 (POM-0.125 gL^{-1} and TiO_2-0.25 gL^{-1}). The experimental results at these optimal conditions were used as basis of control photocatalysis (*no membrane*) to be compared with proposed PMR.

- A simplified (L-H) kinetic model was successfully used to express the photocatalytic degradation data of PEG under control photocatalysis and also batch PMR operation. Reaction kinetics in terms of the obtained K_{app} gave further support to confirm the concept of synergistic combination of POM and TiO_2. This concept of synergistic effect of combined (POM-TiO_2) photocatalysts with their single photocatalysts was confirmed mathematically based on K_{app}.

2) Cross-flow combined (POM-TiO_2) photocatalytic membrane reactor

A. Batch PMR operation:

- The presence of POM (acidic in nature) played a substantial role in changing the pH of (PEG-TiO_2) solution, and then significantly decreasing the effect of adsorption on the TiO_2 concentration. The membrane separation process under combined (POM-TiO_2) PMR could effectively increase the concentration of POM and in particular TiO_2 inside the BSR and the in the photoreactor, thus the concept of membrane enhanced combined (POM-TiO_2) photocatalysis is feasible at the examined photocatalyst loadings of Set 3 (POM-0.03 gL^{-1} and TiO_2-0.03 gL^{-1}). While for the optimal conditions of Set 1 and Set 2, it was not feasible due to increasing the concentration of combined photocatalysts under PMR in the retentate to be higher than that of control photocatalysis, and thus decreasing the %PD of PEG due to light scattering effect.

- For POM and TiO_2 rejections, the PMR could successfully separate them with 100% from (PEG-POM-TiO_2) solution and recycle back into the photoreactor.
- For PEG rejection, the performance of combined (POM-TiO_2) PMR in terms of individual PEG oligomers and total PEG is similar to that of POM homogeneous PMR (chapter 5) where for individual PEG oligomers, the membrane could retain the lightly oxidized PEG oligomers with their MWs > MWCO and return them for further oxidation. While, the greatly oxidized PEG oligomers with their MWs < MWCO could not be predicated in the permeate based on the HPLC methodology and calibration. So, the calculation of true PEG rejection is not accurate.
- For mineralization, the cross-flow combined (POM-TiO_2) PMR could not enhance the photocatalytic mineralization of PEG due to the resistance of formed VFAs to total mineralization and also these VFAs could not considerably pass through the membrane to the permeate because of the effect of a secondary dynamic membrane by the adsorbed VFAs on the TiO_2 particles and on the surface of membrane.
- The permeate fluxes under the synergistic effect of Set 1, Set 2 and Set 3 are higher than that of their single photocatalysts. This is due to a complex physiochemical interactions based on particle-particle, solute-solute and solute-particle, affecting the development of concentration polarization layer and consequently the obtained permeate flux.

B. Continuous PMR operation:

- The proposed cross-flow combined (POM-TiO_2) PMR could successfully convert batch photocatalysis to continuous process for a 12 h operating time at comparable photocatalytic degradation efficiency of PEG to control photocatalysis under the optimal loadings of combined (POM-TiO_2) photocatalysts of Set 2 (POM-0.125 gL^{-1} and TiO_2-0.25 gL^{-1}).
- The membrane could completely reject the POM and TiO_2 photocatalysts and partially reject the identified lightly oxidized oligomers within low range of MWs as well as TOC in relation with formed VFAs. In spite of these rejections, a higher rate of permeate flux continued until the end of operation.
- Monitoring the pH could not gave an accurate indication about the formation of VFAs and the rejection of these acids due to the dilution effect by the continuous addition of fresh PEG feed.
- The overall photocatalytic reaction pathway of PEG under continuous photocatalysis for a 12 h operating time was represented well by three steps of first order reaction kinetic models. The obtained reaction rate constants reflected the photocatalytic reaction mechanism of PEG, which included fast photocatalytic degradation of original PEG oligomers, slower secondary degradation of intermediates and complete mineralization.

Chapter 8

Conclusions, Recommendation and Future Work

8.1 Conclusions

The aim of this thesis was to compare the use and recycle of POM homogeneous, TiO_2 heterogeneous and combined (POM-TiO_2) photocatalysts in a proposed cross-flow PMR for the treatment of PEG as a selected model of synthetic industrial wastewater. The proposed PMR was operated under batch and continuous modes of operation and its performance with these photocatalysts was assessed through the evaluating parameters including primary degradation, reaction kinetics and mineralization with control photocatalysis (*no membrane*) under the examined conditions.

This aim has been achieved in four separate chapters where detailed conclusions are given at the end of each experimental chapter, so this chapter aims to draw together the overall findings of this thesis and provide a general comparison in the performance of these photocatalysts under cross-flow PMR and then recommendations to further studies in this area.

The conclusions resulting from the experimental work are summarized into sections as follows:

8.1.1 Chromatographic method development for PEG oligomers separation and quantification

A RP-HPLC/ELSD method for the separation and quantification of PEG oligomers has been developed based on previous methods. This developed method achieved a high chromatographic resolution of individual PEG oligomers and, stable and straight baseline enabling to obtain an accurate peak area quantification. This method has significant advantages over all existing previously reported methods in the literature where it does not suffer from a non-linear baseline and/or poor peak resolution under different investigated conditions. Given these advantages, this developed method in the current project can now effectively replace the previously methods in the literature for PEG oligomers identification and quantitation.

8.1.2 Effect of POM loading, pH and oxidant on photocatalysis of PEG

1) Non-photocatalytic reaction of POM with PEG

POM homogenous photocatalyst had an ability to react with PEG oligomers under the conditions (*no UV and no control pH*) due to the mechanism of electron transfer reaction. Under controlling the pH using HCl conditions, for example at pH 1, this non-photocatalytic reaction increased significantly due to the presence of chloride ions, which could further increase the charge densities of POM in the form $[PW_{12}O_{40}]^{3-}$ anions, and thus accelerating the non-photocatalytic reaction of POM with PEG oligomers. On the other hand, this non-photocatalytic reaction was not affected under NaOH conditions (pH 3.3-5) based on the concentration of 23 identified oligomers, thus this range was used to investigate the POM homogeneous photocatalysis of PEG.

2) POM chemical stability

POM in the form $[PW_{12}O_{40}]^{3-}$ was not chemically stable under aqueous solution and PEG reactant solution for all examined conditions with and without controlling the pH. It decomposed partially into several lacunary species of *W*. This decomposition in terms of this form of POM and the total elemental concentration of POM based on *W* was significantly affected under the HCl conditions (pH 1), while it was not affected under the NaOH conditions (pH 3.3-5) and also the UV reaction conditions using *CCED*. Under these conditions, POM in the form $[PW_{12}O_{40}]^{3-}$ was still dominant among other identified lacunary species of *W* (oxidative species) and played a vital role in degrading photocatalytically the PEG oligomers.

3) Optimal operating parameters conditions

The optimal operating parameters based on a *CCED* investigated conditions were identified theoretically and confirmed experimentally to be POM loading (0.35 mM-1 gL^{-1}), pH (3.3) and oxidant (14 mgO_2L^{-1}). The pH and oxidant concentration showed a negative impact on photocatalytic degradation activity of PEG where the pH deprotonated the $HO^{\bullet}$ under NaOH conditions, while the oxidant caused in an inner filter effect and then reducing the UV light intensity. So, these parameters were not controlled in the POM homogeneous PMR work.

8.1.3 Separation of POM and TiO_2 (*no UV*)

Initially, dead-end membrane filtration process was used to examine the ability of membrane (NF270) to reject either POM or TiO_2 with PEG separately and together as feed without using UV light. The used membrane could completely separate POM and TiO_2 from PEG reactant solution. These very interesting results were therefore used as a successful choice for the proposed cross-flow PMR.

8.1.4 Batch PMR operation (*membrane enhanced photocatalysis*)

The principal aim of batch PMR operation was to validate if the concept *'membrane enhanced photocatalysis'* is feasible under POM homogeneous, TiO_2 heterogeneous and combined (POM-TiO_2) photocatalysts in a proposed cross-flow PMR. The performance of this PMR for 3 h operating time was assessed based on the following evaluating parameters and compared with control photocatalysis (no membrane).

1) Primary degradation

In terms of POM photocatalyst, the concept of membrane enhanced POM homogenous photocatalysis is feasible based on the evaluating parameters of the %PD of PEG at lower POM loadings of 0.25 and 0.50 gL^{-1}, which are below the optimal POM control loading of photocatalysis (0.75 gL^{-1}). The used membrane could successfully concentrate these lower concentrations of POM in the retentate and then in the photoreactor to be comparable to that of an optimal POM loading, and thus increasing the %PD of PEG. *This successful concept has a valuable advantage in terms of reducing the economical cost of the use of higher photocatalyst loading for the treatment of real industrial wastewater.*

In terms of TiO_2 photocatalyst, the concept of membrane enhanced TiO_2 heterogeneous is not feasible based on the above evaluating parameters at the investigated TiO_2 loadings of 0.125 and 0.25 gL^{-1}. This is because the membrane could not concentrate the TiO_2 inside the BSR where the tendency of TiO_2 particles to adsorb onto the surface of membrane increased with increasing the operating time, reducing the concentration of TiO_2 in the BSR and then in the photoreactor, and thus decreasing %PD of PEG. In order to decrease this tendency of TiO_2 adsorption, increasing the cross-flow velocity is potentially one solution for this and this point is considered in future work.

In terms of combined (POM-TiO_2) photocatalysts, the concept of membrane enhanced combined (POM-TiO_2) photocatalysis at their examined synergistic conditions is feasible at Set 3 (POM-0.03 gL^{-1} and TiO_2-0.03 gL^{-1}). The membrane could effectively increase the concentration of POM and in particular TiO_2 inside the BSR and then in the photoreactor because the presence of POM (acidic in nature) played a substantial role in changing the pH of (PEG-POM-TiO_2) solution and then significantly decreasing the effect of adsorption on the TiO_2 concentration inside the BSR, thus significantly increasing its concentration in the retentate.

2) Reaction kinetics

A simplified Langmuir-Hinshelwood (L-H) kinetic model in terms of K_{app} was successfully used to express the reaction kinetics of photocatalytic degradation data of PEG for batch PMR

operation compared with control photocatalysis for 3 h operating time. The general trend of reaction kinetics was similar to that obtained with the %PD of PEG under the same comparable conditions. So, reaction kinetics results gave further support to confirm that the proof of the investigated concept *'membrane enhanced photocatalysis'* is feasible.

3) Mineralization

The membrane enhanced photocatalytic mineralization of PEG (%TOC removal) for three investigated conditions (POM, TiO_2 and combined photocatalysts) is not feasible. This is due to the formation of a wide range of products including identified and unidentified VFAs as reaction intermediates, lightly oxidized PEG oligomers and oligomeric fractions like ethylene glycol during the photocatalytic reaction. These products expressed by the TOC concentration could not considerably pass through the membrane to the permeate because of the effect of a secondary dynamic membrane, and thus increasing the concentration of TOC in the retentate. This finding was supported by TOC rejection data. In addition, the formed VFAs were resistant to total mineralization. In the respect, further investigation is required to enhance this mineralization and will be part of future work.

8.1.5 Continuous PMR operation (*continuous photocatalysis*)

The proposed cross-flow PMR operation could successfully convert batch photocatalysis (control process-no membrane) to continuous process under the optimal loading of POM (0.75 gL^{-1}), TiO_2 (0.25 gL^{-1}) and combined (POM-TiO_2) photocatalysts of Set 2 (POM-0.125 gL^{-1} and TiO_2-0.25 gL^{-1}) for the end course of operation, 9 h (POM or TiO_2) and 12 h (combined photocatalysts). The performance of continuous photocatalysis was evaluated with the primary degradation, reaction kinetics and mineralization, and compared with batch photocatalysis. In addition, the rejection and flux under this evaluation were considered.

1) Primary degradation

The continuous photocatalysis showed a comparable photocatalytic degradation efficiency of PEG to control photocatalysis under all examined conditions. The general performance of this process was affected by a dilution effect of added fresh PEG feed to the original PEG reactant solution inside the BSR under POM and combined (POM-TiO_2) PMR modes of operation. This dilution effect played a significant role in reducing the concentration of POM for POM PMR and both POM and TiO_2 for combined (POM-TiO_2) PMR in the retentate and then in the photoreactor, thus affecting the %PD of PEG. While for TiO_2 continuous photocatalysis, the performance of this process was not affected by a dilation effect, it was significantly affected by the increase of tendency of TiO_2 to adsorb on the

surface of membrane with increasing the operating time and then reducing its concentration in the retentate and then in the photoreactor, consequently affecting the %PD of PEG.

Among these continuous processes, POM continuous photocatalysis showed the maximum %PD of PEG without supplying a continuous feed of DO in comparison with others. *This is very interesting performance in terms of economical point of view in real wastewater treatment applications.*

2) Reaction kinetics

Three steps of a simplified Langmuir-Hinshelwood (L-H) kinetic models based on K_{app} was proposed to represent the overall photocatalytic reaction pathway of PEG under continuous photocatalysis for the end course of operation. The obtained reaction rate constants reflected the photocatalytic reaction mechanism of PEG, which included fast photocatalytic degradation of original PEG oligomers, slower secondary degradation of intermediates and complete mineralization.

The general trend of reaction kinetics in terms of K_{app} under batch and continuous photocatalysis for 3 h of operating time is similar to that obtained with the %PD of PEG under the same comparable conditions. So, reaction kinetics results gave further support to confirm these photocatalytic degradation results.

3) Mineralization

The photocatalytic mineralization performance of PEG for three investigated continuous photocatalysis (continuous PMR operation) was found to be similar to that of batch PMR operation explained above. To improve this limited mineralization, this is considered in future work.

4) Rejection

In terms of photocatalyst rejection, the used membrane could successfully reject POM, TiO_2 and combined (POM-TiO_2) photocatalysts with 100% for the end course of operation.

In terms of PEG rejection, for POM and combined (POM-TiO_2) photocatalysts, it was found that the concentration of each individual PEG oligomer in the permeate was less than the MIDL of HPLC methodology and calibration, so the calculation of true rejection of PEG is not accurate. While for TiO_2, the same identified MW oligomers were found in the permeate and retentate, and thus the true individual oligomer rejection cannot be valid under these conditions (*this MW identification will be part of future work*). However, in terms of total PEG, it was 33%.

In terms of TOC rejection, the general TOC rejection of POM and combined (POM-TiO_2) continuous photocatalysis for 9 h is similar and higher than that of TiO_2 continuous photocatalysis as shown in Fig. F1 (*Appendix F*). This higher rejection for POM and combined (POM-TiO_2)

photocatalysts indicates that the used membrane could reject a wide range of products including reaction intermediates (identified and unidentified VFAs), lightly oxidized PEG oligomers and oligomeric fractions during the photocatalytic reaction. On the other hand, for TiO_2 rejection, this lower rejection was expected since the individual greatly oxidized PEG oligomers with MWs less than the MWCO of used membrane could pass through the membrane to the permeate and then increasing the TOC concentration, thus reducing the TOC rejection. Further investigation relating to identification of the above products is required and will be part of future work.

In terms of VFAs rejection, the general VFAs rejection of combined (POM-TiO_2) continuous photocatalysis for 9 h is lower than that of POM and TiO_2 continuous photocatalysis as shown in Fig. F1 (*Appendix F*). This lower VFAs rejection for combined (POM-TiO_2) photocatalysts can be attributed to the effect of interfacial interactions of three groups including *'particle-particle'* interactions, *'solute-solute'* interactions and *'solute-particle'* interactions, which played a significant role in developing the concentration polarization layer, and thus permitting these acids to pass through membrane to the permeate and then reducing their rejection to be 61% at 9 h and 50% at 12 h corresponding to their concentration in the permeate to be 0.2 and 0.3 gL^{-1} respectively. *This is very interesting result where these acids are readily biodegradable in either aerobic or anaerobic treatment. It is expected that there is the other unidentified VFAs and thus increasing their concentration in the permeate, further identification of these acids will be part of future work.*

5) Flux

Despite the complete rejection of POM, TiO_2 and combined photocatalysts under continuous photocatalysis, the used membrane (NF270) showed a continuous ability to produce good permeate flux until the end of operation. The general comparison of the permeate flux and permeate volume obtained under continuous photocatalysis for 9 h is shown in Fig. F2 and Fig. F3 respectively (*Appendix F*) and found to be in the following order: combined (POM-TiO_2) > POM > TiO_2. This is attributed to the mechanism of fouling formed under the examined photocatalyst conditions. *The understanding of the fouling mechanism under these conditions will be part of future work.*

This finding in terms membrane flux (POM > TiO_2) proved our expectation (as explained in chapter 1) that POM as homogeneous photocatyst will not foul the membrane to the same extent as compared with TiO_2 heterogeneous photocatalyst, and thus overcoming a reduction in membrane flux and flow throughput.

8.1.6 POM-homogenous vs TiO_2-heterogeneous photocatalysis of PEG

The optimal photocatalytic loadings of POM and TiO_2 photocatalysts were found to be 0.75 and 0.25 gL^{-1}. This give a clear indication that POM homogeneous photocatalyst did not suffer from the effect of light scattering to the same extent as TiO_2 benchmark heterogeneous photocatalyst. Thus, POM can absorb high quantities of UV light, enhancing significantly its photocatalytic activity in the degradation of PEG. The general comparison in terms of %PD of PEG between them is shown in Fig. F4 (*Appendix F*) where it shows that the %PD of PEG for POM (95%) and TiO_2 (63%) based on the total concentration of PEG at 180 min. While for the three selected PEG oligomers, it was found that the %PD of LO, MO and HO for POM was > (84, 86 and 88%) respectively at photocatalytic reaction times (135, 105 and 90 min) respectively since their concentrations would be less than the MIDL of HPLC methodology and calibration. For TiO_2, they were 57, 65 and 73% respectively at 180 min. These results gave evidence that POM is more active than TiO_2 where it could effectively degrade all identified PEG oligomers ranging from LO to HO before 180 min. On the other hand, TiO_2 could not degrade them to be less than the MIDL of HPLC methodology and calibration within 180 min.

The general trend in terms of reaction kinetics (K_{app}) under POM and TiO_2 photocatalysts was similar to that of primary degradation (%PD) of PEG at their optimal loadings as shown in Fig. F5 (*Appendix F*) where it was found that the values of K_{app} for POM and TiO_2 were 0.0188 and 0.0043 min^{-1} respectively. These results gave further support to POM as homogenous photocatalyst is better than TiO_2 heterogeneous photocatalyst of PEG.

Both photocatalysts showed a limited photocatalytic mineralization of PEG (< 3% TOC removal).

8.2 Recommendation

There are a number of general limitations in the current project that should be considered in future work, which can be summarized below:

- A used damper component (Fig. 3.4) should be changed to ensure that it produces a stable pressure and then avoiding the inner filter effect.
- A pump 2 should be replaced by another type that can supply a wide range of hydrodynamic conditions (TMP and CFV) more than that of investigated in the current project. These conditions play a significant role in affecting the efficiency of separation and the quality of permeate.
- A fresh PEG feed should be added at equal rate of the permeate (weight basis) using a computerized feeding system connected with the digital mass balance, which was used to record the weight of permeate.

8.3 Future work

This thesis has presented a range of investigations into comparing the use and recycle of POM homogeneous, TiO_2 heterogeneous and combined (POM-TiO_2) photocatalysts in the proposed cross-flow PMR for the treatment of PEG under batch and continuous modes of operation. This section presents a number of suggestions for future work stemming from the investigations conducted. These suggestions are outlines below:

1) Only one membrane (NF270) was used in the current project. It has shown a superior performance in separating and recycling the POM homogeneous and TiO_2 heterogeneous photocatalysts with the complete rejection under all examined PMR conditions. It is suggested to use other types of membranes such as NF90, NP030 and DS-5DK, which are within NF range **[116]** for examining their ability in terms of the rejection of POM with PEG oligomers and flux, and comparing with that of NF270.

2) One type of POM ($H_3PW_{12}O_{40}$) was investigated in the proposed cross-flow PMR operation. An extent range of POMs can be investigated to extend the knowledge and real application of POMs in the field of industrial wastewater.

3) One type of PEG (PEG1500) was investigated in the current project. Different types of PEGs can be investigated to facilitate easy benchmarking to real industrial wastewater containing soluble polymers with similar properties.

4) In spite of the complete rejection of POM in the form $[PW_{12}O_{40}]^{3-}$ under batch and continuous PMR modes of operation, further investigation is required to identify the types of lacunary species of POM and measure their concentration in the permeate and retentate since these species are oxidative agents and play a significant role in degrading photocatalytically the PEG oligomers.

5) This project does not address the fate of MW of each PEG oligomer during photocatalytic reactions since this is beyond the scope of the work. The identification of MW for each PEG oligomer plays a significant role in understanding the performance of separation process under photocatalytic reaction conditions by knowing the greatly oxidized oligomers passing through the membrane and lightly oxidized oligomers rejecting by the membrane based on the MWCO mechanism. Thus, enabling to calculate the true rejection of individual PEG oligomers. This can be achieved by using a MALDI TOF as explained earlier in chapter 3, 3.2.2.

6) The understanding of fouling mechanism by reaction of photocatalyst with membrane under PMRs system is not obviously understood as reported in literature **[161]**. However,

understanding the detailed mechanism of membrane defouling can assist the timely cleaning of the membrane and improve the membrane long-term performance.

7) The fate of formation of a wide range of products such as unidentified VFAs as reaction intermediates and polymeric fractions like ethylene glycol during the photocatalytic reactions was beyond the scope of the current project. These products should be identified and quantified to give insight with particular emphases into understanding the photocatalytic degradation conditions of these products under PMR operation. This will help in particular to understand why the TOC increased in the retentate with increasing the operating time. After doing this, one way can be a promising solution to optimize the hydrodynamic conditions in terms of TMP and CFV membrane operating conditions to be higher than that of investigated in the current project (25 bar and 1.3 cms^{-1}), potentially overcoming the secondary dynamic effect and then these formed products may pass through the membrane to the permeate. Another way can be found in the next point (8).

8) The total mineralization of PEG, a complete conversion into CO_2 and water-usually the rate-limiting step for TOC in AOPs **[6, 10, 241]**, does not the aim of the current work, a partial mineralization to more biodegradable compounds is. Experimental results confirmed this and put the project in a good position to understand what reaction intermediate compounds are generated since these intermediates like VFAs are resistant to total mineralization. To enhance this mineralization, adding conventional oxidant like H_2O_2 can increase the rate of $HO^{\bullet}$ generation, hence further enhancing the photocatalytic mineralization of PEG.

9) A full kinetic analysis of formed VFAs as reaction intermediate compounds needs to be accounted for the reaction kinetics of PEG to gain an understanding of the photocatalytic degradation of these intermediates under different conditions.

10) A non-photocatalytic reaction of TiO_2 with PEG oligomers was experimentally confirmed as explained in chapter 6, section 6.3.1.1. Further investigation is required to know the main reasons behand this.

11) The concept *'membrane enhanced TiO_2 heterogeneous'* is not feasible under batch PMR operation because the tendency of TiO_2 particles to adsorb onto the surface of membrane increased with increasing the operating time, thus reducing the concentration of TiO_2 in the photoreactor and then decreasing the %PD of PEG. Further investigation is required in terms of increasing the CFV to be higher that of investigated (1.3 cms^{-1}), potentially overcoming this adsorption effect by dislodging the TiO_2 particles from the surface of membrane to the retentate, and thus the membrane may concentrate the TiO_2 concentration and then enhance the photocatalytic degradation of PEG.

8.4 Final Remarks

POM homogeneous photocatalysis is still facing a major barrier to be a promising process in the real applications of industrial wastewater treatment due to the difficulty in separation and recycle of POM photocatalyst. *In the current project*, the preceding results and discussion point to a promising solution in this regard by which the proposed approach of cross-flow PMR under batch and continuous modes of operation could successfully separate and recycle the POM with PEG reactant solution. This successful achievement will make homogeneous photocatalysis using various types of POMs a suitable method for environmental applications and allow to extend the real applications of POMs in the field of industrial wastewater treatment. Therefore, it is recommended from now on to consider the proposed *'POM homogeneous cross-flow PMR'* to be a *'novel approach'* and utilize it as an essential addition to the industrial wastewater treatment toolbox for environmental applications.

The results obtained from this thesis have shown that POM, TiO_2 and combined (POM- TiO_2) PMR under continuous modes of operation are to be an effective process for the degradation of PEG and can be used as a pretreatment step before using conventional biological treatment systems. These results will be useful to facilitate easy benchmarking to real industrial wastewater process scale-up containing soluble polymers with similar properties.

References

1. Herrmann, S., *New synthetic routes to polyoxometalate containing ionic liquids: an investigation of their properties*. 2015: Springer.

2. Ghafoori, S., M. Mehrvar, and P. Chan, *Kinetic study of photodegradation of water soluble polymers.* Iranian Polymer Journal, 2012. 21 (12): p. 869-876.

3. Awaleh, M.O. and Y.D. Soubaneh, *Waste water treatment in chemical industries: the concept and current technologies*. Hydrology: Current Research, 2014. 5 (1): p. 1.

4. Yang, Z.-Z., Q.-W. Song, and L.-N. He, *Capture and utilization of carbon dioxide with polyethylene glycol*. 2012: Springer Science & Business Media.

5. Chen, J., et al., *Polyethylene glycol and solutions of polyethylene glycol as green reaction media.* Green Chemistry, 2005. 7 (2): p. 64-82.

6. Mantzavinos, D., et al., *Wet air oxidation of polyethylene glycols; mechanisms, intermediates and implications for integrated chemical-biological wastewater treatment.* Chemical Engineering Science, 1996. 51 (18): p. 4219-4235.

7. Guo, X., D. Minakata, and J. Crittenden, *Computer-Based First-Principles Kinetic Monte Carlo Simulation of Polyethylene Glycol Degradation in Aqueous Phase UV/H_2O_2 Advanced Oxidation Process.* Environmental science & technology, 2014. 48 (18): p. 10813-10820.

8. Ghafoori, S., M. Mehrvar, and P.K. Chan, *Free-radical-induced degradation of aqueous polyethylene oxide by UV/H_2O_2: experimental design, reaction mechanisms, and kinetic modeling.* Industrial & Engineering Chemistry Research, 2012. 51 (46): p. 14980-14993.

9. Santos, L.C., et al., *The UV/H_2O_2-photodegradation of poly (ethyleneglycol) and model compounds.* Journal of the Brazilian Chemical Society, 2009. 20 (8): p. 1467-1472.

10. Mantzavinos, D., et al., *Catalytic wet air oxidation of polyethylene glycol.* Applied Catalysis B: Environmental, 1996. 11 (1): p. 99-119.

11. Swift, G., *Requirements for biodegradable water-soluble polymers.* Polymer degradation and stability, 1998. 59 (1-3): p. 19-24.

12. Glastrup, J., *Degradation of polyethylene glycol. A study of the reaction mechanism in a model molecule: tetraethylene glycol.* Polymer Degradation and Stability, 1996. 52 (3): p. 217-222.

13. Mantzavinos, D., et al., *Assessment of partial treatment of polyethylene glycol wastewaters by wet air oxidation.* Water Research, 2000. 34 (5): p. 1620-1628.

14. Giroto, J.A., et al., *Degradation of poly (ethylene glycol) in aqueous solution by photo-Fenton and H_2O_2/UV processes.* Industrial & Engineering Chemistry Research, 2010. 49 (7): p. 3200-3206.

15. Chang, C., et al., *Kinetics of decomposition of polyethylene glycol in electroplating solution by ozonation with UV radiation.* Journal of Environmental Engineering, 2001. 127 (10): p. 908-915.

16. Akpan, U. and B. Hameed, *Parameters affecting the photocatalytic degradation of dyes using TiO_2-based photocatalysts: a review.* Journal of hazardous materials, 2009. 170 (2): p. 520-529.

17. Tang, W.Z., *Physicochemical treatment of hazardous wastes*. 2016: CRC Press.

18. Ahmed, S., et al., *Influence of parameters on the heterogeneous photocatalytic degradation of pesticides and phenolic contaminants in wastewater: a short review.* Journal of Environmental Management, 2011. 92 (3): p. 311-330.

19. Sheidaei, B. and M.A. Behnajady, *Determination of optimum conditions for removal of Acid Orange 7 in batch-recirculated photoreactor with immobilized TiO_2-P25 nanoparticles by Taguchi method.* Desalination and Water Treatment, 2015. 56 (9): p. 2417-2424.

20. Ling, C.M., A.R. Mohamed, and S. Bhatia, *Photodegradation of methylene blue dye in aqueous stream using immobilized TiO_2 film catalyst: synthesis, characterization and activity studies.* Jurnal Teknologi, 2004. 40: p. 91-103.

21. Hiskia, A., et al., *Polyoxometallate photocatalysis for decontaminating the aquatic environment from organic and inorganic pollutants.* International Journal of Environmental Analytical Chemistry, 2006. 86 (3-4): p. 233-242.

22. Streb, C., *New trends in polyoxometalate photoredox chemistry: From photosensitisation to water oxidation catalysis.* Dalton Transactions, 2012. 41 (6): p. 1651-1659.

23. ZHONG, J.B., *Photocatalytic Decolorization of Methyl Orange Solution with Phosphotungstic Acid.* 2013.

24. Troupis, A., et al., *Photocatalytic reductive destruction of azo dyes by polyoxometallates: Naphthol blue black.* Journal of Photochemistry and Photobiology A: Chemistry, 2007. 188 (2): p. 272-278.

25. Hu, M. and Y. Xu, *Photocatalytic degradation of textile dye X3B by heteropolyoxometalate acids.* Chemosphere, 2004. 54 (3): p. 431-434.

26. Hiskia, A., et al., *Photocatalytic mineralization of chlorinated organic pollutants in water by polyoxometallates. Determination of intermediates and final degradation products.* Research on Chemical Intermediates, 2000. 26 (3): p. 235-251.

27. Kormali, P., et al., *Photocatalysis by polyoxometallates and TiO_2: A comparative study.* Catalysis Today, 2007. 124 (3): p. 149-155.

28. Chen, L. and B. Bai, *Facile preparation of phosphotungstic acid-impregnated yeast hybrid microspheres and their photocatalytic performance for decolorization of azo dye.* International Journal of Photoenergy, 2013. 2013.

29. Troupis, A., et al., *Photocatalytic reductive–oxidative degradation of Acid Orange 7 by polyoxometalates.* Applied Catalysis B: Environmental, 2009. 86 (1): p. 98-107.

30. Yang, H., et al., *A water-insoluble and visible light induced polyoxometalate-based photocatalyst.* Chemical Communications, 2010. 46 (14): p. 2429-2431.

31. Sivakumar, R., J. Thomas, and M. Yoon, *Polyoxometalate-based molecular/nano composites: Advances in environmental remediation by photocatalysis and biomimetic approaches to solar energy conversion.* Journal of Photochemistry and Photobiology C: Photochemistry Reviews, 2012. 13 (4): p. 277-298.

32. Li, D., et al., *Accelerated photobleaching of Orange II on novel ($H_5FeW_{12}O_{40}10H_2O$)/silica structured fabrics.* Water research, 2004. 38 (16): p. 3541-3550.

33. Zhao, X., et al., *Polyoxometalate-Based Metal–Organic Frameworks as Visible-Light-Induced Photocatalysts.* Inorganic chemistry, 2018. 57 (9): p. 5030-5037.

34. Patel, A. and S. Pathan, *Polyoxomolybdates as Green Catalysts for Aerobic Oxidation*. 2014: Springer.

35. Wen, L.-y., S.-k. Shen, and E.-z. Min, *Physicochemical and catalytic properties of 12-phosphotungstic acid supported on different silica.* Chinese Journal of Catalysis, 2000. 21 (6): p. 524-528.

36. Gao, F., J. Sun, and S. Zhong, *Synthesis and characterization of heteropoly acid catalyst supported on carbonized resin.* Chinese Journal of Catalysis, 1998. 19: p. 190-190.

37. Obalı, Z. and T. Doğu, *Activated carbon–tungstophosphoric acid catalysts for the synthesis of tert-amyl ethyl ether (TAEE).* Chemical Engineering Journal, 2008. 138 (1-3): p. 548-555.

38. Yajun, W., L. Kecheng, and F. Changgen, *Photocatalytic degradation of methyl orange by polyoxometalates supported on yttrium-doped TiO_2.* Journal of Rare Earths, 2011. 29 (9): p. 866-871.

39. Xu, L., et al., *Photocatalytic degradation of atrazine by $H_3PW_{12}O_{40}$/Ag–TiO_2: Kinetics, mechanism and degradation pathways.* Chemical Engineering Journal, 2013. 232: p. 174-182.

40. Janssen, M., C. Mueller, and D. Vogt, *Recent advances in the recycling of homogeneous catalysts using membrane separation.* Green Chemistry, 2011. 13 (9): p. 2247-2257.

41. Ameta, R., et al., *Advanced oxidation processes: basics and applications.* Wastewater Treatment: Advanced Processes and Technologies, 2012: p. 61.

42. Metcalf, E. and H. Eddy, *Wastewater engineering: treatment and reuse. Wastewater Engineering, Treatment, Disposal and Reuse. Techobanoglous G, Burton FL, Stensel HD*. 2003, Tata McGraw-Hill Publishing Company Limited, 4th edition. New Delhi, India.

43. Pera-Titus, M., et al., *Degradation of chlorophenols by means of advanced oxidation processes: a general review.* Applied Catalysis B: Environmental, 2004. 47 (4): p. 219-256.

44. Yonar, T., *Decolorisation of textile dyeing effluents using advanced oxidation processes*, in *Advances in Treating Textile Effluent*. 2011, InTech.

45. Sirés, I., et al., *Electrochemical advanced oxidation processes: today and tomorrow. A review.* Environmental Science and Pollution Research, 2014. 21 (14): p. 8336-8367.

46. Gogate, P.R. and A.B. Pandit, *A review of imperative technologies for wastewater treatment I: oxidation technologies at ambient conditions.* Advances in Environmental Research, 2004. 8 (3-4): p. 501-551.

47. Ikehata, K. and M.G. El-Din, *Aqueous pesticide degradation by hydrogen peroxide/ultraviolet irradiation and Fenton-type advanced oxidation processes: a review.* Journal of Environmental Engineering and Science, 2006. 5 (2): p. 81-135.

48. Neyens, E. and J. Baeyens, *A review of classic Fenton's peroxidation as an advanced oxidation technique.* Journal of Hazardous materials, 2003. 98 (1-3): p. 33-50.

49. Chiron, S., et al., *Pesticide chemical oxidation: state-of-the-art.* Water Research, 2000. 34 (2): p. 366-377.

50. Mantzavinos, D., et al., *Partial wet oxidation of p-coumaric acid: oxidation intermediates, reaction pathways and implications for wastewater treatment.* Water research, 1996. 30 (12): p. 2969-2976.

51. Mantzavinos, D. and E. Psillakis, *Enhancement of biodegradability of industrial wastewaters by chemical oxidation pre-treatment.* Journal of Chemical Technology and Biotechnology, 2004. 79 (5): p. 431-454.

52. Andreozzi, R., et al., *Advanced oxidation processes (AOP) for water purification and recovery*. Catalysis today, 1999. 53 (1): p. 51-59.

53. Ribeiro, A.R., et al., *An overview on the advanced oxidation processes applied for the treatment of water pollutants defined in the recently launched Directive 2013/39/EU.* Environment international, 2015. 75: p. 33-51.

54. Segneanu, A.E., et al., *Waste water treatment methods*, in *Water Treatment*. 2013, Intech.

55. Moyer, E. and P.T. Kostecki, *MTBE remediation handbook*. 2004: Springer Science & Business Media.

56. Legrini, O., E. Oliveros, and A. Braun, *Photochemical processes for water treatment.* Chemical reviews, 1993. 93 (2): p. 671-698.

57. Beltran, F.J., *Ozone reaction kinetics for water and wastewater systems*. 2003: crc Press.

58. Asghar, A., A.A.A. Raman, and W.M.A.W. Daud, *Advanced oxidation processes for in-situ production of hydrogen peroxide/hydroxyl radical for textile wastewater treatment: a review.* Journal of cleaner production, 2015. 87: p. 826-838.

59. Liang, C. and I.-L. Lee, *In situ iron activated persulfate oxidative fluid sparging treatment of TCE contamination—A proof of concept study.* Journal of contaminant hydrology, 2008. 100 (3-4): p. 91-100.

60. Munter, R., *Advanced oxidation processes–current status and prospects.* Proc. Estonian Acad. Sci. Chem, 2001. 50 (2): p. 59-80.

61. Alpatova, A., et al., *Treatment of oil sands process-affected water with ceramic ultrafiltration membrane: Effects of operating conditions on membrane performance.* Separation and Purification Technology, 2014. 122: p. 170-182.

62. Bandala, E.R. and B.W. Raichle, *Solar driven advanced oxidation processes for water decontamination and disinfection.* Solar Energy Sciences and Engineering Applications. CRC Press, EH Leiden, The Netherlands. Print ISBN, 2013: p. 978-1.

63. Muller, P., *Glossary of terms used in physical organic chemistry (IUPAC Recommendations 1994).* Pure and Applied Chemistry, 1994. 66 (5): p. 1077-1184.

64. Hussein, F.H., *Photochemical treatments of textile industries wastewater*, in *Advances in Treating Textile Effluent*. 2011, InTech.

65. Alvarez-Corena, J.R., J.A. Bergendahl, and F.L. Hart, *Advanced oxidation of five contaminants in water by UV/TiO_2: reaction kinetics and byproducts identification.* Journal of environmental management, 2016. 181: p. 544-551.

66. Rao, D.G., et al., *Wastewater treatment: advanced processes and technologies*. 2012: CRC Press.

67. Umar, M. and H.A. Aziz, *Photocatalytic degradation of organic pollutants in water*, in *Organic Pollutants-Monitoring, Risk and Treatment*. 2013, InTech.

68. Ibhadon, A. and P. Fitzpatrick, *Heterogeneous photocatalysis: recent advances and applications.* Catalysts, 2013. 3 (1): p. 189-218.

69. Loures, C.C., et al., *Advanced oxidative degradation processes: fundamentals and applications.* International Review of Chemical Engineering, 2013. 5 (2): p. 102-120.

70. Coronado, J.M., et al., *Design of advanced photocatalytic materials for energy and environmental applications*. 2013: Springer.

71. Zangeneh, H., et al., *Photocatalytic oxidation of organic dyes and pollutants in wastewater using different modified titanium dioxides: A comparative review.* Journal of Industrial and Engineering Chemistry, 2015. 26: p. 1-36.

72. Mozia, S., et al., *Immobilized TiO_2 for phenol degradation in a pilot-scale photocatalytic reactor*. Journal of Nanomaterials, 2012. 2012: p. 16.

73. Thakur, R.S., R. Chaudhary, and C. Singh, *Fundamentals and applications of the photocatalytic treatment for the removal of industrial organic pollutants and effects of operational parameters: a review.* Journal of Renewable and Sustainable Energy, 2010. 2 (4): p. 042701.

74. Dominguez, S., et al., *Influence of radiation and TiO_2 concentration on the hydroxyl radicals generation in a photocatalytic LED reactor. Application to dodecylbenzenesulfonate degradation.* Applied Catalysis B: Environmental, 2015. 178: p. 165-169.

75. Henderson, M.A., *A surface science perspective on TiO_2 photocatalysis.* Surface Science Reports, 2011. 66 (6-7): p. 185-297.

76. Ohama, Y. and D. Van Gemert, *Application of titanium dioxide photocatalysis to construction materials: state-of-the-art report of the RILEM Technical Committee 194-TDP*. Vol. 5. 2011: Springer Science & Business Media.

77. Ohtani, B., *Preparing articles on photocatalysis—beyond the illusions, misconceptions, and speculation.* Chemistry letters, 2008. 37 (3): p. 216-229.

78. Ohno, T., et al., *Morphology of a TiO_2 photocatalyst (Degussa, P-25) consisting of anatase and rutile crystalline phases.* Journal of Catalysis, 2001. 203 (1): p. 82-86.

79. Quiroz, M.A., E.R. Bandala, and C.A. Martínez-Huitle, *Advanced oxidation processes (AOPs) for removal of pesticides from aqueous media*, in *Pesticides-Formulations, effects, fate*. 2011, InTech.

80. Mills, A. and S. Le Hunte, *An overview of semiconductor photocatalysis.* Journal of photochemistry and photobiology A: Chemistry, 1997. 108 (1): p. 1-35.

81. Mozia, S., *Photocatalytic membrane reactors (PMRs) in water and wastewater treatment. A review.* Separation and Purification Technology, 2010. 73 (2): p. 71-91.

82. Chong, M.N., et al., *Recent developments in photocatalytic water treatment technology: a review.* Water research, 2010. 44 (10): p. 2997-3027.

83. Augugliaro, V., et al., *The combination of heterogeneous photocatalysis with chemical and physical operations: A tool for improving the photoprocess performance.* Journal of Photochemistry and Photobiology C: Photochemistry Reviews, 2006. 7 (4): p. 127-144.

84. Hoffmann, M.R., et al., *Environmental applications of semiconductor photocatalysis.* Chemical reviews, 1995. 95 (1): p. 69-96.

85. Lazar, M.A., S. Varghese, and S.S. Nair, *Photocatalytic water treatment by titanium dioxide: recent updates.* Catalysts, 2012. 2 (4): p. 572-601.

86. Zhang, Y., et al., *The influence of operating parameters on heterogeneous photocatalytic mineralization of phenol over $BiPO_4$.* Chemical Engineering Journal, 2014. 245: p. 117-123.

87. Subramonian, W. and T.Y. Wu, *Effect of enhancers and inhibitors on photocatalytic sunlight treatment of methylene blue.* Water, Air, & Soil Pollution, 2014. 225 (4): p. 1922.

88. Andersson, P.G., *Innovative Catalysis in Organic Synthesis: Oxidation, Hydrogenation, and CX Bond Forming Reactions*. 2012: John Wiley & Sons.

89. Papaconstantinou, E., *Photochemistry of polyoxometallates of molybdenum and tungsten and/or vanadium.* Chemical Society Reviews, 1989. 18: p. 1-31.

90. Putaj, P., *Applications of polyoxometalates in heterogenous catalysis*. 2012, Université Claude Bernard-Lyon I.

91. Murzin, D., *Engineering catalysis*. 2013: Walter de Gruyter.

92. Patel, A., et al., *Keggin-type lacunary and transition metal substituted polyoxometalates as heterogeneous catalysts: A recent progress.* Catalysis Reviews, 2016. 58 (3): p. 337-370.

93. Devassy, B.M., F. Lefebvre, and S. Halligudi, *Zirconia-supported 12-tungstophosphoric acid as a solid catalyst for the synthesis of linear alkyl benzenes.* Journal of Catalysis, 2005. 231 (1): p. 1-10.

94. Weinstock, I.A., *Homogeneous-phase electron-transfer reactions of polyoxometalates.* Chemical reviews, 1998. 98 (1): p. 113-170.

95. Zhu, Z., R. Tain, and C. Rhodes, *A study of the decomposition behaviour of 12-tungstophosphate heteropolyacid in solution.* Canadian journal of chemistry, 2003. 81 (10): p. 1044-1050.

96. Oyama, S.T., *Mechanisms in homogeneous and heterogeneous epoxidation catalysis*. Vol. 45. 2011: Elsevier.

97. Hiskia, A., et al., *Sonolytic, photolytic, and photocatalytic decomposition of atrazine in the presence of polyoxometalates.* Environmental science & technology, 2001. 35 (11): p. 2358-2364.

98. Kormali, P., et al., *Photolytic and photocatalytic decomposition of fenitrothion by $PW_{12}O_{40}^{3-}$ and TiO_2: a comparative study.* Applied Catalysis B: Environmental, 2004. 48 (3): p. 175-183.

99. Ozer, R.R. and J.L. Ferry, *Kinetic probes of the mechanism of polyoxometalate-mediated photocatalytic oxidation of chlorinated organics.* The Journal of Physical Chemistry B, 2000. 104(40): p. 9444-9448.

100. Antonaraki, S., et al., *Photolytic degradation of all chlorophenols with polyoxometallates and H_2O_2.* Journal of Photochemistry and Photobiology A: Chemistry, 2002. 148 (1): p. 191-197.

101. Androulaki, E., et al., *Light induced elimination of mono-and polychlorinated phenols from aqueous solutions by $PW_{12}O_{40}^{3-}$. The case of 2,4,6-trichlorophenol.* Environmental science & technology, 2000. 34 (10): p. 2024-2028.

102. Kim, S., H. Park, and W. Choi, *Comparative study of homogeneous and heterogeneous photocatalytic redox reactions: $PW_{12}O_{40}^{3-}$ vs TiO_2.* The Journal of Physical Chemistry B, 2004. 108 (20): p. 6402-6411.

103. Poblet, J.M., X. López, and C. Bo, *Ab initio and DFT modelling of complex materials: towards the understanding of electronic and magnetic properties of polyoxometalates.* Chemical Society Reviews, 2003. 32 (5): p. 297-308.

104. Li, H., et al., *Photoreduction of graphene oxide with polyoxometalate clusters and its enhanced saturable absorption.* Journal of colloid and interface science, 2014. 427: p. 25-28.

105. Hiskia, A., A. Mylonas, and E. Papaconstantinou, *Comparison of the photoredox properties of polyoxometallates and semiconducting particles.* Chemical Society Reviews, 2001. 30 (1): p. 62-69.

106. Qiu, W., Y. Zheng, and K.A. Haralampides, *Study on a novel POM-based magnetic photocatalyst: Photocatalytic degradation and magnetic separation.* Chemical Engineering Journal, 2007. 125 (3): p. 165-176.

107. Junbo, Z., et al., *Photocatalytic decolorization of methyl orange solution with potassium peroxydisulfate.* Central European Journal of Chemistry, 2008. 6 (2): p. 245-252.

108. Baker, R., *Ultrafiltration.* Membrane Technology and Applications, Third Edition, Chichester, UK.: John Wiley & Sons, Ltd, 2012.

109. Gutman, R., *Membrane filtration: the technology of pressure-driven crossflow processes*. 1987: Adam Hilger.

110. Van der Bruggen, B., et al., *A review of pressure-driven membrane processes in wastewater treatment and drinking water production.* Environmental progress, 2003. 22 (1): p. 46-56.

111. ROHANI, R., *Membrane separations: From purifications, minimisation, reuse and recycling to process intensification.* Chemical Processes for a Sustainable Future, 2014: p. 467.

112. Davis, M.L., *Water and wastewater engineering*. 2010: McGraw-Hill.

113. Pinnau, I. and B.D. Freeman, *Membrane formation and modification*. 2000: American Chemical Society.

114. Richardson, J.F. and J.H. Harker, *Chemical engineering-Volume 2: Particle Technology and Separation Processes*. 2002: Butterworth-Heinemann.

115. Pinnekamp, J. and H. Friedrich, *Membrane technology for waste water treatment*. 2006: FiW Verlag.

116. Dogan, E., *Investigation of ciprofloxacin removal from aqueous solution by nanofiltration process.* GLOBAL NEST JOURNAL, 2016. 18 (2): p. 291-308.

117. Nghiem, L.D., C. Espendiller, and G. Braun, *Influence of organic and colloidal fouling on the removal of sulphamethoxazole by nanofiltration membranes.* Water Science and Technology, 2008. 58 (1): p. 163-169.

118. Dolar, D., et al., *Effect of water matrices on removal of veterinary pharmaceuticals by nanofiltration and reverse osmosis membranes.* Journal of Environmental Sciences, 2011. 23 (8): p. 1299-1307.

119. Racar, M., et al., *Application of UF/NF/RO membranes for treatment and reuse of rendering plant wastewater.* Process Safety and Environmental Protection, 2017. 105: p. 386-392.

120. Mänttäri, M., T. Pekuri, and M. Nyström, *NF270, a new membrane having promising characteristics and being suitable for treatment of dilute effluents from the paper industry.* Journal of Membrane Science, 2004. 242 (1-2): p. 107-116.

121. Luo, J. and L. Ding, *Influence of pH on treatment of dairy wastewater by nanofiltration using shear-enhanced filtration system.* Desalination, 2011. 278 (1-3): p. 150-156.

122. Andrade, L., et al., *Nanofiltration and reverse osmosis applied to gold mining effluent treatment and reuse.* Brazilian Journal of Chemical Engineering, 2017. 34 (1): p. 93-107.

123. Wadekar, S.S., et al., *Laboratory and pilot-scale nanofiltration treatment of abandoned mine drainage for the recovery of products suitable for industrial reuse.* Industrial & Engineering Chemistry Research, 2017. 56 (25): p. 7355-7364.

124. Coskun, T., E. Debik, and N.M. Demir, *Treatment of olive mill wastewaters by nanofiltration and reverse osmosis membranes.* Desalination, 2010. 259 (1-3): p. 65-70.

125. Cheah, D., et al., *Performance of Nanofiltration Membrane for Printing Wastewater Treatment.* Journal of Applied Membrane Science & Technology, 2018. 22 (1).

126. Macedo, A.T.Z.N., J.M.O. Pulido, and R. Fragoso, *The Use and Performance of Nanofiltration Membranes for Agro-Industrial Effluents Purification*, in *Nanofiltration*. 2018, IntechOpen.

127. Haan, T.Y., et al., *Pilot-scale integrated pretreatment/membrane filtration system for aerobic palm oil Mill effluent (POME) treatment.* 1960.

128. Tan, Y., et al., *NANOFILTRATION OF AEROBICALLY-TREATED PALM OIL MILL EFFLUENT: CHARACTERIZATION OF THE SIZE OF COLOUR COMPOUNDS USING SYNTHETIC DYES AND POLYETHYLENE GLYCOLS.* Journal of Engineering Science and Technology, 2018. 13 (1): p. 1-10.

129. Greenlee, L.F., et al., *Reverse osmosis desalination: water sources, technology, and today's challenges.* Water research, 2009. 43 (9): p. 2317-2348.

130. Fritzmann, C., et al., *State-of-the-art of reverse osmosis desalination.* Desalination, 2007. 216 (1-3): p. 1-76.

131. Souza, V. and M. Quadri, *Organic-inorganic hybrid membranes in separation processes: a 10-year review.* Brazilian Journal of Chemical Engineering, 2013. 30 (4): p. 683-700.

132. Hsieh, H., *Inorganic membranes for separation and reaction*. Vol. 3. 1996: Elsevier.

133. Green, D., *Perry's Chemical Engineers' Handbook, Eighth*. McGraw-Hill Education.

134. Cheryan, M., *Ultrafiltration and microfiltration handbook*. 1998: CRC press.

135. Evans, P.J., et al., *The influence of hydrophobicity, roughness and charge upon ultrafiltration membranes for black tea liquor clarification.* Journal of Membrane Science, 2008. 313 (1-2): p. 250-262.

136. Makardij, A., X. Chen, and M. Farid, *Microfiltration and ultrafiltration of milk: some aspects of fouling and cleaning.* Food and bioproducts processing, 1999. 77 (2): p. 107-113.

137. Mulder, J., *Basic principles of membrane technology*. 2012: Springer Science & Business Media.

138. Huisman, I.H., et al., *Determining the zeta-potential of ceramic microfiltration membranes using the electroviscous effect.* Journal of membrane science, 1998. 147 (2): p. 187-194.

139. Williams, P.M., *Membrane Charge (Zeta Potential) Effect.* Encyclopedia of Membranes, 2016: p. 1-2.

140. Cheng, S., et al., *Positively charged nanofiltration membranes: review of current fabrication methods and introduction of a novel approach.* Advances in Colloid and Interface Science, 2011. 164 (1-2): p. 12-20.

141. Berg, J.M., et al., *The relationship between pH and zeta potential of∼ 30 nm metal oxide nanoparticle suspensions relevant to in vitro toxicological evaluations.* Nanotoxicology, 2009. 3 (4): p. 276-283.

142. Ortiz-Albo, P., et al., *Phenomenological prediction of desalination brines nanofiltration through the indirect determination of zeta potential.* Separation and Purification Technology, 2019. 210: p. 746-753.

143. Richardson, J. and J. Coulson, *Chemical Engineering: Particle Technology and Seraration Processes*. 2002: Elsevier Engineering Information, Incorporated.

144. Belfort, G., R.H. Davis, and A.L. Zydney, *The behavior of suspensions and macromolecular solutions in crossflow microfiltration.* Journal of Membrane Science, 1994. 96 (1-2): p. 1-58.

145. Zeman and A.L. Zydney, *Microfiltration and ultrafiltration: principles and applications*. 1996: CRC Press.

146. Wijmans, J.G. and R.W. Baker, *The solution-diffusion model: a review.* Journal of membrane science, 1995. 107 (1-2): p. 1-21.

147. Strathmann, H., L. Giorno, and E. Drioli, *Introduction to membrane science and technology*. Vol. 544. 2011: Wiley-VCH Weinheim.

148. Wijmans, J., *The role of permeant molar volume in the solution-diffusion model transport equations.* Journal of membrane science, 2004. 237 (1-2): p. 39-50.

149. Sarkar, S., A.K. SenGupta, and P. Prakash, *The Donnan membrane principle: opportunities for sustainable engineered processes and materials*. 2010, ACS Publications.

150. Schaep, J., et al., *Retention mechanisms in nanofiltration*, in *Chemistry for the Protection of the Environment 3*. 1998, Springer. p. 117-125.

151. Grandison, A.S., *Separation processes in the food and biotechnology industries*. 1996: CRC Press.

152. Cui, Z. and H. Muralidhara, *Membrane technology: a practical guide to membrane technology and applications in food and bioprocessing*. 2010: Elsevier.

153. Song, L. and M. Elimelech, *Theory of concentration polarization in crossflow filtration.* Journal of the Chemical Society, Faraday Transactions, 1995. 91 (19): p. 3389-3398.

154. Miranda, J.M. and J.B. Campos, *Concentration polarization in a membrane placed under an impinging jet confined by a conical wall—a numerical approach.* Journal of Membrane Science, 2001. 182 (1-2): p. 257-270.

155. Cui, Y., et al., *Catalytic water oxidation based on Ag (I)-substituted Keggin polyoxotungstophosphate.* Dalton Transactions, 2014. 43 (46): p. 17406-17415.

156. Bowen, W., J. Calvo, and A. Hernandez, *Steps of membrane blocking in flux decline during protein microfiltration.* Journal of Membrane Science, 1995. 101 (1-2): p. 153-165.

157. Mondal, S., C. Rai, and S. De, *Identification of fouling mechanism during ultrafiltration of stevia extract.* Food and Bioprocess Technology, 2013. 6 (4): p. 931-940.

158. Iritani, E. and N. Katagiri, *Developments of blocking filtration model in membrane filtration.* KONA Powder and Particle Journal, 2016. 33: p. 179-202.

159. Wang, F. and V.V. Tarabara, *Pore blocking mechanisms during early stages of membrane fouling by colloids.* Journal of colloid and interface science, 2008. 328 (2): p. 464-469.

160. Ollis, D.F., *Integrating photocatalysis and membrane technologies for water treatment.* Annals of the New York Academy of Sciences, 2003. 984 (1): p. 65-84.

161. Zhang, W., et al., *Membrane fouling in photocatalytic membrane reactors (PMRs) for water and wastewater treatment: A critical review.* Chemical Engineering Journal, 2016. 302: p. 446-458.

162. Bian, R., K. Yamamoto, and Y. Watanabe, *The effect of shear rate on controlling the concentration polarization and membrane fouling.* Desalination, 2000. 131 (1-3): p. 225-236.

163. Fogler, H.S., *Essentials of chemical reaction engineering*. 2010: Pearson Education.

164. Coker, A.K., *Modeling of chemical kinetics and reactor design*. Vol. 1. 2001: Gulf Professional Publishing.

165. Imoberdorf, G.E., et al., *Optimal design and modeling of annular photocatalytic wall reactors.* Catalysis Today, 2007. 129 (1-2): p. 118-126.

166. Dong, D., et al., *Investigation on the photocatalytic degradation of pyrene on soil surfaces using nanometer anatase TiO_2 under UV irradiation.* Journal of Hazardous Materials, 2010. 174 (1-3): p. 859-863.

167. Fernandez, A., et al., *Preparation and characterization of TiO_2 photocatalysts supported on various rigid supports (glass, quartz and stainless steel). Comparative studies of photocatalytic activity in water purification.* Applied Catalysis B: Environmental, 1995. 7 (1-2): p. 49-63.

168. Denny, F., et al., *CFD modelling for a TiO_2-coated glass-bead photoreactor irradiated by optical fibres: Photocatalytic degradation of oxalic acid.* Chemical Engineering Science, 2009. 64 (8): p. 1695-1706.

169. Bestetti, M., et al., *Photocatalytic degradation activity of titanium dioxide sol–gel coatings on stainless steel wire meshes.* Materials Chemistry and Physics, 2010. 124 (2-3): p. 1225-1231.

170. Kabra, K., R. Chaudhary, and R.L. Sawhney, *Treatment of hazardous organic and inorganic compounds through aqueous-phase photocatalysis: a review.* Industrial & engineering chemistry research, 2004. 43 (24): p. 7683-7696.

171. Galvez, J. and S. Rodriguez, *Solar Detoxification Technology.* Solar Detoxification; UNESCO Publishing: Paris, 2003. 117.

172. Ahmed, S., et al., *Heterogeneous photocatalytic degradation of phenols in wastewater: a review on current status and developments.* Desalination, 2010. 261 (1-2): p. 3-18.

173. Spasiano, D., et al., *Solar photocatalysis: materials, reactors, some commercial, and pre-industrialized applications. A comprehensive approach.* Applied Catalysis B: Environmental, 2015. 170: p. 90-123.

174. Kim, D.H. and M.A. Anderson, *Solution factors affecting the photocatalytic and photoelectrocatalytic degradation of formic acid using supported TiO_2 thin films.* Journal of Photochemistry and Photobiology A: Chemistry, 1996. 94 (2-3): p. 221-229.

175. Hasegawa, K. and P. Neta, *Rate constants and mechanisms of reaction of chloride (Cl_2^-) radicals.* The Journal of Physical Chemistry, 1978. 82 (8): p. 854-857.

176. Yu, X.-Y., Z.-C. Bao, and J.R. Barker, *Free radical reactions involving $Cl^\bullet$, $Cl_2^{-\bullet}$, and $SO_4^{-\bullet}$ in the 248 nm photolysis of aqueous solutions containing $S_2O_8^{2-}$ and Cl.* The Journal of Physical Chemistry A, 2004. 108 (2): p. 295-308.

177. Pope, M.T., *Heteropoly and isopoly oxometalates.* Springer-Verlag, 1983.

178. Habibi, M.H., A. Hassanzadeh, and S. Mahdavi, *The effect of operational parameters on the photocatalytic degradation of three textile azo dyes in aqueous TiO_2 suspensions.* Journal of Photochemistry and Photobiology A: Chemistry, 2005. 172 (1): p. 89-96.

179. Daneshvar, N., D. Salari, and A. Khataee, *Photocatalytic degradation of azo dye acid red 14 in water: investigation of the effect of operational parameters.* Journal of Photochemistry and Photobiology A: Chemistry, 2003. 157 (1): p. 111-116.

180. Konstantinou, I.K. and T.A. Albanis, *TiO_2-assisted photocatalytic degradation of azo dyes in aqueous solution: kinetic and mechanistic investigations: a review.* Applied Catalysis B: Environmental, 2004. 49 (1): p. 1-14.

181. Gaya, U.I., *Heterogeneous photocatalysis using inorganic semiconductor solids*. 2013: Springer Science & Business Media.

182. Palmer, F.L., B.R. Eggins, and H.M. Coleman, *The effect of operational parameters on the photocatalytic degradation of humic acid.* Journal of Photochemistry and Photobiology A: Chemistry, 2002. 148 (1-3): p. 137-143.

183. Malato, S., et al., *Enhancement of the rate of solar photocatalytic mineralization of organic pollutants by inorganic oxidizing species.* Applied Catalysis B: Environmental, 1998. 17 (4): p. 347-356.

184. Parsons, S., *Advanced oxidation processes for water and wastewater treatment*. 2004: IWA publishing.

185. Hernández-Alonso, M.D., R. Portela, and J.M. Coronado, *Turning Sunlight into Fuels: Photocatalysis for Energy*, in *Design of Advanced Photocatalytic Materials for Energy and Environmental Applications*. 2013, Springer. p. 67-84.

186. Rincón, A.-G. and C. Pulgarin, *Use of coaxial photocatalytic reactor (CAPHORE) in the TiO_2 photo-assisted treatment of mixed E. coli and Bacillus sp. and bacterial community present in wastewater.* Catalysis today, 2005. 101 (3-4): p. 331-344.

187. Ohtani, B., *Photocatalysis A to Z—What we know and what we do not know in a scientific sense.* Journal of Photochemistry and Photobiology C: Photochemistry Reviews, 2010. 11 (4): p. 157-178.

188. Matthews, R.W. and S.R. McEvoy, *A comparison of 254 nm and 350 nm excitation of TiO_2 in simple photocatalytic reactors.* Journal of Photochemistry and Photobiology A: Chemistry, 1992. 66 (3): p. 355-366.

189. Yatmaz, H., C. Wallis, and C. Howarth, *The spinning disc reactor–studies on a novel TiO_2 photocatalytic reactor.* Chemosphere, 2001. 42 (4): p. 397-403.

190. Ozer, R.R. and J.L. Ferry, *Photocatalytic oxidation of aqueous 1,2-dichlorobenzene by polyoxometalates supported on the NaY zeolite.* The Journal of Physical Chemistry B, 2002. 106 (16): p. 4336-4342.

191. Magrini, K.A. and J.D. Webb. *Photocatalytic decomposition of aqueous organic compounds as a function of solar irradiation intensity*. in *1990 ASME International Solar Energy Conference*. 1990.

192. Ollis, D.F., *Solar-assisted photocatalysis for water purification: issues, data, questions*, in *Photochemical conversion and storage of solar energy*. 1991, Springer. p. 593-622.

193. Sarasidis, V., S. Patsios, and A. Karabelas, *A hybrid photocatalysis–ultrafiltration continuous process: The case of polysaccharide degradation.* Separation and purification technology, 2011. 80 (1): p. 73-80.

194. Molinari, R., et al., *Photocatalytic processes in membrane reactors.* 2017.

195. Argurio, P., et al., *Photocatalytic Membranes in Photocatalytic Membrane Reactors.* Processes, 2018. 6 (9): p. 162.

196. Dong, X., et al., *Dense ceramic catalytic membranes and membrane reactors for energy and environmental applications.* Chemical Communications, 2011. 47 (39): p. 10886-10902.

197. Westermann, T. and T. Melin, *Flow-through catalytic membrane reactors—principles and applications.* Chemical Engineering and Processing: Process Intensification, 2009. 48 (1): p. 17-28.

198. Fu, J., et al., *A new submerged membrane photocatalysis reactor (SMPR) for fulvic acid removal using a nano-structured photocatalyst.* Journal of hazardous materials, 2006. 131 (1-3): p. 238-242.

199. de Lasa, H., B. Serrano, and M. Salaices, *Novel photocatalytic reactors for water and air treatment*, in *Photocatalytic Reaction Engineering*. 2005, Springer. p. 17-47.

200. Mozia, S., et al., *Comparison of effectiveness of methylene blue decomposition using pristine and carbon-coated TiO_2 in a photocatalytic membrane reactor.* Desalination, 2007. 212 (1-3): p. 141-151.

201. Patsios, S., V. Sarasidis, and A. Karabelas, *A hybrid photocatalysis–ultrafiltration continuous process for humic acids degradation.* Separation and Purification Technology, 2013. 104: p. 333-341.

202. Cooper, G. and M.A. Ratcliff, *Photocatalytic treatment of water*. 1992, Google Patents.

203. Sopajaree, K., et al., *An integrated flow reactor-membrane filtration system for heterogeneous photocatalysis. Part I: Experiments and modelling of a batch-recirculated photoreactor.* Journal of applied electrochemistry, 1999. 29 (5): p. 533-539.

204. Sopajaree, K., et al., *An integrated flow reactor-membrane filtration system for heterogeneous photocatalysis. Part II: Experiments on the ultrafiltration unit and combined operation.* Journal of Applied Electrochemistry, 1999. 29 (9): p. 1111-1118.

205. Zhang, G., et al., *Photocatalytic membrane reactor used for water and wastewater treatment.* Recent Patents on Engineering, 2012. 6 (2): p. 127-136.

206. Kochkodan, V., E. Rolya, and V. Goncharuk, *Photocatalytic membrane reactors for water treatment from organic pollutants.* Journal of Water Chemistry and Technology, 2009. 31 (4): p. 227-237.

207. Wang, P., *Membrane photoreactors (MPRs) for photocatalysts separation and pollutants removal: Recent overview and new perspectives.* Separation Science and Technology, 2016. 51 (1): p. 147-167.

208. Hutanu, D., et al., *Recent applications of polyethylene glycols (PEGs) and PEG derivatives.* Mod. Chem. Appl, 2014. 2 (2): p. 1-6.

209. Plata, M.R., A.M. Contento, and Á. Ríos, *Analytical characterization of PEG polymers by MEKC.* Electrophoresis, 2010. 31 (4): p. 679-687.

210. Jang, H.-J., C.Y. Shin, and K.-B. Kim, *Safety evaluation of polyethylene glycol (PEG) compounds for cosmetic use.* Toxicological research, 2015. 31 (2): p. 105.

211. Bailey, F.E., *Alkylene oxides and their polymers*. Vol. 35. 1990: CRC Press.

212. Santos, L.C., et al., *Photo-fenton degradation of poly (Ethyleneglycol).* Journal of the Brazilian Chemical Society, 2011. 22 (3): p. 540-545.

213. Mantzavinos, D., et al., *Catalytic wet oxidation of p-coumaric acid: partial oxidation intermediates, reaction pathways and catalyst leaching.* Applied Catalysis B: Environmental, 1996. 7 (3): p. 379-396.

214. Rohani, R., M. Hyland, and D. Patterson, *A refined one-filtration method for aqueous based nanofiltration and ultrafiltration membrane molecular weight cut-off determination using polyethylene glycols.* Journal of membrane science, 2011. 382 (1): p. 278-290.

215. Davey, C.J., et al., *Molecular weight cut-off determination of organic solvent nanofiltration membranes using poly (propylene glycol).* Journal of Membrane Science, 2017. 526: p. 221-228.

216. Xu, L., et al., *A wide range and high resolution one-filtration molecular weight cut-off method for aqueous based nanofiltration and ultrafiltration membranes.* Journal of Membrane Science, 2017. 525: p. 304-311.

217. Megoulas, N.C. and M.A. Koupparis, *Twenty years of evaporative light scattering detection.* Critical reviews in analytical chemistry, 2005. 35 (4): p. 301-316.

218. Li, X., et al., *Evaporative light scattering detector: toward a general molecular weight cutoff characterization of nanofiltration membranes.* Analytical chemistry, 2009. 81 (5): p. 1801-1809.

219. Rissler, K., *Improved separation of polyethylene glycols widely differing in molecular weight range by reversed-phase high performance liquid chromatography and evaporative light scattering detection.* Chromatographia, 1999. 49 (11-12): p. 615-620.

220. Marie, A., F. Fournier, and J. Tabet, *Characterization of synthetic polymers by MALDI-TOF/MS: Investigation into new methods of sample target preparation and consequence on mass spectrum finger print.* Analytical chemistry, 2000. 72 (20): p. 5106-5114.

221. Yu, D., N. Vladimirov, and J.M. Frechet, *MALDI-TOF in the characterizations of dendritic−linear block copolymers and stars.* Macromolecules, 1999. 32 (16): p. 5186-5192.

222. Barman, B.N., D.H. Champion, and S.L. Sjoberg, *Identification and quantification of polyethylene glycol types in polyethylene glycol methyl ether and polyethylene glycol vinyl ether.* Journal of Chromatography A, 2009. 1216 (40): p. 6816-6823.

223. Ulbricht, J., R. Jordan, and R. Luxenhofer, *On the biodegradability of polyethylene glycol, polypeptoids and poly (2-oxazoline) s.* Biomaterials, 2014. 35 (17): p. 4848-4861.

224. Davey, C.J., et al., *Nanofiltration and reverse osmosis membranes for purification and concentration of a 2,3-butanediol producing gas fermentation broth.* Journal of Membrane Science, 2016. 518: p. 150-158.

225. Monteagudo, J., et al., *Optimization of pharmaceutical wastewater treatment by solar/ferrioxalate photo-catalysis.* Journal of environmental management, 2013. 128: p. 210-219.

226. Monteagudo, J., A. Durán, and I. San Martín, *Mineralization of wastewater from the pharmaceutical industry containing chloride ions by UV photolysis of H_2O_2/Fe (II) and ultrasonic irradiation.* Journal of environmental management, 2014. 141: p. 61-69.

227. Monteagudo, J., et al., *Application of activated persulfate for removal of intermediates from antipyrine wastewater degradation refractory towards hydroxyl radical.* Journal of hazardous materials, 2016. 306: p. 77-86.

228. Durán, A., et al., *Solar photodegradation of antipyrine in a synthetic WWTP effluent in a semi-industrial installation.* Solar Energy Materials and Solar Cells, 2014. 125: p. 215-222.

229. Durán, A., et al., *Solar-photo-Fenton treatment of wastewater from the beverage industry: Intensification with ferrioxalate.* Chemical Engineering Journal, 2015. 270: p. 612-620.

230. Expósito, A., et al., *Antipyrine removal by TiO_2 photocatalysis based on spinning disc reactor technology.* Journal of Environmental Management, 2017. 187: p. 504-512.

231. Einaga, H. and M. Misono, *Photocatalysis of $H_3PW_{12}O_{40}$ for 4-chlorophenol decomposition in aqueous media.* Bulletin of the Chemical Society of Japan, 1996. 69 (12): p. 3435-3441.

232. Tseng, D.-H., L.-C. Juang, and H.-H. Huang, *Effect of oxygen and hydrogen peroxide on the photocatalytic degradation of monochlorobenzene in aqueous suspension.* International Journal of Photoenergy, 2012. 2012.

233. Lee, H., et al., *Contribution of dissolved oxygen to methylene blue decomposition by hybrid advanced oxidation processes system.* International Journal of Photoenergy, 2012. 2012.

234. Weston, A., P.R. Brown, and F. Foret, *HPLC and CE, Principles and Practice.* Analytical Biochemistry, 1998. 255 (1): p. 164.

235. Sakharov, A., L. Mazaletskaya, and I. Skibida, *Catalytic oxidative deformylation of polyethylene glycols with the participation of molecular oxygen.* Kinetics and catalysis, 2001. 42 (5): p. 662-668.

236. Shirayama, H., Y. Tohezo, and S. Taguchi, *Photodegradation of chlorinated hydrocarbons in the presence and absence of dissolved oxygen in water.* Water research, 2001. 35 (8): p. 1941-1950.

237. Sivalingam, G., M. Priya, and G. Madras, *Kinetics of the photodegradation of substituted phenols by solution combustion synthesized TiO_2.* Applied Catalysis B: Environmental, 2004. **51 (1): p. 67-76.**

238. Elrod, M., *An Introduction to Chemical Kinetics (Margaret Robson Wright)*. 2005, ACS Publications.

239. Ozer, R.R. and J.L. Ferry, *Investigation of the photocatalytic activity of TiO_2− polyoxometalate systems.* Environmental science & technology, 2001. 35(15): p. 3242-3246.

240. Jin, H., Q. Wu, and W. Pang, *Photocatalytic degradation of textile dye X-3B using polyoxometalate–TiO_2 hybrid materials.* Journal of hazardous materials, 2007. 141 (1): p. 123-127.

241. Mantzavinos, D., et al., *Reaction mechanisms and kinetics of chemical pretreatment of bioresistant organic molecules by wet air oxidation.* Water Science and Technology, 1997. 35 (4): p. 119-127.

242. Sarkar, B., *A combined complete pore blocking and cake filtration model during ultrafiltration of polysaccharide in a batch cell.* Journal of Food Engineering, 2013. 116 (2): p. 333-343.

243. Peeva, P.D., et al., *Cross-flow ultrafiltration of protein solutions through unmodified and surface functionalized polyethersulfone membranes–effect of process conditions on separation performance.* Separation and purification technology, 2012. 92: p. 83-92.

244. Hellenbrand, R., et al., *Integration of wet oxidation and nanofiltration for treatment of recalcitrant organics in wastewater.* Industrial & engineering chemistry research, 1997. 36 (12): p. 5054-5062.

245. Chen, B., et al., *Integrated membrane process for wastewater treatment from production of instant tea powders.* Desalination, 2015. 355: p. 147-154.

246. Zuriaga-Agustí, E., et al., *Performance of ceramic ultrafiltration membranes and fouling behavior of a dye-polysaccharide binary system.* Water research, 2014. 54: p. 199-210.

247. Hong, S., R.S. Faibish, and M. Elimelech, *Kinetics of permeate flux decline in crossflow membrane filtration of colloidal suspensions.* Journal of colloid and interface science, 1997. 196 (2): p. 267-277.

248. Sharma, C., et al., *Clarification of Stevia extract by ultrafiltration: selection criteria of the membrane and effects of operating conditions.* Food and Bioproducts Processing, 2012. 90 (3): p. 525-532.

249. Darvishzadeh, T. and N.V. Priezjev, *Effects of crossflow velocity and transmembrane pressure on microfiltration of oil-in-water emulsions.* journal of membrane science, 2012. 423: p. 468-476.

250. Ellouze, E., N. Tahri, and R.B. Amar, *Enhancement of textile wastewater treatment process using nanofiltration.* Desalination, 2012. 286: p. 16-23.

251. Akdemir, E.O. and A. Ozer, *Investigation of two ultrafiltration membranes for treatment of olive oil mill wastewater*. Desalination, 2009. 249 (2): p. 660-666.

252. Shariffuddin, J.H., M.I. Jones, and D.A. Patterson, *Greener photocatalysts: hydroxyapatite derived from waste mussel shells for the photocatalytic degradation of a model azo dye wastewater.* chemical engineering research and design, 2013. 91 (9): p. 1693-1704.

253. Song, L., et al., *Hybrid processes combining photocatalysis and ceramic membrane filtration for degradation of humic acids in saline water.* Membranes, 2016. 6 (1): p. 18.

254. Lee, S.-A., et al., *Use of ultrafiltration membranes for the separation of TiO_2 photocatalysts in drinking water treatment.* Industrial & engineering chemistry research, 2001. 40 (7): p. 1712-1719.

255. Jiang, H., et al., *Photocatalytic membrane reactor for degradation of acid red B wastewater.* Chemical Engineering Journal, 2010. 156 (3): p. 571-577.

256. Fotiou, T., et al., *Evaluation of the photocatalytic activity of TiO_2 based catalysts for the degradation and mineralization of cyanobacterial toxins and water off-odor compounds under UV-A, solar and visible light.* Chemical Engineering Journal, 2015. 261: p. 17-26.

257. Grassian, V.H., *Environmental catalysis*. 2005: CRC press.

258. Choo, K.-H., et al., *Use of an integrated photocatalysis/hollow fiber microfiltration system for the removal of trichloroethylene in water.* Journal of hazardous materials, 2008. 152 (1): p. 183-190.

259. Weimin, X. and S.-u. Geissen, *Separation of titanium dioxide from photocatalytically treated water by cross-flow microfiltration.* Water Research, 2001. 35 (5): p. 1256-1262.

260. Joseph, C.G., et al., *Operating parameters and synergistic effects of combining ultrasound and ultraviolet irradiation in the degradation of 2,4,6-trichlorophenol.* Desalination, 2011. 276 (1): p. 303-309.

261. Duran, A., et al., *Modeling the sonophoto-degradation/mineralization of carbamazepine in aqueous solution.* Chemical Engineering Journal, 2016. 284: p. 503-512.

Appendices

Appendix A

A1. Gradient method used for HPLC analysis of PEG1500

Table A1: HPLC gradient profiles for the elution of PEG1500.

Elution time (min)	Gradient (%acetonitrile)	Gradient (% Water)
0	15	85
5	25	75
20	50	50
22	25	75
25	15	85

A2. Calibration curve of PEG1500

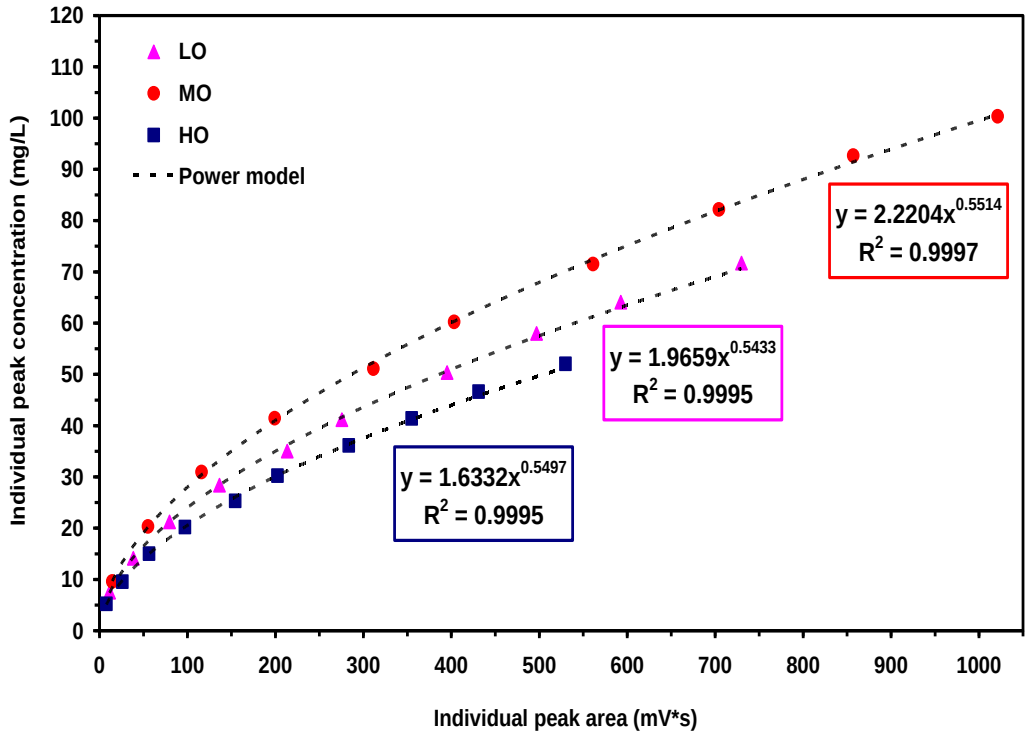

Fig. A1: Calibration curve of PEG1500 oligomers.

Table A2: Correlation of the PEG oligomers' MW with calibration equation.

Peak No.	PEG oligomer MW ($gmol^{-1}$)	Calibration equation ($C=aA^b$)		R^2	MIDL	
		a	*b*		*A* (mV)	*C* (mgL^{-1})
1	1097.6	0.8492	0.3872	0.9835	1.75	1.15
2	1141.7	0.8650	0.4900	0.9890	2.16	1.42
3	1185.7	0.9648	0.5375	0.9985	2.52	1.66
4	1229.7	1.2174	0.5402	0.9960	4.65	3.06
5	1273.7	1.4350	0.5499	0.9996	5.76	3.79
6	1317.8	1.6393	0.5540	0.9996	7.64	5.04
7	1361.8	1.9659	0.5433	0.9995	11.41	7.52
8	1405.8	2.0912	0.5480	0.9996	12.94	8.52
9	1449.9	2.2119	0.5474	0.9996	14.66	9.66
10	1493.9	2.2154	0.5508	0.9997	14.41	9.49
11	1537.9	2.2204	0.5514	0.9996	14.56	9.59
12	1581.9	2.0924	0.5545	0.9998	12.99	8.55
13	1626.0	2.0435	0.5475	0.9998	12.22	8.05
14	1670.0	1.8905	0.5458	0.9993	9.75	6.42
15	1714.0	1.6332	0.5497	0.9995	7.93	5.22
16	1758.1	1.3450	0.5599	0.9997	5.12	3.37
17	1802.1	1.1311	0.5609	0.9997	3.44	2.27
18	1846.1	0.9198	0.5642	0.9993	2.13	1.40
19	1890.1	0.7702	0.5540	0.9962	1.30	0.86
20	1934.2	0.6981	0.5098	0.9908	1.22	0.80
21	1978.2	0.6747	0.4236	0.9867	1.15	0.76
22	2022.2	0.6297	0.4075	0.9782	1.13	0.74
23	2066.2	0.6003	0.2781	0.9500	1.01	0.67
						$MDL = \sum_{n=1}^{23} MIDL = 100\ mgL^{-1}$

A3. Investigation on intermediates formation

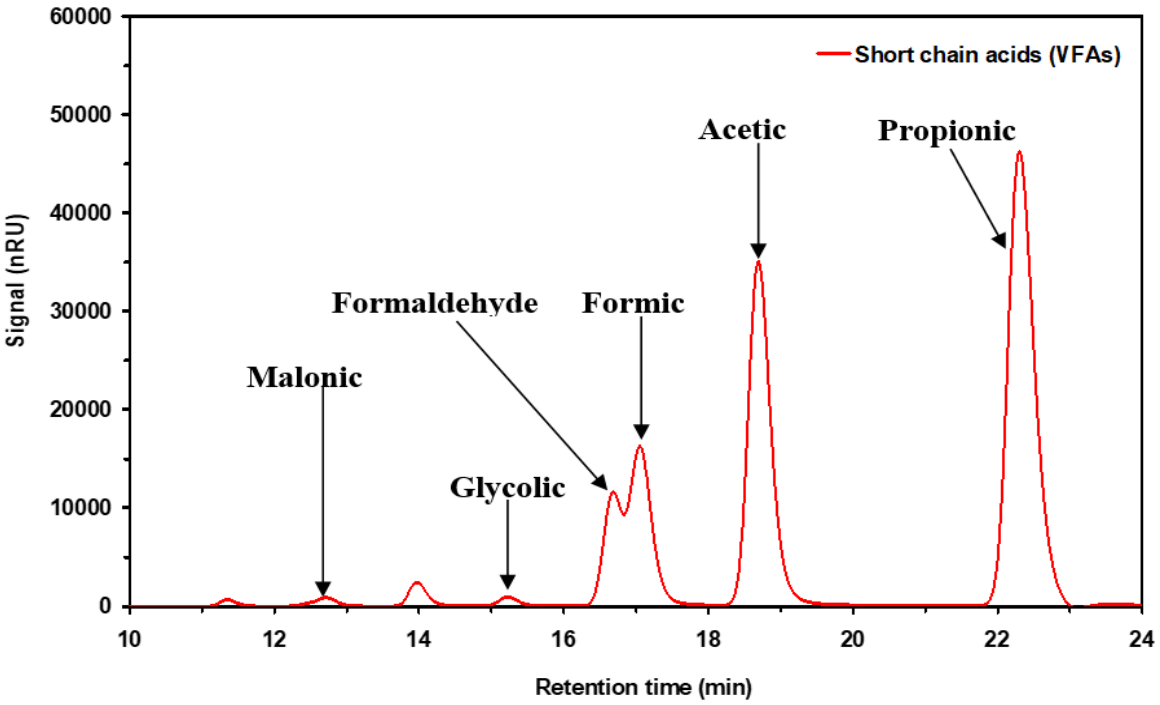

Fig. A2: Chromatographic analysis of mixed external standard solutions.

A4. Calibration curve of identified intermediates

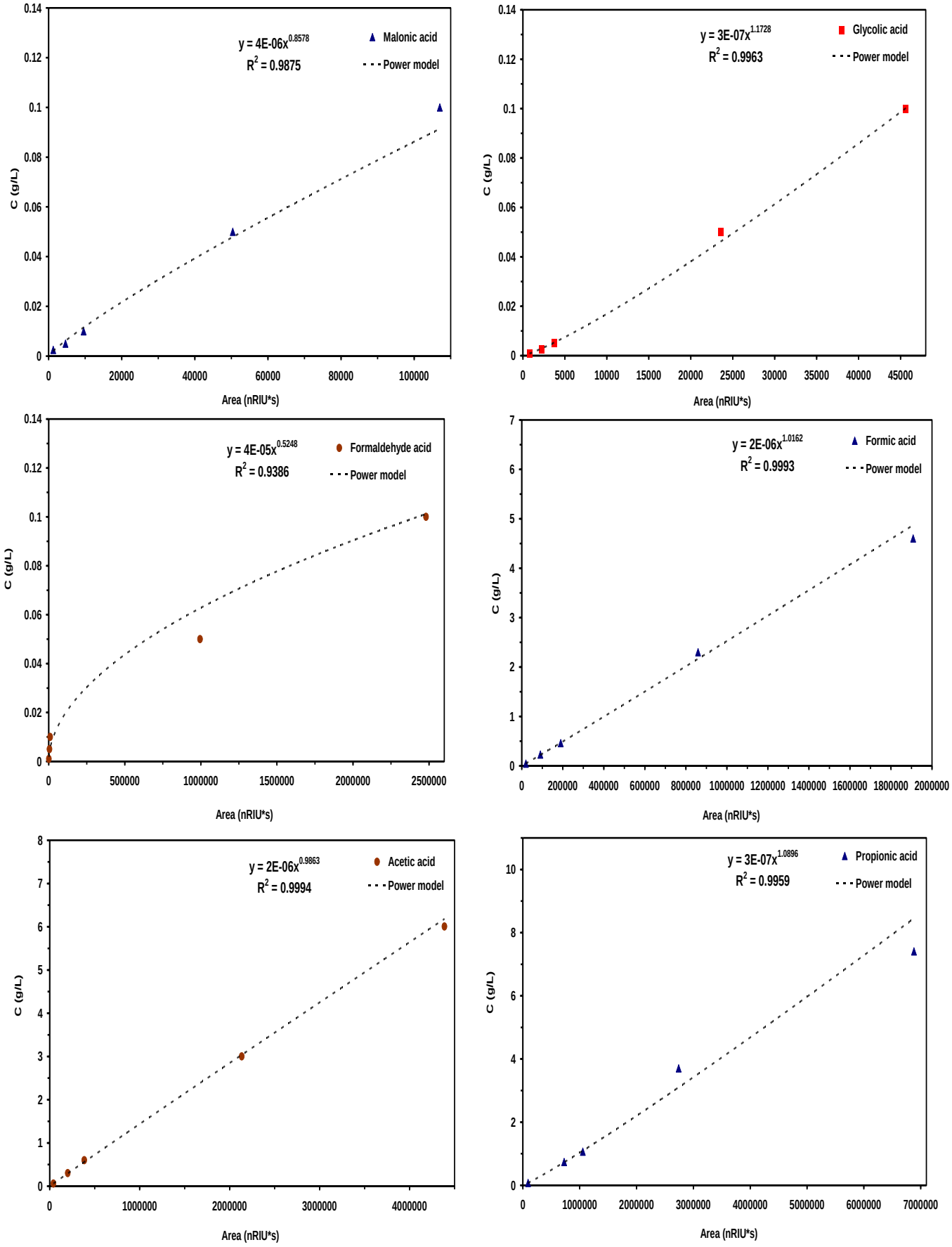

Fig. A3: Calibration curve of identified intermediate compounds.

A5. POM calibration curve

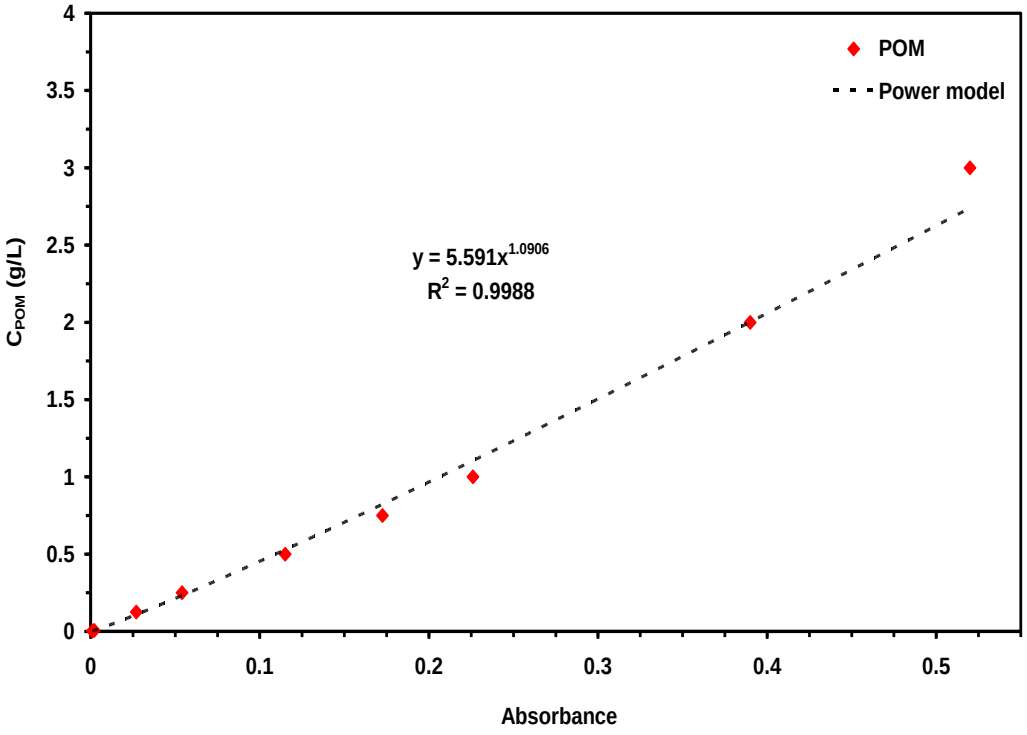

Fig. A4: Calibration curve of POM in aqueous solution.

A6. TiO_2 calibration curve

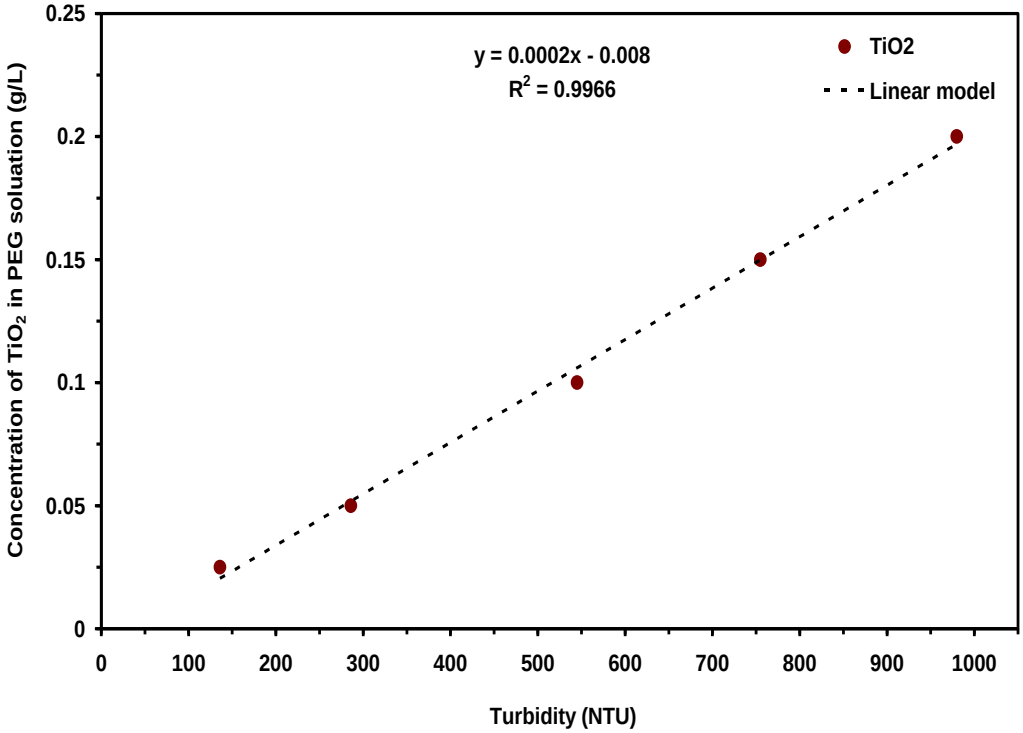

Fig. A5: Calibration curve of TiO_2 in PEG reactant solution.

A7. Dead-end cell components and operating parameters

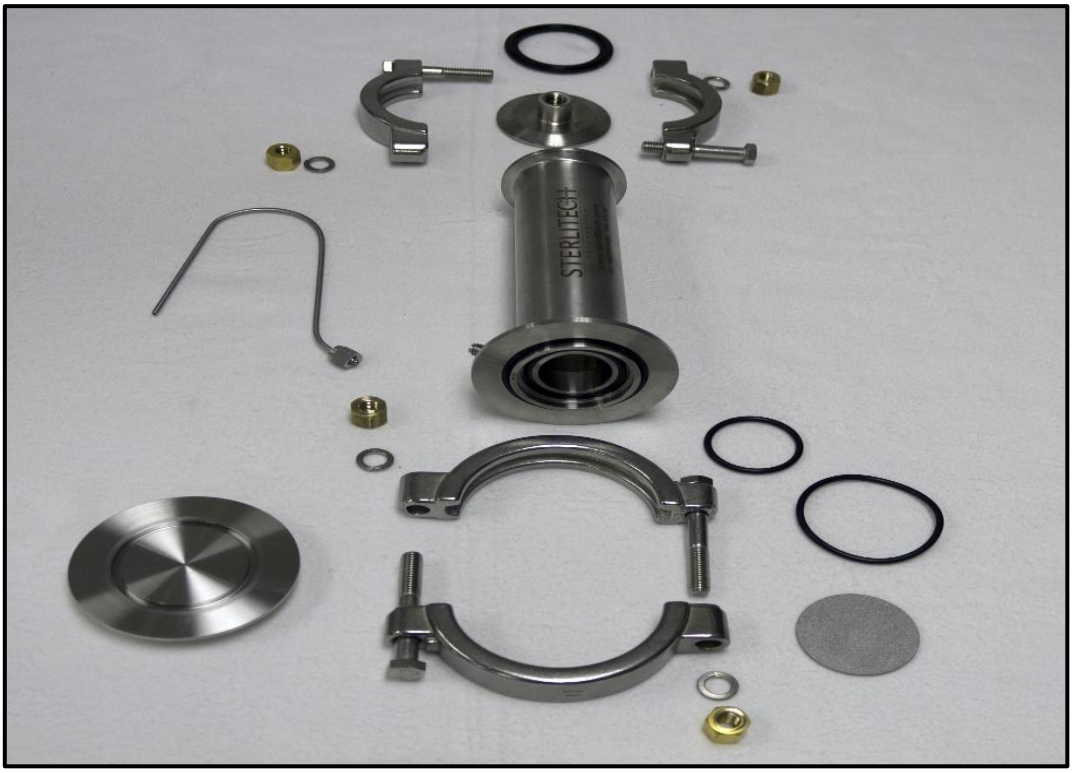

Fig. A6: Assembly photograph of a dead-end membrane filtration cell components.

Table A3: The operating parameters of HP4750 stirred cell from supplier.

Parameter	Description
Membrane Size:	47-49 mm diameter (1.93 inches)
Active Membrane Area:	14.6 cm^2 (2.26 in^2)
Processing Volume:	300 mL
Hold-Up Volume:	1 mL
Maximum Pressure:	69 bar (1000 psig)
Maximum Temperature:	121 °C (250 °F) at 55 bars (800 psig)
PH Range:	Membrane dependent
Connections:	
Permeate Outlet:	1/8-inch diameter 316L SS tubing
Pressure Inlet:	¼ inch FNPT
Wetted Materials of Construction	
Cell Body:	316L Stainless Steel
O-rings:	Buna-N, others available as options
Gaskets:	Buna-N, others available as options
Stir Bar:	PTFE-coated magnet
Dimensions:	
Cell Diameter:	5.1 cm (2.0 inches)
Cell Height:	22.4 cm (10.0 inches)
Autoclavable	Yes

A8. Specifications of the annular photoreactor

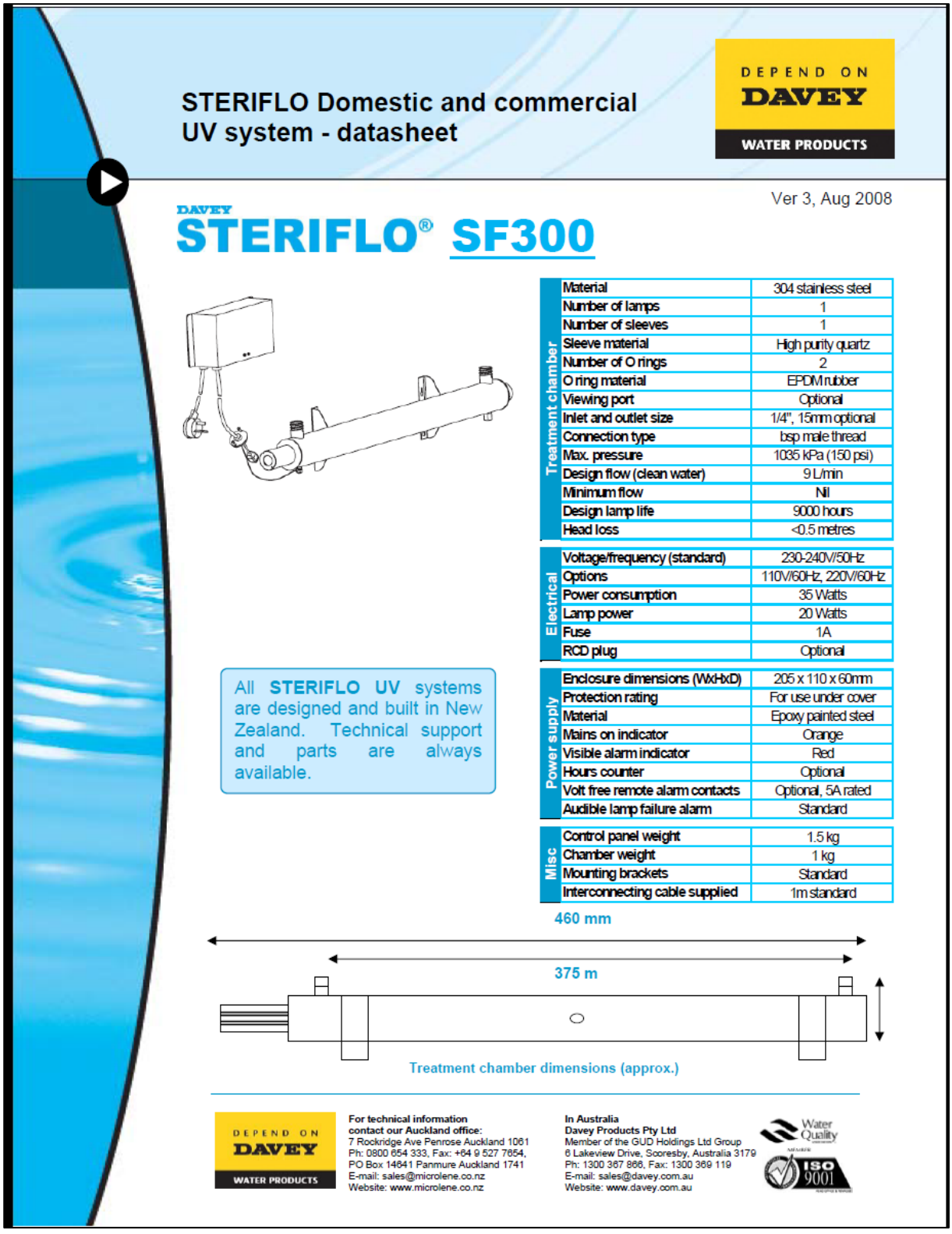

STERIFLO Domestic and commercial UV system - datasheet

DEPEND ON DAVEY WATER PRODUCTS

Ver 3, Aug 2008

DAVEY STERIFLO® SF300

Treatment chamber	Material	304 stainless steel
	Number of lamps	1
	Number of sleeves	1
	Sleeve material	High purity quartz
	Number of O rings	2
	O ring material	EPDM rubber
	Viewing port	Optional
	Inlet and outlet size	1/4", 15mm optional
	Connection type	bsp male thread
	Max. pressure	1035 kPa (150 psi)
	Design flow (clean water)	9 L/min
	Minimum flow	Nil
	Design lamp life	9000 hours
	Head loss	<0.5 metres
Electrical	Voltage/frequency (standard)	230-240V/50Hz
	Options	110V/60Hz, 220V/60Hz
	Power consumption	35 Watts
	Lamp power	20 Watts
	Fuse	1A
	RCD plug	Optional
Power supply	Enclosure dimensions (WxHxD)	205 x 110 x 60mm
	Protection rating	For use under cover
	Material	Epoxy painted steel
	Mains on indicator	Orange
	Visible alarm indicator	Red
	Hours counter	Optional
	Volt free remote alarm contacts	Optional, 5A rated
	Audible lamp failure alarm	Standard
Misc	Control panel weight	1.5 kg
	Chamber weight	1 kg
	Mounting brackets	Standard
	Interconnecting cable supplied	1m standard

All STERIFLO UV systems are designed and built in New Zealand. Technical support and parts are always available.

460 mm

375 m

Treatment chamber dimensions (approx.)

DEPEND ON DAVEY WATER PRODUCTS

For technical information contact our Auckland office:
7 Rockridge Ave Penrose Auckland 1061
Ph: 0800 654 333, Fax: +64 9 527 7654,
PO Box 14641 Panmure Auckland 1741
E-mail: sales@microlene.co.nz
Website: www.microlene.co.nz

In Australia
Davey Products Pty Ltd
Member of the GUD Holdings Ltd Group
6 Lakeview Drive, Scoresby, Australia 3179
Ph: 1300 367 866, Fax: 1300 369 119
E-mail: sales@davey.com.au
Website: www.davey.com.au

Water Quality ISO 9001

Fig. A7: A datasheet of steriflow annular photoreactor.

A9. The relationship between pH and POM loading

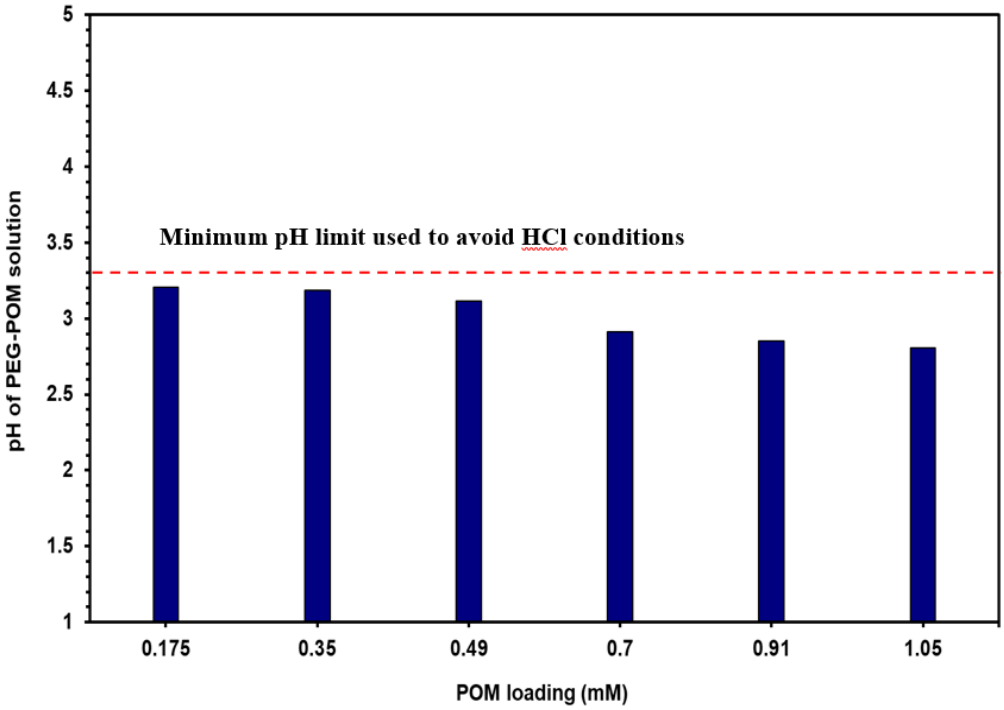

Fig. A8: pH of PEG-POM reactant solution as a function of POM photocatalyst loading (mM).

Appendix B

B1. POM Consumption

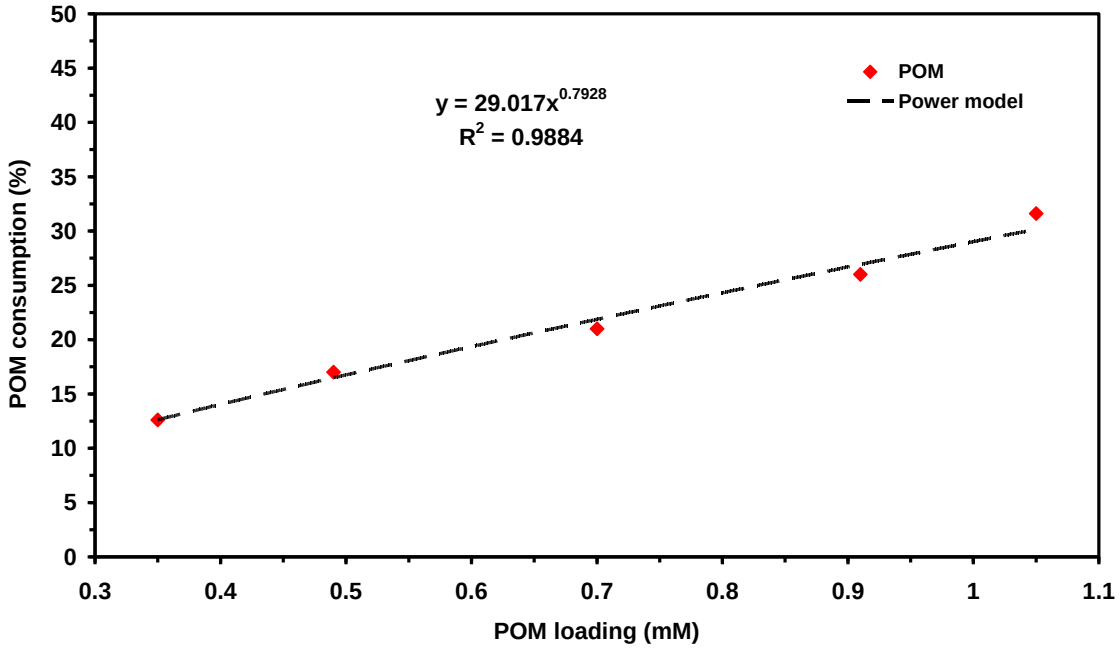

Fig. B1: percent POM consumption under various POM loadings (mM).

B2. Effect of PH on the non-photocatalytic reaction of POM with PEG

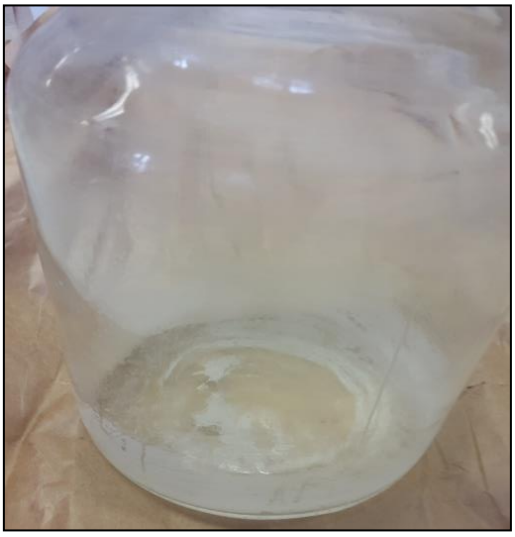

Fig. B2: The formation and precipitation of a white and very sticky material during the non-photocatalytic reaction of POM with PEG at pH 1, POM loading (0.35 mM) and mixing time (30 min).

B3. Equation and parameters for the *NN* fittings

Table B1: Equation and parameters of *NN* for the %PD and K_{app} of the three oligomers and total PEG by POM homogeneous photocatalysis.

%PD or K_{app} $=N_1$ (1/(1+1/EXP ($a_1W_{11}+a_2W_{12}+a_3W_{13}$))) + N_2 (1/(1+1/EXP ($a_1W_{21}+a_2W_{22}+a_3W_{23}$)))									
Neuron and weight factors	Parameters	Values of neurons and factors							
		%PD				K_{app}			
		LO	*MO*	*HO*	*Total PEG*	*LO*	*MO*	*HO*	*Total PEG*
N_1	**Neuron**	0.566	0.996	0.857	0.632	0.356	0.594	0.950	0.995
W_{11}	a_1	-0.625	-0.864	-0.446	-0.719	-0.592	-0.488	-0.764	-0.942
W_{12}	a_2	-1.255	-0.971	-0.733	-0.890	-1.551	-1.470	-1.170	-1.589
W_{13}	a_3	-0.493	-0.235	-0.281	-0.202	-0.331	-0.180	-0.143	-0.275
N_2	**Neuron**	0.546	0.685	1.124	0.879	0.411	0.762	1.347	0.720
W_{21}	a_1	-0.624	-0.808	-0.474	-0.768	-0.645	-0.498	-0.839	-0.882
W_{22}	a_2	-1.256	-1.021	-0.718	-0.858	-1.484	-1.368	-1.147	-1.589
W_{23}	a_3	-0.494	-0.217	-0.293	-0.231	-0.419	-0.130	-0.097	-0.286

W_{11}-W_{13} and W_{21}-W_{23} were normalized to the interval of 0.01.

a_1 (POM loading (mM)), a_2 (pH) and a_3 (oxidant concentration (mgO_2/L)).

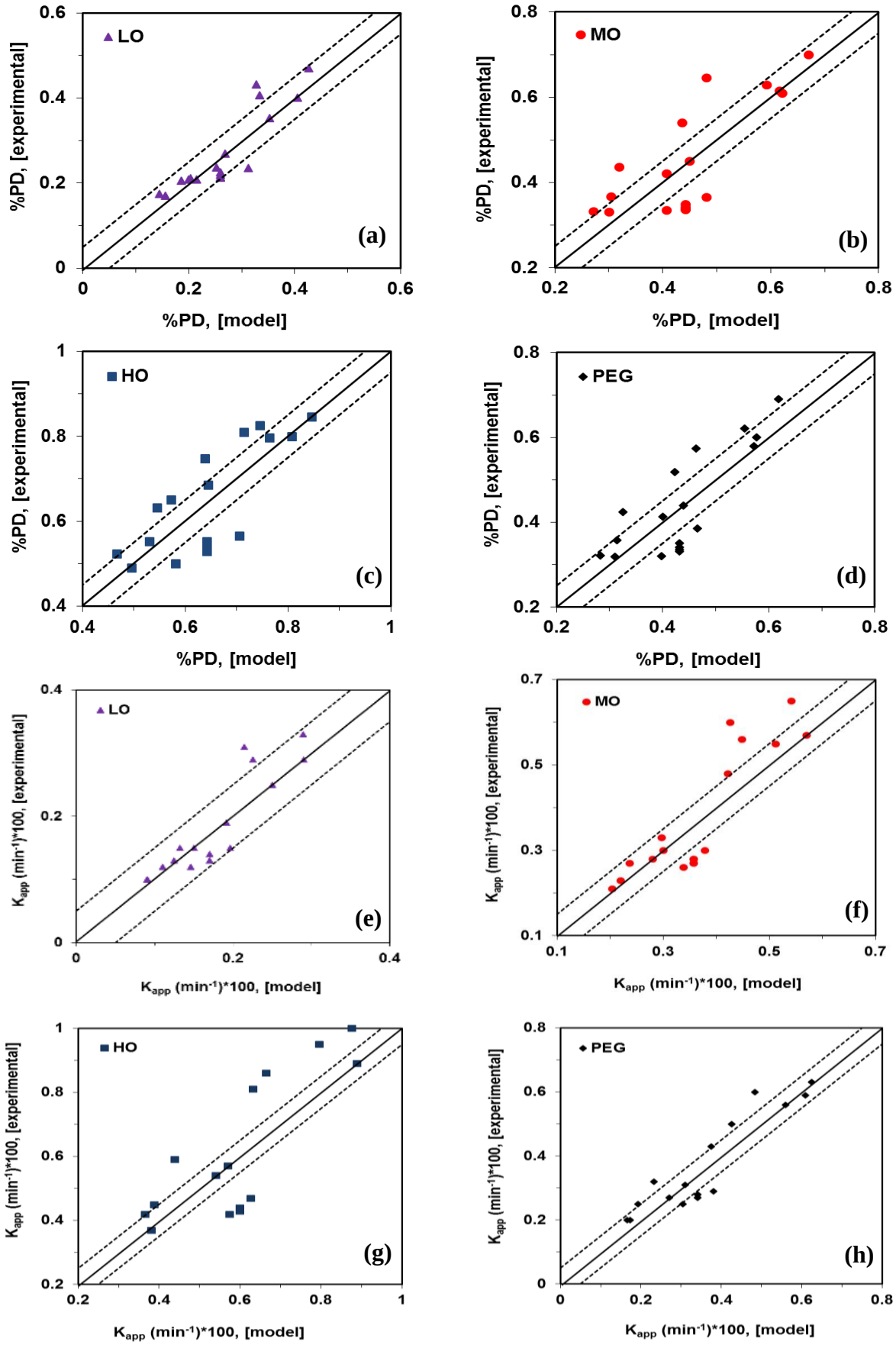

Fig. B3. Experimental and model neural network fittings of three selected oligomers and total PEG with the average error of fittings: (a-d) %PD; LO (2.47%), MO (6.25%), HO (6.87%), total PEG (6.13%) and (e-h) K_{app}; LO (2.93%), MO (5.90%), HO (11.63%), PEG (4.91%).

B4. HPLC chromatograms

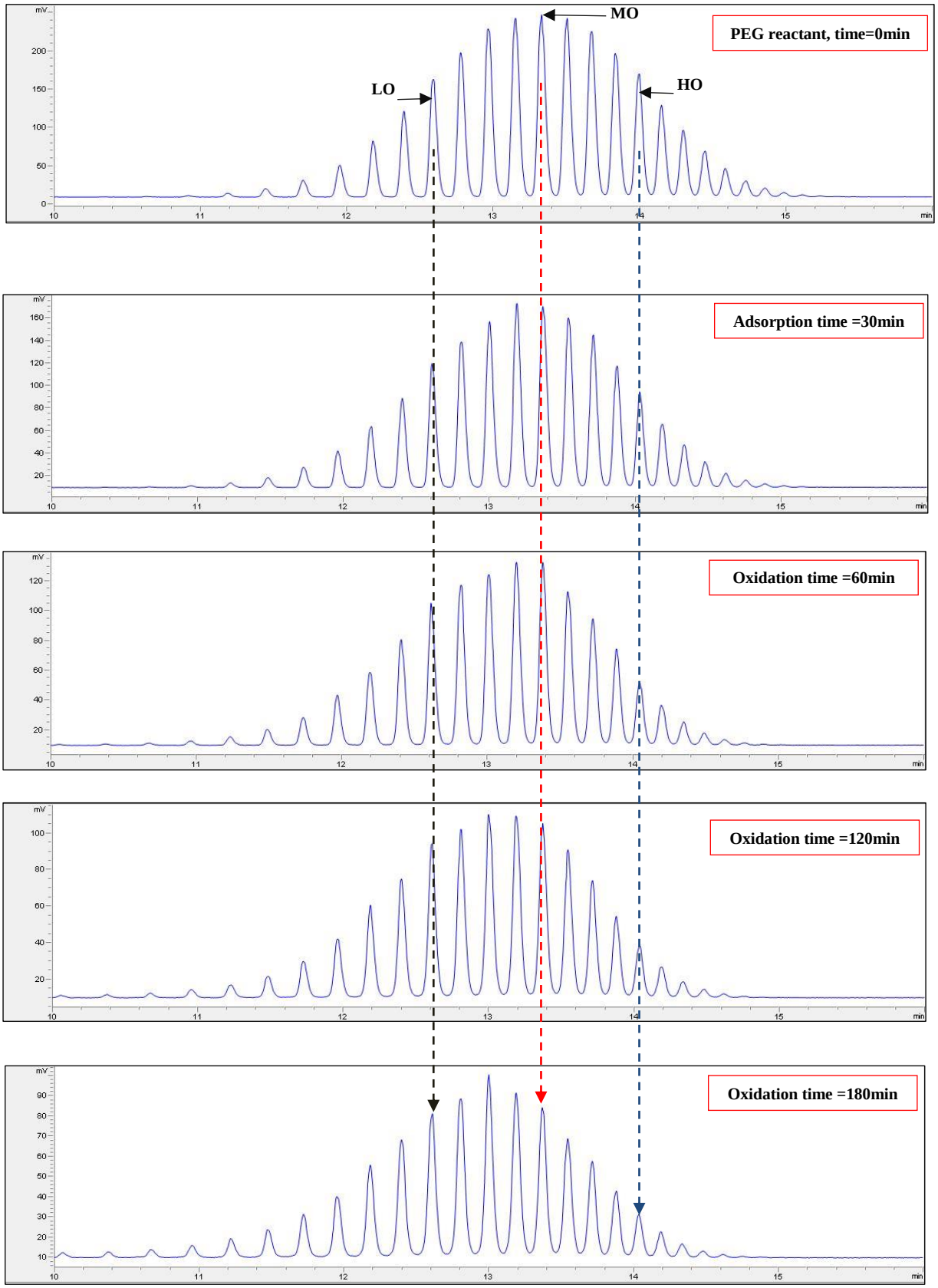

Fig. B4: HPLC chromatograms showing the relationship between the primary degradation of selected oligomers and the oxidation times under POM photocatalysis, loading (0.91 mM), pH (4.66) and oxidant concentration (58.65 mgO_2L^{-1}).

B5. Effect of pH and oxidant concentration on %PD

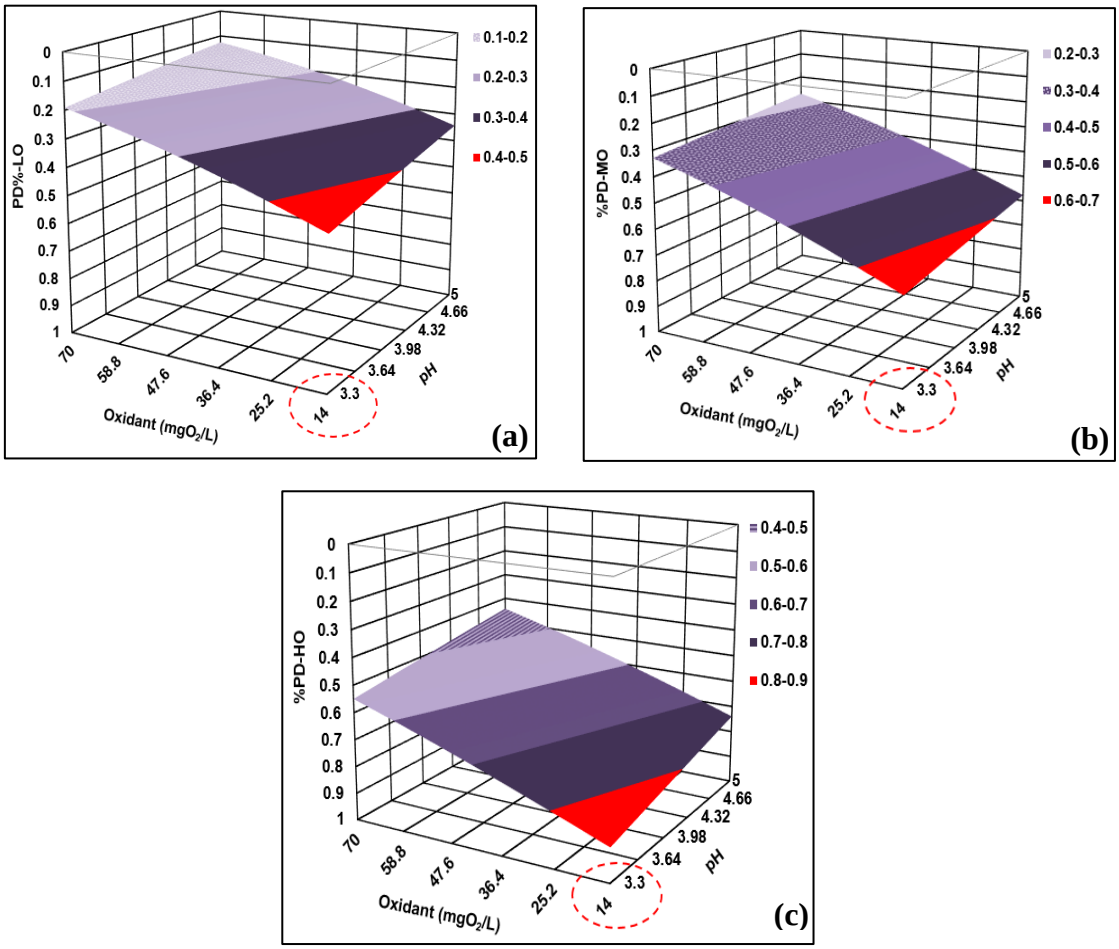

Fig. B5: *NN* simulation of %PD of LO, MO and HO under pH and oxidant concentration; (a) LO, (b) MO and (c) HO.

B6. Investigation on kinetic model

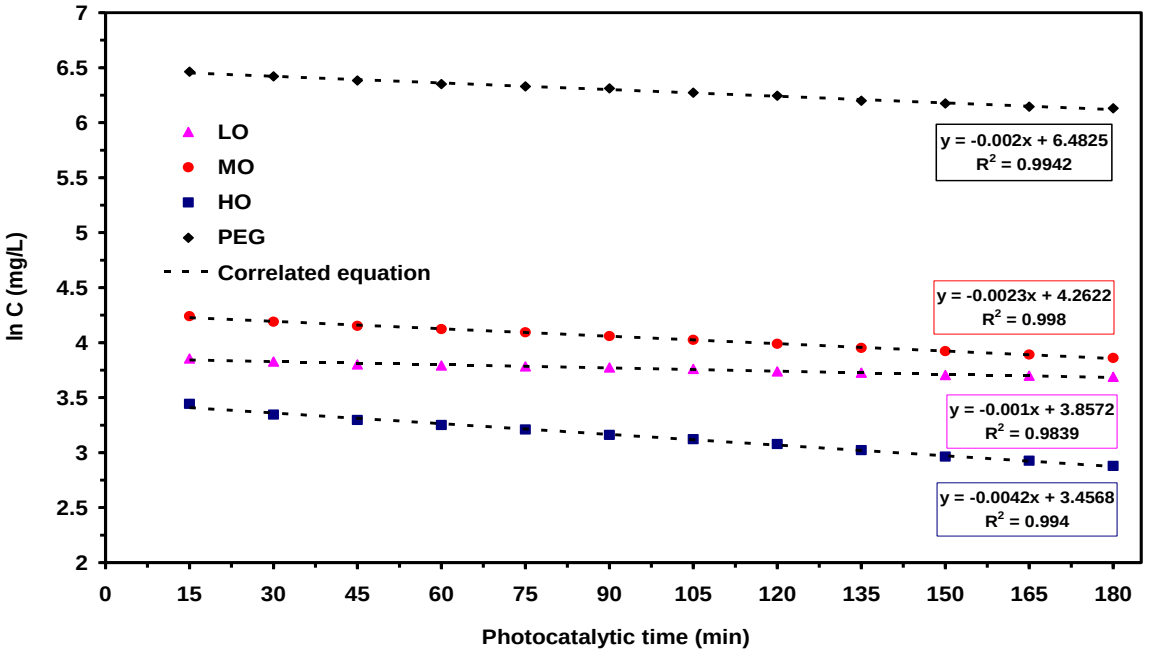

Fig. B6: Experimental photocatalytic data of PEG fitted with correlated equation at induction period (15 min), loading (0.91 mM), pH (4.66) and oxidant concentration (58.65 mgO_2L^{-1}).

B7. Effect of pH, loading and oxidant concentration on K_{app}

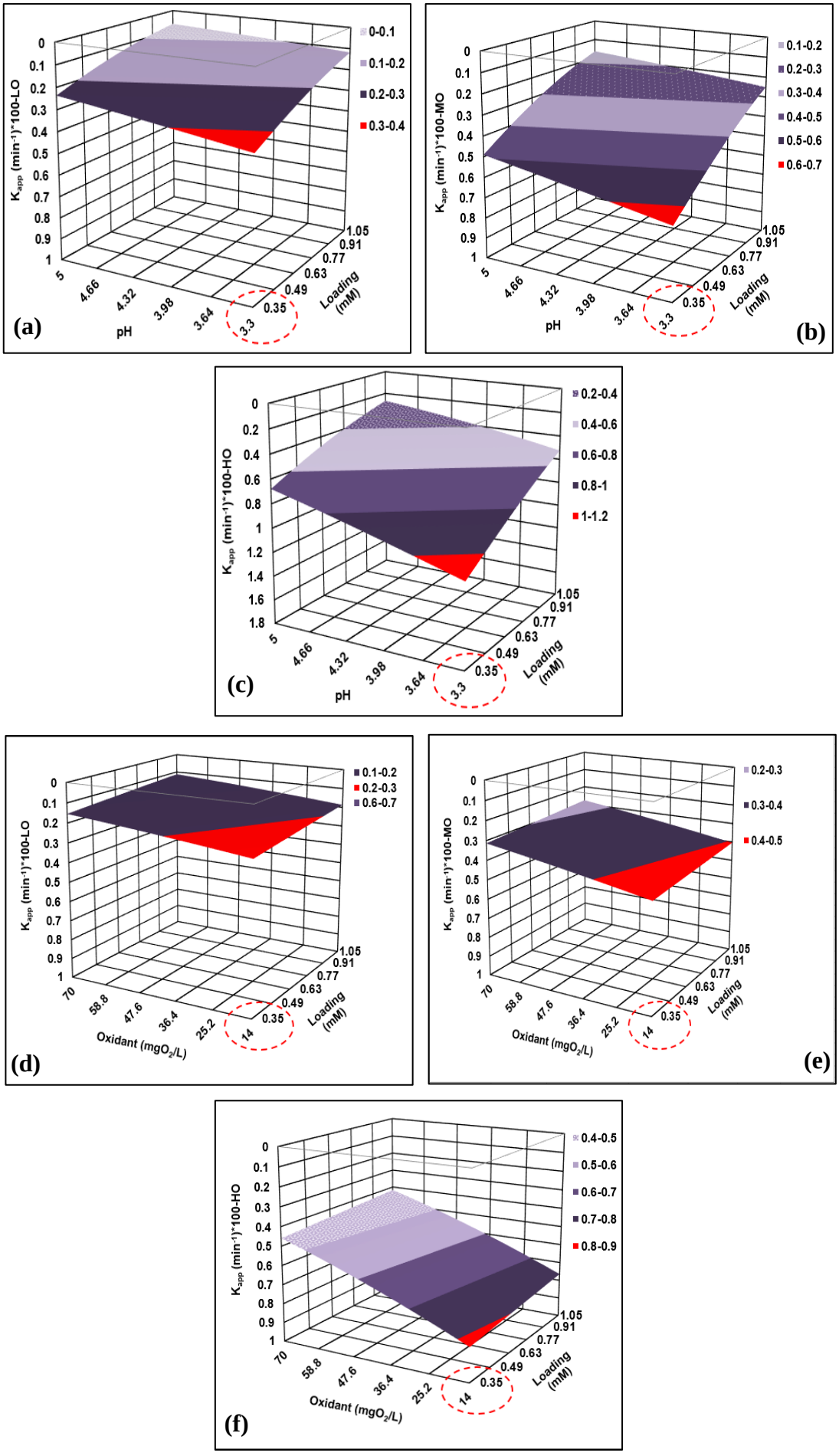

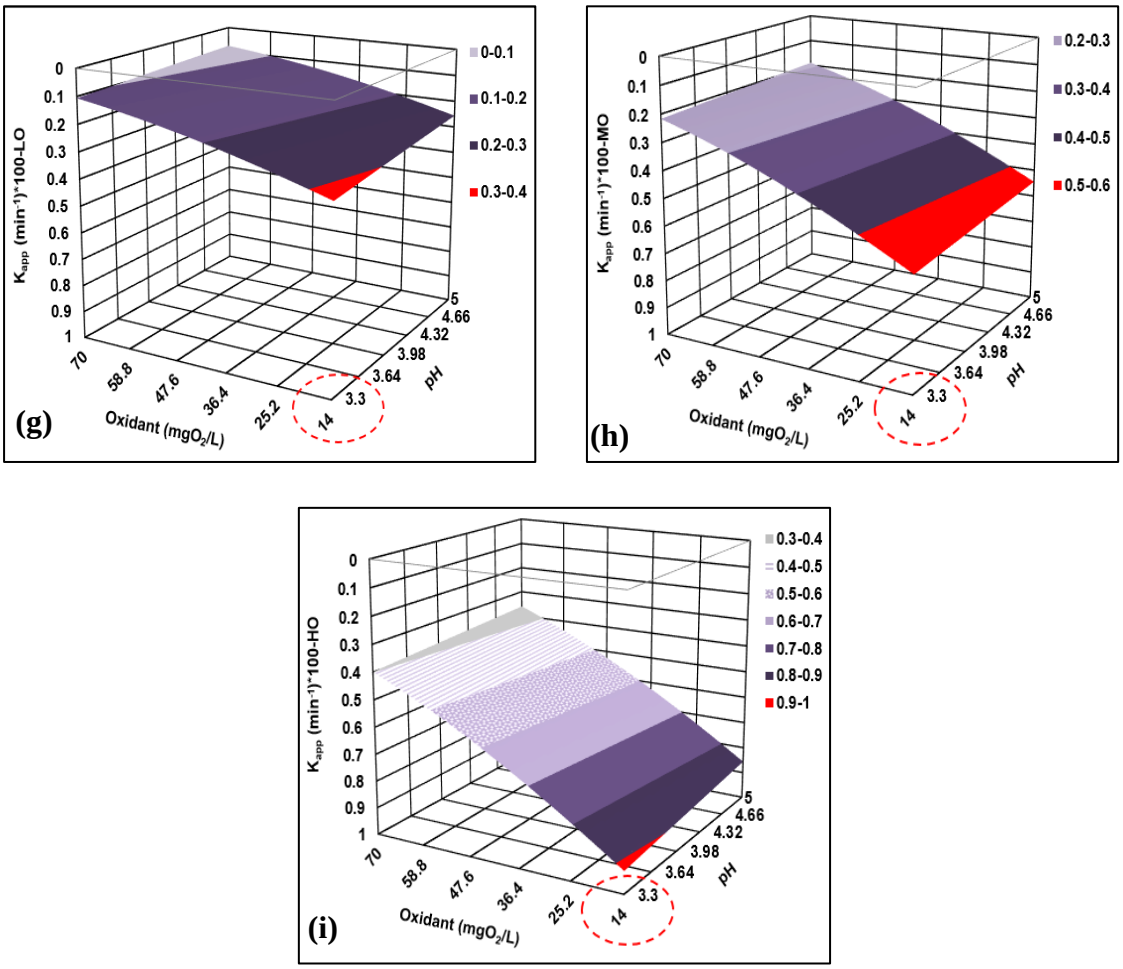

Fig. B7: *NN* simulation of a K_{app} of LO, MO and HO under various operating conditions: (a-c) POM loading and pH, (d-f) POM loading and oxidant concentration and (g-i) oxidant concentration and pH.

Appendix C

C1. Comparison of %PD of PEG with and without controlling the pH.

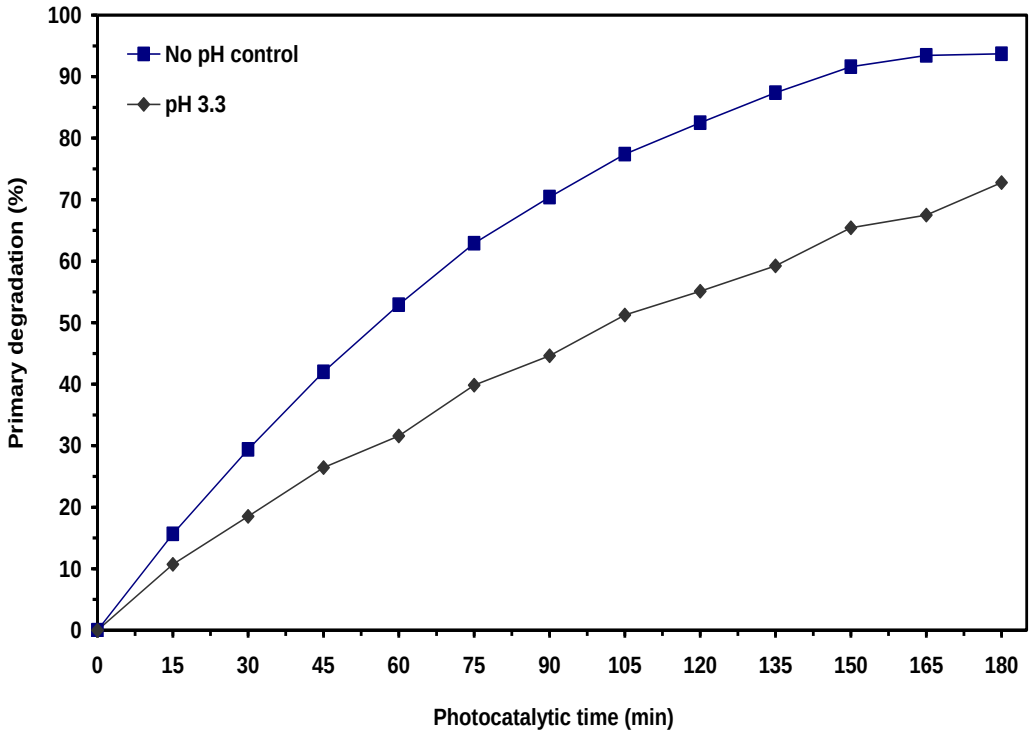

Fig. C1: Comparative performance of %PD of PEG without and with controlling the pH 3.3 and oxidant concertation (14 mgO_2L^{-1}) under POM loading (0.35 mM-1 gL^{-1}).

Appendix D

D1. Intermediates formation during TiO_2 control photocatalysis.

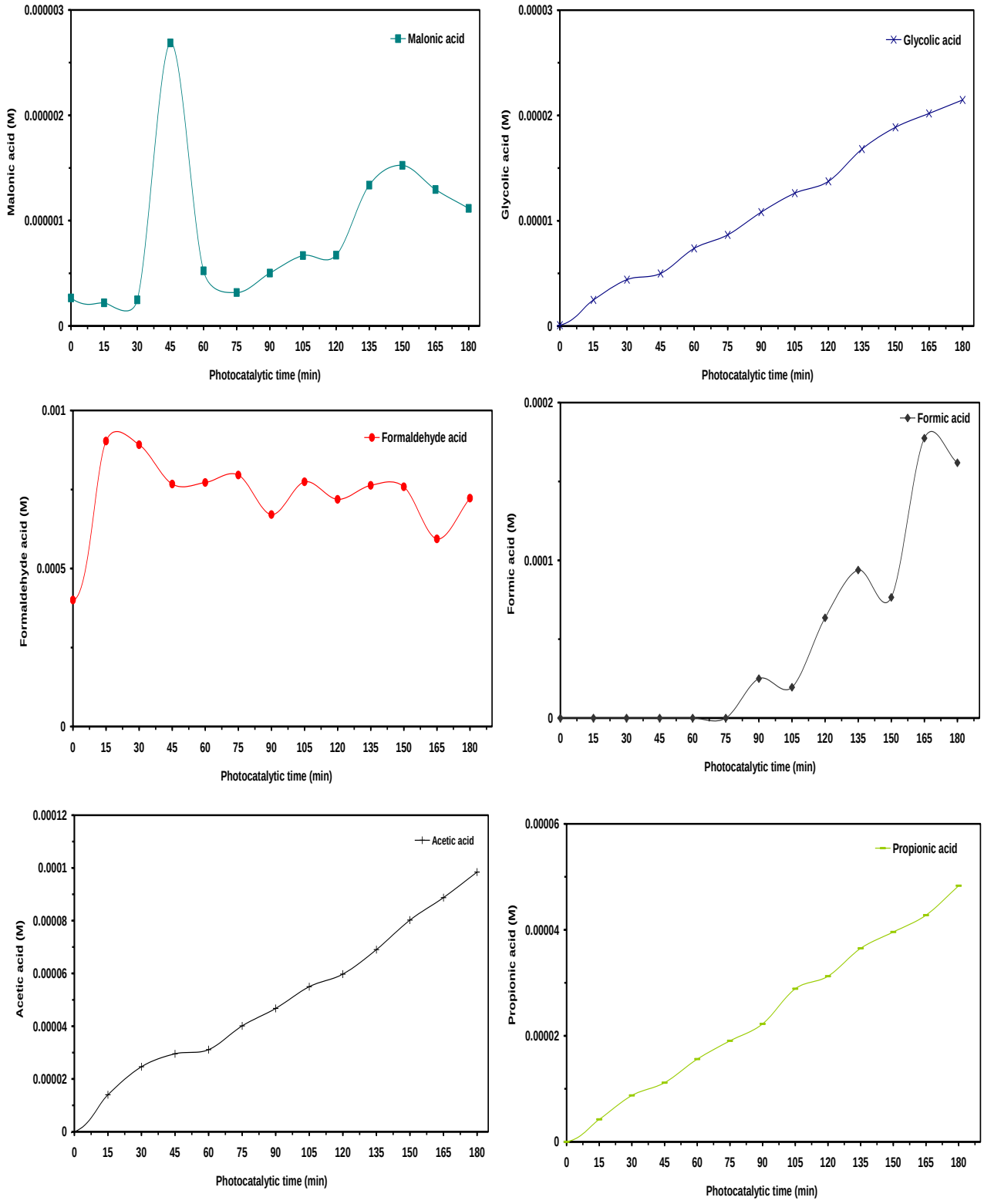

Fig. D1: Identified VFAs over a TiO_2 photocatalytic reaction time.

D2. SEM images under cross-flow heterogeneous PMR

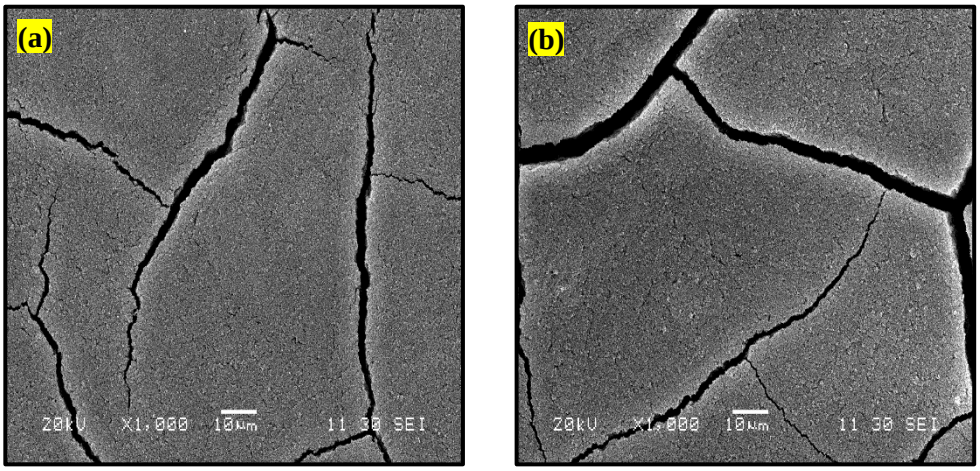

Fig. D2: SEM images of the top surface of a fouled membrane with PEG and two TiO_2 loadings using cross-flow PMR, magnifications: x 1000 and scale 10 µm, (a) 0.125 gL^{-1} and (b) 0.250 gL^{-1}.

Appendix E

E1. SEM images under cross-flow Combined (POM-TiO_2) PMR

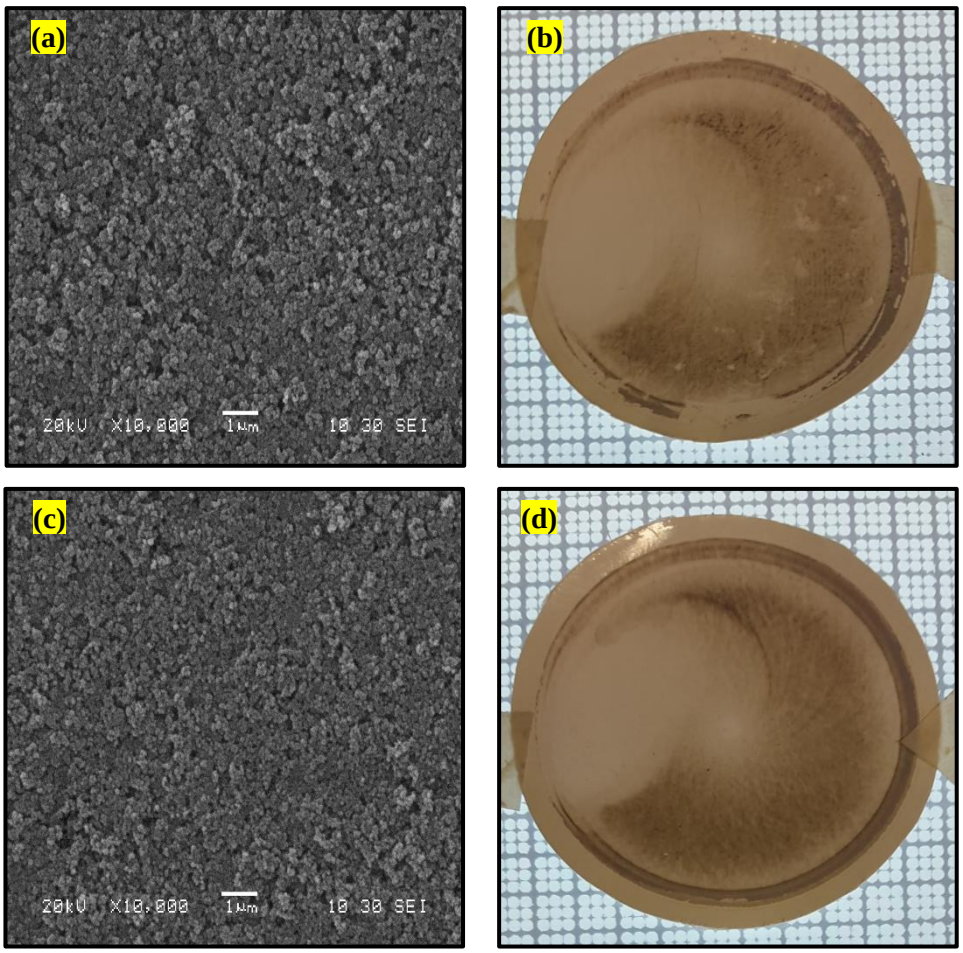

Fig. E1: SEM images (a, c) and real photos (b, d) of the top surface of a fouled membrane with PEG and combined (POM-TiO_2) photocatalysts using cross-flow PMR, magnifications: x 10,000 and scale 1 µm, (a-b) Set 1 and (c-d) Set 2.

Appendix F

F1. TOC and VFAs rejections under POM, TiO_2 and combined photocatalysts of continuous photocatalysis

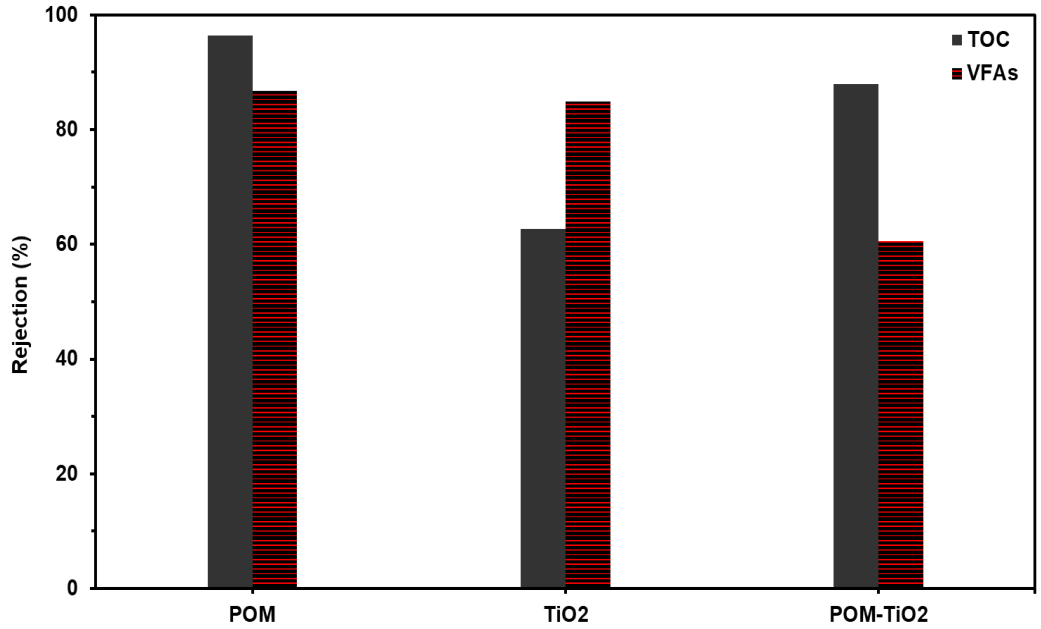

Fig. F1: Comparison of TOC and formed VFAs rejection under continuous photocatalysis with POM (0.75 gL^{-1}), TiO_2 (0.25 gL^{-1}) and combined (POM-TiO_2) photocatalysts (POM-0.125 gL^{-1}, TiO_2-0.25 gL^{-1}) at 9 h operating time.

F2. Comparative fluxes under POM, TiO_2 and combined photocatalysts of continuous photocatalysis

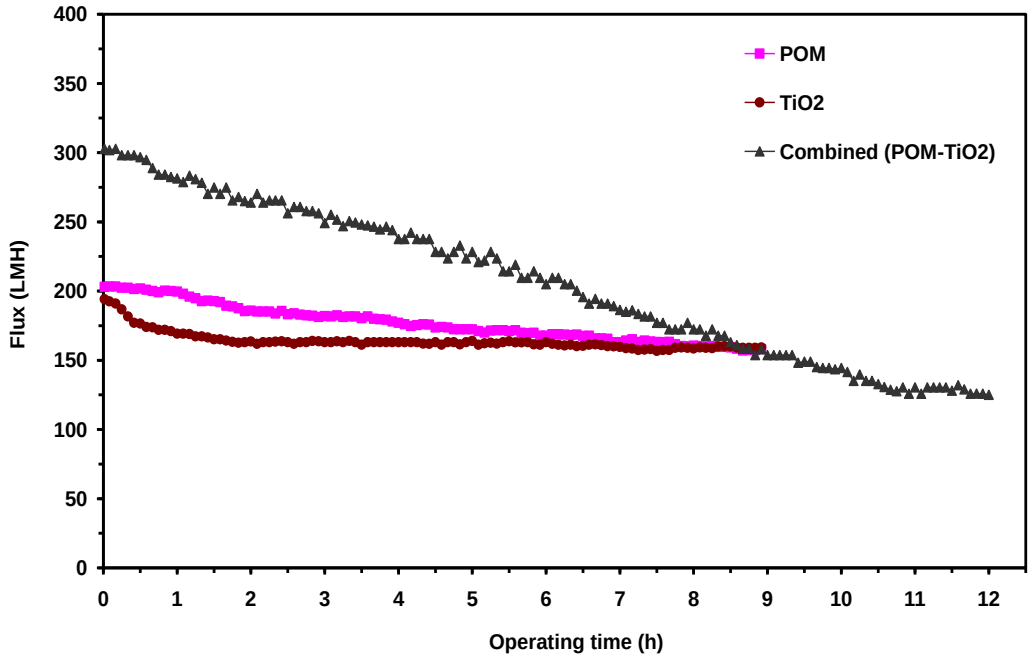

Fig. F2: Comparison of permeate flux under continuous photocatalysis with POM (0.75 gL^{-1}), TiO_2 (0.25 gL^{-1}) and combined (POM-TiO_2) photocatalysts (POM-0.125 gL^{-1}, TiO_2-0.25 gL^{-1}) at 9 h operating time.

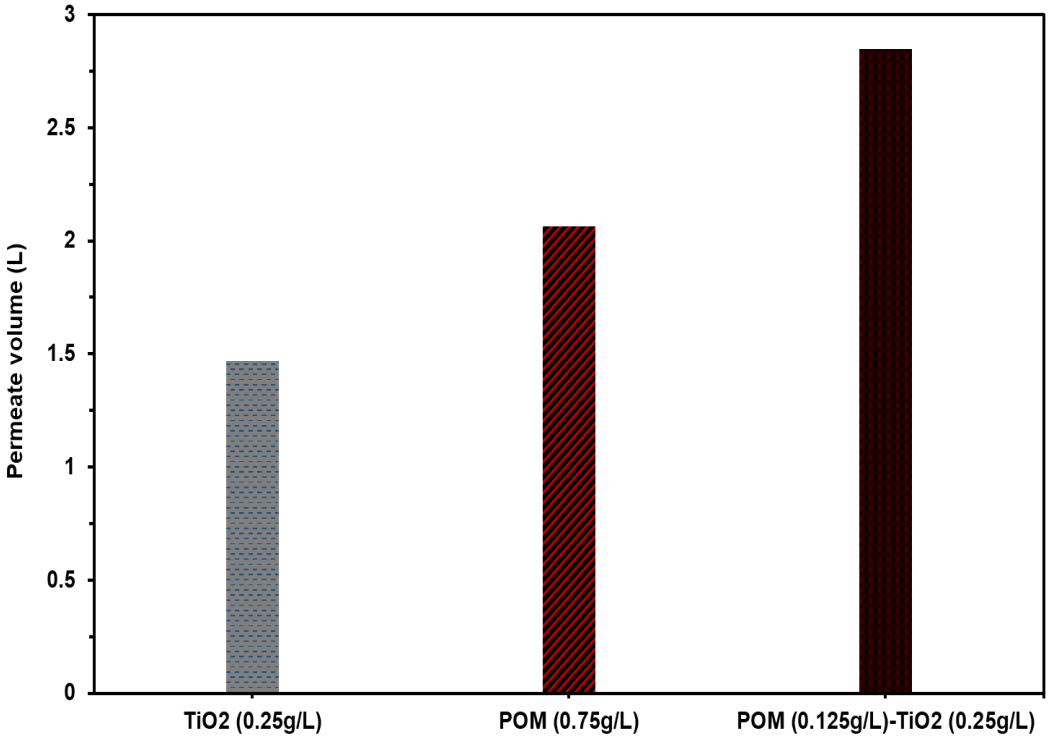

Fig. F3: Comparison of permeate volume under continuous photocatalysis with POM (0.75 gL^{-1}), TiO_2 (0.25 gL^{-1}) and combined (POM-TiO_2) photocatalysts (POM-0.125 gL^{-1}, TiO_2-0.25 gL^{-1}) at 9 h operating time.

F3. POM Vs TiO_2 photocatalysis of PEG

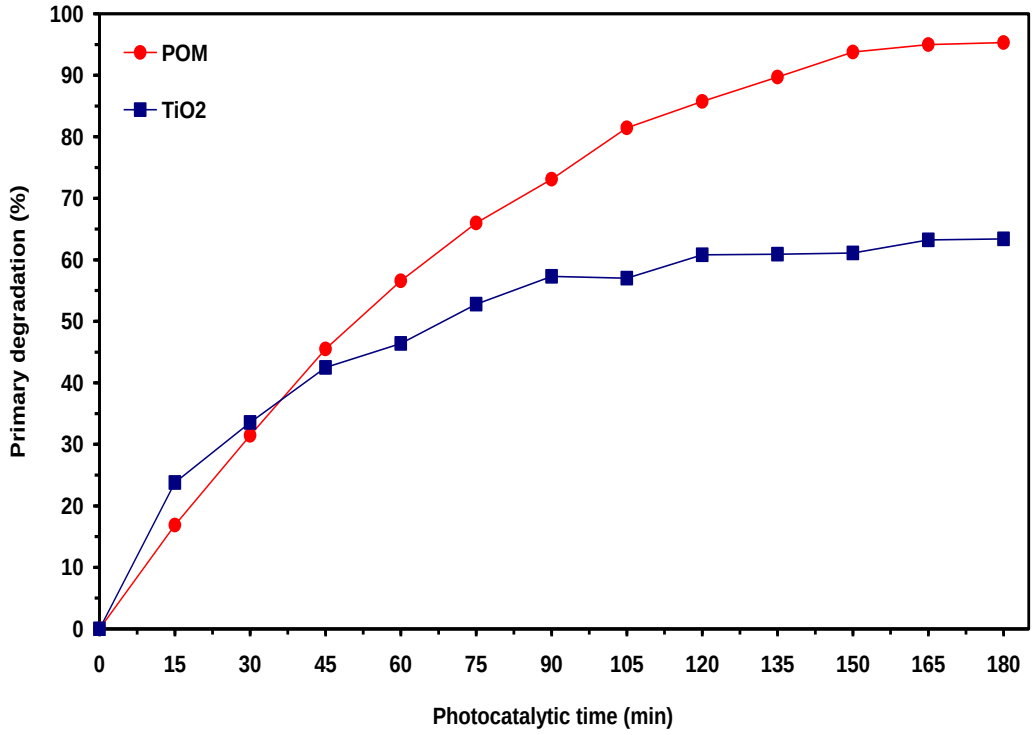

Fig. F4: Comparative performance of the %PD of PEG for 3 h between POM-homogeneous TiO_2-heterogeneous photocatalysts under their optimal loading, POM (0.75 gL^{-1}) and TiO_2 (0.25 gL^{-1}).

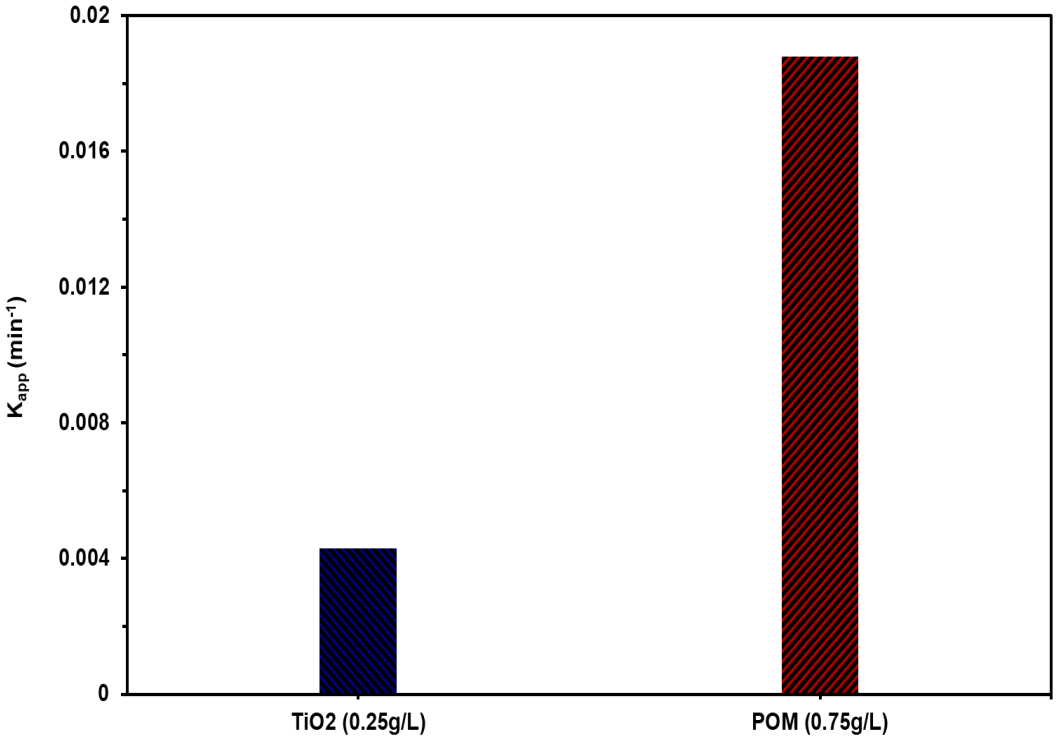

Fig. F5: Comparative performance of the K_{app} between POM-homogeneous TiO_2-heterogeneous photocatalysts under their optimal loading, POM (0.75 gL^{-1}) and TiO_2 (0.25 gL^{-1}).